DOCTOR OF PHILOSOPHY

Shear dispersion in the surface layers of the sea.

Shield, S. R.

Award date:
1991

Awarding institution:
Bangor University

SHEAR DISPERSION IN THE SURFACE LAYERS OF THE SEA

A thesis submitted in accordance with the requirements
of the
University of Wales for the Degree of Doctor of Philosophy

by

S.R. Shield.

ACKNOWLEDGEMENTS

I would like to thank Dr. A. J. Elliott for his forebearance, encouragement and guidance throughout this project. I am also very grateful to the Director and Staff of the Department of Nuclear Science and Technology, Royal Naval College, Greenwich, for allowing me the time and resources to complete the work. My thanks are also due to the staff of the Warren Spring Laboratory, Stevenage, for making available their dye and oil release data and for allocating time and resources for the current meter experiment.

The support of my wife, Dr. N. C. Reynolds, and of her family, has been unstinting.

The work was funded by the Department of Nuclear Science and Technology, Royal Naval College, Greenwich.

ABSTRACT

The kinetic energy density, k, and lifetime, t, of a turbulent eddy, volume V, are shown to be related to a characteristic length scale, ℓ, by:

$$\ell^3 = V \qquad k = \varepsilon^{2/3}\ell^{2/3} \qquad t = \varepsilon^{-1/3}\ell^{2/3}$$

where ε is the energy dissipation rate. A self similar cascade of discrete eddy sizes is derived, each size related to the next larger by:

$$\ell_{i+1} = C\ell_i$$

where $C = 8^{1/2}$. With some simple assumptions as to the turbulent production process the mean logarithmic velocity profile is derived. The relationship between the friction velocity and Reynolds stress is explained in terms of the large eddy intermittency, n. Below a critical free stream velocity, U', n is proportional to the free stream velocity. The dissipation rate, ε, is then constant and given by:

$$\varepsilon = U'^3/N^3L$$

where N is the number of discrete eddy sizes in the boundary layer. When the boundary layer has reached the surface N = 11. The observed turbulent spectral characteristics are derived from the eddy equations without using dimensional reasoning and an explanation of the mechanism behind surface layer similarity scaling is proposed.

An experiment was carried out in the North Sea to test the model predictions. Correlations showed that, except at slack water, the largest eddies were approximately cubic, occupying the whole flow depth, and were advected with the mean flow. Frequency spectra provided evidence that the cascade formulation was correct. The turbulent intermittency was proportional to the current speed and the value of ε, calculated by several methods, was found to be constant with a value:

$$\varepsilon = 0.3 \text{ cm}^2/\text{s}^3$$

The characteristics of the largest eddies were isolated using a spectral cropping technique and plotted as a phase portrait of the turbulent strange attractor. This demonstrated that the boundary layer sat at preferred, discrete energy levels. The levels observed could be related to the discete cascade model. A computer code based on the model equations was tested against a series of large scale oil and dye releases in the North Sea. The observed intermittency, meandering, and dispersion were well simulated with the value of ε given above.

CONTENTS

LIST OF FIGURES AND TABLES

CHAPTER 1 INTRODUCTION

This thesis was driven by the need to quantify the mechanisms involved in contaminant dispersion in the surface layers of estuaries and shallow seas. This need is significant since most contaminant releases have their environmental effects in such areas. Buoyant contaminants necessarily remain in the surface layers, and neutrally buoyant contaminants released near the surface may mix downwards comparatively slowly allowing the near-surface mixing mechanisms to be effective for a significant time.

Four mechanisms are important in their effect on the temporal evolution of the concentration of a contaminant:

1. Advection. A contaminant is carried along by the mean current in which it finds itself. Such mean currents may be tidally or density driven, generated by a wave field or driven by a wind stress on the surface. Secondary currents, which may be thought of as large semi-permanent swirls or eddies are often caused by coastal topography. In this thesis the expression "mean current" is avoided wherever possible, the expression "bulk flow" being more descriptive of the macroscopic water motions. Such bulk flows are commonly approximated by two-dimensional, depth averaged, numerical models; the detail available being limited by computational efficiency and grid size. Here the assumption is made that such bulk flows can be predicted sufficiently well that an improvement in accuracy of mixing models can be achieved by the inclusion of the more detailed fluid motions.

2. Turbulent mixing. All tidally driven flows are turbulent over a large part of the tidal cycle. The significant characteristic of a turbulent flow is its ability to mix and disperse a contaminant effectively. Three mechanisms generate such turbulent mixing, these are illustrated in Figure 1.

a. Large, essentially two-dimensional eddies are generated by side boundaries. In an estuary these often occupy the whole width

(1) Bulk flow generated by estuarine model

(2) 2D eddy or secondary flow

(3) 3D anisotropic bottom turbulence

(4) small 3D isotropic eddy

(5) Wind wave turbulence

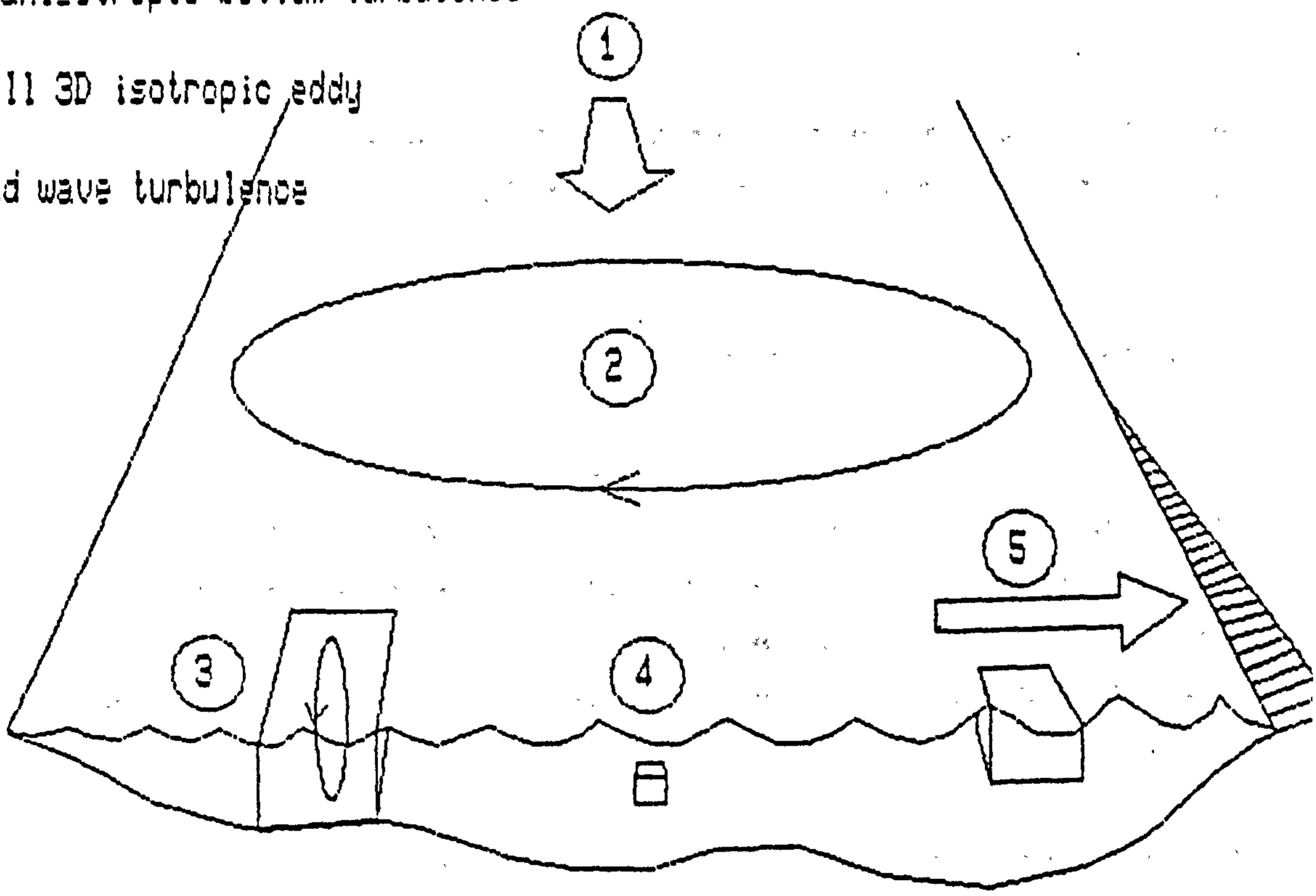

Figure 1. Turbulent mixing mechanisms.

of the flow and are advected for considerable distances before dissipating. Their scale makes them impossible to distinguish from secondary bulk flows and their prediction is thus a function of the accuracy of the bulk flow model and is outside the scope of this thesis.

b. Bottom generated, rough turbulent boundary layers often reach to the surface in shallow seas and generate active mixing. This thesis is concerned with predicting and modelling these turbulent effects.

c. Wind generated surface waves both transport contaminants in the surface layers and generate turbulence and its associated mixing, especially when they break.

3. Molecular diffusion. Molecular diffusion is an essential mechanism for smoothing out the large concentration gradients produced by the turbulent mixing and in converting turbulent kinetic energy into heat. In the flows considered here the dispersive effect of molecular diffusion will be insignificant when compared to that of the turbulence although molecular influences are essential to the determination of turbulent mixing parameters.

4. Contaminant Interactions. Some contaminants degrade in sea-water through biological or chemical reaction. For example radionuclides decay as they disperse. Many contaminants react with the suspended solids in the flow and are dispersed with them rather than following the motions of the fluid. Drying banks retain contaminants which may be re-suspended on the following tide. Oil slicks behave as a collection of droplets but exhibit colloidal and surface tension effects.

Previous work on turbulent mixing has followed two main streams, neither of which has proved entirely satisfactory. The first originated before powerful computers became readily available and predicts concentrations in an Eulerian frame. In recognition of the fact that turbulent dispersion is not a

property of the contaminant or of its local concentration, the diffusion coefficients are replaced by "apparent eddy diffusivities" which are made functions of both space and time. Csanady (1972) noted that this leads to a mismatch between the formulation and the physical processes taking place.

Often the mean shear, itself a product of the turbulent structure, is modelled separately in an attempt to represent the large scale flow structure, diffusion then representing the smaller scales. Unfortunately there are few adequate correlations for predicting the eddy diffusivities as a tidally driven flow develops (Smith, 1982). Mean shear measurements also show a wide variation which limits the efficacy of shear diffusion modelling. Further progress in quantifying the mixing mechanisms demands a more physically realistic method of modelling the turbulence itself.

The second technique employed has been to predict the Lagrangian paths of particles dispersing in a turbulent flow field. Either particle velocity or acceleration is treated as a random walk process, the magnitude and time scales of the random steps being coupled to the turbulence.

Durbin (1983) showed that a simple random walk of fixed step length equates to a diffusion model with constant diffusivity and suffers from the same physical unrealism. Langevin models, in which some past velocity history is recalled at each time step, are more successful since they go some way to acknowledging the longer term influences of the large scale motions in the flow. Again turbulent accelerations at a point are not a local property and have to be predicted from a model of the mean turbulent characteristics or measured in the field.

Much work has been carried out in trying to predict the mean properties of turbulent flows. This is because almost all engineering flows are turbulent, indeed they are almost always designed to be fully turbulent so that their characteristics can be empirically predicted. Turbulent flows can be represented by

the Navier Stokes equations but these equations cannot be solved analytically because they are non-linear. If they were linear, then the dispersion problem would be solved since the passive contaminant would be transported as a marked fluid packet moving in the flow. The resolution of the dispersion would then be determined by the grid size and the numerical integration technique.

Information can be gained from a study of the time averaged equations if time averaged quantities are regarded as characteristic of the fluid properties. The continuity and Navier-Stokes equations, decomposed into mean and fluctuating parts for a constant density fluid are given by Tritton (1977):

$$\partial(U_i + u_i)/\partial x_i = 0 \qquad (1.1)$$

Averaging this equation (the processes of averaging and differentiation are interchangeable in order) shows that:

$$\partial U_i/\partial x_i = 0 \quad \text{and} \quad \partial u_i/\partial x_i = 0 \qquad (1.2)$$

The same division applied to the Navier Stokes equation yields:

$$U_j \partial U_i/\partial x_j = -1/\rho \; \partial P/\partial x_i + \nu \partial^2 U_i/\partial x_j^2 - \partial(\overline{u_i u_j})/\partial x_j \qquad (1.3)$$

for steady flow. This equation for the mean velocity U differs from the laminar flow equations by the addition of the last term which arises from the non-linearity of the Navier Stokes equation. The tensor:

$$-\rho(\overline{u_i u_j}) \qquad (1.4)$$

is called the Reynolds stress.

A similar equation can be derived for the transport of turbulent kinetic energy, $q = 1/2\ (\overline{u_i u_i})$, giving, in the absence of buoyancy effects:

$$U_k \partial q/\partial x_k = -\overline{u_i u_k}\,\partial U_i/\partial x_k - \nu(\partial \overline{u}_i/\partial x_k)^2 - \partial/\partial x_k\,[1/2\ \overline{u_i(\overline{u_i u_k})} - \nu\partial q/\partial x_k + P\overline{u}_k/\rho] \qquad (1.5)$$

(1) (2) (3) (4)

The terms represent:

(1) advection by the mean flow
(2) production of q by mean strain
(3) viscous dissipation
(4) diffusive transport ($P^2 = 1/2\ p_{ii}^2$)

If this turbulent kinetic energy equation is written for a pure shear flow (u_1 in the streamwise direction) in the absence of buoyancy effects, then the entire production occurs in the equation for $u_1^2/2$ and the equations for $u_2^2/2$ and $u_3^2/2$ have no production terms since there is no shear perpendicular to the 2 and 3 axes. The u_2 and u_3 components must therefore receive their energy from the pressure interaction terms.

Because the sum of the pressure terms is zero, the pressure terms exchange energy between components without changing the total amount of energy. Also if the 2 and 3 terms are to maintain themselves despite dissipative losses, $p\partial u_2/\partial x_2$ and $p\partial u_3/\partial x_3$ must be positive and $p\partial u_1/\partial x_1$ must be negative. This can only be the case if the turbulence is not isotropic. In most shear flows this is indeed found to be the case with the r.m.s streamwise component being roughly twice as large as the vertical (Raudkivi and Callander, 1975).

The turbulent energy equation shows that the Reynolds stresses work against the mean velocity gradient to remove energy from the mean flow and provide energy for the turbulence. In order to calculate the development of the mean flow schemes that predict the Reynolds stresses have been devised. The simplest (writing in 2D for clarity, U and u being mean and fluctuating velocities in the x direction, v being the fluctuating velocity in the y direction) are:

$$-\overline{uv} = \nu_T \partial U/\partial y \qquad (1.6)$$

where ν_T, the eddy viscosity, can be taken as a constant or a function of position derived from a model of the turbulence or empirically determined (Boussinesq, 1877). Unfortunately since turbulence involves large scale coherent motions, the Reynolds stresses at any point depend on the whole velocity profile and not just on the local gradient.

Prantle's momentum transfer hypothesis (Prantle, 1925) better reflects these larger scale motions by allowing an appropriate length scale to be applied to the geometry. Here:

$$-\overline{uv} = \ell^2 \partial U/\partial y \; |\partial U/\partial y| \qquad (1.7)$$

where ℓ, the mixing length, must be specified.

The mixing length theory suffers from the same theoretical limitations as above. To its credit, however, if ℓ is taken as proportional to the distance from a solid boundary then a logarithmic velocity profile is predicted (Landahl and Mollo-Christensen, 1987). Much of the literature is concerned with fitting coefficients to this logarithmic profile which is widely held to be representative of turbulent shear flows, although striking departures from the logarithmic form are often reported (Soulsby, 1983). Tennekes and Lumley (1972), while rejecting the mixing length hypothesis, show by dimensional reasoning that a logarithmic profile should exist over some part of a boundary layer.

A higher level model recognises that the Reynolds stresses must be related to the turbulent kinetic energy level and its dissipation rate, ε. It is possible to derive an exact equation for ε from the Navier Stokes equations (Jones, 1971). Unfortunately this is again difficult to solve except in the simplest restricted geometries. Having solved for, or proscribed, q and ε, the expression:

$$\varepsilon = q^{3/2}/\ell \qquad (1.8)$$

gives ℓ, where ℓ is a length scale characterising the energy containing motions (Launder et al., 1972). The Reynolds stresses are then predicted using ℓ and the Prantle-Kolmogoroff expression (Prantle, 1945):

$$-\overline{u_i u_j} = C_1 \, q^{1/2} \, \ell \, \partial U_i/\partial x_j \qquad (1.9)$$

or that:

$$\nu_T = C_1 \, q^{1/2} \, \ell \qquad (1.10)$$

where C_1 is a constant. The length ℓ may be directly specified, thus saving the need to solve an equation for ε. This has the advantage that ν_T can reflect transport processes but in complex flows ℓ is difficult to specify. An alternate form (Jones and Launder, 1972) gives the eddy viscosity directly from:

$$\nu_T = C_2 q^2/\varepsilon \qquad (1.11)$$

where the constant C_2 now has to be found from experiment or specified.

For complex flows progress has been made by deriving equations for the transport of the Reynolds stresses themselves. Unfortunately if the unknown stresses are represented as dependent variables in conservation equations, higher order correlations appear. The level at which truncation of this process takes place is referred to as the level of "closure" of the modelling. Various closures have been developed with some success in predicting complex flows in relatively restricted geometry and scale (Bradshaw, Cebeci and Whitelaw, 1981). Computationally a 3D closure model of an estuary is expensive and a typical three dimensional estuarine model (Smith, 1982) scales the magnitude of the eddy viscosity on the depth-mean turbulence kinetic energy and a proscribed depth mean turbulence energy dissipation rate while

the vertical structure is described by a suitable similarity function derived by experiment.

To summarise: The temporal and spatial evolution of mean turbulent flows can only be calculated using prescribed functions which do little to reflect the underlying physics. In many simple cases they work adequately when the unknowns are found from experiment or trial and error, and any new model that seeks to refine the turbulence modelling must give the same result as these prescriptions in the cases where they have been shown to work well. The varying temporal and spatial characteristics of the turbulence in a real flow cannot be predicted by these models except in the case of Reynolds stress closures in very simple geometries. The development of a real geophysical flow, and the associated turbulent mixing cannot be quantified unless a more physical representation of the turbulence is modelled. As a first step towards this it is necessary to discuss the concept of coherent turbulent structures or "eddies".

It appears from observations of turbulent wakes, plumes and flows, that turbulence has a structure and some universal characteristics. Coherent structures can be seen or extracted from records using statistical analysis techniques. These structures are known as eddies. Eddies of different "sizes" co-exist in the turbulent flow and appear to interact with each other, some eddies being of the same scale as the flow (the same "size" as the width of a smoke plume or the diameter of a pipe), some being very much smaller (Tritton, 1977).

Turbulence will decay in the absence of a continuing generating mechanism. It is thought that in three-dimensional flows large eddies which initially contain most of the turbulent energy break down or decay into smaller and smaller eddies until the very smallest eddies dissipate energy as heat by the effects of molecular diffusion (Tennekes and Lumley, 1972). There is a cascade of energy from the larger to the smaller scales. In largely two dimensional flows, for example in the atmospheric boundary layer or the Gulf Stream, eddies are also observed to

coalesce, transferring energy from smaller to larger scales.

Either the most unstable mode of breakdown to turbulence is at the largest scale or the large eddies are produced by interactions from smaller scales. The theory of instability of laminar flows indicates, at least in two dimensions, that the earliest wave mode to go unstable is the one that occupies the whole flow (Yalin, 1977). Unfortunately the theory is unable to deal with anything more complex than a singular instability in simple geometry.

The growth of a boundary layer over a flat plate is a good example of a situation where the underlying mechanism appears to be different. Turbulent spots developing in the laminar boundary layer appear to be derived from the development and interaction of hairpin vortices revealed by numerical and flow visualisation experiments (Utami and Uemo, 1987). The implication is that the large eddies, occupying and defining the full thickness of the boundary layer, are generated by a mechanism which originates at small scales close to the plate. The resulting turbulent patch is then transported and decays until laminar flow is re-established (Raukivi and Callander, 1975).

Fine scale velocity records in wakes and boundary layers show that turbulence is "intermittent" except in the region very close to a rough boundary (Csanady, 1972). Fluctuating portions of the record are separated by regions of smooth mean flow. All classical models of turbulent flows ignore this intermittency which is still present at high Reynolds numbers. A similar intermittency is observed in records of dye concentrations, (Nakamura, Sakai and Miyata, 1987) showing that the mixing associated with the turbulence also occurs in a patchy fashion. If the turbulent flow is decomposed into eddies, each of which is being advected by the mean flow and by larger eddies, then this intermittency can be conceptualised.

An eddy can be thought of as a volume in which local instability, overturning and mixing is taking place. Since

turbulence is dispersive so must be an eddy, implying that a line of marked fluid particles affected by the eddy motion must be stretched as well as deformed. In attempting to extract eddies from velocity records the assumption is made that in an eddy there is some form of organised structure and that the velocity of the particles in an eddy are in some way correlated to each other (Woods, 1977a).

Correlations extracted from records are often normalised with an appropriate r.m.s value and may be either space or time averages. Thus they may be the average product of, for example, velocity components measured at two different points in space or the average product of velocities measured at the same point at different time delays. The particular case of the product average of a velocity measured in the same direction at the same point after some time delay is, when normalised with the r.m.s value, called the autocorrelation (Tennekes and Lumley, 1972). The integral time scale is often regarded as a measure of the memory time over which particle velocities are related to each other.

Concentration, velocity or correlation records can be analysed to determine the proportion of the signal being received within a narrow frequency band. If a measure of the signal strength is plotted against frequency this is called a spectrum. Although only individual points can be derived from records, the magnitude of the contribution being averaged over the (small) bandwidth of the filter, continuous spectra are often derived and compared with those predicted theoretically.

Frequency spectra can be converted to space spectra by associating the frequency band in which the contribution is measured with a "wave number", k, using Taylor's hypothesis (Tennekes and Lumley, 1972). This states that if a probe is moved through the turbulent field much faster than the field changes then the time record from the probe is equivalent to a space record, taken over the distance that the probe has moved, at a particular time. The frequency is then converted to a wave number using the probe velocity.

Taylor's hypothesis is often applied to velocity records taken at a fixed point as the turbulent flow passes. The criterion then is that the mean flow must be much larger than the turbulent fluctuation change rate. A wave number is representative of a wave which exists in all space, whereas eddies are localised. The interpretation of wave number spectra in terms of their component eddies must recognise this. In this thesis the majority of spectra presented are raw frequency spectra, allowing their interpretation to be discussed case by case.

Two dimensional wave number spectra can be measured directly at the sea surface and ensemble average spectra of horizontal variance of sea surface temperature exhibit a k^{-2} trend (Woods, 1977b). Local spectra however show wide fluctuations in slope and the temperature variance is concentrated into hills and ridges in the (x,k) plane. The kurtosis of horizontal temperature gradient ranges up to 40 confirming that the temperature variations are distributed very intermittently.

Woods (1977b) states that the patchy distribution of temperature variance reveals, by definition, the patterns associated with eddies, uncontaminated by internal waves. Vertical profiles of temperature microstructure show the same kurtosis of temperature gradient and the same intermittency and this leads to a picture of turbulent motion at the sea surface characterised by discrete eddies, distributed so that only a selection of eddies is present at any given location at any instant.

To elucidate this process Kolmogorov (1941) predicted the existence at sufficiently high Reynolds numbers of a universal equilibrium range of eddy sizes where a transfer of energy proceeds towards smaller scales of motion, each having increased statistical independence of the mean flow as the scale reduces. The rate of energy supply to this range is governed by, and in equilibrium with, its rate of removal. The only two parameters controlling this process are ε (the rate of turbulent kinetic energy dissipation per unit mass) and ν (the kinematic viscosity).

If the energy containing and dissipating scales are sufficiently well separated then energy transfer will occur with negligible dissipation. This is called the "inertial subrange" and dimensional analysis shows that the 3D energy spectrum, $E(k)$, is given by (Tennekes and Lumley, 1972):

$$E(k) = \text{const.}\varepsilon^{2/3} k^{-5/3} \qquad (1.12)$$

For isotropic turbulence the same authors show that the 1D energy spectrum $\Phi_1(k)$ is given by:

$$\Phi_1(k) = A \alpha \varepsilon^{2/3} k^{-5/3} \qquad (1.13)$$

where k is the radian wave number, A is a constant determined from considerations of isotropy and normally taken as 18/55 and α is 1.44. The inertial subrange is only expected to exist at sufficiently high Reynolds numbers and is well supported by 1D measurements in high Reynolds number flows if Taylor's hypothesis is used to transform records from time to space (Tennekes and Lumley, 1972). It should be noted that 1D spectra are only expected to follow the $k^{-5/3}$ law if the turbulence is isotropic. Unfortunately a region of the spectrum exhibiting this relationship is often found when an inertial subrange should not exist on dimensional grounds (Turner, 1973) or when the turbulence is known to be anisotropic (Heathershaw, 1979). Ozmidov (1965) suggested that the $k^{-5/3}$ dependence may be characteristic of the eddy cascade wherever energy is not being supplied to the turbulence.

Tennekes and Lumley (1972) show that one dimensional spectra of velocity fluctuations plotted against a frequency, σ, associated with the eddy timescale (or strain rate), are predicted to follow a σ^{-2} relationship in the inertial subrange although spectra of this kind have not been directly measured. Later in this thesis these dependencies will be shown to follow from the characteristic relationships derived for individual eddies in a cascade and time spectra will be presented.

The turbulent motions in a shear flow are never isotropic, however the smaller scale motions should be randomly orientated since they have little statistical dependence on the large scale motion characterising the flow. At small scales therefore the isotropic assumption should be valid. This is called local isotropy (Tennekes and Lumley, 1972). If this assumption is made then the value of ε can be calculated from measured 1D spectra. The dissipation rate may also be measured by assuming local isotropy and measuring the temporal derivative of the longitudinal velocity fluctuation (equation (1.5), term 3). Browne, Antonia and Shah (1987) made detailed studies in a low Reynolds number wake and showed that the assumption of local isotropy is unlikely to be true in any shear flow, even at high Reynolds numbers. The values of ε achieved by assuming local isotropy were underestimated by factors of about 45% on a wake centreline and 80% at the edge, values verified by considering the turbulence kinetic energy budget.

Heathershaw (1979) compared the value of ε found from spectra with that calculated from the assumption that in a constant stress layer the production should equal dissipation, ie:

$$\tau/\rho \; \partial U/\partial z = \varepsilon \qquad (1.14)$$

This is another common method for estimating ε which assumes that the advection and diffusion are negligible. He found that ε was anomalously high so that the budget did not balance. Also the ratio of the magnitudes of the longitudinal and transverse space spectra was $S_{11}(k)/S_{22}(k) \simeq 1$ instead of 4/3 as it should be for isotropy. Therefore there was only qualitative experimental support for the theory as it stands.

The ensemble mean dissipation rate, $\bar{\varepsilon}$, should lie somewhere in the range of values measured at small scales. Published values of $\bar{\varepsilon}$ show a wide scatter and Woods (1975a) noted that the actual dissipation rate within a turbulent patch should be related to $\bar{\varepsilon}$ by the intermittency factor of the turbulence. Heathershaw (1979) and Woods (1977a) both reviewed published values of $\bar{\varepsilon}$ for

$= 10 \ (W m^{-3})$

VALUE $(cm^2 s^{-3}) = 10^{-4} (m^2 s^{-3})$	LOCATION
0.02	1 m above the sea bed in a stratified estuary
≤ 1.02	The surface layers of a tidal flow
≤ 0.08	The upper layers of the ocean
0.14 - 0.32	Tidally averaged estuary values
0.10	Patches in the equatorial undercurrent

Table 1. Summary of published values of the energy dissipation rate.

comparison with their own measurements. These are summarised in Table 1 in units of cm^2/s^3:

It is important to achieve some quantitative results for the extent of the range of turbulent eddy sizes. Let us first consider the dissipative scales. Heathershaw used his estimate for ε (0.6 cm^2/s^3) to estimate the Kolmogorov microscales at which eddies with unity Reynolds number are able to dissipate kinetic energy into heat and noted that a typical dissipation wave number will be a couple of orders of magnitude larger than any that can be measured. These estimates were:

η	.04 cm	the dissipative length scale
τ	.14 s	the dissipative timescale
ω	.30 cm/s	a characteristic velocity in the dissipative eddies

At the largest scales the formation of seabed sand dunes can be described in terms of the action of the large scale turbulent eddies in the flow (Yalin, 1977). This argument is particularly revealing. It is a significant empirical fact that the dune wavelength is very directly correlated with the water depth (h). The build up of the dunes is described in terms of the ringing in the autocorrelation of the horizontal velocity which has a wavelength 1/h. The theory predicts dunes of wavelength $\Lambda=2\pi h$ which is very close to the field measurements. The implication is that the driving velocity must have a narrow spectrum centred around 1/h or that the size of the energy containing eddies must be centered around h, this being the average length scale over which horizontal velocities are just correlated.

Although the probabilistic characteristics of u vary with depth, the characteristics of the largest eddies, those with the lowest spectral frequencies, remain remarkably constant over the majority of the channel depth (Heathershaw, 1979), implying again that the large scale eddies have the same length scale as the flow. Sand dunes undoubtedly form and thus the presence of energy containing eddies of the same scale as the flow must be taken as established. These eddies are similar to those scaling with the

outer dimensions of a boundary layer and it is a reasonable assumption that the largest eddies occupy the whole depth when the boundary layer does, as is the case in many sea areas within an hour or two of slack water (Soulsby, 1983).

Contributions to the Reynolds stress are large and intermittent both in laboratory and geophysical shear flows (Heathershaw, 1979). At sea the strength of the contributions is not known more than 2 m from the bed although they are of constant strength within that layer (Bowden and Ferguson, 1980). In the laboratory there is little variation over the flow depth (Anwar, 1981). These contributions are believed to have causal similarity to bursting phenomena observed in laboratory shear flows where a well ordered sequence has been established:

$w>0,\ u<0$	Ejection
$w<0,\ u>0$	Sweep
$w>0,\ u>0$	Outward interaction
$w<0,\ u<0$	Inward interaction

Ejections and sweeps make large negative contributions to the Reynolds stresses, interactions make weak positive contributions. Whereas u and w are distributed normally around their means, $\overline{uw}$ is skewed and kurtosed. For large values of the kurtosis $K(\overline{uw}) = 3/\gamma$ where γ is an indicator of the time in a total record length for which the signal is effectively "switched on" (Heathershaw, 1979). If the quantity being examined is intermittent the kurtosis will take on large values. Applying this criterion to the Reynolds stress he showed that the signal was typically "on" for 25 -30% of the time and that the mean period between bursts, T_p, remained fairly constant across the boundary layer and could be scaled with the outer flow parameters :

$$T_p = \text{const}.d/U_0 \qquad (1.15)$$

The specification of the boundary layer depth, d, is fairly arbitrary except where the boundary layer has grown to occupy the

whole flow. U_0 is the free stream velocity. The correlation time for the events (their average duration), T_d, is related to the period between bursts and the intermittency calculated from the kurtosis of the signal by:

$$T_d/T_p = \gamma \tag{1.16}$$

showing that the Reynolds stresses are mainly associated with the large eddies which occupy the whole flow. Reynolds stresses are associated with anisotropy (Tritton, 1977) so that these large eddies are anisotropic.

It has been shown that there exists a range of eddy scales from the largest size equal to the major dimensions of the turbulent flow down to the smallest, dissipative size where kinetic energy is irreversibly turned into heat. The main spectral characteristics of the inertial subrange seem to apply outside the range of scales for which they are predicted, leading to the hope that if some general characteristics of turbulent eddies can be found, both in space and time, then a more effective modelling of the turbulence can be made.

All turbulent flow dispersion experiments exhibit meandering in the early stages after release. The plume from a chimney, oil slick or dye release wanders so that the meandering is much greater than the plume dimensions. The averaged properties of the plume as a whole are described by "absolute" diffusion theory and the spreading of the plume relative to its centre of gravity by "relative" diffusion theory. These theories are described in detail by Csanady (1972) and are illustrated in Figure 2. They are particularly applicable to the dispersion of some toxic chemicals where a threshold level is hazardous. Some extra mathematical derivations are given here since they will be used later in the thesis.

Absolute diffusion theory (Csanady, 1972) predicts the ensemble averaged properties of a diffusing cloud or plume in a constant mean flow. The ensemble average concentration

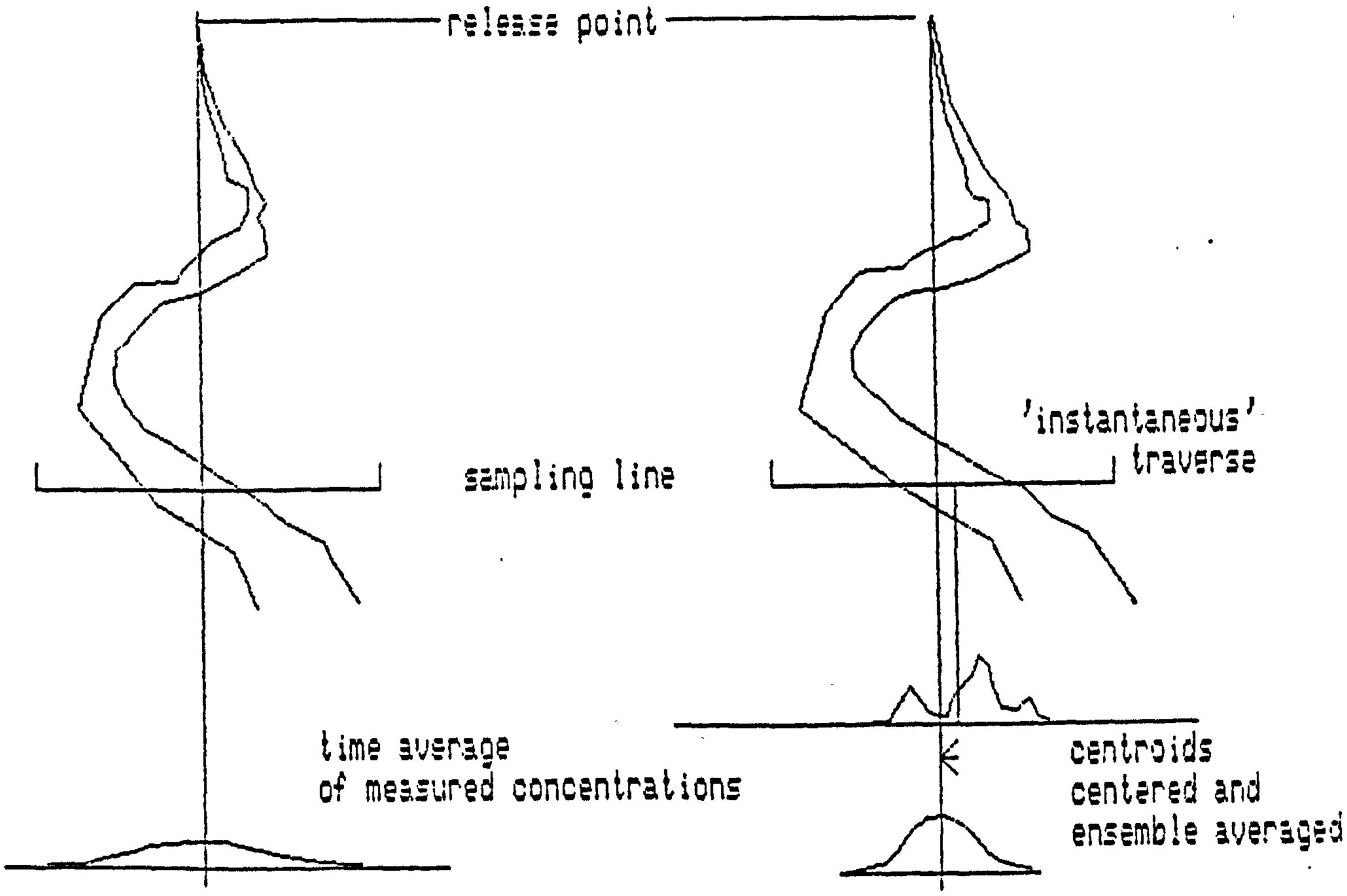

Figure 2. Absolute and relative dispersion.

distribution is assumed to be Gaussian and no account is taken of intermittency or velocity shear. Fick's law provides a relationship between the spatial distribution of concentration and flux provided that the continuum approach to the density distribution is valid and that the 'flight time' of a particle is small compared to the time step under consideration. Mathematical closure using the equation of continuity results in the diffusion equation for the concentration, χ:

$$\partial\chi/\partial t + \mathbf{u}.\nabla\chi = D\nabla^2\chi \qquad (1.17)$$

where D is the "diffusivity", a material quantity. For a constant diffusivity and in one dimension, a point source diffusing under this relationship exhibits a Gaussian concentration distribution with the variance $\sigma^2 = 2Dt$ so that σ increases with the square root of time. In the turbulent diffusion approximation this is replaced by the eddy diffusivity which must be related to the turbulence. Csanady showed that the spreading of an initially concentrated cloud can be related to the Lagrangian autocorrelation, $R(\tau)$, of the stationary velocity field by Taylor's theorem (Taylor 1922). This is:

$$\sigma_x^2 (t) = 2\, u^2 \int_0^t (t - \tau)\, R(\tau)\, d\tau \qquad (1.18)$$

The predicted dispersion is relatively insensitive to the form of the Lagrangian autocorrelation. Two examples show this. If dispersion in stationary, homogeneous turbulence is a Markov process then Durbin (1983) showed that:

$$R(\tau) = \exp\ (-\tau/t_L) \qquad (1.19)$$

where t_L is a timescale associated with the largest turbulent eddies. There is laboratory evidence for a Lagrangian autocorrelation of this form although it is known to be incorrect at the origin. Substituting and integrating gives:

$$\sigma_x^2 = 2\, u^2 t_L\, t - 2\, u^2\, t_L^2\, (1-\exp(-t/\, t_L)) \qquad (1.20)$$

which for $t >> t_L$ implies that:

$$\sigma_x^2 = 2\ u^2\ t_L(t - t_L) \qquad (1.21)$$

Thus the standard deviation tends to grow with the square root of time from an origin at t_L.

If an alternate extreme form of $R(\tau)$ is chosen to reflect the spatial distribution of eddies so that:

$$R(\tau) = 1,\ t \leq t_L$$
$$R(\tau) = 0,\ t > t_L \qquad (1.22)$$

then integration gives:

$$\sigma_x^2 = 2\ u^2 t_L\ (t - t_L\ /2) \qquad (1.23)$$

and once again the standard deviation grows with the square root of time, here from an origin at $t_L/2$. In practice this would be indistinguishable from the first formulation at times greater than t_L.

If dispersion is modelled as a simple random walk, step length ut_L occurring every t_L, then after many steps the particle distribution approaches the Gaussian with variance:

$$\sigma^2 = u^2 t_L t \qquad (1.24)$$

and the standard deviation grows with the square root of time as before. This demonstrates that a random walk model with constant step length is the equivalent of a diffusion model with constant diffusivity (Durbin, 1983). An isotropic two dimensional random walk in x and y, although at large times Gaussian in x and y, approaches a Rayleigh distribution for r, the dispersion distance from the moving origin (Bartlett, 1978). Thus:

$$r^2(t) = x^2(t) + y^2(t)$$

$$f_r(t) = (2r/u^2 t_L t) \exp(- r^2/4u^2 t_L t)$$

with a mean η_r now increasing as:

$$\eta_r(t) = (\pi u^2 t_L t/4)^{1/2} \quad (1.25)$$

and variance given by:

$$\sigma_r^2(t) = (1 - \pi/4)\, u^2 t_L t \quad (1.26)$$

The mean and standard deviation of r increase with the square root of time as before.

Real plumes meander (Bowden and Lewis, 1973). An ensemble average concentration distribution in a fixed frame at a certain distance x downstream from the source will show a wider and lower profile than that achieved by averaging in a moving frame of reference centred on the realised centre of gravity of the plume at each traverse. Accepting that the averaged, centred, concentration distribution will be Gaussian, whatever the fluctuation concentration distribution at a point, provided that at each point the fluctuation distribution profile is the same (Bartlett, 1978) it is instructive to study spreading in a moving frame. Indeed when making dispersion measurements in the sea relative diffusion measurements are often the only ones that it is practicable to make.

If the initial dispersion of a point source cloud relative to its centre of gravity is governed by the action of turbulent eddies in the inertial subrange, Batchelor (1950,1952) predicted on dimensional grounds:

$$u^2(t) = a_1 s^{2/3} \varepsilon^{2/3} \quad (1.27)$$

$$t_R(t) = a_2 s^{1/3} \varepsilon^{-1/3} \quad (1.28)$$

where ε is the energy dissipation rate, s the standard deviation of the cloud concentration about its centroid, a_1 and a_2 constants

of order unity and t_R a Lagrangian time scale for relative diffusion. Assuming a Gaussian concentration distribution and defining a standard deviation relative to the centroid, s(t), Batchelor (1952) showed that:

$$s^2(t) = 2 \int_0^t u^2(t') \; t_R(t') \; dt' \qquad (1.29)$$

so that substituting (1.27) and (1.28) into (1.29) gives:

$$s(t) = (2a_1a_2/3)^{3/2} \varepsilon^{1/2} \; t^{3/2} \qquad (1.30)$$

when the cloud is initially concentrated at a point. The standard deviation relative to the centroid should grow with $t^{1.5}$. There is much evidence that this is a good representative model (Csanady, 1972). As in the spectral evidence already discussed, however, the $t^{1.5}$ growth is found over a much wider range of physical scales than those for which inertial subrange eddies could possibly account (Okubo, 1971). Attempts to explain this discrepancy invoke shear dispersion, a recognition in itself that the mean characteristics of the large eddies in the flow exhibit the same dispersive characteristics as the smaller ones.

The discrepancy between theory and observation could also be explained if the constants a_1 and a_2 in (1.27) and (1.28) were significantly less than unity. The scales over which meandering is observed (until relative and absolute diffusion are equal) would then be extended. Batchelor's (1952) argument assumed a continuous distribution of eddy sizes in the inertial subrange. There would always therefore be an eddy size available to spread the patch efficiently (eddies much smaller or larger than the patch being ineffective in causing spreading). The constants can only be reduced if the distribution of eddies is itself patchy, so that some of the possible sizes are absent. A distribution where some sizes are preferred may be termed a "discrete" distribution.

The statistical characteristics of such discrete eddy cascades have been examined previously (Yaglom, 1966) but have not

been related to practical turbulence models. Mandelbrot (1974) has clearly pointed out the dependence of measured parameters on the measuring technique when one dimensional, eulerian, measurements are taken of an intermittent and three-dimensional process. He has introduced the concept of fractional dimension, a self similarity dimension for geometrical constructions that need not be integer. Mandelbrot (1973) calls this fractional dimension Δ and shows that for a spatially intermittent set of such figures, it is necessary for Δ to be less than 3 and suggests that:

$$1/3\ \Delta > \Delta-2 \qquad (1.31)$$

The advantage of a fractional dimension is that it allows the mathematics to be performed without the necessity for the geometry of the self-similar structure to be known. As a concept it removes a traditional constraint, that of being able to mentally visualise the geometric form under consideration. In this thesis the dissipative cascade of eddies will be shown to necessarily have a fractal dimension within the Mandelbrot limits given above.

More recently the evolving understanding of non-linear dynamics, generically termed "Chaos Theory", has demonstrated that many natural phenomena may be described without resorting to statistical methods. Since by their very nature non-linear systems of equations are mathematically intractable, computer simulations are used to track particles moving in a non-linear fashion at each time step. This is similar to Langevin modelling but without the random input at each step. Applications to dispersion are rare and the non-linear equations are often not derived from physical principles. It has been shown, for example, (Okubo, Andreasen and Mitchell, 1984) that particles moving under an amplified climbing-sine model of the form:

$$X_{t+1} = X_t + a\ |X_t|^p \sin X_t \qquad (1.32)$$

exhibit a rate of growth of displacement variance which is faster than linear in time, rather like the explosive phase of cloud growth in relative diffusion. Other work has shown (for example

Cox, Darzin, Ryrie and Slater, 1990) that particle paths can be chaotic in simple systems of perturbed irrotational cellular flows or in irrotational flows containing simple, but non-linear, wave fields. The development of turbulence and its dispersive properties are both governed by the non-linear Navier Stokes equations. Even simplified versions of these are intractable to analysis. It appears, however, that such families of equations exhibit solutions which, although unstable, are structured. A fuller understanding of these structures may be the only way to link fundamental dynamical theory to the phenomenum of turbulence. This would restore randomness to its natural position of modelling the motion of the super-molecular fluid packets and the statistical description to its position as the target against which models are run. To summarise the introduction, an improved model of turbulent eddies must:

a. Recognise the spatial distribution of eddies and the intermittency of the turbulence.

b. Give the mean velocity distributions found by observation.

c. Give the correct frequency and wave number spectral characteristics, possibly over a wider range than those derived for the inertial subrange.

d. Give values for parameters such as ε which are within the band of values measured by experiment.

e. Predict dispersion which agrees with the measurements of relative and absolute dispersion, meandering and intermittency.

f. Model the Reynolds stresses and justify the models currently in use for their prediction.

g. Give eddy characteristics which are derived from the fundamental equations of motion, so that the physics of the turbulent process is made more clear.

CHAPTER 2. THE EDDY ENERGY CASCADE IN THE ABSENCE OF BOUNDARIES.

An isolated eddy

Let us consider how an isolated eddy might behave. Clearly the eddy has to be spatially limited and we shall define its volume V as ℓ^3, where V may vary during the existence of the eddy and ℓ is a representative length scale. V is chosen to be big enough to encompass the fluid motions induced by the eddy but small in comparison with the total volume of fluid in which the eddy is embedded. Clearly V contains vorticity or the eddy would not exist.

Consider now an infinite volume of stationary irrotational fluid into which the eddy is placed at time t=0. There is an immediate dilemma. Any motion involving fluid shear dissipates kinetic energy by the action of viscosity, and the presence of vorticity implies the presence of velocity gradients and energy dissipation. Lamb (1932) shows, however, that the total kinetic energy of this system should remain invariant. How can this be? The implication is that the flow structure should arrange itself so that the induced velocities within V are such that the average gain in kinetic energy exactly balances the loss. To see the implications of this we now need to consider vorticity dynamics in some detail.

The equation of motion for a fluid at any point can be written in the form known as the "vorticity equation" (Batchelor, 1967):

$$\partial \mathbf{w}/\partial t = -(\mathbf{u}.\nabla)\mathbf{w} + (\mathbf{w}.\nabla)\mathbf{u} + \nu\nabla^2\mathbf{w} \qquad (2.1)$$

Alternatively, following the motion of a marked fluid packet:

$$D\mathbf{w}/Dt = (\mathbf{w}.\nabla)\mathbf{u} + \nu\nabla^2\mathbf{w} \qquad (2.2)$$

The advantage of describing the flow field in terms of vorticity is that the pressure terms are absent from the equations of motion. Vorticity is a mathematical property of the fluid motion

and not a property of the fluid itself, however if the behaviour of the vorticity distribution can be characterised then the motion as a whole is defined.

A line in the fluid whose tangent is everwhere parallel to the local vorticity is termed a "vortex line" and a useful result (Batchelor, 1967) is that the vorticity vector behaves like a material line element coinciding instantaneously with the vortex line, even in a real fluid. Batchelor (1967) showed that as a result the flux of vorticity across a material surface element changes only as a result of diffusion. There are two consequences to this for our postulated isolated eddy. First, although V might change radically in shape while the eddy exists, it will change in size only as a result of vorticity diffusing under the action of viscosity. Secondly if V is allowed to encompass all the rotational flow, then the total "amount" of vorticity in V will remain invariant. Defining an "amount"' of **w** as the square of the magnitude of the vector **w**.**w** or ω^2 and Ω_0^2 as the total "amount" of vorticity in the eddy:

$$\int_V \omega^2 \, dV' = \text{constant} = \Omega_0^2 \qquad (2.3)$$

Defining the average amount of vorticity per unit volume as ω_1^2, then:

$$\omega_1^2 = \Omega_0^2/V \qquad (2.4)$$

Locally, within the eddy, the vortical regions will be being deformed. Raudkivi and Callender (1975) noted that the deformation will involve an overall stretching of fluid elements because of the dispersive nature of turbulence. Batchelor (1967) showed that vorticity when stretched concentrates into lines or sheets (a sheet can be considered as being made up of a set of adjacent vortex lines). Solutions exist in simple geometries and we consider here the dynamics of a small element of vortex sheet to illustrate the main effects of stretching. The geometry is illustrated in Figure 3.

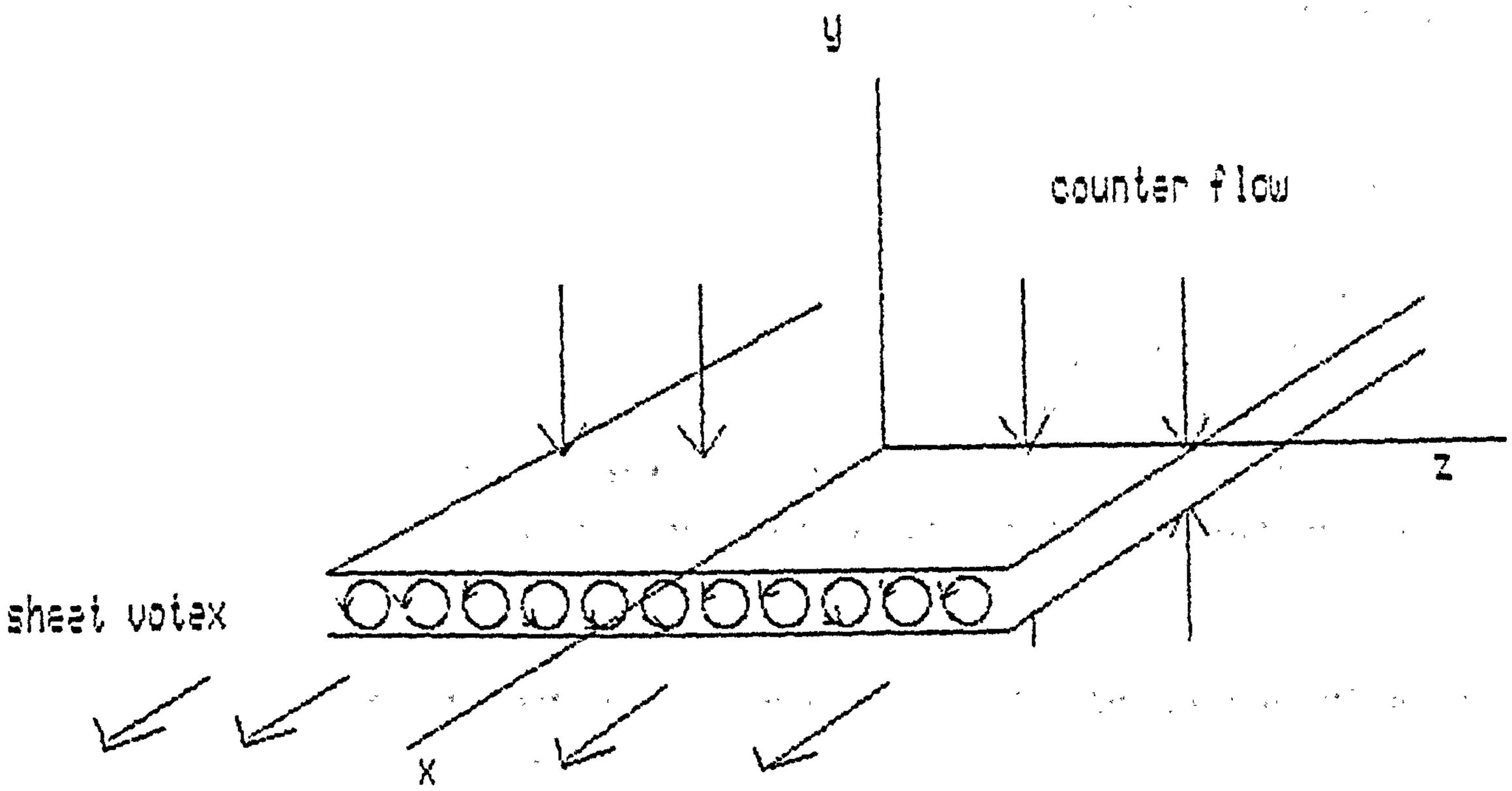

Figure 3. Geometry of a stretching vortex sheet element.

The solution for a sheet which is being stretched in one direction only is given by Batchelor (1967). The sheet exists in the x,z plane and the stretching is in the x direction such that $u(x)=\beta x$. If all the resulting contraction is in the y direction then the vorticity is ultimately concentrated into a Gaussian distribution about y=0 thus:

$$\omega(y) = \omega_s \exp(-\beta y^2/2\nu) \qquad (2.5)$$

where ω_s is now the amount of vorticity per unit area of the elemental sheet. The standard deviation, σ, of the Gaussian vorticity distribution is given by:

$$\sigma = (\nu/\beta)^{1/2} \qquad (2.6)$$

and 95% of the vorticity will be found within a layer 4σ thick, 98% in a layer 8σ thick. This steady solution (time does not appear in the equation) exists because the diffusion of vorticity away from the y=0 plane is exactly balanced by the inward flux of fluid necessary for continuity within the control volume under consideration.

If the vorticity vector was originally wholly in the direction of the stretching, so that:

$$\mathbf{w} = (\omega_x, 0, 0) \qquad (2.7)$$

then the concentration will result in an increase of vorticity within a control volume containing the sheet. This is known as vortex stretching (Tennekes and Lumly, 1972; Batchelor, 1967). We can find an equation for ω_s in these circumstances by assuming that the vorticity is concentrated into the (x,z) plane. The vorticity equation becomes, following the motion of the small element:

$$D\omega_x/Dt = \omega_x \partial u_x/\partial x + \nu\partial^2\omega_x/\partial x^2 \qquad (2.8)$$

and ignoring diffusion in the direction of stretching the solution

is:

$$\omega_x = \text{const.}\exp(\beta t) \qquad (2.9)$$

which increases exponentially. The sheet element has enlarged because of the stretching since there is no contraction in the z direction. Thus, calling the sheet area A:

$$DA/Dt = \beta A \qquad (2.10)$$

and:

$$A = \text{const. } \exp(\beta t) \qquad (2.11)$$

The vorticity per unit area, $\omega_* = \omega_x/A$, therefore remains constant as expected from the steady state solution given above.

If the original vortex vector is wholly in the z direction, so that:

$$\mathbf{w} = (0, 0, \omega_z) \qquad (2.12)$$

the Gaussian solution still applies since the vorticity diffuses in the same manner and the stretching and influx are the same. The value of ω_* may be obtained as before by considering the vorticity equation with all the vorticity concentrated into the x,z plane. Thus:

$$D\omega_z/Dt = \nu\, \partial^2\omega_z/\partial x^2 \qquad (2.13)$$

and ignoring viscous diffusion in the direction of stretching this becomes, following the motion of a fluid packet:

$$D\omega_z/Dt = 0 \qquad (2.14)$$

therefore ω_z remains constant and ω_* decreases exponentially with time as the sheet stretches normal to the vortex lines.

The formulation implies that if β is negative so that the sheet is being compressed, then ω_s should increase exponentially. In practice this does not occur since the sheet can only thicken by diffusion and a consequential stretching in the z direction would have to be induced. Rogers and Moin (1987) found that on compression a vortex sheet buckles or folds and, since a perturbed sheet is unstable (Batchelor, 1967), the folding becomes increasingly complex as compression continues, without thickening the sheet.

Batchelor (1967) and Raudikvi and Callender (1975) showed that the vorticity equation implies that the increase in one component of the vorticity of a fluid packet is at the expense of the other components without a reduction in the total amount of vorticity. This is because the pressure terms in the turbulent kinetic energy equation transfer energy between components without loss and the local vorticity vector moves instantaneously with the fluid. If w is neither parallel to nor normal to the direction of stretching then it will tend to turn to align itself with the stretching axis since downstream fluid particles instantaneously coincident with the vortex line are moving faster than upstream ones.

Suppose that the instantaneous vorticity distribution within V can be approximated by a large number of small vortex sheet elements, each of which is being stretched. If the many elements are examined at an instant in time then the central limit theorem (Bartlett, 1978) tells us that an ensemble average of the vorticity distribution across each element will be Gaussian. If the sheet elements are chosen to be small enough so that each is two-dimensional then Batchelor (1967) gives for the kinetic energy dissipation rate per unit area of such an element:

$$(\partial KE/\partial t)_{\text{per unit area}} = -\nu \int_{-\infty}^{\infty} \omega(y)^2 dy \qquad (2.15)$$

Substituting the Gaussian vorticity distribution, (2.5), into the integral gives (Dwight 1961):

$$(\partial KE/\partial t)_{\text{per unit area}} = -\nu(\omega_s)^2(\pi\nu/\beta)^{1/2} \qquad (2.16)$$

If we define the element thickness, δ, as 8σ so that almost all the vorticity is contained in the sheet then, using (2.6):

$$\delta = 8\sigma = 8(\nu/\beta)^{1/2} \qquad (2.17)$$

The average kinetic energy dissipation rate per unit volume within the element is given by:

$$(\partial KE/\partial t)_{\text{per unit volume}} = (1/\delta)(\partial KE/\partial t)_{\text{per unit area}} \qquad (2.18)$$

and substituting from (2.16) and (2.17) into (2.18) gives:

$$(\partial KE/\partial t)_{\text{per unit volume}} = -\nu(\omega_s)^2\pi^{1/2}/8 \qquad (2.19)$$

which is independent of element thickness.

The total kinetic energy dissipation rate within the eddy is found by summing the dissipation within each elemental volume dV′, thus:

$$\partial KE/\partial t \;\alpha\; \sum_{\text{elements}} (\omega_s)^2 dV' \qquad (2.20)$$

and since by summing over all the vortical elements we account for all the vorticity within the eddy, we can use (2.3) to give:

$$\partial KE/\partial t \;\alpha\; -\nu\,\Omega_0^2 \qquad (2.21)$$

If the vorticity distribution within V can be approximated by a suitable selection of elemental Gaussian sheets then it is also valid to consider the Gaussian as a distribution function whose properties reflect the average manner in which the vorticity is diffusing and therefore of the manner in which the boundary of V is increasing by diffusion.

The representative length scale ℓ will therefore increase with time as:

$$\ell^2 = 2\nu(t+t_0) \tag{2.22}$$

where t_0 reflects the finite size of ℓ at t=0. Since V is equal to ℓ^3:

$$V \alpha (\nu(t+t_0))^{3/2} \tag{2.23}$$

and:

$$V = V_0(1+\nu t/V_0^{2/3})^{3/2} \tag{2.24}$$

where V_0 is the volume at t=0. Now the kinematic viscosity of water is very small. The value varies with temperature and salinity but is of the order of 10^{-2} cm^2/s (Batchelor (1967), Appendix 1). If V_0 was 1 m^3 then it would take 16 hours for the eddy to increase in volume by 10%. A 40 m eddy (V_0=64000 m^3) will increase its volume by 3% in one hour. A 1 cm eddy might double its volume in 100 s. Turbulence decays in much shorter timescales than these (Tennekes and Lumley, 1972) and it is therefore safe to assume, to a high level of approximation, that V is constant over the lifetime of the eddy. The same argument applies to the shape of V. Since V is constant, ℓ is a constant and is the average magnitude of a vector stretching from the centroid of V to the surface at any point. Defining this vector as (ℓ_x, ℓ_y, ℓ_z) then if ℓ_x, say, is increasing then ℓ_y and ℓ_z can reduce at any rate to conserve volume but $d\ell_x/dt$ can never become greater than the rate of diffusion of vorticity in the x direction. Thus:

$$(d\ell_x/dt)_{max} \alpha \nu^{1/2}(t+t_0)^{-1/2} \tag{2.25}$$

so that soon after the eddy is established we would expect its shape to stabilise.

The average kinetic energy dissipation rate in the eddy, ε, is constant since Ω_0^2 is constant and V is constant. From (2.21):

$$\varepsilon V = dKE/dt \ \alpha \ -\nu \ \Omega_0^2 \qquad (2.26)$$

and ε is constant.

This dissipation has to be accounted for by an increase in the kinetic energy in V so that the total kinetic energy remains invariant. This can only be achieved as a result of the vorticity re-arranging itself to amplify certain components by vortex stretching so that net circulations are increased around certain closed loops within the eddy. The vorticity distribution must dynamically order itself such that the average kinetic energy due to the self induced motions increases thus:

$$(dKE/dt)_{induced} = const.\nu \ \Omega_0^2 \qquad (2.27)$$

and a representative averaged kinetic energy density for the induced velocities, k, varies as:

$$dk/dt = const.\nu \ \Omega_0^2/V \qquad (2.28)$$

which is a constant since $\Omega_0{}^2$ and V are constant. Thus:

$$k(t) = const.\nu \ \Omega_0^2(t+t_0)/V \qquad (2.29)$$

where t_0 again reflects the initial conditions. Since at t=0 there has been no dissipation and k(t) reflects the additional induced energy required to compensate for subsequent dissipation, equation (2.4) gives:

$$k(t) = const.\nu \ \omega_1^2 t \qquad (2.30)$$

and if an averaged induced velocity in the eddy is defined as u(t) so that:

$$u(t)^2 = k(t) \qquad (2.31)$$

then:

$$u(t) \ \alpha \ \omega_1 (\nu t)^{1/2} \tag{2.32}$$

At some time the induced kinetic energy must equal the total original kinetic energy of the eddy. It certainly cannot exceed it since there is then no kinetic energy to be dissipated. Calling the invariant total kinetic energy KE_0 then at some time, t_{max}:

$$KE_0 = \text{const.} \nu \ \Omega_0^2 t_{max} \tag{2.33}$$

and:

$$t_{max} \ \alpha \ KE_0 / \nu \Omega_0^2 \tag{2.34}$$

giving, from equation (2.30):

$$k(t_{max}) \ \alpha \ \nu \ \omega_1^2 t_{max} \ \alpha \ KE_0 / V \tag{2.35}$$

The fact that there must be a maximum time for which the motion can proceed can also be demonstrated as follows; the induced velocities can only increase if the vorticity in one direction is being amplified and vortex lines do not induce velocities in the direction of the vorticity vector (Batchelor, 1967). When all the original vorticity has aligned itself into one component, say ω_x, there is maximum circulation around the x axis and none around the y or z. It is not possible then to induce stretching in the x direction. With no stretching the vorticity will diffuse away from the x axis and kinetic energy will be lost. This cannot occur in this system. At some point before this maximum level of organisation can take place the eddying motion must change in character. Since it cannot suddenly get larger, it must break-down in such a way as to produce smaller eddies which are able to sustain themselves. In this break-down the total kinetic energy and amount of vorticity in the system should be preserved.

In time t_{max} an average particle within the eddy will be transported by a distance ℓ such that, using (2.32):

$$\mathcal{L} = \int_0^{t_{max}} u(t)\,dt \;\alpha\; \omega_1 \nu^{1/2} t_{max}^{3/2} \tag{2.36}$$

and since the particle must remain within V, $\mathcal{L}$ must be proportional to ℓ. Thus we can write equation (2.36) in terms of ℓ:

$$t_{max} \;\alpha\; \nu^{-1/3}\; \omega_1^{-2/3}\; \ell^{2/3} \tag{2.37}$$

and:

$$k(t_{max}) \;\alpha\; \nu\omega_1^2 t_{max} \tag{2.38}$$

At t_{max}, $k(t_{max})$ is equal to the invariant average kinetic energy density of the eddy. Calling this k_ℓ and calling t_{max} the mean eddy lifetime, t_ℓ:

$$k_\ell / t_\ell \;\alpha\; \nu\omega_1^2 \tag{2.40}$$

and from (2.26) we can identify this value as ε, the constant energy dissipation rate within the eddy. There follows:

$$k_\ell = \varepsilon^{2/3}\; \ell^{2/3} \tag{2.41}$$

$$t_\ell = \varepsilon^{-1/3}\; \ell^{2/3} \tag{2.42}$$

$$\varepsilon \;\alpha\; \nu\omega_1^2 \tag{2.43}$$

These formulae often appear in turbulence models. Tennekes and Lumley (1972) give for the lifetime, τ, of the dissipation eddies:

$$\tau = \varepsilon^{-1/3}\lambda^{2/3} \tag{2.45}$$

For all eddies in the inertial subrange Woods (1975) gives:

$$\ell = (\varepsilon t_\ell^{\,3})^{1/2} \tag{2.46}$$

both of which are the same formulation as (2.42). Woods (1975a)

gives for eddies at the beginning of the buoyancy range with $\tau^{-1}=N$, N being the buoyancy frequency:

$$\ell_N = (\varepsilon/N^3)^{1/2} \tag{2.47}$$

which again has the same form as (2.42).

The turbulence theory (k/ε) model described in the introduction uses, rewriting equation (1.8):

$$k = (\varepsilon\ell)^{2/3} \tag{2.48}$$

which is the same as (2.41). If the Prantle-Kolmogorov and Jones and Launder expressions for eddy viscocity, (1.10) and (1.11), are equated then:

$$k^{1/2}\ell = k^2/\varepsilon \tag{2.49}$$

which is the same as (2.41).

Tennekes and Lumley (1972) give, for high Reynolds number flows:

$$\varepsilon \approx \nu\ \omega_i\omega_i \tag{2.50}$$

which has the same form as (2.43). In the absence of knowledge of ω_1 we can use (2.31) to write:

$$u_\ell^2 = k_\ell \tag{2.51}$$

and (2.41) to give:

$$\varepsilon = u_\ell^3/\ell \tag{2.52}$$

Tennekes and Lumley (1972) give this expression as an approximation for ε when a length scale is known.

The value of ε determines the time for which kinetic energy can exist at a particular scale. The value depends on the

kinematic viscosity and the square of the vorticity per unit volume in the eddy. One would expect, therefore, that ε will be the same for similar fluids and for eddies with the same value of ω_1^2. If an eddy breaks down into smaller ones then they must occupy the same volume of fluid as the large eddy since V can only grow (slowly) by the diffusion of vorticity and the breakdown is assumed to occur instantaneously. Therefore there can be no loss of total kinetic energy due to the breakdown itself, nor can there be a change in Ω_0^2. Since V is constant and Ω_0^2 is constant, ω_1^2 remains constant. Thus ε is the same just after the breakdown has taken place. This must be true for each subsequent breakdown and ε is independent of scale. The implication is that eddies of all scales have the same fundamental energy and time characteristics (given by (2.41) and (2.42)) as the large eddy producing them.

This assertion is normally made in the literature. In deriving the dimensional characteristics of eddies breaking down in the inertial subrange, for example, (Tennekes and Lumley, 1972), ε is taken as independent of wave number, or eddy size. The same authors show that large eddies contain smaller ones. On average, therefore, the amount of vorticity per unit volume within the smaller eddies must be the same as that of the larger ones containing them, producing the same result.

It is now necessary to consider how the various possible scales are related. It has been shown in the introduction that for meandering to be observable there cannot be a smooth distribution of eddy sizes and since ε remains constant there must be some common relationship between possible sizes at each stage of the breakdown. Taking the scales, ℓ, as discrete, and ℓ_i as a typical scale:

$$\ell_{i-1} = f(\ell_i) \tag{2.53}$$

$$\ell_{i-2} = f(\ell_{i-1}) \tag{2.54}$$

where $f(\ell)$ is the same function each time since the mechanism causing the breakdown has the same characteristics at each stage.

Although each individual eddy will be physically different, when the average characteristics of a breakdown is considered all the available smaller sizes must be allowed to appear. The smallest eddy which can be created will be taken at the Kolmogorov dissipation scale λ (Tennekes and Lumley, 1972). Here the smallest eddies are irreversibly converting energy, and vorticity, into heat.

When the next size down breaks down, some time later, the smaller eddy sizes should have the same distribution as for the first breakdown since ε is constant and $f(\ell)$ is the same function at each stage. Now to conserve kinetic energy at the first breakdown (V is constant, ε is constant and therefore Ω_0^2 is already being preserved):

$$k_L \Rightarrow \sum_{\lambda}^{L-1} k_\ell \tag{2.55}$$

where L is the size of the largest eddy and the summation is taken over all the smaller sizes down to λ. When the next largest size breaks down:

$$k_{L-1} \Rightarrow \sum_{\lambda}^{L-2} k_\ell \tag{2.56}$$

where k_{L-1} is the kinetic energy density in the largest eddy size created by the first breakdown. For a consistent model this must be true all the way down the cascade to λ. Reverting to the largest eddy and the first breakdown, substituting (2.53) and (2.41) into (2.55):

$$\sum_{\lambda}^{f(L)} \varepsilon^{2/3}\ell^{2/3} = \varepsilon^{2/3}L^{2/3} \tag{2.57}$$

and since ε is constant:

$$\sum_{\lambda}^{f(L)} \ell^{2/3} = L^{2/3} \tag{2.58}$$

For the subsequent breakdown:

$$\sum_{\lambda}^{f(f(L))} \ell^{2/3} = (f(L))^{2/3} \tag{2.59}$$

and subtracting the second series from the first retains only the top term so that:

$$f(L)^{2/3} = L^{2/3} - (f(L))^{2/3} \tag{2.60}$$

and so on for every step. Thus from equation (2.60):

$$2f(\ell_i)^{2/3} = (\ell_i)^{2/3} \tag{2.61}$$

for every step. The only way for this to be possible is for:

$$\ell_{i+1} = 2^{3/2} \ell_i \tag{2.62}$$

This states that the discrete scales are logarithmically distributed as first suggested by Kolmogorov (1941) from dimensional reasoning. He did not, however, consider the cascade as discrete. The proposition that the eddies are related by a constant C such that $\ell_{i+1} = C \ell_i$ and:

$$C = 8^{1/2} \cong 2.83 \tag{2.63}$$

is original to this thesis. This scaling factor is within the limits that Mandelbrot (1974) suggested as appropriate for the turbulent cascade (equation (1.31)). Taking $C = 8^{1/2}$ gives:

$$k_{i+1} = 2 k_i \tag{2.64}$$

and:

$$t_{i+1} = 2 t_i \tag{2.65}$$

A temporal view of the energy cascade is given in Figure 4. This represents the eddy sizes on the vertical axis which will on

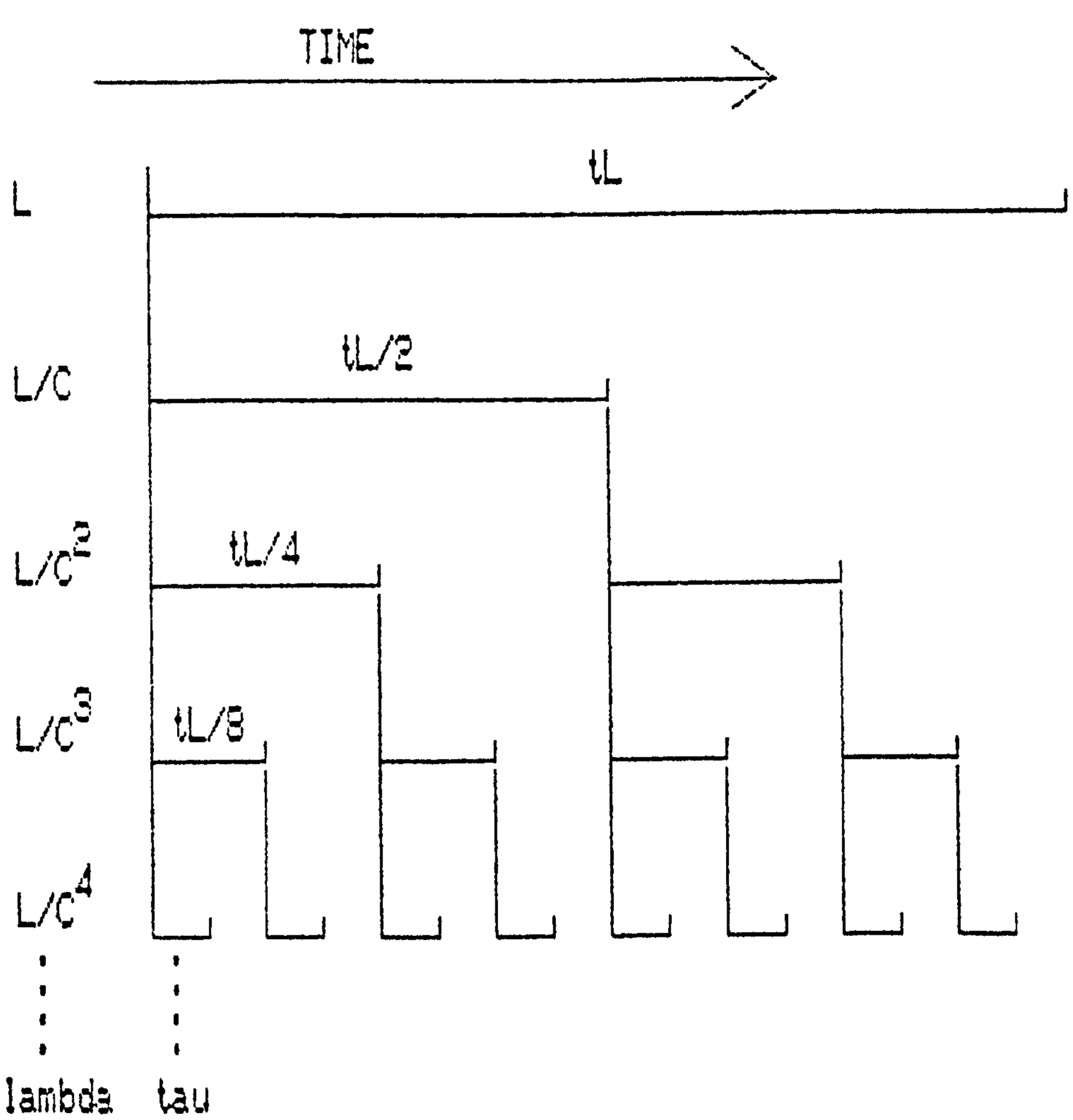

Figure 4. Temporal view of the dissipation cascade.

average be present at a point, time being the horizontal axis. It shows that each size exists in total for precisely half the time that the largest eddy exists. If we define the (one dimensional) probability that a large eddy exists as n_L, then the probability that a smaller eddy will be found at any particular location and time is $n_L/2$. All the energy in an eddy size L will dissipate into heat in time t_L, preserving the physical nature of ε as both an energy dissipation rate and as a factor which determines how long energy can remain in an eddy at a particular scale.

Since it is possible for the small eddies from a previous large eddy breakdown to be contained in a newly forming large eddy, it is possible for turbulence to become fully developed. This is illustrated in Figure 5 for n_L=0.5 and n_L=1. The large eddy production process will be discussed in the next chapter.

If n_L is equal to 1 then Figure 5 shows that the average turbulent kinetic energy present in the flow, q, is given by:

$$q = (3/2)k_L \tag{2.66}$$

since the kinetic energy from a breakdown at L is dissipated at a constant rate over t_L.

The cascade formulation can now be applied to a simple geometry. Define the largest size present at any instant as L′ and the associated time as t with t=0 at the first breakdown. It may be seen from Figure 4 that:

$$t= t_L - t_{L'} \tag{2.67}$$

where $t_{L'}$ is the lifetime at L′. If (2.42) is substituted into (2.67) there results:

$$L' = (L^{2/3} - \varepsilon^{1/3}t)^{3/2} \tag{2.68}$$

If the decaying eddies are being transported with a mean velocity U and their properties measured at x such that:

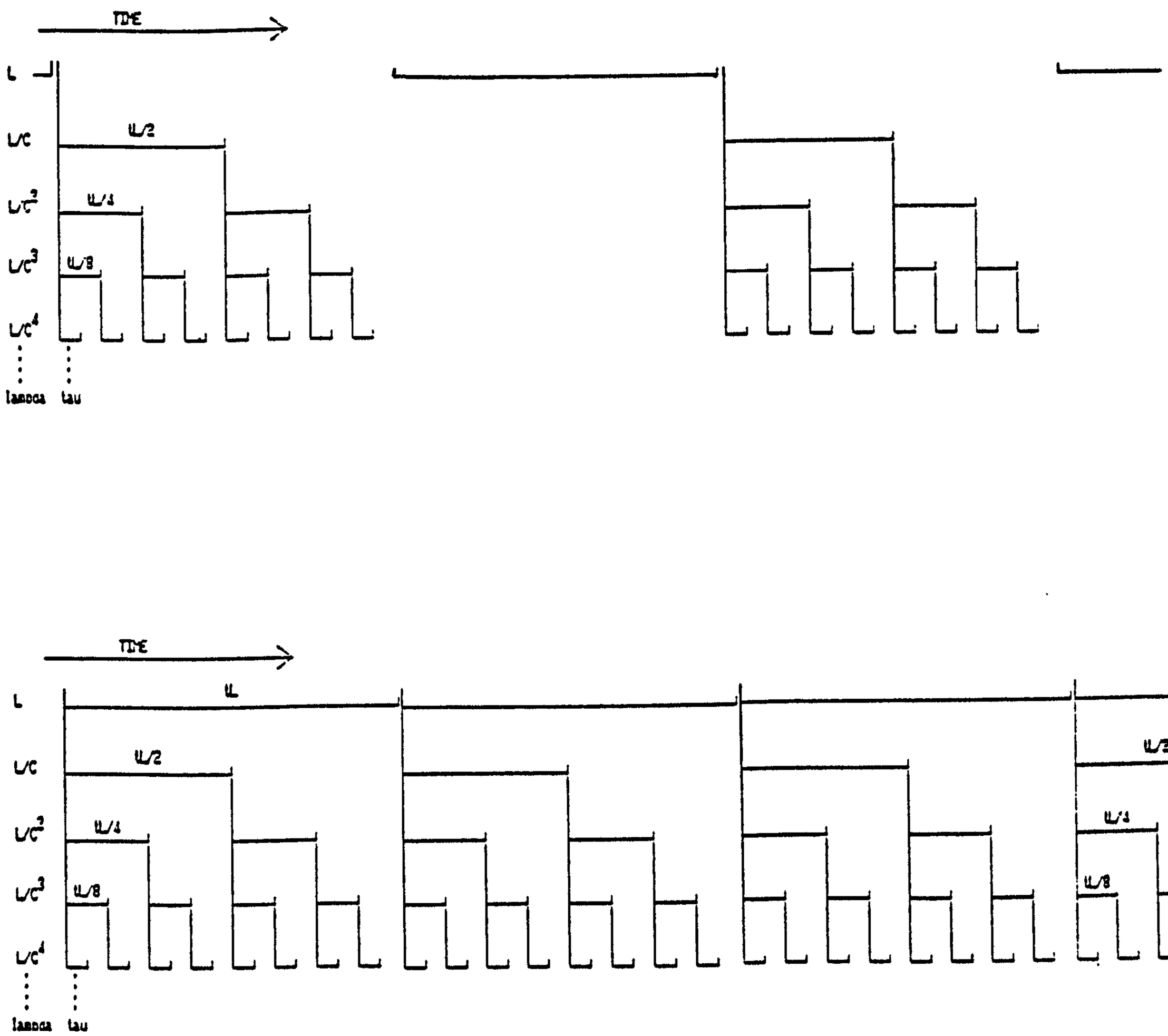

Figure 5. Temporal view of successive eddy cascades: (top): $n_L = 0.5$. (bottom): $n_L = 1$.

$$t = x/U \tag{2.69}$$

then:

$$L' = (L^{2/3} - \varepsilon^{1/3} x/U)^{3/2} \tag{2.70}$$

These conditions approximate to wind tunnel turbulence for which Tennekes and Lumley (1972) derive from dimensional reasoning (writing L′ as their "integral length scale"):

$$L' = \text{const.}(x/U)^{1/2} \ (L' u_{L'})^{1/2} \tag{2.71}$$

so that, using (2.52):

$$L' = \text{const.}(x/U)^{1/2} \ L'^{1/2} \ \varepsilon^{1/6} \ L'^{1/6} \tag{2.72}$$

giving:

$$L' = \text{const.} \varepsilon^{1/2} \ (x/U)^{3/2} \tag{2.73}$$

which has the same form as (2.70). Since the integral scale must be related to the largest eddies present, the model formulation agrees well with Tennekes and Lumley's theory for the decay of (isotropic) wind tunnel turbulence for which they quote experimental support.

It is also possible to construct a model of how such a cascade might disperse a contaminant. To do this we consider each particle in an eddy to be moved randomly by a simple random walk step length $u_\ell t_\ell$ for each period t_ℓ equal to the lifetime of the eddy. The step length will have to be modified dependant on the geometry under consideration. For example at the surface, when the vertical velocity component is supressed (Brumley and Jirka, 1987):

$$u_s^2/2 + v_s^2/2 = u_\ell^2 \tag{2.74}$$

so that if the surface turbulent velocities are isotropic:

$$u_s = u_\ell \tag{2.75}$$

For three dimensional isotropic mixing:

$$3u^2/2 = u_\ell^2 \tag{2.76}$$

and:

$$u = (2/3)^{1/2}\, u_\ell \tag{2.77}$$

The dispersion of a concentrated patch of contaminant from a homogeneous and stationary field of such eddies is given by (1.24). Putting $u = u_\ell$, so that surface dispersion is being modelled (equation (2.74)):

$$\sigma^2 = u_\ell^2 t_\ell t \tag{2.78}$$

If the eddy size is intermittent, so that the step occurs with a probability n_ℓ then:

$$\sigma^2 = n_\ell u_\ell^2 t_\ell t \tag{2.79}$$

This is equivalent to diffusion with a constant diffusion coefficient, D_ℓ, given by:

$$D_\ell = n_\ell u_\ell^2 t_\ell / 2 \tag{2.80}$$

The dispersion from a superposition of such eddy fields is given by adding the diffusion coefficients (Csanady 1972), thus:

$$\sigma^2 = (\sum n_\ell u_\ell^2 t_\ell)\, t \tag{2.81}$$

Summing the geometric series from λ to L, using $\ell_{i+1} = C\, \ell_i$, and using $n_L/2$ for eddies smaller than L, then, keeping ε constant, the summation is (Dwight, 1961):

$$\sigma^2 = n_L u_L^2 t_L t + n_L t_L u_L^2 t/6$$

$$= (7/6) n_L u_L^2 t_L t \qquad (2.82)$$

when L >> λ. This represents absolute diffusion when the cascade is as described.

In the explosive phase of cloud growth (representing the early stages of relative diffusion) then following Batchelor's argument given in the introduction (equation (1.29)):

$$ds^2/dt = 2(n_L/2) \sum_{\lambda}^{s} u_\ell^2 t_\ell \qquad (2.83)$$

since eddies of dimension ℓ > s will move the patch as a whole rather than causing individual particles to separate. Summing as before:

$$ds^2/dt = (1/3) n_L u_s^2 t_s \qquad (2.84)$$

Substituting (2.51), (2.41) and (2.42) into (2.84) gives:

$$ds^2/dt = (n_L/3) \varepsilon^{1/3} s^{4/3} \qquad (2.85)$$

Integrating (2.85) we achieve:

$$s = (n_L/9)^{3/2} \varepsilon^{1/2} (t - t_0)^{3/2} \qquad (2.86)$$

where t_0 reflects the finite size of the patch at t=0. For a point source release, the cascade model predicts relative diffusion at the surface by:

$$s = 0.037\ n_L^{3/2} \varepsilon^{1/2} t^{3/2} \qquad (2.87)$$

The same argument for the isotropic three dimensional case where u = $(2/3)^{1/2} u_\ell$ gives:

$$s = (2n_L/9)^{3/2}\ \varepsilon^{1/2} t^{3/2} \qquad (2.88)$$

Recalling (1.30), Batchelor's (1952) result for the 3D isotropic case given in the introduction:

$$s = (2a_1a_2/3)^{3/2}\varepsilon^{1/2}t^{3/2} \qquad (1.30)$$

we see that the model gives $n_L/3$ for the product of the non-dimensional constants a_1 and a_2. Knowledge of this value is necessary to relate ε to measured relative dispersion. Using the model results we would expect absolute and relative diffusion to be the same when $s \approx \sigma$, so that from (2.82) and (2.87):

$$0.037n_L^{3/2}\ \varepsilon^{1/2}t^{3/2} \approx 1.08n_L^{1/2}\varepsilon^{1/6}\ L^{2/3}\ t^{1/2} \qquad (2.89)$$

which gives:

$$0.034n_L\varepsilon^{1/3}\ t = L^{2/3} \qquad (2.90)$$

If the maximum time for which meandering will be observable is defined as T_2, then substituting (2.42) into (2.90) gives:

$$T_2 = 29.4\ t_L/n_L \qquad (2.91)$$

With L = 45 m, ε = 0.3 cm^2/s^3 and n_L = 1 meandering should occur for a period of about 12000 s from the release. In a mean flow of 1 m/s then the meandering of a plume should extend over about 12000 m from the release point. The figures here have been chosen to reflect oil and dye release experiments reported in Chapter 8 where meandering over such distances is observed.

Csanady (1972) relates absolute dispersion (characterised by its standard deviation σ), relative dispersion (characterised by s) and the standard deviation of the meandering, m, by:

$$\sigma^2 = m^2 + s^2 \qquad (2.92)$$

This equation gives for the explosive phase, from (2.82) and (2.87):

$$m^2 = 1.17 n_L \varepsilon^{1/3} L^{4/3} t - 0.0012 n_L^3 \varepsilon t^3 \qquad (2.93)$$

There should be a period where the equation simplifies. This is when the relative diffusion is not "explosive" and the spreading is being caused by all sizes up to and including L/C, the meandering being caused by the large eddies L only. Then the model gives:

$$m^2 = n_L u_L^2 t_L t \qquad (2.94)$$

or, substituting for u_L^2 and t_L as before:

$$m^2 = n_L \varepsilon^{1/3} L^{4/3} t \qquad (2.95)$$

Equating (2.93) and (2.95) we would expect (2.95) to be dominant after a time, T_1, given by:

$$T_1 = 11.9 \, \varepsilon^{-1/3} L^{2/3} / n_L \qquad (2.96)$$

which can be rewritten in terms of the large eddy lifetime, t_L, giving:

$$T_1 = 11.9 t_L / n_L \qquad (2.97)$$

Csanady (1972), without a model for the non-dimensional constants a_1 and a_2 in (1.30), predicted that the explosive phase would end at $T_1 \approx t_L$. Were this the case then meandering on the scale reported in Chapter 8 would not be observed. By substituting the values used above for L, ε and n_L into (2.96), then the meandering should follow (2.94) from about 5000 m from the release point. During this second phase s^2 is found by substituting (2.82) and (2.95) into (2.92) giving:

$$s^2 = (1/6) n_L \varepsilon^{1/3} L^{4/3} t \qquad (2.98)$$

or:

$$s = 0.4 \, n_L^{1/2} \varepsilon^{1/6} L^{2/3} t^{1/2} \qquad (2.99)$$

The model has predicted two phases in the development of the relative diffusion. In the first phase the growth is explosive, following a $t^{3/2}$ relationship as larger eddy sizes contribute to the growth of the patch. In the second phase the growth slows to follow a $t^{1/2}$ relationship because of the wide gap between the eddy sizes at L/C and L. Two distinct phases of growth are reported in Chapter 8 and provide evidence that this formulation is correct. From (2.91) and (2.97):

$$T_2 \approx 2.5\ T_1 \tag{2.100}$$

and from (2.82):

$$\sigma = 1.08\ n_L^{1/2} \varepsilon^{1/6} L^{2/3} t^{1/2} \tag{2.101}$$

so that during the second phase, using (2.99):

$$s \approx 0.4\ \sigma \tag{2.102}$$

so that the development of the absolute and relative dispersion can be approximated by:

$$\begin{aligned} T_2 &\approx 2.5\ T_1 \\ s &\approx 0.03\ \sigma^3/L^2 && 0 < t < T_1 \\ s &\approx 0.4\ \sigma && T_1 < t < T_2 \\ s &\approx \sigma && t > T_2 \end{aligned} \tag{2.103}$$

CHAPTER 3. EDDIES IN THE BOTTOM BOUNDARY LAYER

Aim.

The structure of the eddies in a turbulent boundary layer must reflect the turbulent production process as well as the dissipation cascade. The mean eulerian velocity profile reflects the passage of the turbulent eddies past the sensing point. If the mean velocity profile can be associated with the turbulence then it should be possible to relate the amount of turbulence present, and its dispersive effect, with some easily measurable quantity such as the surface velocity U_0. That is the aim of this chapter.

When the boundary conditions are changing slowly (for example if the channel width and depth are constant) the average velocity of the eulerian profile, U_m, will equal the bulk flow, U_b. The bulk flow is a measure of the average streamwise Lagrangian velocity since the turbulent mixing will cause fluid packets to sample all positions within the boundary layer if their motion is followed for long enough. The distinction is made since the variation in the "mean" velocity profile during the eddy production process will be discussed.

In the following derivations the logarithms (written as log) are to the base e. The size of the eddies in the dissipation cascade is characterised as a geometric series whose base is $C = \sqrt{8}$. Since $\log_c x = 1.034 \log_e x$, the natural logarithm is a sufficiently good approximation to the cascade for use in the derivations below.

General considerations.

If an eddy V is placed into a uniform bulk flow U_b, then Lamb (1932) shows that since the pressure forces exerted on the surface of V are equal to the forces exerted in the fluid at all points just outside V, the eddy will move with the fluid at U_b. Small eddies existing within bigger ones will be transported by the larger eddy velocities. Since none of the fluid particles within a large eddy leave its volume V during its lifetime, a

small eddy finding itself within a larger one will remain within it.

If an eddy V is placed into a shearing bulk flow then the same argument implies that the volume V must distort with the mean shear. Batchelor (1967) showed that any velocity field may be represented as the superposition of a symmetrical expansion, two simple shearing motions and a rigid rotation. Further, he showed that each simple shearing motion may be regarded as a superposition of a pure straining motion (with zero rate of expansion) and a rigid rotation. Since V is constant throughout eddy lifetime (Chapter 2), it is reasonable to characterise its distortion as the resultant of two pure straining motions, which are equivalent to a single pure straining motion. It will also rotate as a rigid body.

As far as the characteristics of V are concerned (which are encompassed in the value of ε) rigid body rotation will have no effect since all the vorticity components within V will rotate in the same manner. To consider the effect of straining by shear it is convenient to give some two dimensional examples. If the only velocity is in the x direction and is sheared such that U(y) = f(y) then putting:

$$DU/Dy = f'(y) = \text{constant} \qquad (3.1)$$

characterises a local mean shear on an eddy if ℓ (the characteristic eddy dimension) is of order Δy. The total derivative is used since we are following the translational and rotational motion of V. Batchelor gives the maximum rate of extension of a unit element in V as:

$$D\ell/Dt = A\,\ell \qquad (3.2)$$

where:

$$A = (DU/Dy) / (2^{1/2}) \qquad (3.3)$$

If the eddy lifetime is characterised by (2.42):

$$t_\ell = \varepsilon^{-1/3}\ \ell^{2/3} \qquad (2.42)$$

and a representative value of ε is in the higher regions of those found in the sea, 0.3 cm^2/s^3, then for:

$$\ell = 1\ m$$

$$DU/Dy = 0.03\ s^{-1}$$

which represents a small eddy in the bulk of a geophysical stream 30 m deep and whose free surface velocity is about 1 m/s; the maximum extension of ℓ due to the shear is 2% in t_ℓ. For:

$$\ell = 10\ cm$$

$$DU/Dy = 10\ s^{-1}$$

which is an extreme case of a small eddy in a high shear layer of the same dimensions as the eddy (a situation which might occur at a solid boundary), then in t_ℓ the maximum extension of ℓ is about 20%. The value of ε for large eddies in a weak shear should therefore remain substantially unaffected by the shear. The value may increase for small eddies in a high shear layer near a boundary.

Summary of the production process.

The details of the process by which the large eddies are produced are unclear (Landahl and Mollo-Christensen (1988) give a recent review) but in a flow moving over a solid boundary it is the no-slip condition at the surface which generates vorticity and this is the source of vorticity for the turbulent eddies since vorticity cannot be created within the fluid (Batchelor, 1967).

In the laboratory the vortical surface layer is observed to remain thin (Tennekes and Lumley, 1972) and a large part of the streamwise velocity shear can occur in this layer. The transport

of vorticity and momentum from this layer into the bulk of the flow results in the turbulent eddies and the mean velocity profile.

Flow visualisation studies reported by Utami and Ueno (1987) and numerical simulations reported by Rogers and Moin (1987) show that the disruption to the vortical layer is characterised by the evolution of hairpin vortices which themselves interact in a complex manner. Such hairpin structures induce a fluid velocity within themselves which is counter to the streamwise velocity and away from the wall. This induced flow exhibits the characteristic correlation of the intermittent bursting event found when measuring Reynolds stress in the laboratory and at sea (Heathershaw, 1979).

Kim, Kline, and Reynolds (1971) showed, in the laboratory, that much of the turbulence production was associated with the bursting events. Heathershaw (1979) has correlated the bursting events with large eddies in the sea and, since such events can transport vorticity away from the boundary, the burst of negative Reynolds stress must be an event characterising the production of the large eddies in the flow or their passage, once formed, past the sensing point.

Kim, Kline and Reynolds (1971) also used high speed photographs of hydrogen bubbles to show that when an eddy from the turbulent flow outside the surface layer impinges on it, the eddy penetrates to the wall, disrupting the layer and causing a burst. The ejected low momentum fluid retards the fluid in its new surroundings, giving rise to a further eddy. To that extent when turbulence exists, it is self propagating.

The implication is that the eddies in the flow are both responsible for the continued generation of eddies and for the subsequent transport of momentum and vorticity from the wall to the outer flow regions. Their disruptive effect on the wall layer is to scour vorticity away from the layer, keeping it thin.

Tennekes and Lumley (1972) showed that the amount of turbulence in a shear flow is determined by a strongly non-stationary dynamic process. In a geophysical flow the driving forces (primarily tidal) of the flow as a whole are continuously changing and the turbulence varies so that the resulting mean profile changes to match the boundary conditions. Here it is intended to highlight only those features of a steady, two dimensional, turbulent shear flow which the discrete eddy model is able to describe.

Production and large eddies.

If the boundary layer has thickness L, so that the largest eddies have characteristic size L, and if they are produced in a characteristic time, t_p, then the average velocity at which vorticity moves vertically away from the boundary is equal to L/t_p. This cannot be larger than the largest measured vertical velocities measured in the flow. Thus:

$$L/t_p < u_L \tag{3.4}$$

and:

$$t_p > L/u_L \tag{3.5}$$

and since the average large eddy lifetime, t_L, is given by:

$$t_L = L/u_L \tag{3.6}$$

then:

$$t_p > t_L \tag{3.7}$$

The intermittency is related to these times since it is the probability that an eddy exists. Thus:

$$n_L = t_L/t_p \tag{3.8}$$

and (3.7) implies that:

$$n_L \leq 1 \tag{3.9}$$

Soulsby (1983) reported that the standard deviation of the vertical velocity fluctuations measured in boundary shear layers is characteristically 0.46-0.5 times the horizontal, and 0.66 times the cross-stream. Writing,for the mean vertical velocity, w:

$$(w/0.5)^2/2 + (w/0.66)^2/2 + w^2/2 = u_\ell^2 \tag{3.10}$$

then repeating (3.5) - (3.8) gives:

$$n_L \leq 0.5 \tag{3.11}$$

implying that the turbulence in a shear flow may always be found to be significantly intermittent.

The kinetic energy density of the largest eddies is k_L and this is produced in t_p. Thus the energy production rate is given by:

$$D(KE)/Dt_{prod} = n_L k_L / t_L = n_L \varepsilon \tag{3.12}$$

which is equal to the dissipation rate, as it should be if the conditions are steady. In the mean the turbulent kinetic energy is produced and dissipated at a constant rate if the conditions are steady.

Since the boundary of an eddy volume V can only move through the surrounding fluid at a (slow) diffusion velocity proportional to $(\nu t)^{-1/2}$, then to maintain its identity throughout its lifetime t_L, a large eddy L must move relative to the boundary without being substantially influenced by the vortical layer at the boundary surface even though the layer can be disturbed by its passage. The streamwise fluctuations in a large eddy L are proportional to u_L and any mean shear within the large eddy can only be as a result of these fluctuations being more likely to be in the upstream direction than the down stream, or to the strain

induced in the eddy throughout its lifetime which we have seen to be small. Since u_L is normally much less than U_b, the eddy volume V is moving with the flow relative to the boundary. Since small eddies within larger ones move with the larger ones, then it follows that in the mean and outside the surface layer, all the eddies are moving at U_b.

Fluctuations in the bulk flow.

The turbulence kinetic energy equation quoted in the introduction, shows that the turbulent kinetic energy is produced at the expense of the bulk flow. The mean flow, U_m is a constant in steady conditions but since the production of the large eddies is characterised by a burst, then, following the motion at U_m, the bulk velocity U_b should show a negative fluctuation where eddies are being produced and a subsequent positive fluctuation so that U_m has a steady value. For a single large eddy whose lifetime is t_L then we should expect this variation to have a fundamental period equal to t_L. If the fluctuation can be approximated by a sine wave then the maximum amplitude of the disturbance, ΔU_{max}, should be sufficient to supply all the kinetic energy of the large eddy size since the turbulent kinetic energy equation (equation (1.5))shows that the energy is initially supplied to the streamwise component. Thus, using (2.51) for u_L:

$$\Delta U_{max}^2/2 = k_L = u_L^2 \qquad (3.13)$$

and:

$$\Delta U_{max} = (2^{1/2})u_L \qquad (3.14)$$

so that the r.m.s value of the fluctuation is equal to u_L. If the turbulence is intermittent then the fluctuation should have r.m.s. value $n_L u_L$.

If the boundary layer has not occupied the full flow depth then we can define the free-stream velocity as U_0 so that the bulk velocity, U_b, within the boundary layer caused by the production process should be:

$$U_b = U_0 - n_L u_L \tag{3.15}$$

If the turbulence is significantly developed, and especially if the boundary layer has grown to occupy the full depth of the flow, then the requirements of continuity dictate that a streamwise succession of eddies L should show similar fluctuations in U_b over a distance equal to $U_m t_L$ indicating that approximately $U_m t_L/L$ successive eddies will be at significantly correlated stages of their history. It will be shown in the next section that a significant spectral peak is found at a frequency equal to $1/t_L$ and of energy u_L^2.

Derivation of the mean velocity profile.

The mean flow does not exist as a separate entity from the turbulence and when measured by a fixed sensor is the time average of the velocities caused by the eddies passing that point superimposed on the bulk flow U_b. Since this cannot be measured until the mean profile is known, the most convenient velocity on which to base the derivation is the mean surface velocity, U_0. A discrete cascade of eddies is assumed, with the largest eddies having size L and intermittency n_L. A fixed eulerian sensor is situated at height h from the bottom boundary.

For an eddy size ℓ to disturb the vortical surface layer it must be in contact with it. It can exchange vorticity or momentum to a distance ℓ from the boundary during its lifetime since $u_\ell t_\ell$ is equal to ℓ. The transported property may become part of the eddy, altering its characteristics, or may exist separately from the eddy which has disturbed the vortical layer. Here it is considered that such an eddy assumes different characteristics when in contact with the bottom, which simplifies the formulation.

Let it be assumed that each eddy size in the dissipative cascade is equally likely to disturb fluid from the vortical layer at the boundary. Further, let it be assumed, crudely, that the disturbed low momentum fluid is instantaneously mixed throughout the eddy. The probability that a packet will be transported to a

distance greater than h from the surface, P(h), is then given by:

$$P(h) = \frac{\text{number of eddy sizes greater than h}}{\text{total number of eddy sizes}} \qquad (3.16)$$

If the smallest eddy size in the dissipation cascade is defined as λ, then we can define the largest size L as:

$$L = C^N \lambda \qquad (3.17)$$

where N is an integer. By defining N in this fashion the cascade contains N+1 distinct eddy sizes including the smallest at λ. It will be shown that the value of N is an important parameter in characterising the boundary layer. Since logC $\approx$ 1 we can write:

$$N = \log(L/\lambda) \qquad (3.18a)$$

If the sensor height, h, is chosen so that:

$$C^n \lambda = h \qquad (3.19)$$

then there are n+1 eddy sizes smaller than h and (N-(n+1)) sizes greater than h. Putting these numbers into (3.16) gives:

$$P(h) = (N-(n+1))/N \qquad (3.18b)$$

The fluid packets carrying the momentum defect originate at the boundary where they are effectively stationary compared to U_0. Thus on average we should expect the momentum exchange by the eddies to give a profile of the form:

$$U(h) = U_0 - U_0(N-(n+1))/N \qquad (3.20)$$

Since the eddies smaller than L extend to a distance L/C from the boundary, the surface velocity should extend down to h=L/C. Equation (3.20) gives, for h = L/C and n = N-1:

$$U(L/C) = U_0 - U_0(N-(N-1+1))/N = U_0 \qquad (3.21)$$

as expected. The velocity at $h=\lambda$ is given by:

$$U(\lambda) = U_0 - U_0(N-1)/N = U_0/N \qquad (3.22)$$

This mean profile is stepped since (3.20) has only been calculated at discrete values of h and is illustrated in Figure 6. Near the bed when the discrete values of h are closely spaced the profile will appear logarithmic. From (3.19):

$$n = \log(h/\lambda) \qquad (3.23)$$

then using (3.18a):

$$(N-n+1) = \log(L/h) + 1 \qquad (3.24)$$

so that (3.20) can be rewritten as:

$$U(h) = U_0 - (U_0/N)\log(L/h) + U_0/N \qquad (3.25)$$

which is the profile in the velocity defect form (Tennekes and Lumley, 1972). Using equation (3.22) this may be written as:

$$U(h) = (U_0/N)\log(h/\lambda) + U_0/N \qquad (3.26)$$

which is in the familiar logarithmic form. The criterion that h should be small is as given by Tennekes and Lumley (1972) who predict a logarithmic profile on dimensional grounds if $L \gg h$ and $hu_L \gg \nu$, the latter condition being always valid in the sea where ν is very small. A mean velocity profile of logarithmic form is usually found in the sea near the bed (Soulsby, 1983) and in the laboratory (Anwar, 1981).

The mean value of the velocity profile, U_m, is found by integrating (3.25) and is given by:

$$U_m = U_0 - U_0/N \qquad (3.27)$$

which is found at a height L/C or 0.353L. Prandle (1982) has found

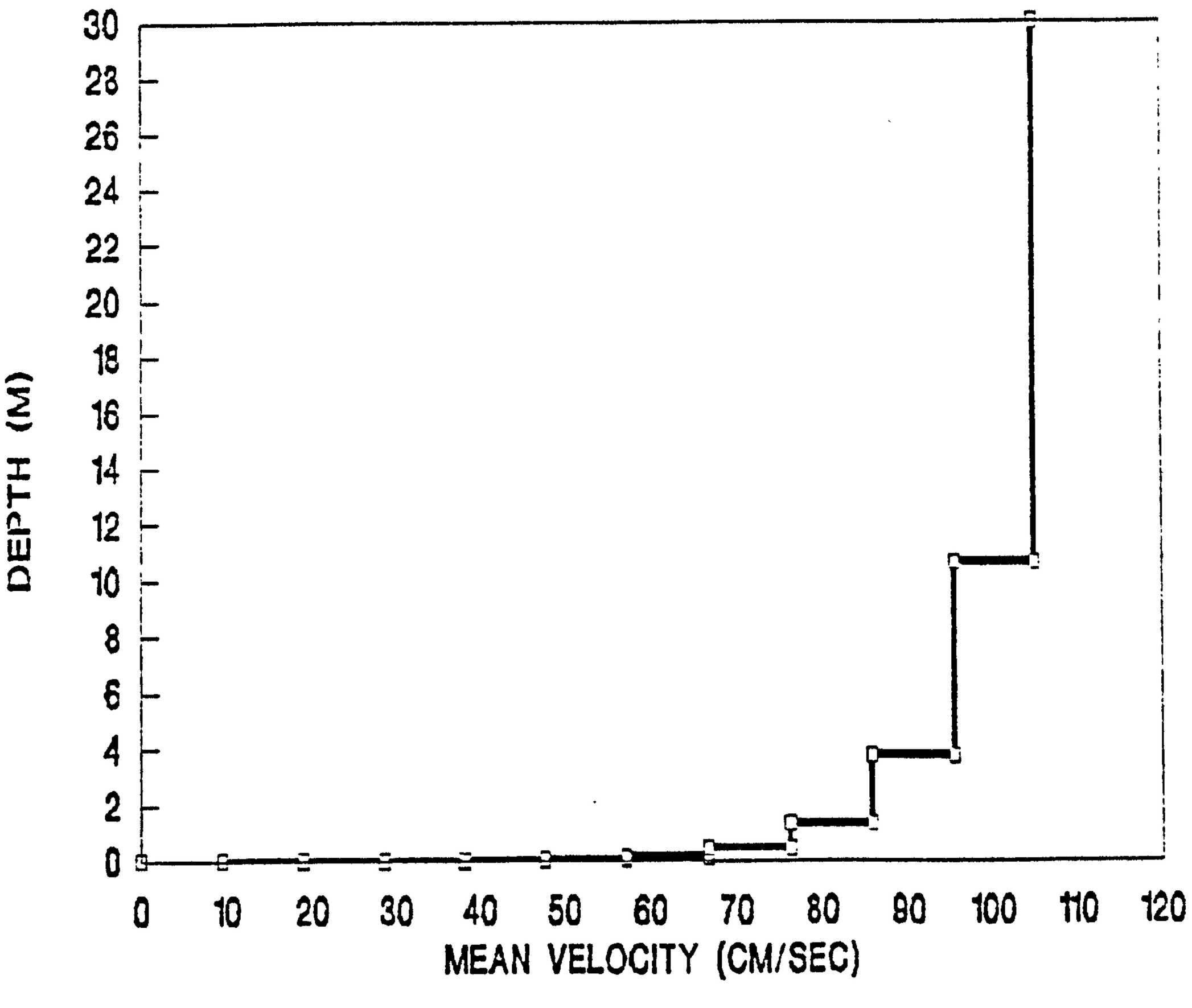

Figure 6. A stepped mean velocity profile derived from instantaneous eddy mixing characteristics and the discrete dissipation cascade (3.20).

from experiments in the sea that the mean velocity is measured at approximately 0.4 of the depth when the boundary layer has reached the surface. Since we are associating the mean profile with the production process we can equate (3.15) and (3.27) to write:

$$U_0/N = n_L u_L \tag{3.28}$$

and the mean profile (3.26) as:

$$U(h) = n_L u_L \log h/\lambda + n_L u_L \tag{3.29}$$

Two formulae which are immediately derived from the above are, using (2.41)and (3.28):

$$u_L = U_0/n_L N = \varepsilon^{1/3} L^{1/3}$$

so that using $u_L t_L = L$:

$$\varepsilon = U_0^3/n_L^3 N^3 L \tag{3.30}$$

$$n_L N L = U_0 t_L \tag{3.31}$$

Noting that each eddy size touching the bottom contributes an extra velocity defect over the sizes larger than it equal to $n_L u_L$, it is a straight-forward proposition to generate a smooth profile by assuming that within each size the defect is distributed linearly. Writing the extra defect in a size ℓ as:

$$\Delta u_\ell(h) = (1-h/\ell) n_L u_L \tag{3.32}$$

when $\ell > h$. This models the fact that an eddy size ℓ can only mix low momentum fluid a maximum distance ℓ from the boundary during its lifetime t_ℓ. Summing over the sizes greater than h gives the profile:

$$U(h) = n_L u_L \log h/\lambda + 1.5\, n_L u_L h/L + n_L u_L \tag{3.33}$$

This profile is shown in Figure 7 together with the stepped

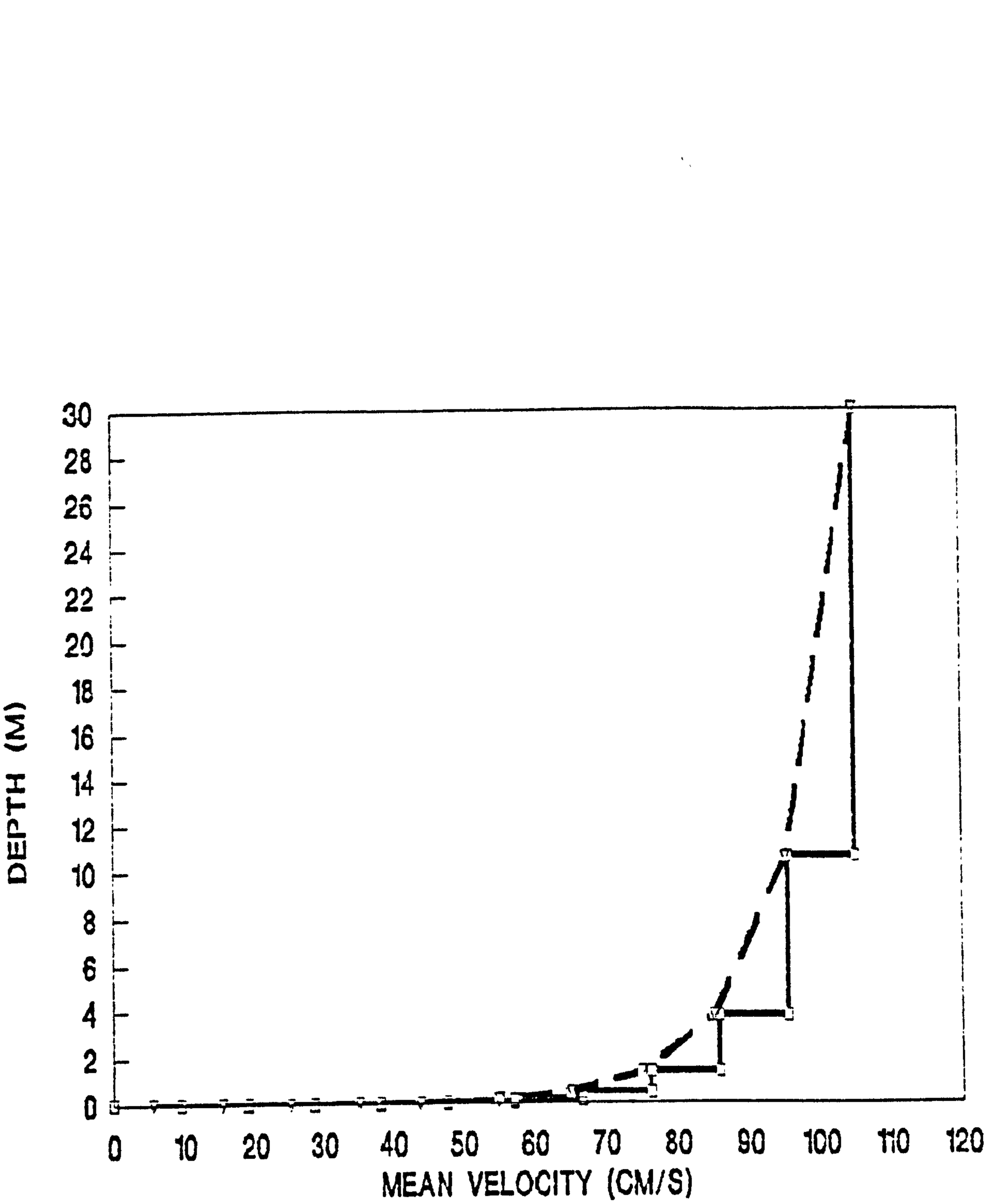

Figure 7. A comparison of the profiles given by equations (3.20) and (3.33) (N = 11).

profile (equation (3.20)). It may be seen that both profiles are similar in the bottom half of the flow. In Chapter 7 an equation similar to (3.33) will be shown to accurately model the mean profile found at sea when the parameters n_L and ε are known.

The smallest eddy size.

The smallest eddy size, λ, may be identified with the Kolmogorov dissipation scale and is given by (Tennekes and Lumley, 1972):

$$\lambda = (\nu^3/\varepsilon)^{1/4} \tag{3.34}$$

This is the only length scale which is of the same order of magnitude as the values of the roughness length, z_o, given by Heathershaw (1979) and Soulsby (1983) for unrippled beds (approximately 0.03 cm). No other derivations give results close to those found in the sea in these conditions.

Using (3.30) and (3.34) gives:

$$\lambda^4 = N^3 n_L^3 \nu^3 L/U_0^3 \tag{3.35}$$

so that using (3.17) we obtain:

$$n_L N\ C^{4N/3} = U_0 L/\nu \tag{3.36}$$

which is the Reynolds number. Taking typical values as:

$$L = 30 \text{ m}$$

$$U_0 = 1 \text{ m/s for } n_L = 1$$

$$\nu = 0.014 \text{ cm}^2/\text{s}$$

gives:

$$N = 11 \tag{3.37}$$

If the bed is rippled or strewn with substantial obstacles

then the value of z_0 is dependent on the ripple wavelength or obstacle separation. Soulsby (1983) gives proscriptions from several workers if the bed structure is known. These suggest that z_0 may be an order of magnitude larger in some conditions (0.3 - 0.6 cm), equivalent to a change of 2 in the value of N. For all the results given by Heathershaw (1979) the value of N lies between 7 and 15 and the mean value of N = 11 agrees well with $z_0 = \lambda$ for the experiments where he has published the values of ε.

A length scale which may be more applicable to rippled or very rough beds, λ', can be derived from (3.22) and (3.28):

$$U(\lambda') = U_0/N = n_L u_L \tag{3.38}$$

If the vorticity between h = 0 and h = λ is primarily cross-stream, then from the definition of ε, (2.43) gives:

$$\varepsilon = \nu u_L^2/\lambda'^2 \tag{3.39}$$

and:

$$\lambda' = (\nu t_L)^{1/2} \tag{3.40}$$

which is the diffusion distance related to large eddy lifetime. With typical values of ε , ν and L, λ' is 1-2 cm.

A useful result is that taking mean velocity measurements at two heights, h_1 and h_2 and substituting into (3.33):

$$U(h_1) = n_L u_L \ (\log \ (h_1/\lambda) + (1.5h_1/L) + 1) \tag{3.41}$$

$$U(h_2) = n_L u_L \ (\log \ (h_2/\lambda) + (1.5h_2/L) + 1) \tag{3.42}$$

so that eliminating $n_L u_L$:

$$\lambda = \frac{h_2}{\exp\left[\frac{U(h_2)\left(\log(h_1/h_2)+(1.5(h_1-h_2)/L)\right)}{U(h_1)-U(h_2)} - \frac{1.5h_2}{L} - 1\right]} \qquad (3.43)$$

an equation which allows the calculation of λ when other parameters are unknown. An increase in λ implies that if the true value of λ varies only with bottom conditions then L has decreased. This result, which does not invoke the intermittency n_L, will be useful in analysing the results given in Chapter 7 where the boundary layer development is examined over a tidal cycle.

We are now in a position to consider Yalin's result (Yalin (1977), see Introduction) that the wavelength of sand-dunes generated by turbulence is between 2π and 20 times the water depth. We would expect particles which are being transported by the large eddies occupying the whole depth to travel approximately $U_0 t_L$ if they are suspended when the eddy is formed and settle when it breaks down. Equation (3.31) with n_L equal to 1 (since no transport will occur if the eddy is not there):

$$NL = U_0 t_L \qquad (3.44)$$

shows that the wavelength should be approximated by NL. The mean (11) and spread (7 - 15) for N derived from Heathershaw's (1979) results agree well with Yalin's sand-dune wavelength distribution of $2\pi < N < 20$.

Reynolds stress.

The average level of Reynolds stress near the bed is defined in the literature as ρu^{*2}, where u* is the friction velocity. It is found to be roughly constant near the bed outside the vortical layer at the boundary (Soulsby, 1983). The Reynolds stresses are associated with the anisotropic eddies, those affected by the bottom which are creating the mean velocity profile. The

contribution to the averaged Reynolds stress from an eddy size ℓ must be proportional to the product of the averaged eddy velocity components which make up the correlation. Using $u^{*2}(\ell)$ for the stress in an eddy size we can see that it must be proportional to the product of the streamwise velocity defect $n_L u_L$ (which is the same for each eddy size) and the mean vertical transport velocity within the size which is proportional to $n_L u_\ell$. Thus:

$$u^{*2}(\ell) \ \alpha \ n_L^2 u_L \ u_\ell \tag{3.45}$$

and taking the constant of proportionality to be independent of eddy size, then summing as before over all the sizes greater than h:

$$u^{*2}(h) \ = \ \beta \ n_L^2 (u_L^2 - u_L u_h) \tag{3.46}$$

so that the stress is zero at L as we would expect. If h << L then:

$$u^{*2} = \beta n_L^2 u_L^2 \tag{3.47}$$

which is independent of h. Thus a constant stress layer will be found near the bottom of a geophysical flow. The model implies that the measured stress is proportional to the turbulent kinetic energy. Heathershaw (1979) states that over a wide range of conditions, the stress and measured turbulent kinetic energy, q, are related by:

$$u^{*2} \approx 0.2 \ q \tag{3.48}$$

so that using (2.66):

$$u^{*2} \approx 0.3 \ n_L^2 \ u_L^2 \tag{3.49}$$

Equations (3.47) and (3.49) indicate that the value of β is approximately 0.3. Soulsby (1983) reported that on average, and under widely varying conditions the quadratic friction law holds so that:

$$u^{*2} \approx 0.0025\ U_0^2 \qquad (3.50)$$

For fixed L, (3.31) and (3.34) imply that if ε is constant then n_L is proportional to U_0, so that u* is proportional to U_0 (equation (3.49)). Equation (3.48) can also be true if the turbulence is fully developed. It may be that the intermittency accounts for the wide scatter reported when measuring the Reynolds stress (Soulsby, 1983).

The mean velocity profile is normally characterised by u*/K where K is Von Karman's constant. Equating the two formulations for the log profile (equation (3.29)):

$$u^*/K \equiv n_L u_L \qquad (3.51)$$

and substituting (3.50) into (3.49) gives:

$$K \approx (0.3)^{1/2} \approx 0.5$$

Von Karman's constant is found to be approximately 0.4 when the friction velocity is fitted to logarithmic profiles measured in the sea (Soulsby, 1983). Equating (3.49) and (3.50) gives:

$$0.0025\ U_0^2 \approx 0.3\ n_L^2 u_L^2 \qquad (3.52)$$

so that (3.28) gives:

$$N \approx 11 \qquad (3.53)$$

The production term in the tubulence kinetic energy equation, (1.5), is given by $u^{*2}\partial U/\partial y$ for a two dimensional boundary layer. The mean shear $(\partial U/\partial y)_h$ between h/C and h in the mean profile (3.33) is given by:

$$(\partial U/\partial y)_h = 1.5 n_L u_L/L + \sum_h^L n_L u_L/h \approx 1.5\ n_L u_L/L + n_L u_L/(C-1)h$$

so that using (3.47) for the Reynolds stress with $\beta = 0.3$, summing over all sizes with $n_L = 1$ and equating production to dissipation gives:

$$\sum_{\lambda}^{L} 0.3\ (u_L^2 - u_L u_h)\left((u_L/((C-1)h)+(1.5u_L/L)\right)h(1-1/C) = L\varepsilon \qquad (3.54)$$

so that using (2.52) for ε:

$$0.1\ ((N+1)-2.62) = 1 \qquad (3.55)$$

and:

$$N \approx 11 \qquad (3.56)$$

Direct substitution of (3.38) into the logarithmic profile gives:

$$u^{*2} = \text{const.}\ u_L\ h\ \partial U/\partial h \qquad (3.57)$$

which is the Prantle-Kolmogorov expression for the Reynolds stress near a wall (equation (1.9)). Substituting again gives:

$$u^{*2} = \text{const.}\ h^2(\partial U/\partial h)^2 \qquad (3.58)$$

which is equivalent to the mixing length formulation (equation (1.7)).

A crude model of the bursting sequence.

We have shown that a smooth logarithmic profile (equation (3.33)) can be generated by the dissipation cascade of eddies if each size is assumed to have a linear velocity defect given by (3.32) additional to the defect induced by sizes larger than itself when the eddies are touching the bottom. Recalling:

$$\Delta u_\ell(h) = (1-h/\ell)\,n_L u_L \qquad (3.32)$$

$$U(h) = n_L u_L \log h/\lambda + 1.5\ n_L u_L h/L + n_L u_L \qquad (3.33)$$

This is equivalent to each size containing an extra mean cross-stream vorticity equal to u_L/ℓ. The production event takes place in t_L/n_L. Since the dissipative cascade only lasts for t_L we shall initially assume that the production event takes place in t_L and ignore the intermittency.

The average extra vorticity associated with an eddy size ℓ touching the bottom is u_L/ℓ, and the maximum vorticity that such an eddy can support is U_0/ℓ (since the mean profile cannot be negative). Therefore the production event may be modelled as a sequence of N profiles, each lasting t_L/N, and each reflecting a different eddy size ℓ_i which is carrying vorticity U_0/ℓ_i. Since, using (3.28):

$$t_L(u_L/\ell) = (t_L/N)(Nu_L/\ell) = (t_L/N)(U_0/\ell) \qquad (3.59)$$

the average extra vorticity in each size is retained. The profile sequence is, for N profiles $U_i(h)$ each lasting t_L/N:

$$U_i(h) = \begin{cases} =(U_0 h/\ell_i) & h < \ell_i \\ =(U_0) & h > \ell_i \end{cases}$$

$$\ell_i = C^i\lambda$$

$$i = 1 \to N \qquad (3.60)$$

The intermittency is now included by assuming that each step takes t_L/Nn_L so that the process is complete in the correct production time. Integrating over the sequence of increasing sizes over time gives the mean profile:

$$U(h) = n_L u_L \log h/\lambda + 1.5\, n_L u_L h/L + 0.5 n_L u_L \qquad (3.61)$$

which is very similar to (3.33).

The crude model of the bursting sequence simulates the time variation of the velocity profile at a fixed point. If the eddies are essentially cubic and pass the point in approximately L/U_0 then since we have derived (equation (3.31)):

$$n_L NL = U_0 t_L \tag{3.31}$$

each eddy will pass the measuring point in time:

$$t_{passage} = L/U_0 = t_L/Nn_L \tag{3.62}$$

so that each time interval in this model is equal to the individual eddy passage time. Modelling the bursting event as a sequence reflects the earlier result that a sequence of N eddies should be at co-ordinated stages of their lifetimes because of continuity. Such a group would give the correct mean velocity profile and reflect the production process into frequency spectra at a frequency of $1/t_L$. It is the contention of Chapters 5 - 7 that this is indeed the case.

The variation of intermittency with bulk velocity.

The following equations are repeated from this chapter for ease of reference:

$$U_0/N = n_L u_L \tag{3.28}$$

$$\varepsilon = U_0^3/n_L^3 N^3 L \tag{3.30}$$

$$U(h) = n_L u_L \log h/\lambda + 1.5 n_L u_L h/L + n_L u_L \tag{3.33}$$

$$\lambda = (\nu^3/\varepsilon)^{1/4} \tag{3.34}$$

$$n_L N C^{4N/3} = U_0 L/\nu \tag{3.36}$$

These equations simplify to a closed set if it is assumed that at some velocity, U_1, n_L is equal to 1 and that below this velocity n_L varies linearly with current speed as implied by (3.49) and (3.50). Writing:

$$n_L = U_0/U_1 \tag{3.63}$$

then if n_L can be determined and plotted against U_0 the value of

U_1 can be found (such a plot would verify (3.63)). Rewriting (3.36) using (3.63):

$$N\, C^{4N/3} = U_1 L/\nu \qquad (3.64)$$

which implies that if the turbulent boundary layer has grown to fill the whole depth so that L is known, then N is constant below U_1. This implies, from (3.28) and (3.30) which can be written as:

$$U_1/N = u_L \qquad (3.65)$$

$$\varepsilon = U_1^3/N^3 L \qquad (3.66)$$

that the dissipation rate is also a constant.

Forced turbulence.

If the velocity exceeds the critical value U_1, the turbulence, already being fully developed and still being constrained by the flow boundaries, can only change by an alteration in the value of ε. Tennekes and Lumley (1972) reported that in laboratory experiments where L is constant an increase in Reynolds number decreases the size of the smallest eddies so that we would expect λ to decrease and N to increase. Writing (3.34) and (3.66) for these conditions:

$$\lambda = (\nu^3/\varepsilon)^{1/4} \qquad (3.66)$$

$$\varepsilon = U^3/N^3 L \qquad (3.67)$$

shows that to find ε the following equation has to be solved numerically:

$$\log\,(L\varepsilon^{1/4}/\nu^{3/4}) = U/\varepsilon^{1/3}L^{1/3} \qquad (3.68)$$

It is clear that an increase in U at constant L causes an increase in the dissipation rate and a decrease in λ. Figure 8 shows the expected variation of the velocity profile for L = 30 m and ε = 0.29 cm^2/s^3 (which result in N = 11 and U_1 = 105 cm/s) for three

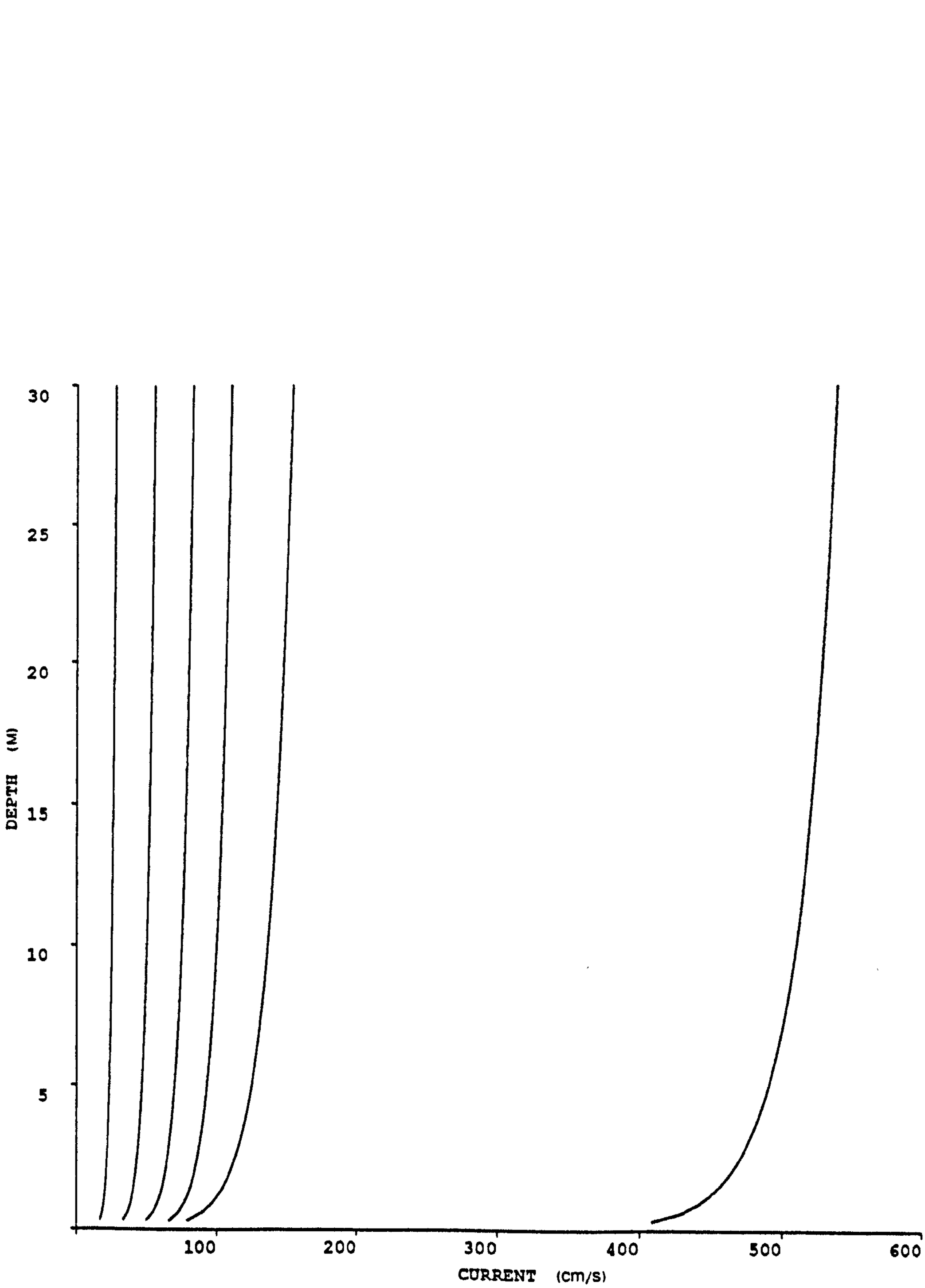

Figure 8. The development of the mean velocity profile.

velocities up to U_1 = 105 cm/s, and for $5U_1$ for the same inputs.

A model for intermittent turbulence.

The following model is proposed:

a. Below a critical velocity U_1 the energy dissipation rate is constant and the large eddy intermittency is proportional to the current speed.

b. The velocity profile is given by (3.33) with a value of N approximately equal to 11, the model roughness length λ being close to the dissipation scale over a flat bed.

c. The eddies should exhibit group behaviour because of continuity and the effect of the production process on the bulk flow. This grouping may vary with intermittency. When the turbulence is fully developed a sequence of NL large eddies should show related behaviour.

The remainder of this thesis is concerned with testing these model propositions against spectral evidence and direct measurement made at sea. Turbulent spectra are a useful tool for establishing the value of the energy dissipation rate, ε, and are discussed in the next chapter.

CHAPTER 4 TURBULENT SPECTRA

Wave number spectra

Tennekes and Lumley (1972) showed that the energy contribution from each eddy size to a true one dimensional wave number spectrum of a field of spatially discrete and intermittent eddies would be associated with a wave number, k, such that:

$$k = 2\pi/\ell \tag{4.1}$$

and that if the magnitude of the spectral estimate at k is $\Phi_1(k)$ then the energy associated with a discrete disturbance whose size is ℓ will be found within a spectral band of width k centred on k. This is because the fourier transform of a narrow band around k is a wave of wavelength $2\pi/k$ with an envelope whose width is the inverse of the bandwidth. The mean energy contribution from each size is given by $n_\ell k_\ell$ since:

$$n_\ell k_\ell = (1/L)\ (L/\ell)\ (n_\ell)\ (k_\ell \ell) \tag{4.2}$$

(1) (2) (3) (4)

the individual terms being:

(1) The averaging term over the record length L
(2) The number of discrete sites ℓ in the record
(3) The probability that a site is active
(4) The 1D energy contribution from each site

Substituting (4.1) into (4.2), using (2.41), and associating the mean energy per size with the energy in the spectrum at that wave number $k\Phi_1(k)$:

$$k\Phi_1(k) = n_k k_k = n_k \varepsilon^{2/3} (2\pi/k)^{2/3} \tag{4.3}$$

$$\Phi_1(k) = 3.4\ n_k\ \varepsilon^{2/3} k^{-5/3} \tag{4.4}$$

The energy cascade proposed in Chapter 2 is characterised by all the eddy sizes smaller than the largest having the same

intermittency, equal to $n_L/2$. Such a cascade would exhibit the $k^{-5/3}$ dependence throughout the range of wave numbers higher than the peak:

$$\Phi_1(k) = 1.7\ n_L \varepsilon^{2/3} k^{-5/3} \qquad (4.5)$$

This result for the one dimensional wave-number spectrum is of the same form as (1.13) which was derived from Batchelor's result for the three dimensional wave-number spectrum in the inertial subrange (equation (1.12)) and the assumption that the turbulence is isotropic in that range. Here the formulation is derived without regard to isotropy or the conditions under which the inertial subrange is expected to exist.

If the spectrum is sharply cut off by the outer flow parameters so that the peak is at a wave number, k_L given by:

$$k_L = 2\pi/L \qquad (4.6)$$

then using equation (2.41):

$$\int_{k_L}^{\infty} \Phi_1(k)\ dk \approx 0.74\ n_L u_L^2 \qquad (4.7)$$

and the mean square measured turbulent velocity is directly proportional to the kinetic energy density of the energy containing eddies.

Surface spectra

Woods (1975a) reported that two dimensional wave number spectra of horizontal temperature variance which have been directly measured at the sea surface exhibit a k^{-2} trend. If, as he suggests (see Introduction) the distribution of temperature variance reflects the spatial distribution of the eddies, then we can write immediately:

$$k\Phi_2(k) \ \alpha\ \ell \qquad (4.8)$$

so that using (4.6):

$$\Phi_2(k) \propto k^{-2} \tag{4.9}$$

Frequency spectra

Tennekes and Lumley (1972) show a direct equivalence between the frequency and wave number spectra of a property, thus:

$$\sigma\phi_1(\sigma) = k\Phi_1(k) \tag{4.10}$$

where $\phi(\sigma)$ is the frequency spectral estimate at frequency σ. This relationship is used to transform time records taken at a point into wave number spectra using Taylor's Hypothesis (Heathershaw, 1979). In this transformation the wave number is related to the frequency by:

$$k = 2\pi\sigma/U \tag{4.11}$$

where U is the mean velocity at the point of recording. For equivalence with equation (4.1) the frequency must be associated with the eddy passage time. Equating (4.1) and (4.11):

$$k = 2\pi/\ell = 2\pi\sigma/U$$

so that:

$$\sigma = U/\ell \tag{4.12}$$

The eddy passage time, $t_{passage}$, being given by:

$$t_{passage} = \ell/U \tag{4.13}$$

We should therefore expect to see a $\sigma^{-5/3}$ dependence in the frequency spectrum which is then transformed directly into the $k^{-5/3}$ wave number spectrum when Taylor's hypothesis is valid. If the spectrum is cut-off by the outer flow parameters then the peak frequency, σ_p, will be given by:

$$\sigma_p = U/L \tag{4.14}$$

and the $\sigma^{-5/3}$ dependence will be seen at higher frequencies than σ_p.

If it were possible to measure a spectrum so that the energy in a particular eddy size was associated with a frequency related to the eddy lifetime, t_ℓ, so that:

$$\sigma = 1/t_\ell \tag{4.15}$$

then, calling this spectrum $\phi(\sigma)$, and using (4.3),(4.10) and (4.14):

$$\sigma\phi(\sigma) = \phi(\sigma)/t_\ell = n_\ell k_\ell$$

so that:

$$\phi(\sigma) = n_\ell k_\ell t_\ell \tag{4.16}$$

We can now use (2.41) and (2.42) to give:

$$\phi(\sigma) = n_\ell \varepsilon t_\ell^2 \tag{4.17}$$

so that resubstituting for σ using (4.15), and putting n_ℓ equal to $n_L/2$ as before, this spectrum has the form:

$$\phi(\sigma) = 0.5 n_L \varepsilon\ \sigma^{-2} \tag{4.18}$$

This is the form predicted by Tennekes and Lumley (1972) and described in Chapter 1. If this spectrum is cut-off by the outer flow parameters then the peak should be at a frequency, σ_t, given by:

$$\sigma_t = 1/t_L \tag{4.19}$$

and the σ^{-2} dependence should be seen above that frequency.

The peak frequencies σ_p and σ_t are related by:

$$\sigma_p/\sigma_t = Ut_L/L \tag{4.20}$$

Substituting (3.26):

$$n_L NL = U_0 t_L \tag{4.21}$$

into (4.20) gives:

$$\sigma_p/\sigma_t = n_L NU/U_0 \tag{4.22}$$

If the turbulence is well developed (4.22) can be approximated by:

$$\sigma_p \approx N\sigma_t \tag{4.23}$$

We have seen in the previous chapter that in a boundary layer energy is expected to exist at frequencies equivalent to $1/t_\ell$ due to the production process. If the time spectral estimate at σ_t is equal to ϕ_p then the time spectral estimate at σ_t is given approximately by (4.18) and (4.23):

$$\phi(\sigma_t) \approx \phi_p/N^2 \tag{4.24}$$

and with N approximately equal to 11 we should expect the time spectrum, ϕ, to be greatly reduced before the passage time spectrum, ϕ, is measured. We should expect, therefore, to see a spectrum from the bottom boundary layer having two distinct peaks. This will happen if the energy in a particular eddy size is divided equally between the ϕ and ϕ spectra since in that circumstance:

$$\sigma_t\phi(\sigma_t) = \sigma_p\phi(\sigma_p) \tag{4.25}$$

and (4.23) gives:

$$\phi(\sigma_t) \approx N\phi(\sigma_t) \tag{4.26}$$

so that from (4.24):

$$\phi(\sigma_t) \approx \phi(\sigma_t)/N \qquad (4.27)$$

The lack of previous reporting of the time spectra, $\phi(\sigma)$, can be explained by considering some published results. Figure 9 shows two figures taken from Heathershaw (1979). The top figure (Figure 9(a)) shows a typical analogue record in which the u signal shows a clear variation about the mean with a period of about 300 seconds. The lower figure (Figure 9(b)) gives his derived spectra, the lowest wave number of which (approximately 0.002 cm^{-1}) corresponds to a period of 60 seconds at a mean velocity of 50 cm/s. Figure 10 is taken from Bowden and Ferguson (1980). Figure 10(a) showing analogue records where the u component displays a clear 9 minute periodicity. Figure 10(b) shows the resulting spectra in which the minimum wave number equates to an 80 second period. It seems likely that in both cases the systematic variation in the u component shown in Figures 9(a) and 10(a) were removed as a linear trend in the data since each record length was only slightly longer than the fundamental period.

Surface layer similarity scaling

Many spectra have been measured near the sea bed in marine boundary layers. These are reported in detail in monographs by Soulsby (1983) and Heathershaw (1979). In his original paper (Soulsby, 1977), Soulsby reported that spectra calculated over a wide range of wave numbers, with reasonably tight confidence limits, together with spectra from other authors and atmospheric results, collapsed to a universal form when scaled with variance and measuring height, h, thus:

$$\frac{k\Phi\ (k)}{\int_0^\infty \Phi(k)\,dk}.v.kh$$

collapsed the spectra irrespective of the value of ε (since atmospheric spectra also collapse). The spectra were ensemble averaged one dimensional velocity spectra. Heathershaw (1979)

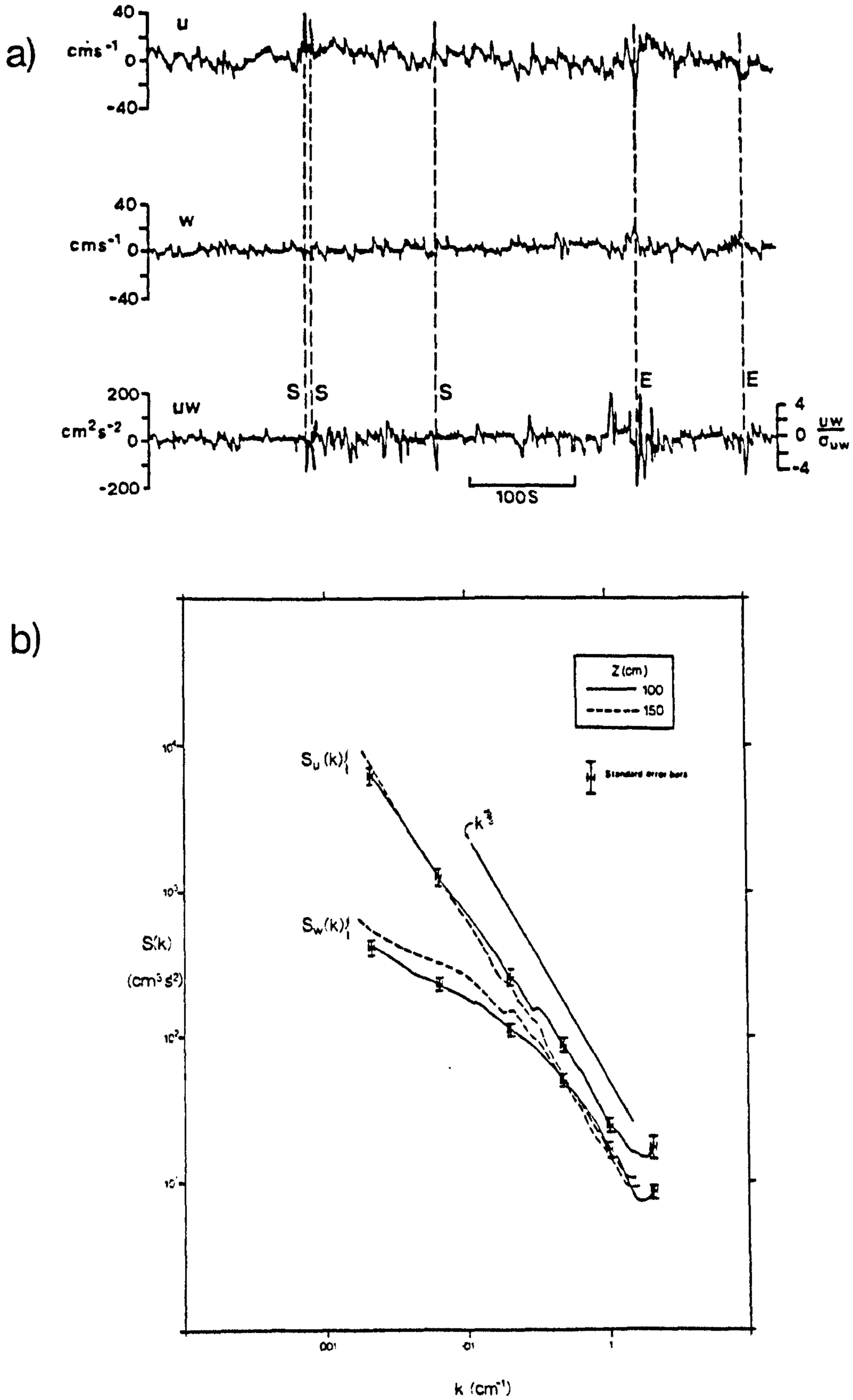

Figure 9. (a) Analogue records from Heathershaw (1979), (b) spectra from the same author.

a)

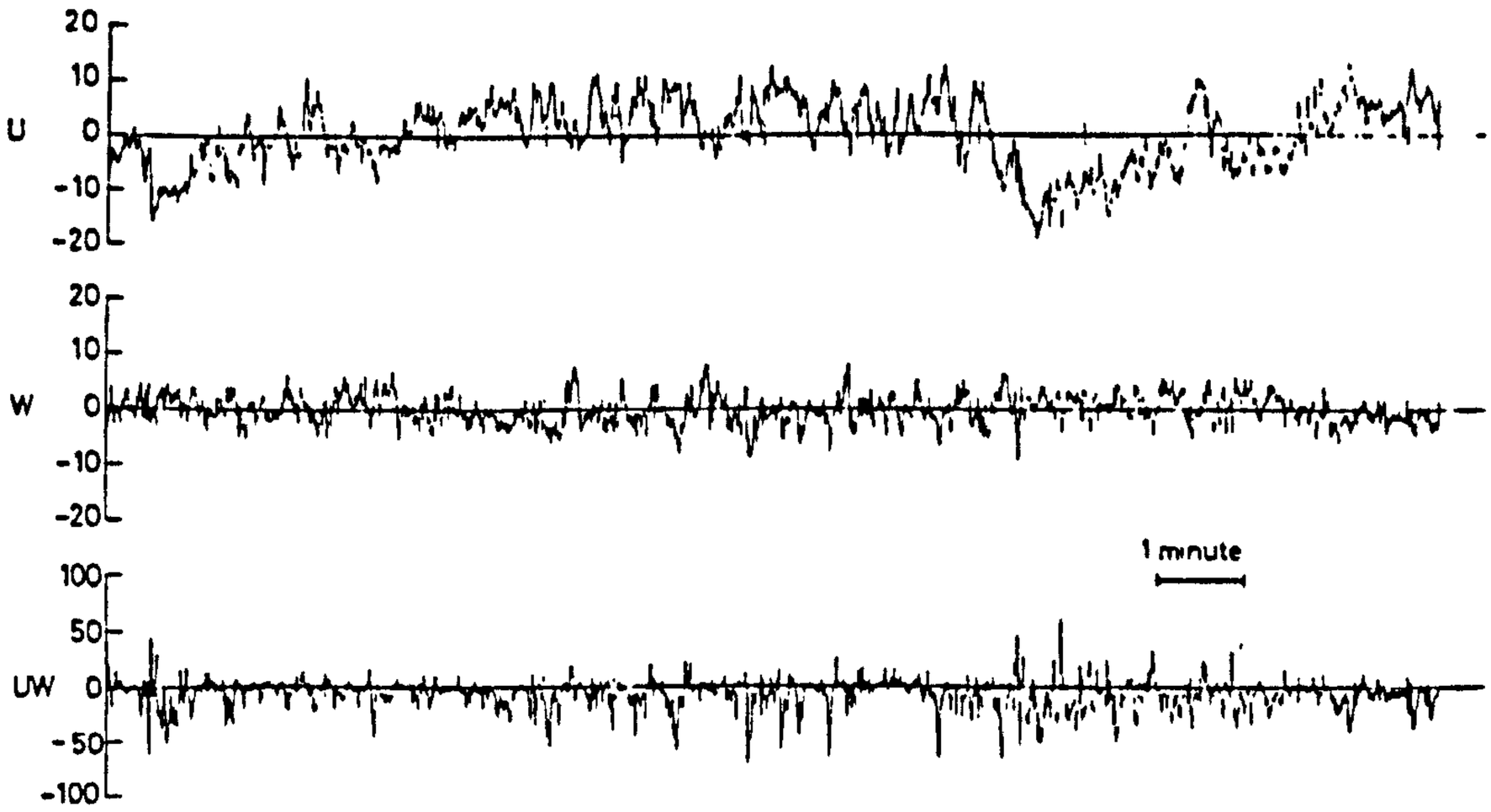

b)

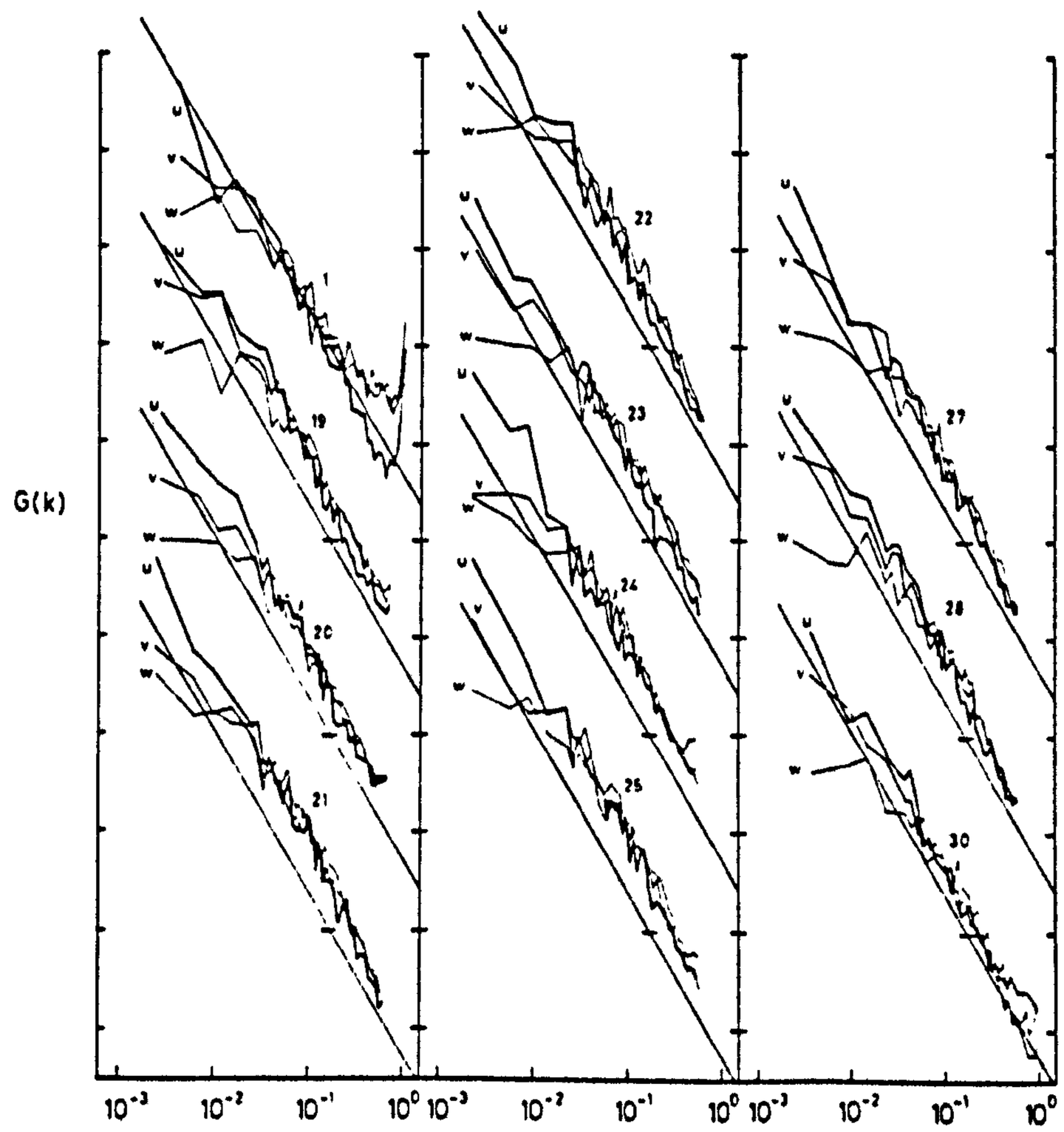

Figure 10. (a) Analogue records from Bowden and Ferguson (1980), (b) Spectra from the same authors.

commented that this scaling appears to undermine the similarity scaling (which should be with u*) and the assumptions which go with it. An inertial subrange (i.e. a $k^{-5/3}$ dependance in the spectra) could be discerned at higher wave numbers although the Reynold's numbers were less than those at which an inertial subrange should exist. The scaling must be examined for its significance since it implies some universality of structure. It should be noted that the scaling is not as successful in laboratory flows (Anwar, 1981) where better collapse is achieved by scaling with flume depth. Figure 11 is taken from Soulsby (1983) and illustrates the scaling.

To begin to explain the scaling the collapse of the spectral peaks is considered first. If the spectrum is sharply cut-off by the outer flow parameters and displays a power law dependence at higher wave numbers, so that using (4.4):

$$\Phi(k) = A\ \varepsilon^{2/3}k^{-5/3} \qquad k > k_p \tag{4.28}$$

$$\Phi(k) = 0 \qquad k < k_p$$

where A is a constant. At the peak the spectral estimate, $\Phi(k_p)$ is given by:

$$\Phi(k_p) = A\ \varepsilon^{2/3}k_p^{-5/3} \tag{4.29}$$

so that:

$$k_p\Phi(k_p) = A\ \varepsilon^{2/3}k_p^{-2/3} \tag{4.30}$$

The integral under such a spectrum is given by:

$$\int_{k_p}^{\infty}\Phi(k)\,dk = (3/2)A\ \varepsilon^{2/3}k_p^{-2/3} \tag{4.31}$$

Thus:

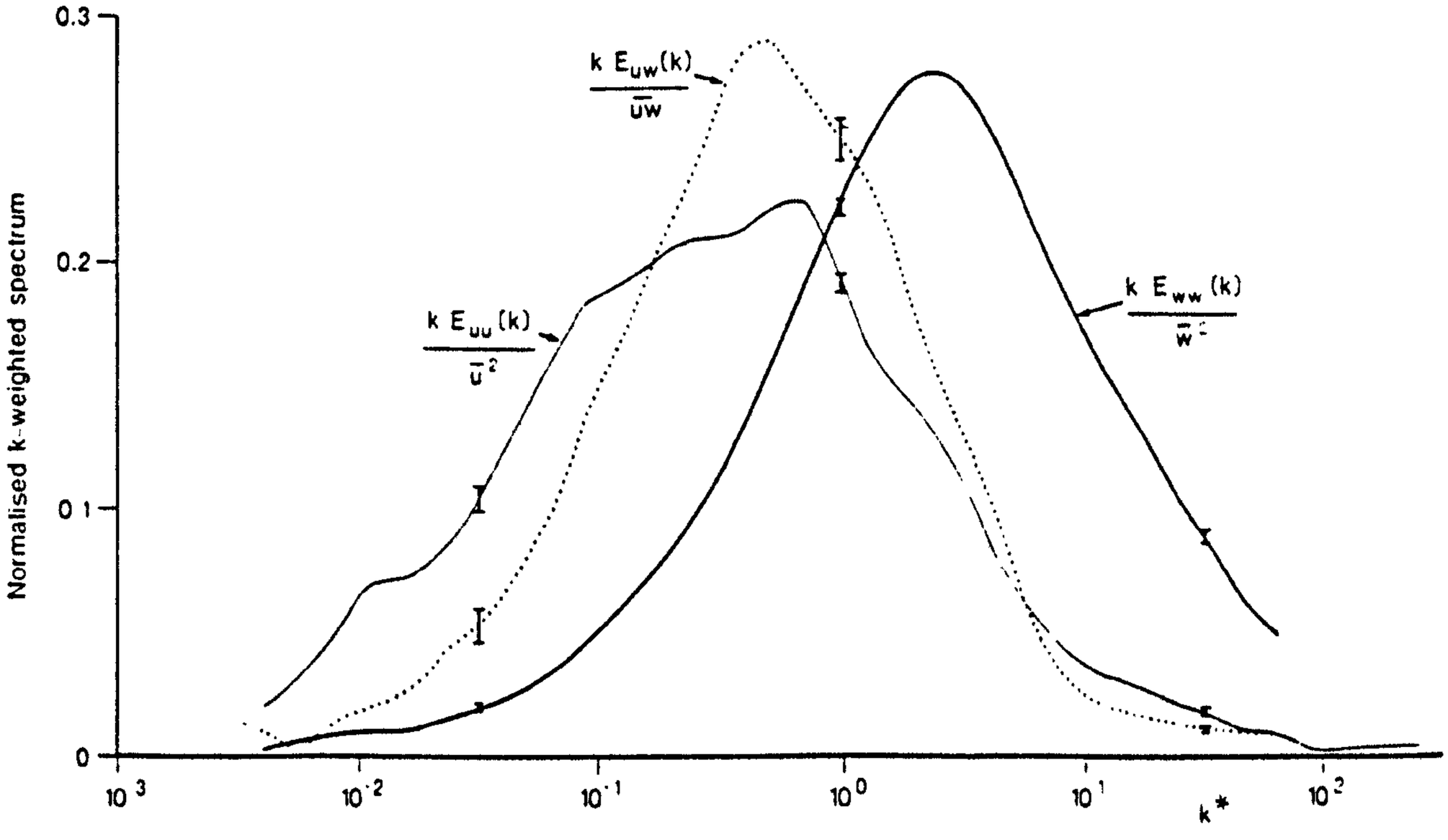

Figure 11. Surface layer similarity scaling from Soulsby (1983).

$$\frac{k_p \Phi(k_p)}{\int_0^\infty \Phi(k)\,dk} = 2/3 \qquad (4.32)$$

irrespective of the value of A or of ε. The published spectra scaled under surface layer similarity scaling collapse to approximately 1/2 this value indicating that about half the spectral energy lies below the peak.

To explain the scaling completely it is necessary to investigate the fact that the peak wave numbers collapse with the sensor height. We have seen that these spectra are associated with the eddy passage times and peak at a frequency given by (4.14). Using (4.11) to convert to peak wave number we achieve:

$$k_p = 2\pi/L \qquad (4.33)$$

implying that the non-dimensional peak, k_p^*, should be located at:

$$k_p^* = k_p h = 2\pi h/L \qquad (4.34)$$

which at first sight cannot be constant since there is no interdependence between the sensor height, h, and the boundary layer thickness L. After detailed analysis, Soulsby (1983) recognised that the value of k_p^* increases with sensor height as we would expect from equation (4.34). It appears that two phenomena contribute to the collapse of k_p^*. The first is that, at least in the marine records, the ratio of the sensor height to boundary layer depth all fall within a small band on the logarithmic *k*h scale. For all the marine spectra calculated by Soulsby (1983), Heathershaw (1979) and Bowden and Ferguson (1980) the value of the ratio falls in the band:

$$0.06 < h/L < 0.1 \qquad (4.35)$$

when the boundary layer depth is defined as the water depth at the measuring point. Using (4.34):

$$0.37 < k_p^* < 0.62 \tag{4.36}$$

which is well within the range of values over which the spectral peaks lie as may be seen in Figure 11.

The second point of interest is that k_p^* for the vertical velocity spectra is about ten times the value for the horizontal peak. It is likely that the vertical component is reflecting more of the fine scale structure of each eddy as it passes than the horizontal component since it is less constrained by continuity. If this is so then we might expect the peak wave numbers to be related by an equation similar to (4.23). Substituting (4.11) into (4.23) and (4.34) gives:

$$(k_p^*)_{\text{passage time}} \approx N(k_p^*)_{\text{eddy lifetime}} \tag{4.37}$$

and substituting N = 11 (as found in the previous chapter) into (4.37) would explain the observed spectral shift.

Spectral ratios.

In order to examine isotropy, Bowden and Ferguson (1980) calculated spectral ratios from 3000 spectral estimates for the inertial subrange and plotted $\Phi_w(k)/\Phi_u(k)$ against kh where h was again the sensor height. Within the scatter the ratio increased linearly from 1 to 1.33 as kh increased to 2π and then remained at 1.33 indicating that the turbulence was isotropic above that wave number. At $kh = 2\pi$, (4.1) gives:

$$kh = 2\pi h/\ell > 2\pi \tag{4.38}$$

so that for the turbulence to appear isotropic:

$$h > \ell \tag{4.39}$$

This equation is eqivalent to the condition used to calculate the mean velocity profile from the passing eddy structure; namely that only the eddies of a particular size which were in contact with the bottom would be anisotropic, and that these eddies would only

be detected if the eddy size was greater than sensor height (otherwise they would pass beneath the sensor).

The discrete eddy cascade model has been shown to be consistent with the turbulent spectra found in the sea. It is shown below that by using current meters, frequency spectra which reflect the production process can be resolved and related to the model. It is also shown that if the fourier components associated with a particular eddy size are isolated, then the discrete nature of the eddy cascade is revealed.

CHAPTER 5. DESCRIPTION OF A CURRENT METER EXPERIMENT

A current meter experiment was carried out in the North Sea in August 1989 using the facilities of the Warren Spring Laboratory, Stevenage. The aim of the experiment was to collect detailed current data over several tidal cycles in two locations using two arrays of three current meters suspended vertically at varying separations. In the event, bad weather and instrumentation failure curtailed the experiment, fortunately without detriment to the major results.

The experiment was carried out from the SEASPRING a 194.5 foot converted sewage vessel at anchor 15 miles to the east of Felixtowe at 51° 57.31′ N, 1° 46.06′ E in about 30 m of water over a flat sandy bottom (the variation in chart depth is 3 m in 1000 m), fixed by Decca and bearings on the Shipwash light. The tidal streams in the area had been previously measured (Elliott, 1986).

The experiment can be conveniently divided into two parts. The first part was conducted overnight on the second of August with both arrays of current meters deployed from the anchored SEASPRING. The current meter deployment is shown in Figure 12. One set of current meters were always deployed from SEASPRING and are hereafter described as the fixed set. The meters which recorded successfully were suspended at depths of 10 m and 22 m below the surface from a derrick on the starboard side. In this part of the experiment the second set of current meters, called hereafter the moving set, was suspended overnight from a crane on the port side, separated laterally at a distance of 20 m and longditudinally by 5 m. In the moving set only one meter functioned correctly. Fortunately this was a meter suspended at 22 m, allowing direct comparison with the bottom fixed meter. The top fixed and bottom moving current meters were DNC-2B meters constructed by NBA (Controls) Ltd and record current by propeller revolution count and direction by internal compass.

The bottom meter of the fixed array was a DNC 2M meter, similar to the above but with a slightly different fin geometry

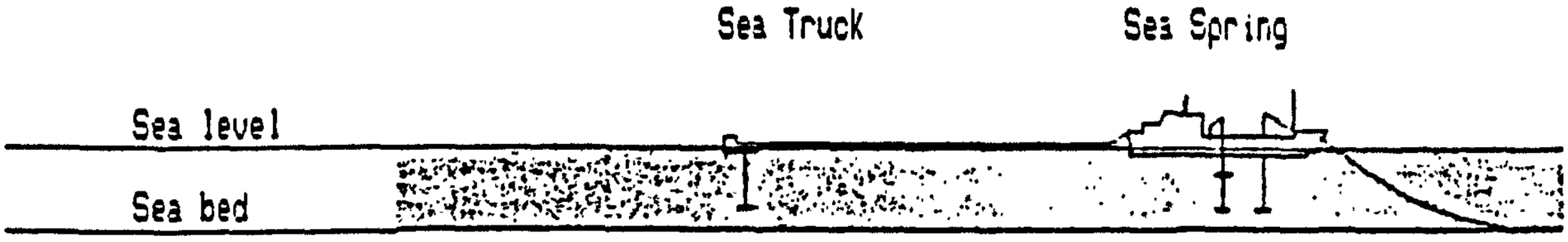

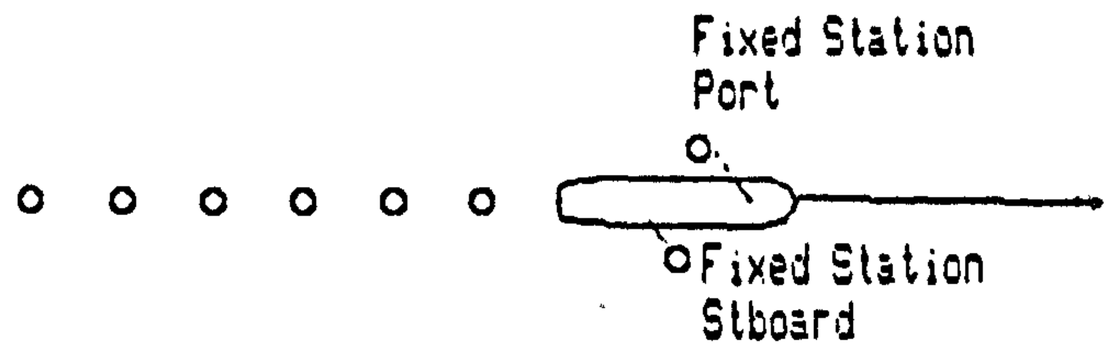

Geometry of Current Meter
Experiment
(Approximately to scale)
1 cm = 20 m

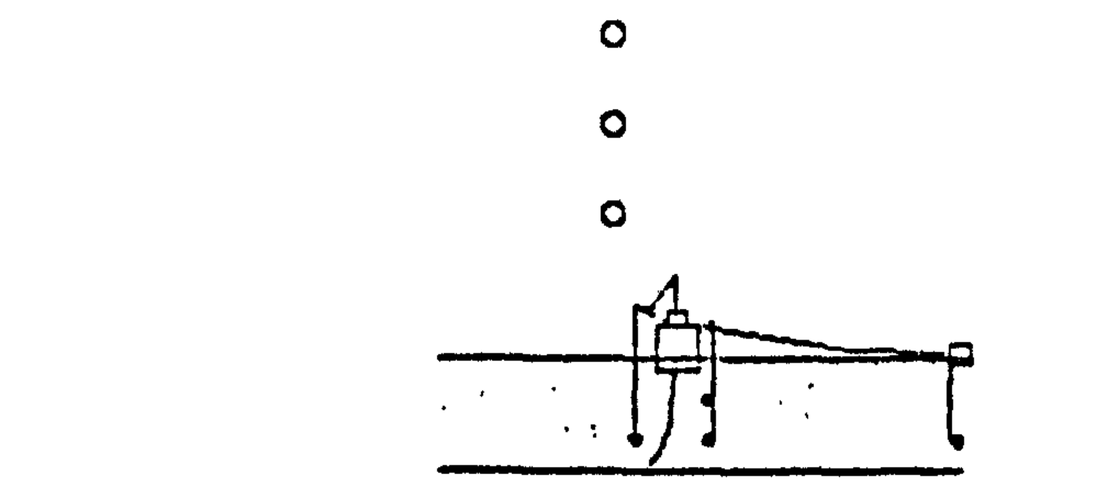

Figure 12. Deployment of current meters.

and capable of measuring temperature, salinity and conductivity as well as speed and direction. The meters were calibrated by the manufacturers in preparation for the experiment and set-up in accordance with the handbooks. The data recording rate (the meters record digitally onto magnetic tape) was set at the minimum interval of 15 s and the scaling factor selected such that the meters would record accurately at well above the predicted maximum water velocity. All the meters were started at the same time at 0850 on the 2nd August and ran throughout the experiment until switched off at 1308 on the 3rd. It is not known what caused two meters to be defective although rough handling in poor weather conditions 30 miles further out to sea on the 2nd was probably the most significant factor. An AML salinometer was used to measure salinity profiles at slack water, it not being possible to take readings when the current was running fast, and the readings from this equipment and the DNC-2M meter confirmed that the tidal stream was unstratified throughout the whole experimental period.

The second part of the experiment was conducted during the morning of the 3rd August. The moving array of meters was detached from SEASPRING and suspended (at the same depth below the surface) from a 13 m utility vessel called SEATRUCK. Simultaneous readings were then taken from fixed and moving arrays at grid positions as shown in Figure 12 while the tide was flooding (the flood being when the water level was rising). The sampling time at each position was chosen to be between 15 and 25 minutes so that as much detail as possible could be recorded without the weather and tidal conditions changing significantly over the period during which the different stations were sampled.

Overnight on the 2/3rd August and during the second part of the experiment there was little wind and no wind-generated waves. There was a slight residual swell overnight which decreased as the second experiment progressed. The only effect of this was to cause SEASPRING to roll and pitch at a frequency of 0.2 Hz, a frequency which as will be seen in the results is far removed from that of the turbulence. Further the maximum vertical displacement of the meters at their suspension points was 0.6 m, a quantity which was

much smaller than any systematic motion from the different suspension mechanisms.

The ship was anchored with 120 m of cable and had only 2 m of draft making it very unlikely that the current meter readings would be influenced by the presence of the ship or by its wake although the actual measuring position could be expected to vary slowly as the ship swung at anchor. The hardest problem was to accurately and consistently position SEATRUCK relative to SEASPRING during Part 2 of the experiment. This was achieved by running a light, buoyant line between the vessels, the line being marked at 20 m intervals. SEATRUCK's outboard was used to maintain line tension and position when the lateral stations were being measured. Astern the current was such that the measuring line remained taut although there was some lateral swing about the mean current bearing at the 20 m and 40 m stations.

To check the surface current and relative diffusion coefficients, dye patches were released from the stern of SEASPRING at each astern measuring station and their spreading and transport time measured. This sequence of dye releases was recorded on video film to aid later analysis. The current meters recorded the total number of turns of the propeller in each 15 second sampling interval. The specified accuracy is +/- 2% above 3.1 cm/s. When the tidal stream reversed at slack water the ship was swinging at its anchor but this minimum restriction is unimportant since readings in these periods were not used.

Direction was recorded using a magnetic compass at each 15 s sampling interval. This was an instantaneous reading and not an average over the interval as the current reading was. The specified resolution is 2°. The clock accuracy was +/- 2 s a day.

At maximum current the angle made between the suspension wire and the vertical reached 12° - 15°. This would imply a maximum of 0.7 m variation in bottom meter depth below the surface and a maximum streamwise displacement of 6 m since the bottom meters were suspended on 22 m of wire. The top fixed meter was suspended

on 10 m of wire so the maximum streamwise separation between the two meters should have been less than 3 m since a very heavy weight was attached to the bottom of the array. Finally, although the compasses were calibrated, the data processing recognised that systematic errors in direction measurement could exist between meters.

The data were recovered from the meters on magnetic tape and processed on a Hewlett Packard PC using software supplied by NBA (Controls) Ltd and validated by their test program to convert the recorded signals to ASCII format. At a sampling interval of 15 s and a record length of 27.5 hours there was a considerable quantity of data. The data was time-matched and then transferred to the PRIME 9955 Mark 2 mini computer in the Department of Nuclear Science and Technology, Royal Naval College Greenwich, for processing. The records were compared to check that the transfer had been completed without corruption and split into separate files for access by the data handling program. In particular each file was checked for notable features (such as zero readings when the meters were removed from the water) to ensure that the time matching was correct.

Two data handling processes were fundamental to all the subsequent results and their interpretation. First the current and direction readings had to be converted to streamwise and cross-stream (u and v) components. The vertical velocity component was not measured. It is possible for a component of the vertical velocity to contribute to the other components if the current meter angle of attack varied in the vertical plane. For this reason the coherence between the derived u and v components was calculated.

Secondly a representative mean value had to be chosen from each signal so that the fluctuating signal could be extracted and processed. The raw data consisted of a current averaged over the sampling interval, R, and a direction, ϑ, measured at each interval. Taking these as the raw data the following simple algorith was used to produce u and v velocity components. First ϑ

was smoothed (smoothing is discussed below) to produce a mean, and this was subtracted from the raw direction signal to achieve a fluctuating angle, ϑ', with a zero mean. The fluctuating angle, ϑ', is therefore a direction relative to the tidal stream. All smoothing processes induce numerical diffusion and the fact that a satisfactory mean value had been achieved was checked by computing rms fluctuation values at discrete (short) intervals and by comparing the mean with the lowest frequency components of a Fast Fourier Transform of the signal.

The data were then processed using the following simple algorithms to give u and v, the streamwise and cross-stream velocity fluctuations:

ϑ' is averaged over the interval

$$v = R \sin\vartheta'$$

$$U = R \cos\vartheta'$$

where U is the total streamwise velocity, fluctuating around its mean $\overline{U}$:

$$U = \overline{U} + u$$

and the U signal was smoothed again (and checked as above) to find a mean, $\bar{U}$ and this then subtracted to produce u. $\bar{U}$ is taken as the mean streamwise velocity at that current meter. This algorithm, although simple, balances the forces against the current meter fins while assuming the meter to be in the steady state over the averaging interval. No better algorithm is recommended by the manufacturer or has been used in the literature.

The data was non-stationary in every respect. The mean streamwise velocity varied with time, the mean square value of the fluctuating components varied with time and the frequency structure was also time varying. This made the data very difficult to handle as there is no totally satisfactory algorithm which can

handle all types of non-stationary situation, primarily because the very nature of the non-stationarity is the first unknown. The subject is well reviewed in the last chapter of Bendat and Piersol (1971). It is only possible to sensibly process the data into usable form and clearly compare and report the effects of the mathematical techniques used.

With such large data sets it proved impractical to attempt a polynomial or cubic spline fit to elucidate the mean values even using the NAG library sub-routines available on the PRIME. It was therefore decided find to mean values using a smoothing process known as "Hanning" (Bendat and Piersol (1971) and Kinsman, (1965)). This process is normally used to remove spectral leakage when producing spectra from correlation functions. The process consists of taking a weighted average value of each data point and its adjacent data points, the weighting factors a and b (following Kinsman the programs use a = 0.54, b = 0.23) being applied without carrying the new value across to the next average:

$$\langle x_i \rangle = bx_{i-1} + ax_i + bx_{i+1} \qquad (5.1)$$

Repeating the smoothing process 1000 times to ϑ and subsequently U gave non-stationary mean values which when subtracted from the original signal left component velocities which fluctuated evenly around zero. The original signal was then converted to a complex spectrum using the FFT algorithm in the PRIME NAG library and the resulting spectrum cropped and transformed back for comparison with the mean derived from the smoothing process. The result depended on the amount of spectral cropping (equivalent to passing the signal through a low-pass filter) but the spectrum peaked severely at the frequency of the tidal period, and a transform of the frequencies close to the peak showed a very similar mean signal to that derived from the smoothing process. This double check showed that the separate mean and fluctuating signals produced were valid since similar results were obtained from two very different techniques. The result is demonstrated in Figure 13 where the whole data set for the bottom fixed meter is shown. In this figure the top graph is depth versus

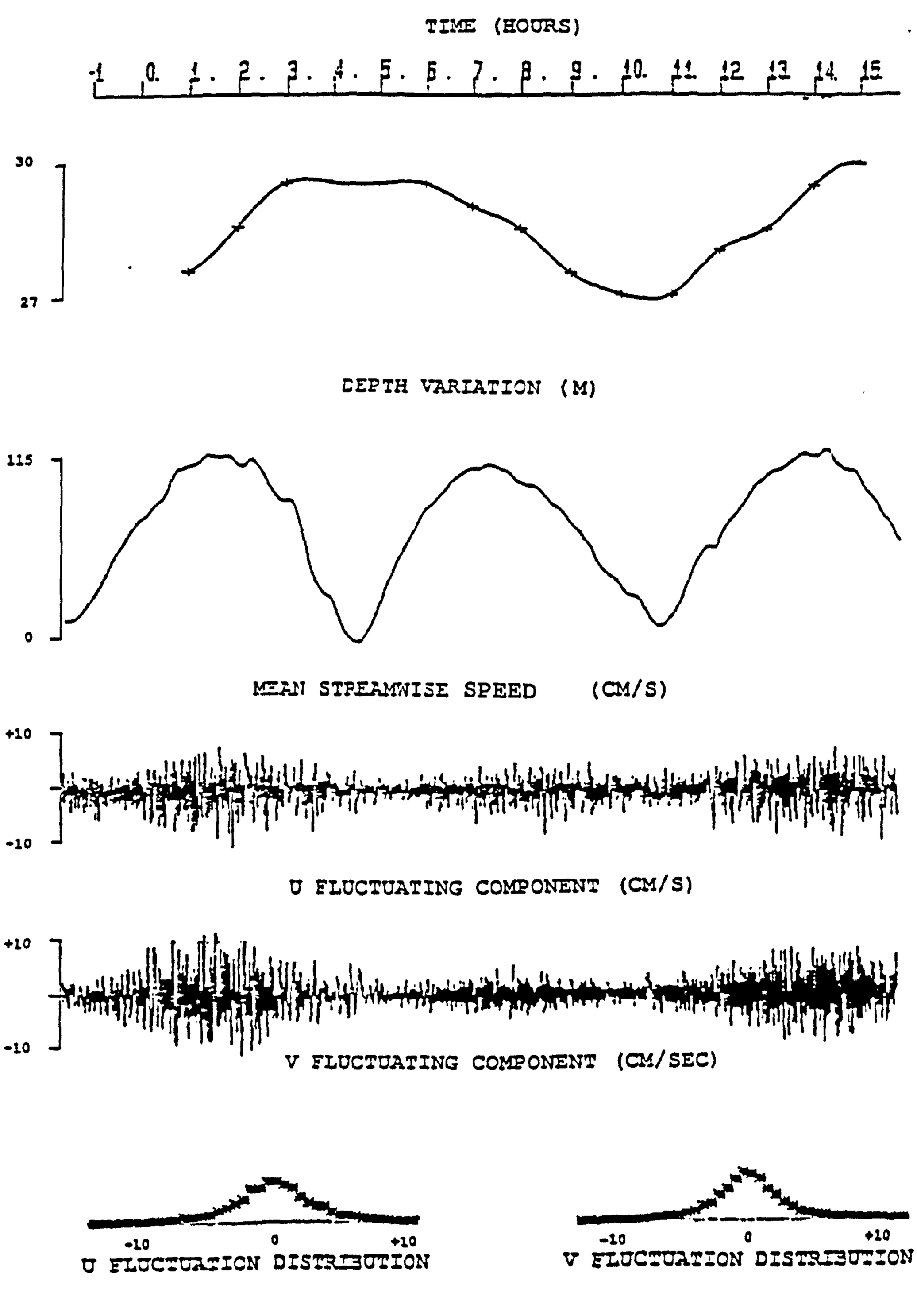

Figure 13. Full data set from Part 1 of the current meter experiment.

time (the depth readings were taken by echo-sounder, corrected for keel depth and the curve fitted by a cubic spline interpolation). The second graph shows the mean streamwise velocity U and the third and fourth the u and v fluctuating components.

The two lowest graphs show the statistical distributions of u and v taken over the whole record. These are approximately Gaussian. Figures 14 and 15 show the autocorrelations and derived spectra for the u and v components, calculated from the record as a whole. Each autocorrelation time lag is 15 seconds. One would expect some distortion in the spectral estimates due to the varying r.m.s. value of the signals but it is encouraging that the correlations and spectra are well behaved and have the expected form. A record length of 4160 and an autocorrelation sample length of 50 gives around 80 degrees of freedom and a reasonable confidence that the derived spectrum is representative of the underlying process (Kinsman, 1965).

Both autocorrelations are characterised by negative portions of roughly equal area to the positive, reflecting the fact that the mean values achieved are good representations. The spectra exhibit sharp peaks at the same frequency and the logarithmic spectra exhibit the predicted characteristic -2 power dependence. The r.m.s. value of the v component and the height of its spectral peak show that the v component is of the same order of magnitude as (and may be in some circumstances larger than) the u. The horizontal turbulence as measured is essentially isotropic.

Figures 16 shows the coherence function between the u and v components from the whole data set, bottom fixed meter. Normally a coherence function is used to establish limits in a non-linear system within which the output is directly related to the input without distortion due to extraneous effects such as system noise. It is defined as the square of the modulus of the co-spectrum divided by the product of the component spectral values at the same frequency. Aside from at zero frequency (where departures from mean values may be significant) the coherence is very small, indicating that the measuring techniques and mathematical

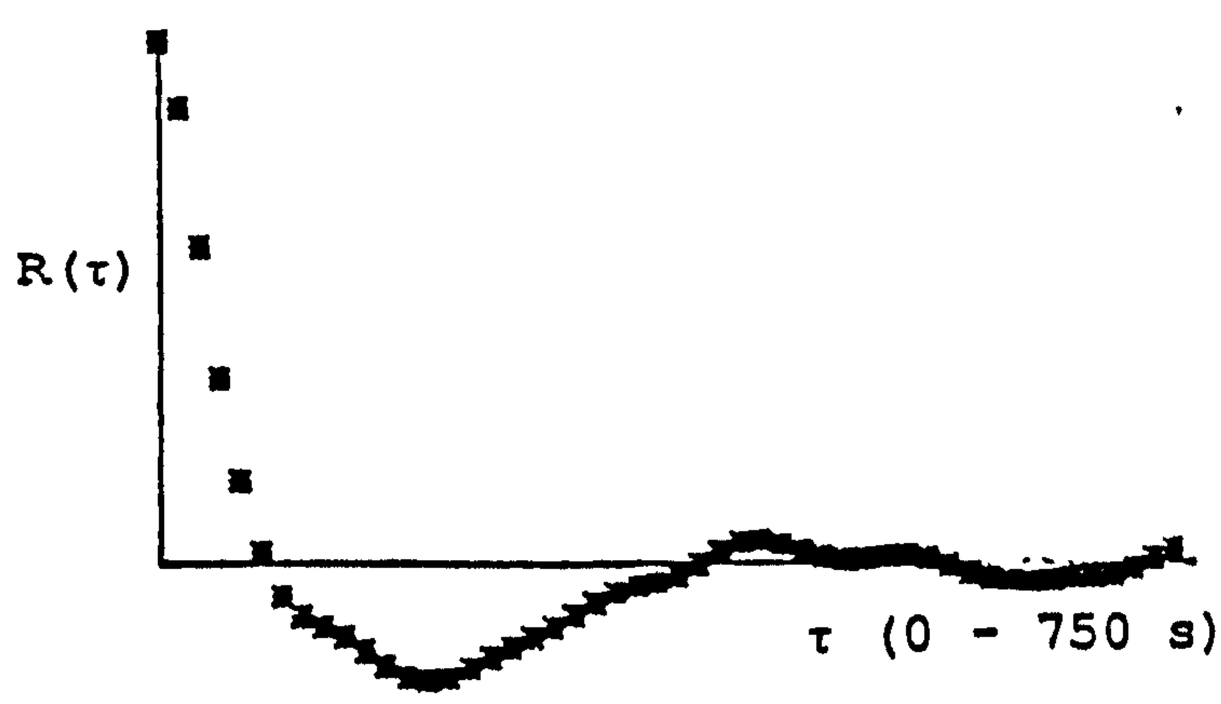

U FLUCTUATION CORRELATION

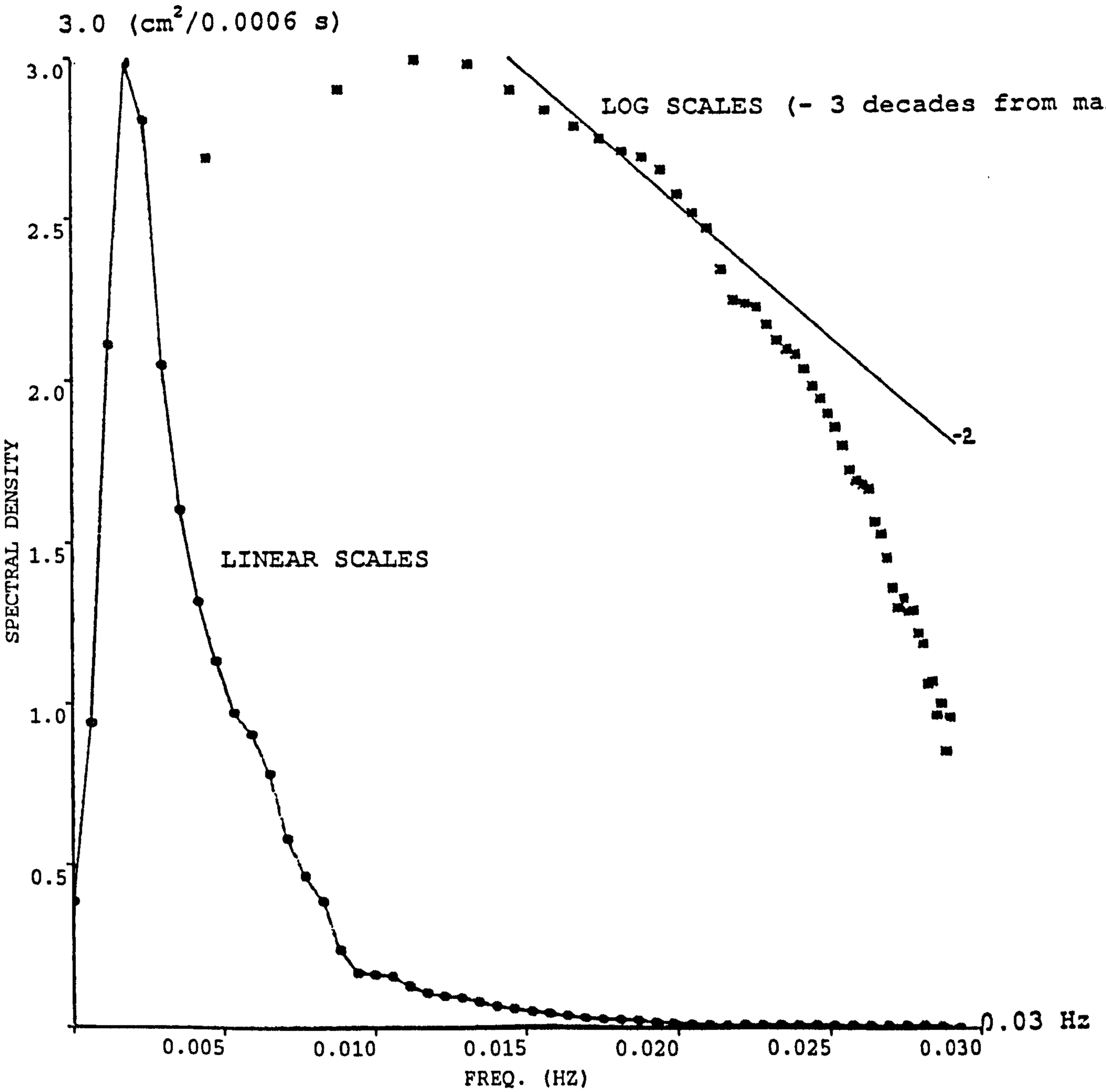

Figure 14. Streamwise fluctuation autocorrelation and spectrum for whole data set.

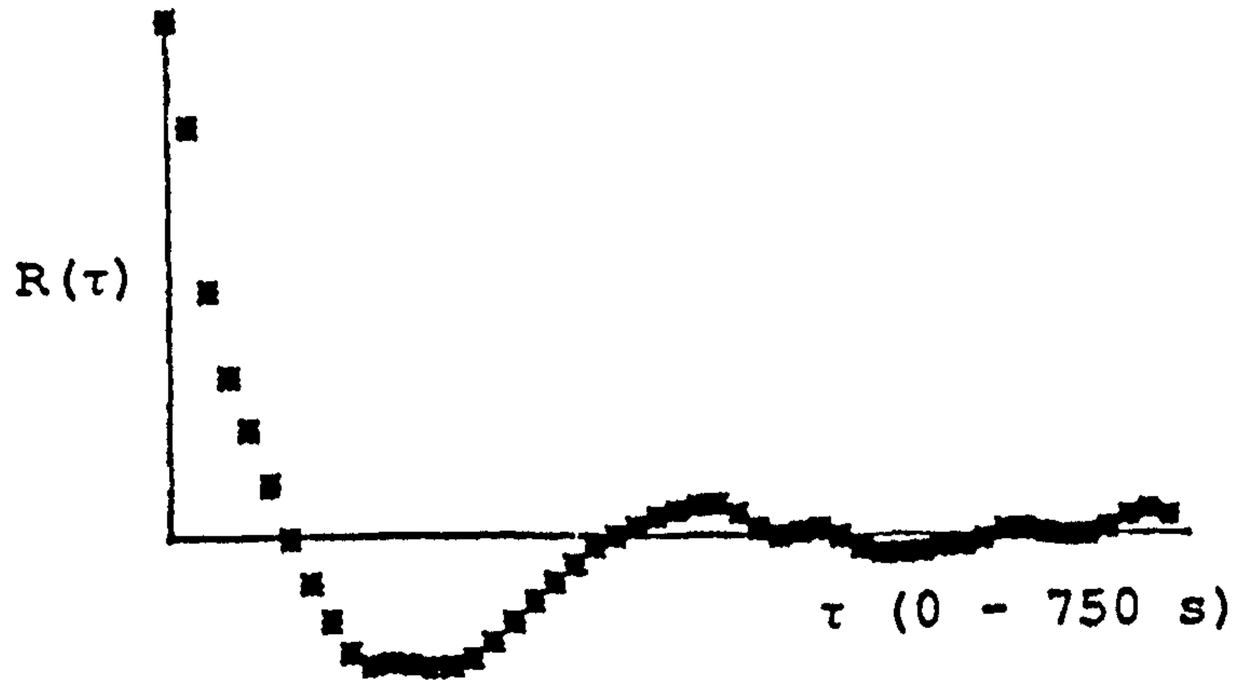

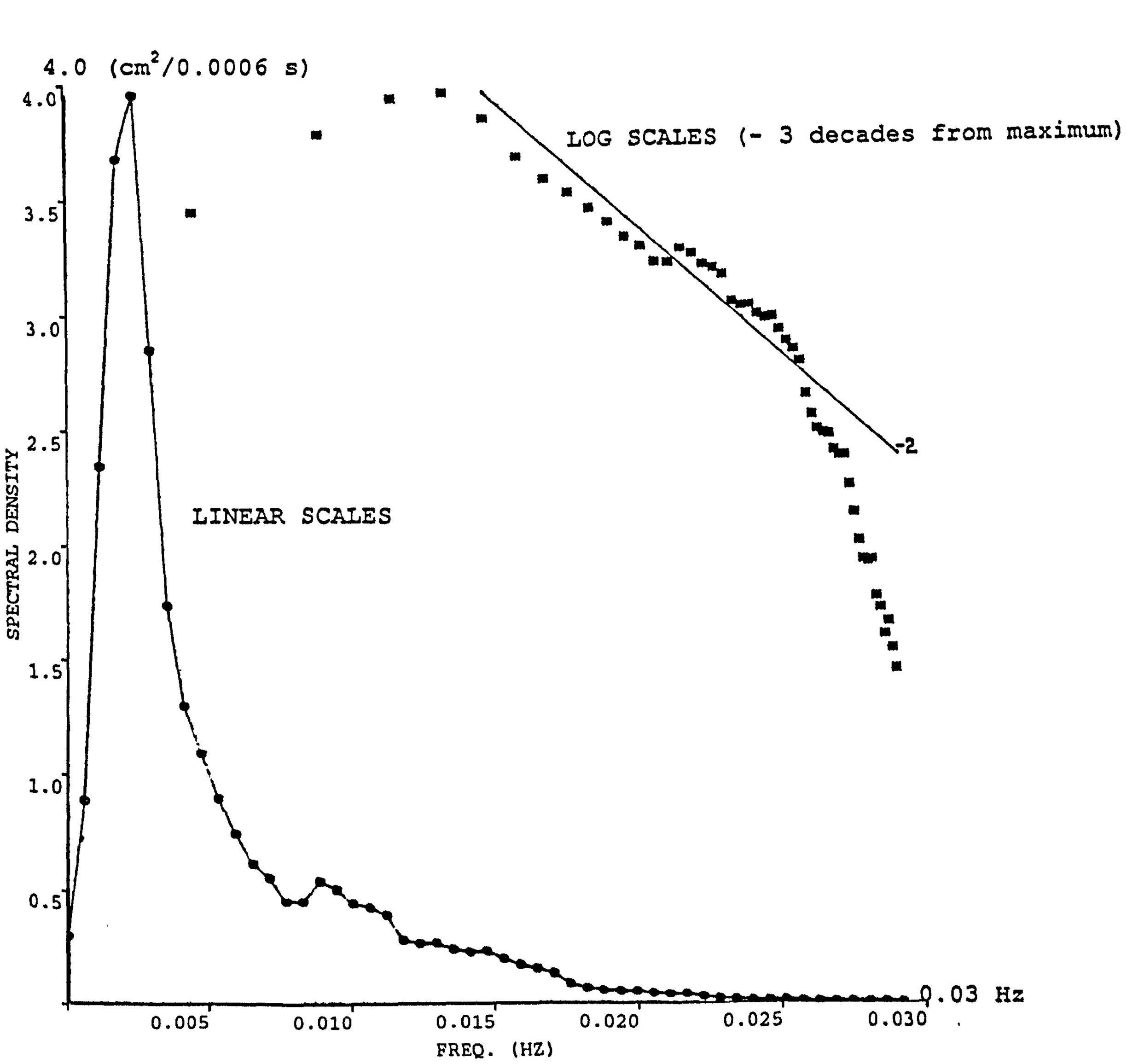

Figure 15. Cross-stream fluctuation autocorrelation and spectrum for the whole data set.

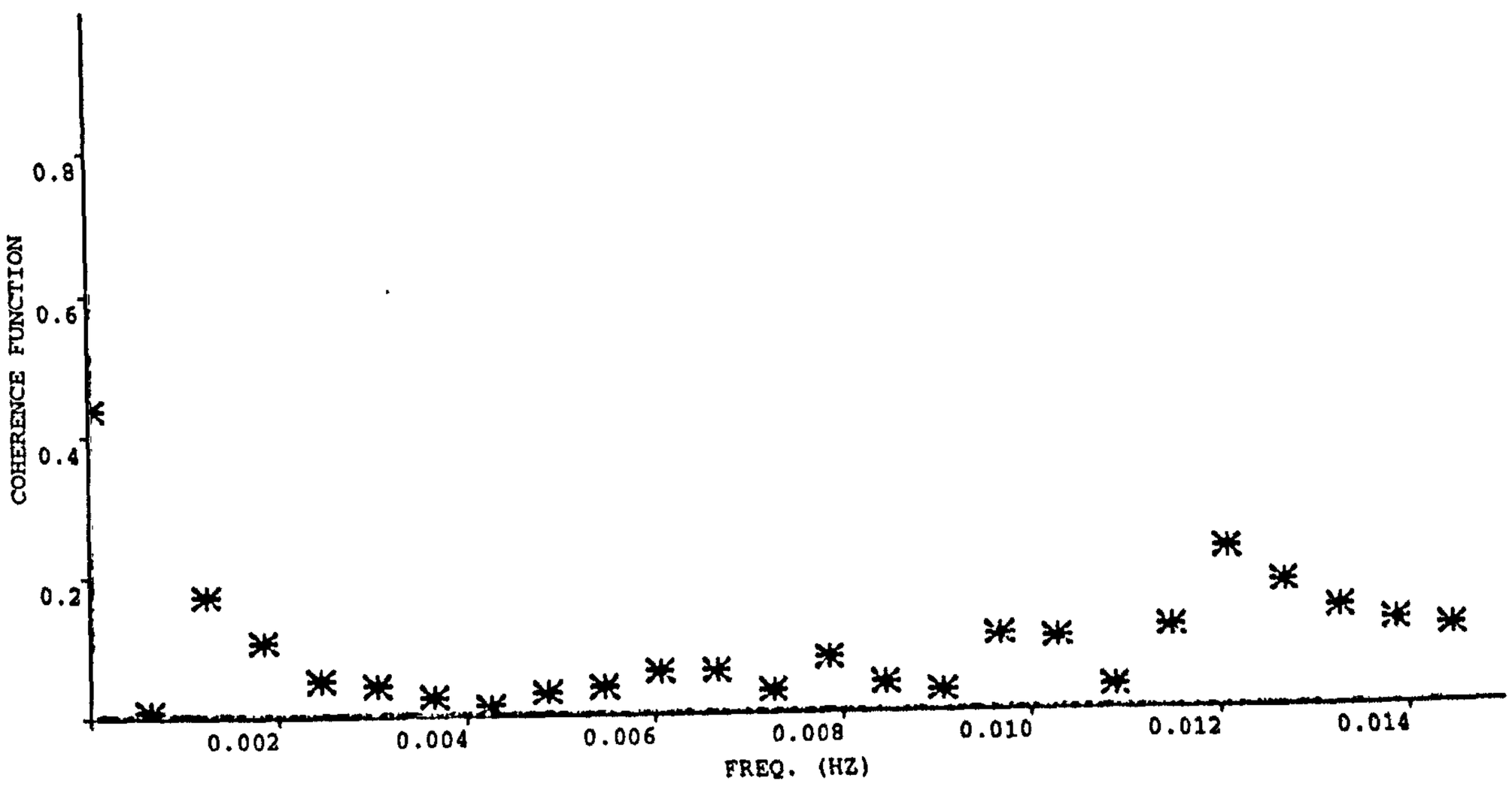

Figure 16. Coherence function between u and v components.

algorithms are unlikely to be introducing any significant systematic error into the resulting statistics.

The Nyquist frequency is 0.033 cps and calculated spectral estimates will be aliased if the physical process being measured has energy at frequencies higher than this. This frequency is at the maximum of the frequency axes in Figures 14 and 15 and since the spectrum becomes very small at much lower frequencies than this, the sampling criterion is satisfied.

The residual swell had a frequency of 0.2 Hz, a much higher frequency than the energy containing range of the spectra. The spectral peaks in both the u and v records occur with a period close to 600 s or 10 minutes. This period is far from the tidal period, measured in hours, and the swell or instrument pendulum effects which were measured in seconds. The only events occurring in the sea at these intermediate periods are the turbulent eddies of the bottom-generated boundary layer. It appears that the signals derived from the current meters are representative of the turbulence without being contaminated by other effects. It is therefore expected that useful qualitative results about these eddies might be obtained from shorter record segments where stationary conditions were better realised, and that quantitative comparisons might be obtained for each component as variations take place over a tidal period.

Stern and side space correlations.

The energy peak in the whole record component spectra was centred around a period of 10 minutes and there was energy in the spectra down to a period of about 40 s. In carrying out space correlation estimates a compromise had to be achieved between getting sufficient readings per location to reveal the detail of the motion (ideally each record should be 5 or 6 times longer than the 10 minute period) and achieving results at sufficient locations for the spatial distribution to be established before the environment changed appreciably. This maximum period was obviously less than the 6 hour half-tidal cycle. In the event practical considerations dictated a compromise and the runs

achieved are shown in Table 2.

It was unsafe to try and control SEATRUCK at a 20 m separation abeam of SEASPRING, therefore to complete the beam data set records were extracted from the equivalent period in the previous tidal cycle when the moving array was suspended from SEASPRING.

The experiment was terminated at 1230 on the 3rd August in order that the chemical speciation experiments required by Warren Spring could be conducted within the sea-time available to SEASPRING. During the experiment the mean streamwise velocity increased but the turbulent fluctuations were much better behaved than shown in the overall record. Space correlations for the further 2 hour period, as the velocity decreased towards high water were, unfortunately, not achieved. Figures 17 - 20 show the records, probability distributions, autocorrelations, spectra and coherence function calculated over the 4 hour period of this experiment.

The correlations show a flattening at the origin and coherence over a longer time than they did for the whole 15 hour record. The correlations indicate coherence extending to 8 minutes in the u component and 5 minutes in the v. The spectral peaks have a period near to 6 minutes. The spectra still have the same form as those derived for the whole record. Since the mean flow is varying less over the shorter record period the coherence function is now very small over the whole range. In the next chapter, where property variations over a tidal cycle are studied, the results will be taken from even shorter records and the lack of coherence between u and v implies that the characteristics of the turbulent structure, rather than those of the current meters themselves, will be properly reflected in the data.

The runs were first processed to determine the spatial extent over which the signals were well correlated, thus giving an indication of the largest eddy size. For each fluctuating component the correlations were calculated for simultaneous

RUN	START TIME	FINISH TIME	NOTES
Stern 45 m	0900	0921	
Stern 65 m	0923	0949	
Stern 85 m	0951	1015	Dye release 1014
Stern 105 m	1016	1027	Dye release 1021
Stern 125 m	1028	1055	Dye release 1050
Stern 145 m	1056	1125	Dye release 1103
Beam 40 m	1135	1154	
Beam 60 m	1155	1209	
Beam 80 m	1210	1225	

Table 2. Correlation experiment.

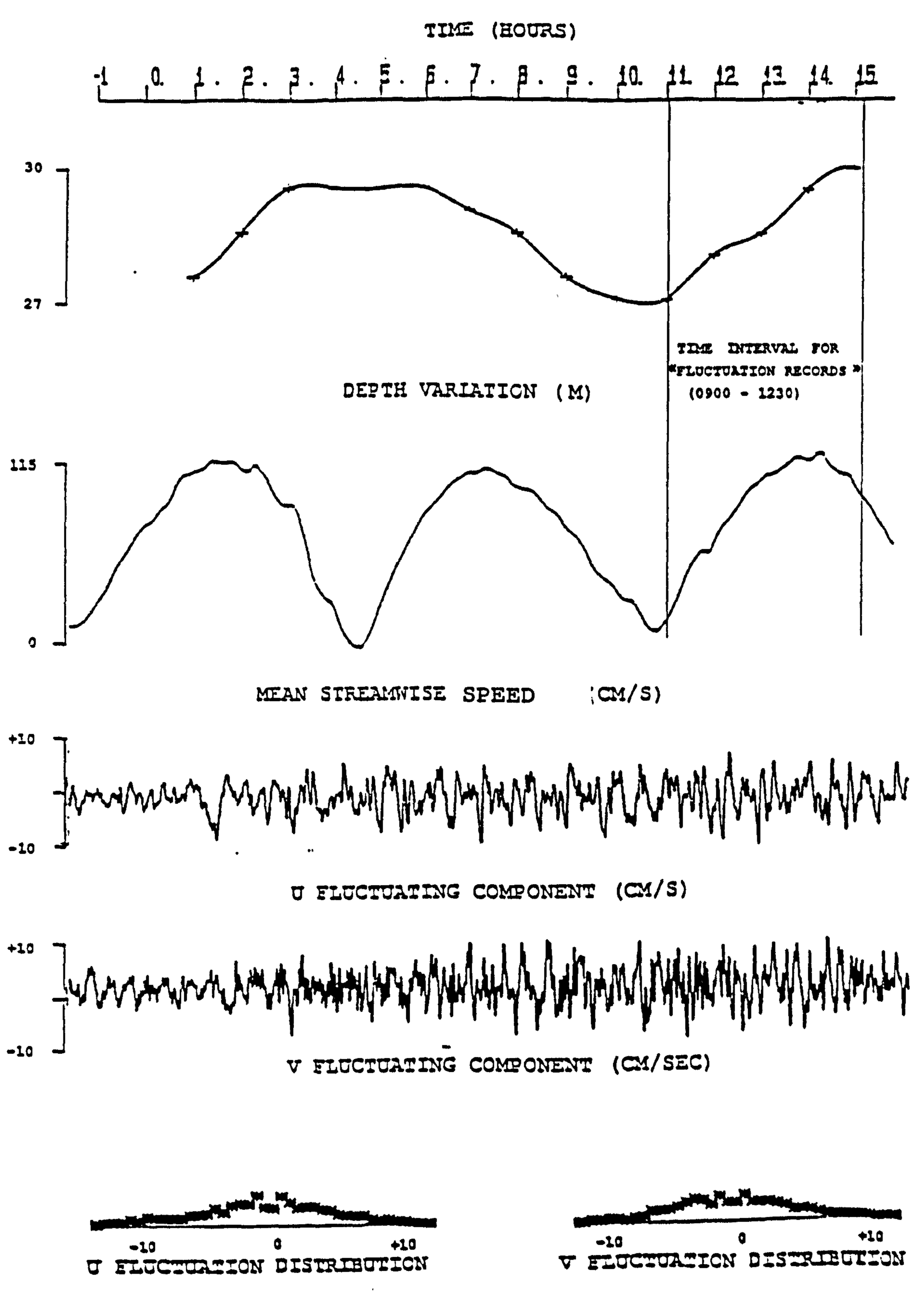

Figure 17. Data set for the interval 0900 - 1230, bottom fixed meter.

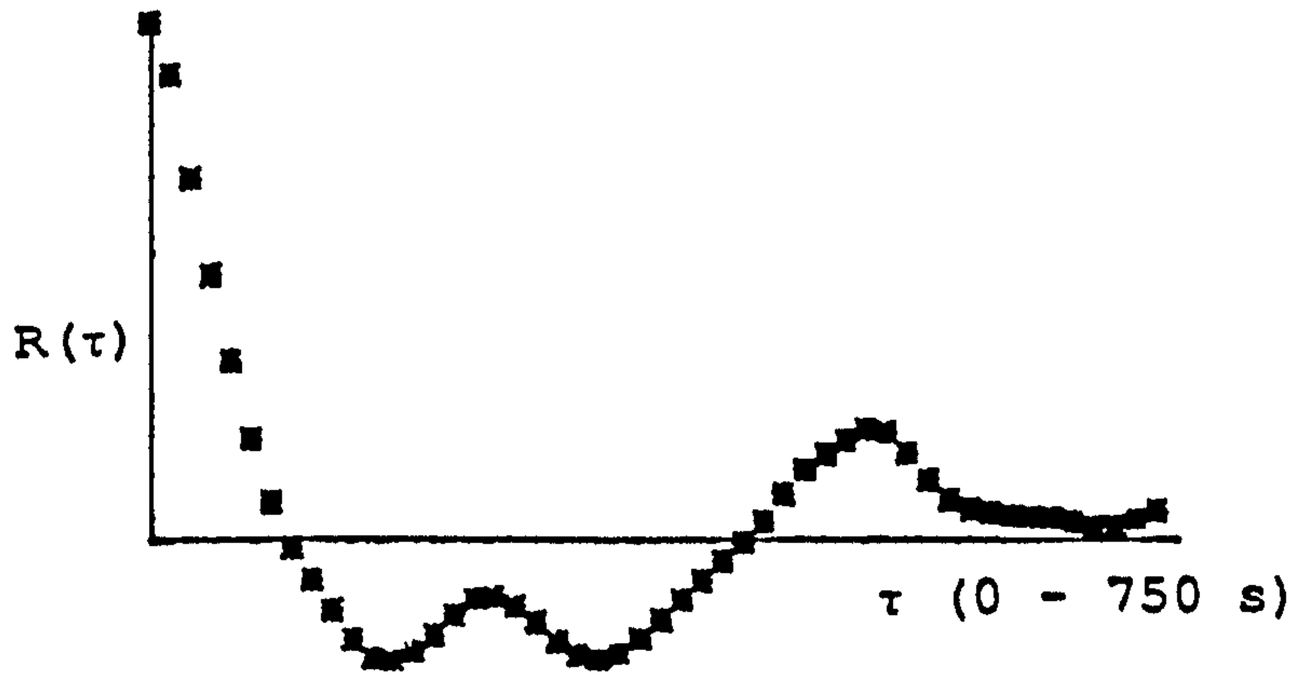

U FLUCTUATION CORRELATION

Figure 18. Streamwise fluctuation correlation and spectrum for 0900 - 1230 data set.

Text cut off in original

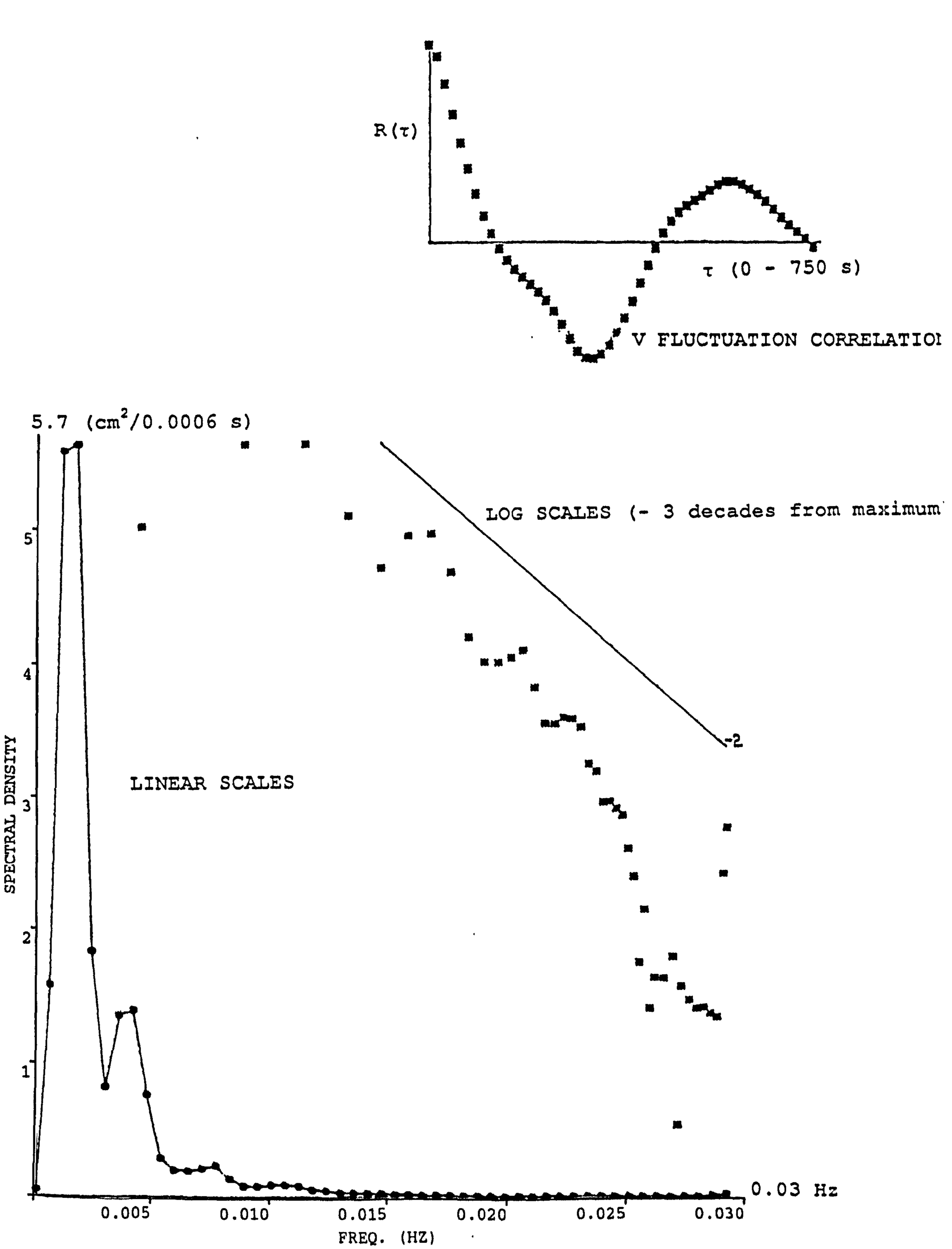

Figure 19. Cross-stream fluctuation correlation and spectrum for 0900 - 1230 data set.

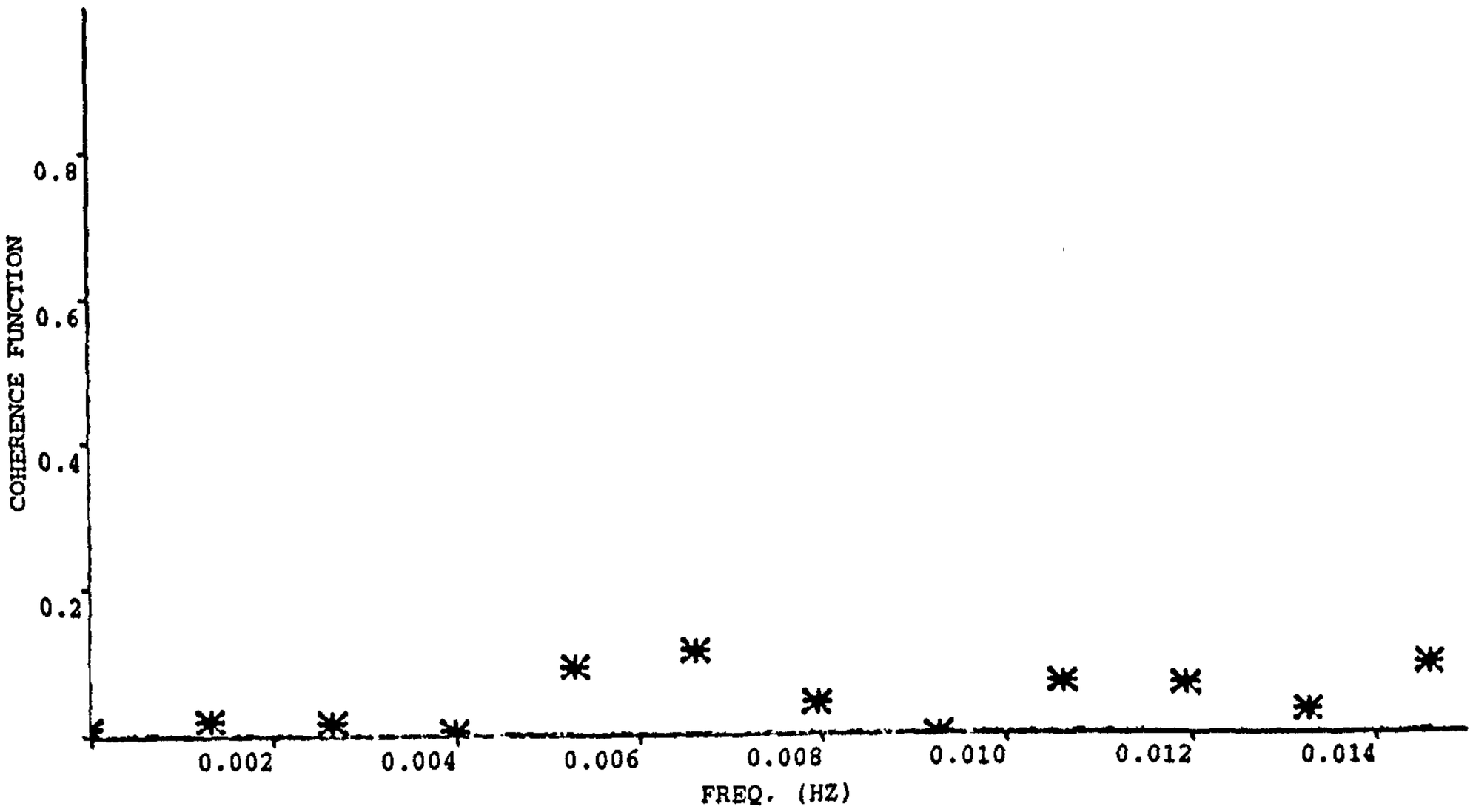

Figure 20. Coherence function for 0900 - 1230 data set.

records measured at different spatial separations. The results are given in Figure 21 for the beam runs and Figure 22 for the stern runs.

The u and v correlations display variability and this is not surprising owing to the constraints on the sampling duration at each station. The overall trend is, however quite clear. Abeam the signals are well correlated over 20 - 30 m and then rapidly become uncorrelated. Astern the result is similar except that there is more noise in the signal.

There are two aspects in the interpretation of such space correlations. First how "long", or "wide" is the eddy, and, second, is it moving during its lifetime relative to the mean line of advance through the sampling point? The answer is that one cannot tell. It appears that the eddy is about 30 m wide and long, approximately the same as the depth of water at the time the record was taken. It may be that the eddy width or length is distributed around this size or that the coherent motion involves a moving spatial mean. This will be discussed further in Chapter 7 where all the results are summarised and the parameters used in the model given.

The astern correlations were next examined to find the time delay at which the correlation between two simultaneous records taken at varying separations was a maximum. This reveals the mean propagation velocity of the eddy structures (Townsend, 1976). The results are shown in Figure 23. The separation distance was divided by the mean velocity to give an expected time delay (if the turbulent structures were moving at the mean velocity of the flow) which is plotted on the x axis.

Determination of the mean velocity was complicated by the fact that the current meters were suspended from the surface and therefore were not at a fixed distance above the sea-bed. Mean current profiles from top and bottom sensors and the surface dye release experiments showed that during this period the boundary layer occupied the whole flow depth. The mean velocity was

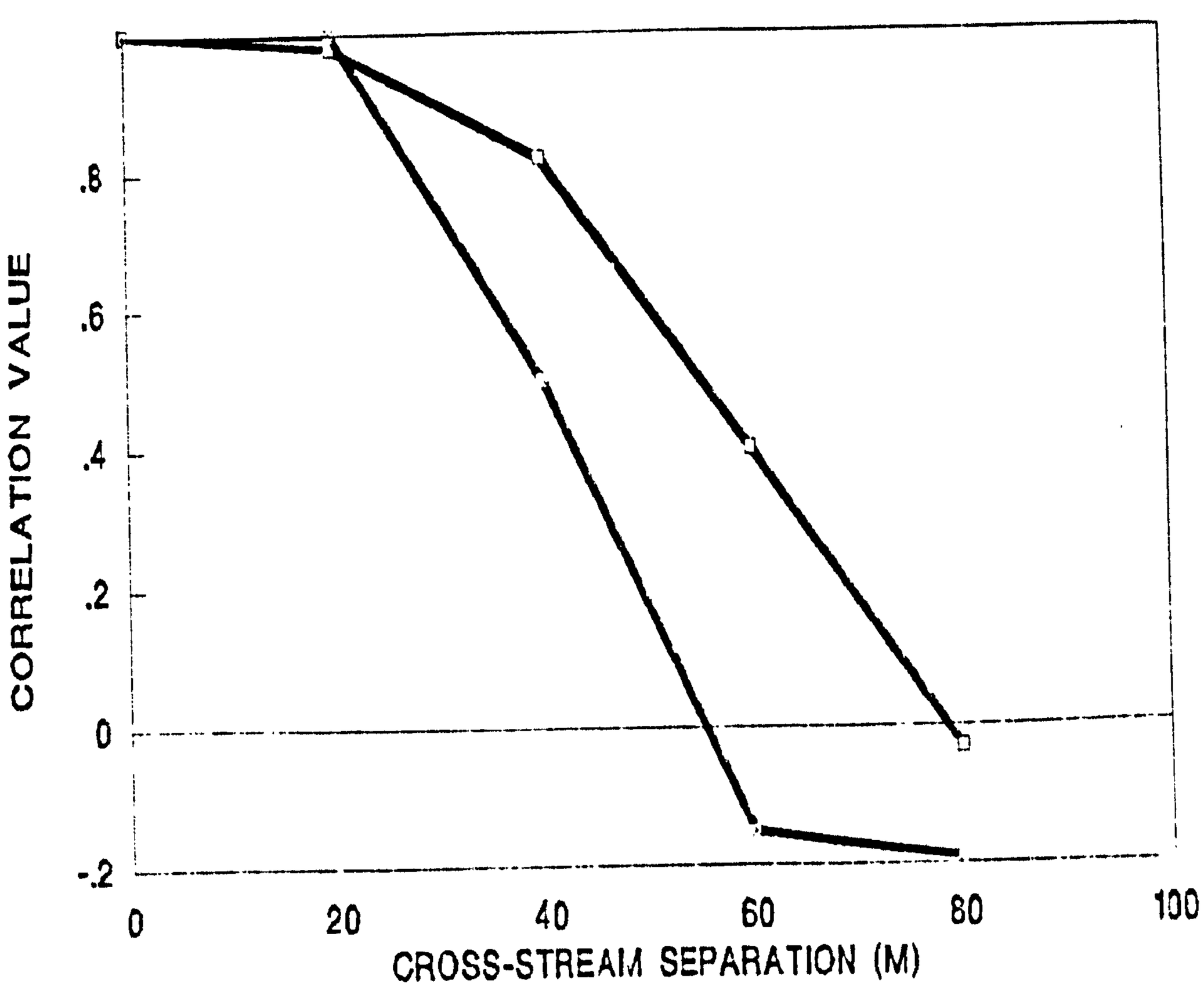

Figure 21. Cross-stream spatial correlation.

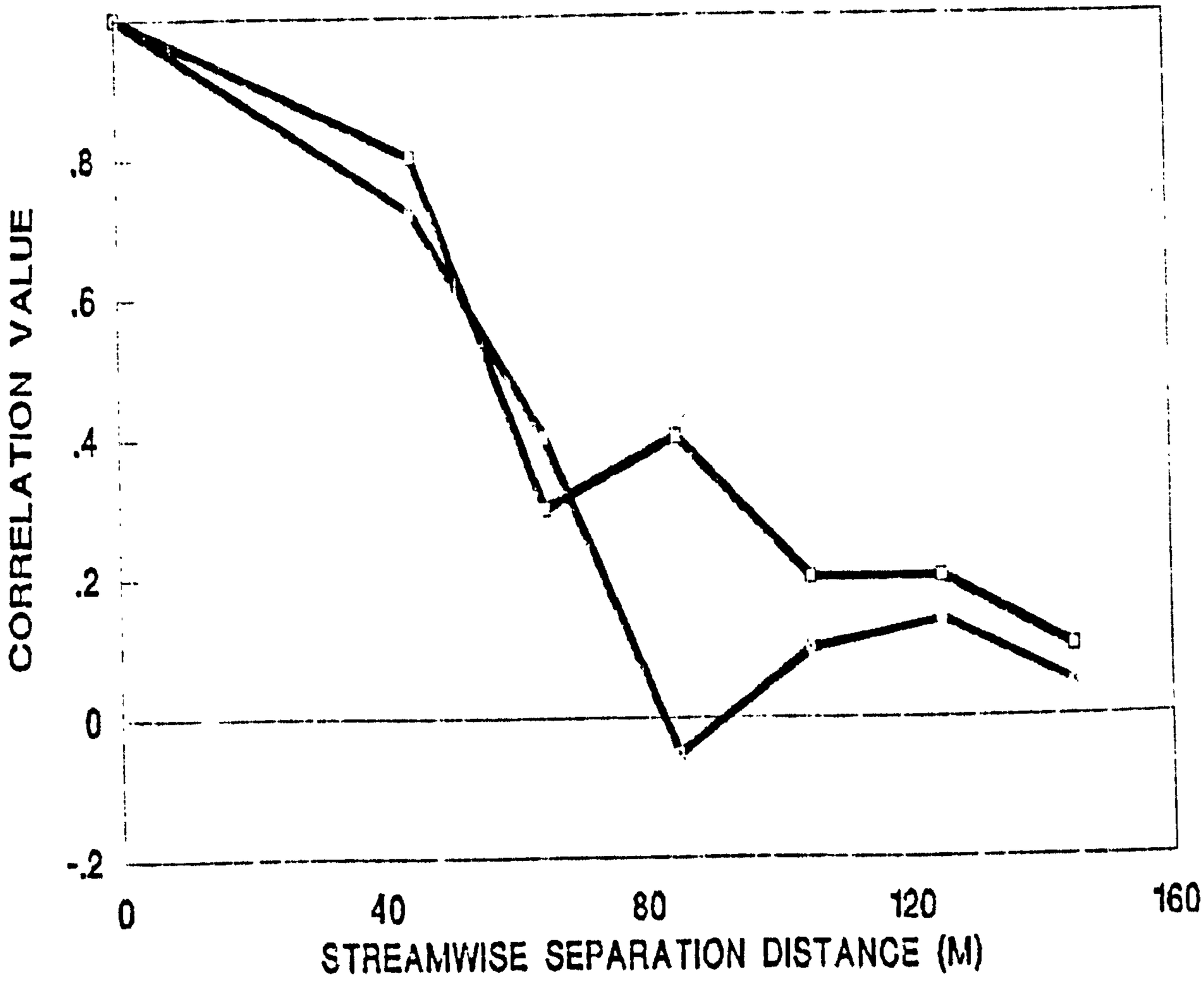

Figure 22. Streamwise spatial correlation.

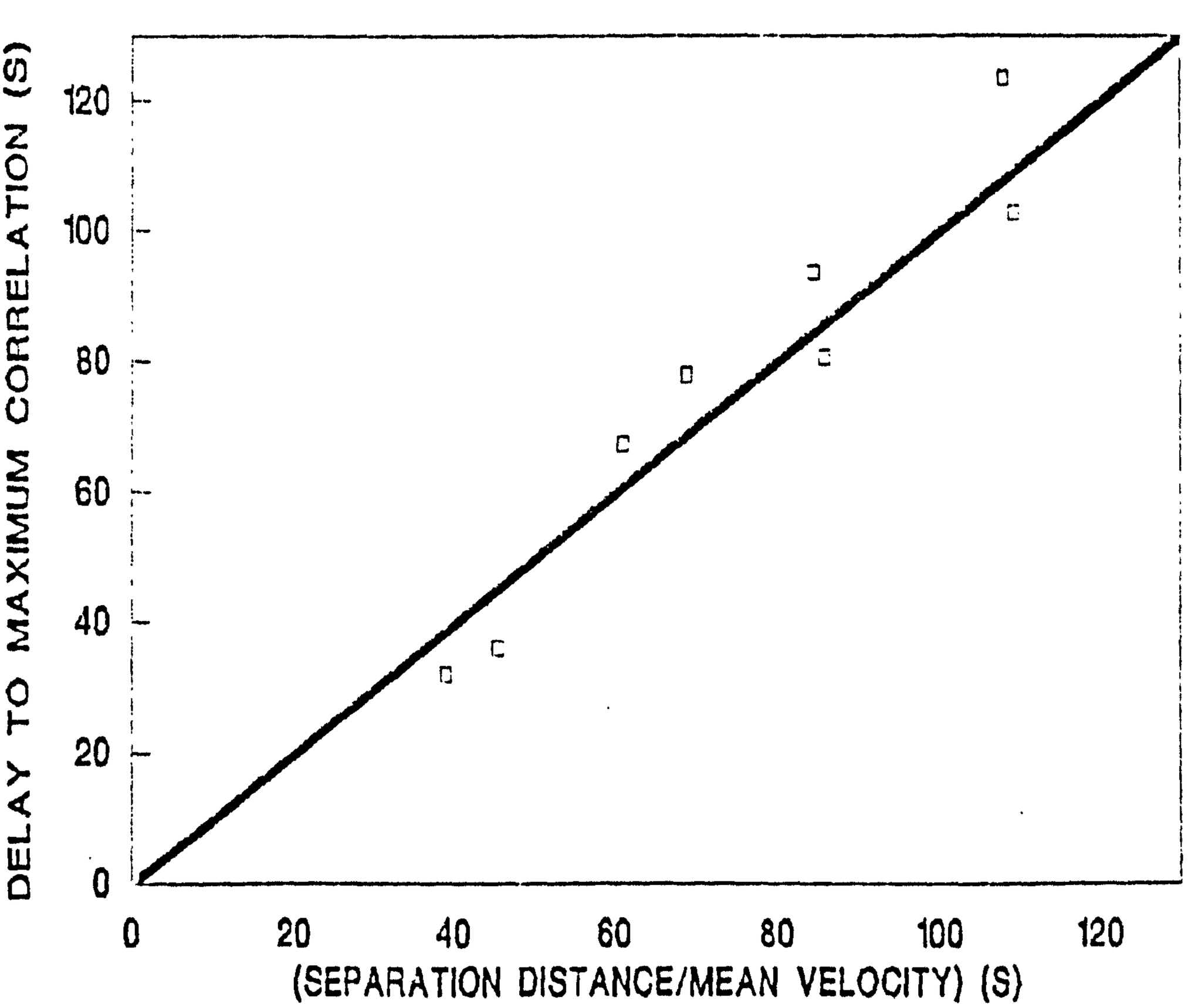

Figure 23. Advection time against transport time at bulk velocity.

therefore taken as the average of the mean currents measured at the two bottom sensors since the bulk flow is found close to 0.4 of the depth in these conditions (Prandle, 1982). It may be seen that the actual and expected time delays in Figure 23 are nearly equal, implying that the largest eddies move at the bulk velocity of the flow as was anticipated in Chapter 3.

CHAPTER 6 PROPERTY VARIATIONS OVER A TIDAL CYCLE

General Characteristics

To investigate the variation of the turbulent properties over a tidal cycle, the 12 hours from the first measured slack water to the second was divided into 2 hour intervals and correlations and spectra produced as before. Figures 24-26 show the results for a typical interval. Each record is 480 samples long and the correlations and spectra have been kept to 50 intervals giving 10 degrees of freedom. This is a compromise between gaining definition and achieving confidence that the spectra reflect the underlying process. The correlations and spectra showed the following characteristics:

a. The frequency at which the spectral peak occurred was the same for both the u and v components and was always close to a frequency corresponding to a period of approximately 350 s. The streamwise correlations show that the eddies are about 30 m "long", implying that the eddy passage time should be between 30 s and 60 s dependent on the mean bulk velocity during the 2 hour interval. The peak is therefore associated with the eddy lifetime as was predicted by the crude model of the bursting sequence given in Chapter 3.

b. The resolution in the spectra was sufficient to show that each spectrum is made up of a set of discrete, but overlapping, peaks. The peak heights followed a σ^{-2} trend at higher frequencies. This was predicted by (4.18) and is not inconsistent with the logarithmic plots in Figures 25 and 26. The frequencies at which obvious peaks occur are at 2 and 4 times the frequency associated with the major peak, indicating that the periods of the eddies causing the peaks follow (2.65).

c. The integral value of all the correlations was close to zero. This indicated that the non-stationary mean flow derived for each of the 2 hour intervals was a good representation. The time delay between each point in the correlations shown in Figures 25 and 26 is the data sampling interval, 15 s. The correlations all had a

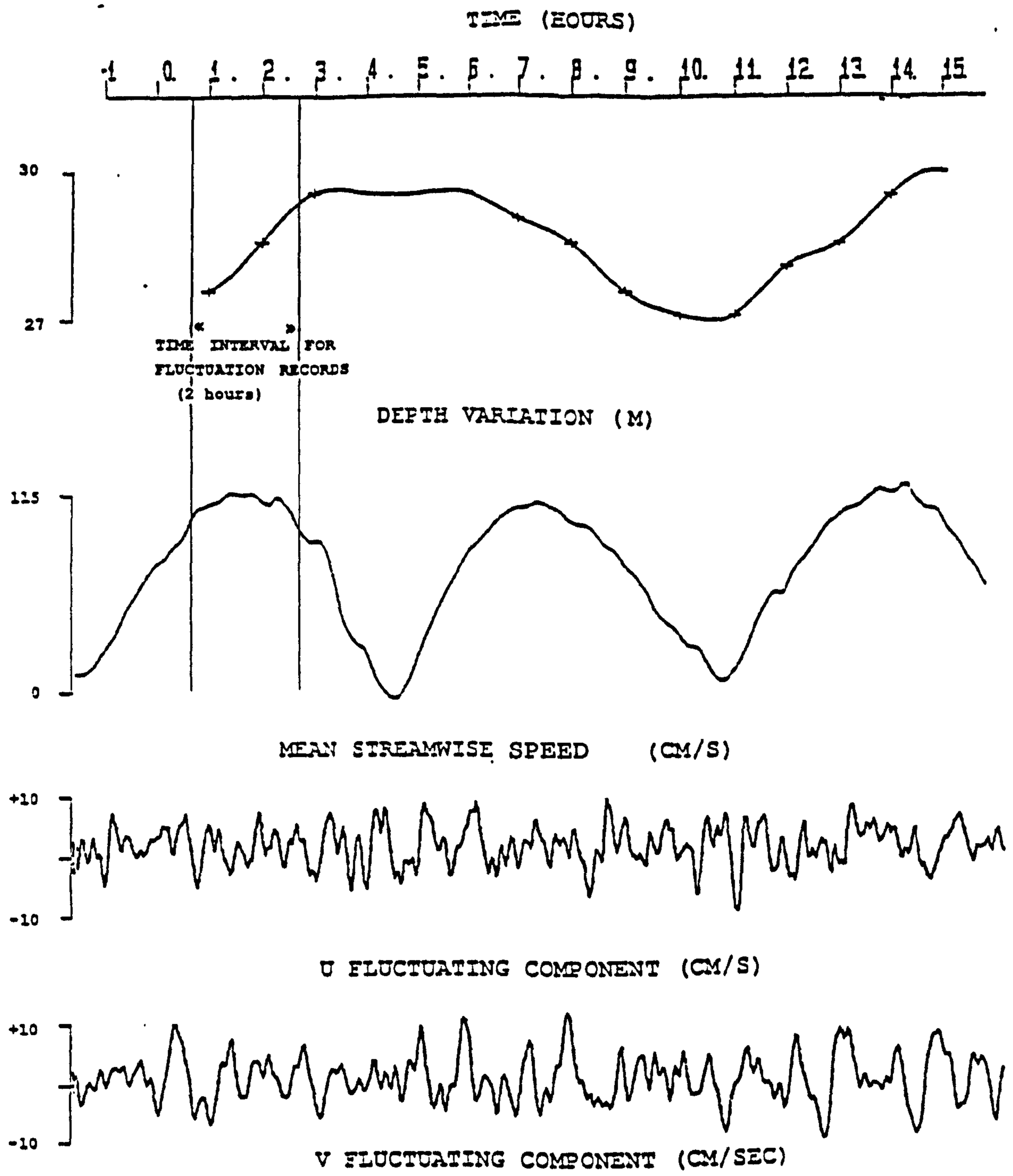

Figure 24. Record from a typical 2 hour interval.

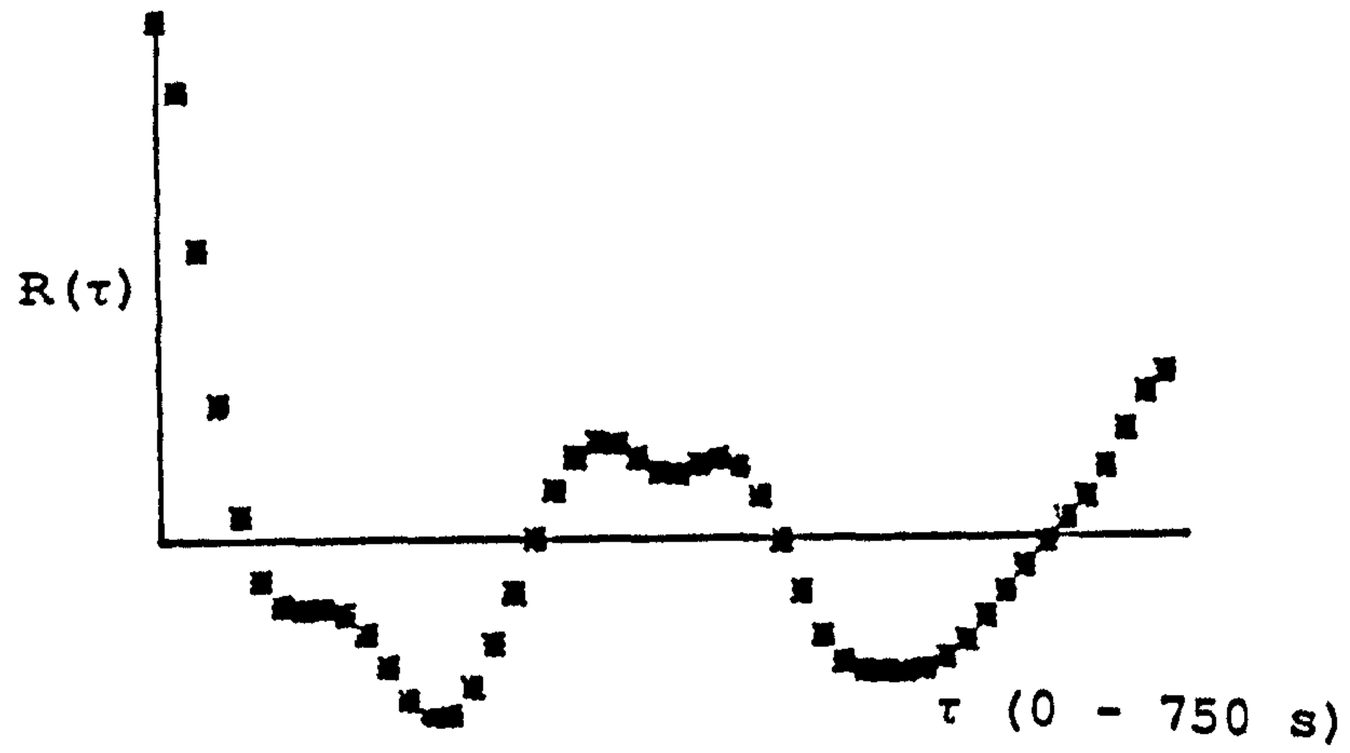

Figure 25. Typical streamwise correlation and spectrum.

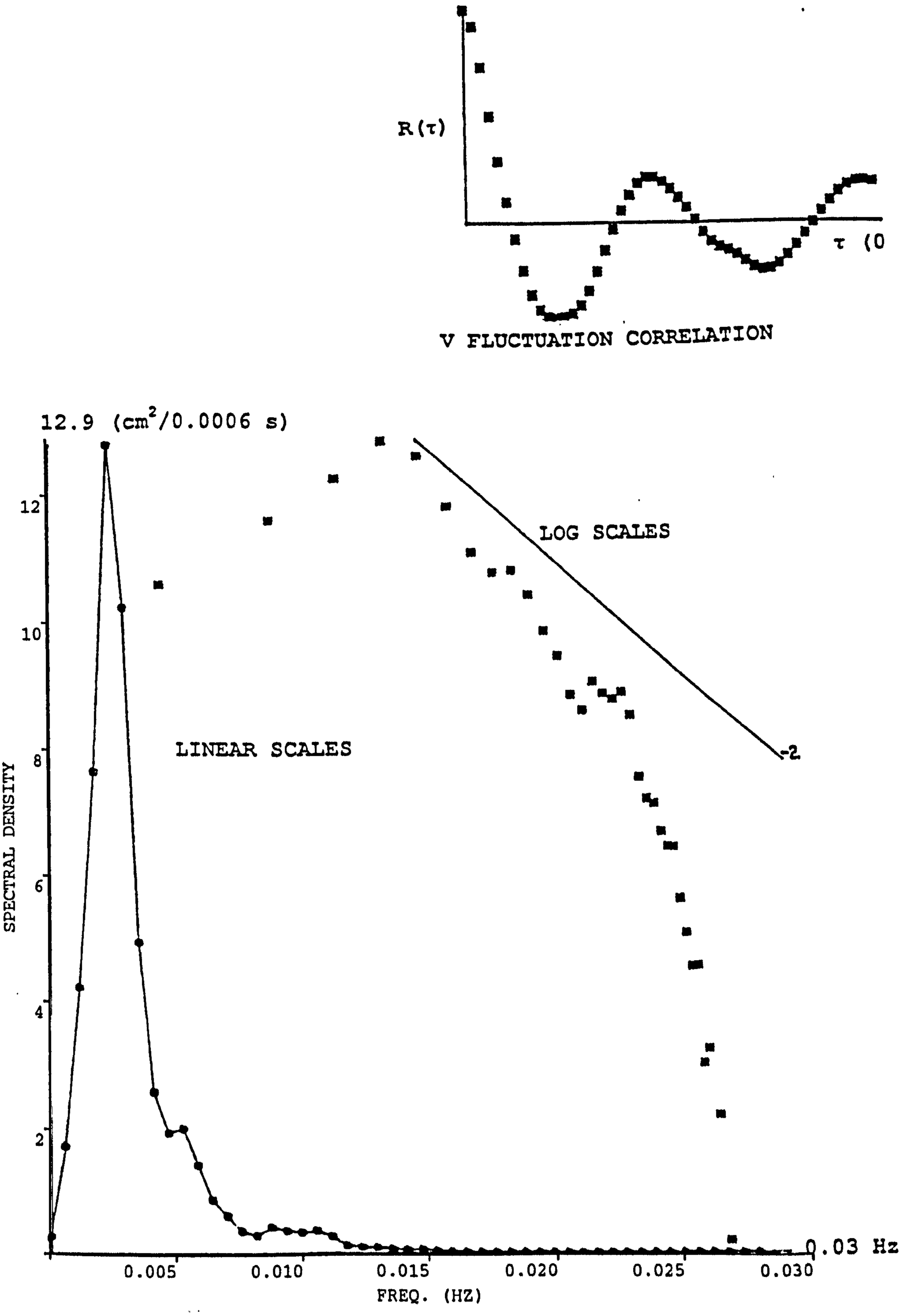

Figure 26. Typical cross-stream correlation and spectrum.

positive value for time delays between 0 and 60 s, indicating that within this period the velocity structure is dominated by a single passing eddy. The integral value always became zero close to a time delay of 350 s, the period corresponding to the frequency of the main spectral peak. The total time lag shown for each correlation is 750 s and a second near sinusoidal positive/negative variation is often apparent when the lag is between 350s and 750s, indicating the recurrent nature of the process.

The mean and fluctuating components from the top and bottom fixed meters are shown in Figure 27. The sum of the component squares, a measure of the horizontal kinetic energy, is shown for later use. Individual component fluctuations from the two meters followed each other consistently, fluctuations at the top meter being sensed 15 - 30 s before the lower. This indicated that the eddies may have a characteristic slope to the vertical of about 45 degrees as suggested by Utami and Uemo (1987). The fluctuations had similar magnitude. The mean streamwise velocities were approximately sinusoidal with the lower meter recording approximately 0.85 the current speed of the upper.

Mean velocity profile variation.

The following equations are repeated for convenience:

$$u_L = \varepsilon^{1/3} L^{1/3} \tag{2.52}$$

$$N = \log L/\lambda \tag{3.18}$$

$$U_0/N = n_L u_L \tag{3.28}$$

$$n_L = U_0/U_1 \tag{3.63}$$

$$U_1/N = u_L \tag{3.65}$$

$$U(h) = n_L u_L \log(h/\lambda) + 1.5 n_L u_L h/L + n_L u_L \tag{3.33}$$

$$\lambda = (\nu^3/\varepsilon)^{1/4} \tag{3.34}$$

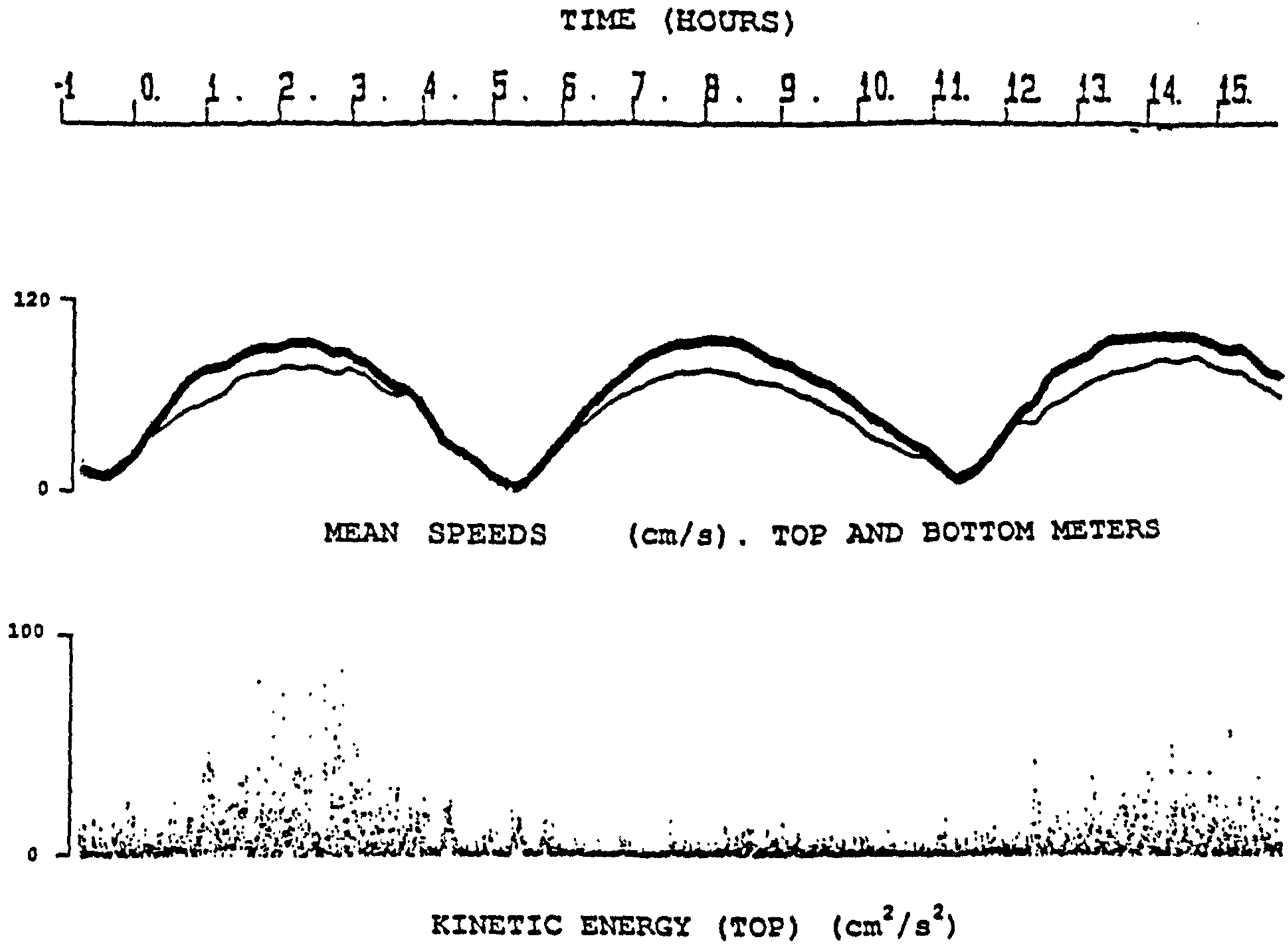

Figure 27. Mean speed and turbulent kinetic energy variation over the whole record, top and bottom fixed meters.

$$\lambda = \frac{h_2}{\exp\left[\frac{U(h_2)\left(\log(h_1/h_2)+(1.5(h_1-h_2)/L)\right)}{U(h_1)-U(h_2)} - \frac{1.5h_2}{L} - 1\right]} \qquad (3.43)$$

The value of λ was calculated over the whole record using (3.43). The mean value of λ was found to be 0.052 cm with a standard deviation of 0.022 cm. Departures from the mean were greatest when the mean current was small and SEASPRING was swinging. Substituting a value for λ of 0.05 cm into (3.34), and using a value for the kinematic viscosity of 0.014 cm^2/s, gives a value for the energy dissipation rate ε equal to 0.3 cm^2/s^3.

Substituting λ into (3.18) and putting L equal to 30 m gives N equal to 11. This is the median of the values derived in Chapter 3.

Substitution of 0.3 cm^2/s^3 as the value of ε into (2.52) and putting L equal to 30 m gives a value of u_L equal to 9.65 cm/s. Substituting this value of u_L into (3.65) with N equal to 11 implies that a value for U_1, the velocity where the turbulence is fully developed, equal to 105 cm/s. This is close to the highest surface velocities measured with the dye releases in part two of the experiment and shown in Figure 27. The necessary implication is that over most of the record the turbulence is intermittent.

<u>The variation of intermittency.</u>

The variation in the intermittency of the turbulence was studied by comparing values directly measured from the data with values calculated from (3.28) using the values of u_L and N calculated above and assuming that the boundary layer occupied the full water depth. The intermittency was assessed in two ways. First the signal was processed to give a plot of measured kinetic energy against time. Figure 28 (top) shows a plot of a portion of this record. The measured kinetic energy record was used since

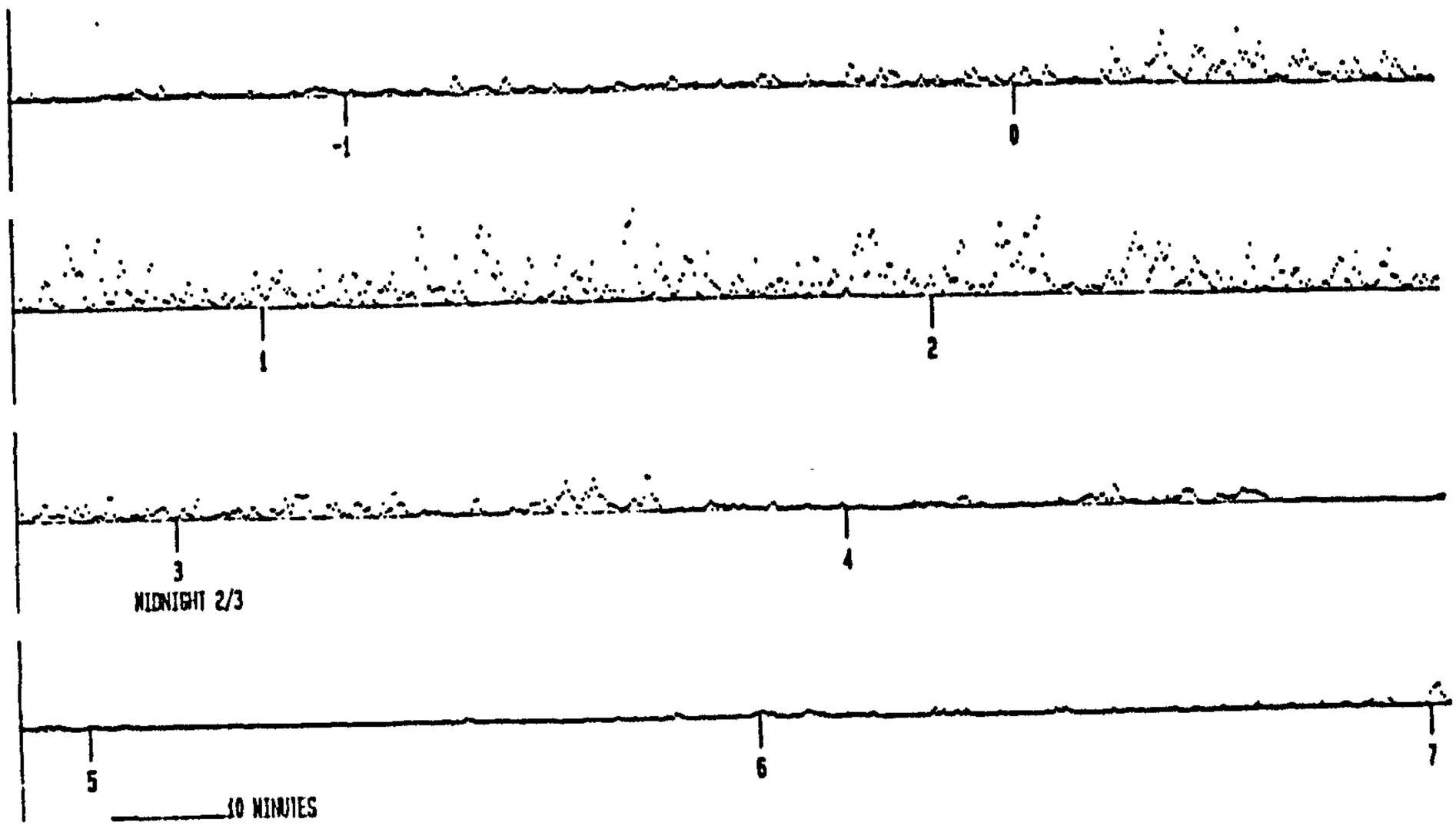

Figure 28. (top): Typical raw kinetic energy plot. (bottom): Kinetic energy plot from cropped spectrum.

being the sum of the squares of the signal it enhanced the peaks and supressed the low values, giving a better indication of the passage of the larger eddies with which the intermittency is associated, especially as the (unmeasured) kinetic energy in the vertical component is known to be well correlated with the streamwise (Heathershaw, 1979).

The intermittency was first determined by assessing where the magnitude of the signal exceeded a threshold value. This threshold was kept the same value throughout the record at a value equal to one half of the maximum peak measured. These results were measured for same 12 intervals as above and are plotted as "n_L-amp" points in Figure 29.

The intermittency was then assessed in the following way. First the u and v component records were calculated and the records Fast Fourier Transformed to produce a complex spectrum. The spectrum was inspected and cropped on either side of the peak so that the only non-zero spectral components remaining were those in a band around the peak. The spectral peak was then transformed back to give modified u and v records which were squared and added. The resulting signal was insensitive to the actual cropping points provided that the peak was retained and a portion is illustrated in Figure 28 (bottom). By retaining only the spectral components around the peak at $1/t_L$ it was expected that the resulting signal would reflect only the large eddy production process. The intermittency was then assessed as the proportion of the time at which energy was apparent in the smoothed signal. These results are plotted as "n_L-t_L" in Figure 29.

The plot of measured versus calculated intermittency in Figure 29 clearly shows that during the flood tides (when the water level is rising) the model formulation correctly reflects the intermittency measured by either method.

The points on Figure 29 which strongly depart from the expected relationship are the "n_L-amp" points for the majority of the ebb tide. Here the calculated intermittency is significant but

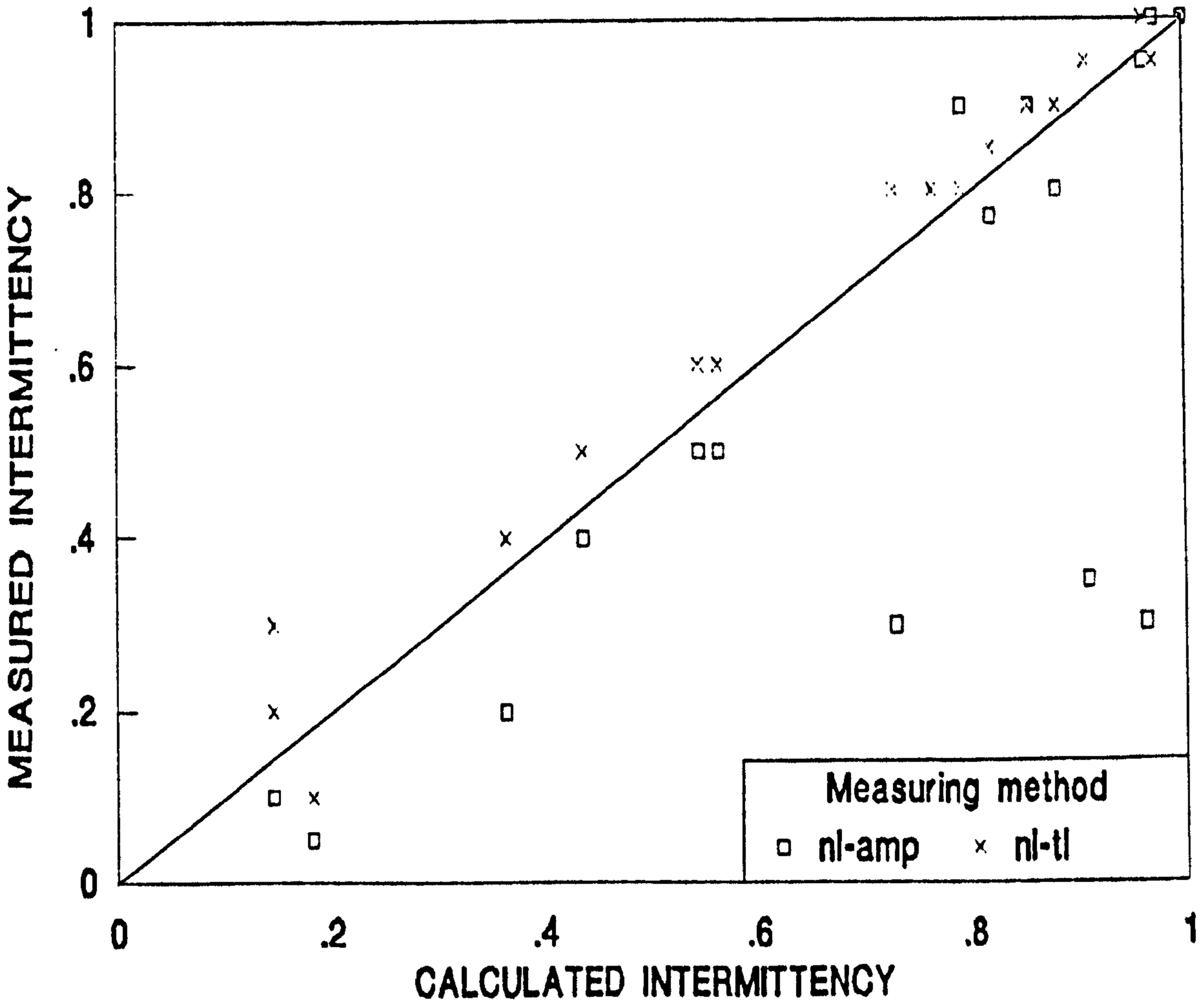

Figure 29. Calculated against measured intermittency.

the magnitude of the measured turbulence was small, despite there still being energy at the $1/t_L$ spectral peak. A detailed investigation of the vertical profile during this period showed an intermittent 10 to 20 fold increase in the value of λ when (3.43) was calculated at every 15 s data interval. This indicated that the boundary layer may have dropped away from the surface at high slack water and taken some time to recover. It is clear from the kinetic energy plot in Figure 27 that there was a reduced level of turbulence during the accelerating phase of the ebb tide (that following the first slack high water) than during either of the flood tides, despite the mean velocity shear being similar in both cases. This will be discussed below.

Calculated values of the energy dissipation rate.

Figure 29 shows good agreement over the flood tides for ε equal to 0.3 cm^2/s^3. This value also gives a value of the Kolmogorov scale, λ, here associated with the profile roughness length, equal to that derived from a fitted logarithmic profile and well within the range that Heathershaw (1979) and Soulsby (1982) give as typical for this type of sea-bed. The derived value of λ also gives a number of eddy sizes, N, equal to 11, which is as predicted in Chapter 3 and consistent with Yalin's (1977) sand-dune results.

The energy dissipation rate was calculated from the u and v spectra calculated for each 2 hour interval. The average value of the intermittency was assessed from the mean current and Figure 29 and (4.18) was used to calculate ε from the most linear part of the logarithmic spectral plots. Recalling:

$$\phi(\sigma) = 0.5\ n_L \varepsilon\ \sigma^{-2} \qquad (4.18)$$

The result of the 12 calculations was a mean value of ε of 0.28 cm^2/s^3 with a standard deviation of 0.09 cm^2/s^3. Given the sensitivity to the resultant value to exactly where the spectral curve fitting was made this is considered a very stable result.

The energy dissipation rate was then calculated from (2.52)

which may be rewritten as:

$$\varepsilon = L^2/t_L^3 \qquad (7.1)$$

The calculation was performed for the 12 intervals used in the intermittency calculation. The periods, t_L, were measured from the cropped kinetic energy plots (Figure 28(bottom)). The period t_L was taken as the mean time for which a peak existed within each interval. The mean measured value of ε derived in this way was found to be 0.304 cm^2/s^3 with a standard deviation of 0.02 cm/s. Here there was no correction for intermittency and the result was more stable.

The dissipation rate ε was also assessed by making the reasonable assumption that at some stage during the record the full value of u_L would be measured in one velocity component by one of the current meters. Searching through the record for this maximum value gave u_L equal to 9.55 cm/s at a depth water depth of 29.5 m in the middle of period 2 of the experiment. This corresponded to a value of ε from (7.1) equal to 0.295 cm^2/s^3.

The values for ε found in this thesis are shown in Table 3 along with those measured by other authors in similar conditions. The energy dissipation rate remains substantially constant over the tidal cycle and has a value close to 0.3 cm^2/s^3. This result was tested against oil and dye release experiments made in a 45 m water depth and reported in Chapter 8. An immediate test was made by modelling the mean velocity profiles found over the cycle. A plot of measured and calculated profiles is shown in Figure 30. The best fit was achieved by using a mean profile given by (7.2):

$$U(h) = n_L u_L \log(h/\lambda) + 1.5 n_L u_L (h/L) + 0.5 n_L u_L \qquad (7.2)$$

the maximum error being 4% at the peak of the ebb tide. The inputs to the equation were calculated as follows:

REFERENCE	SOURCE	VALUE
Table 1	Tidally averaged estuary values	0.23
Table 1	Surface layers of tidal flow	0.51
Heathershaw (1979)	Revised estimate	0.41
Woods (1975)	Ensemble average	0.31
This thesis	Fitting of logarithmic profile	0.30
This thesis	Frequency spectra (4.18)	0.28
This thesis	Lifetime relationship (7.1)	0.30
This thesis	Maximum fluctuation (7.1)	0.29

Table 3. Summary of values of energy dissipation rate (cm^2/s^3).

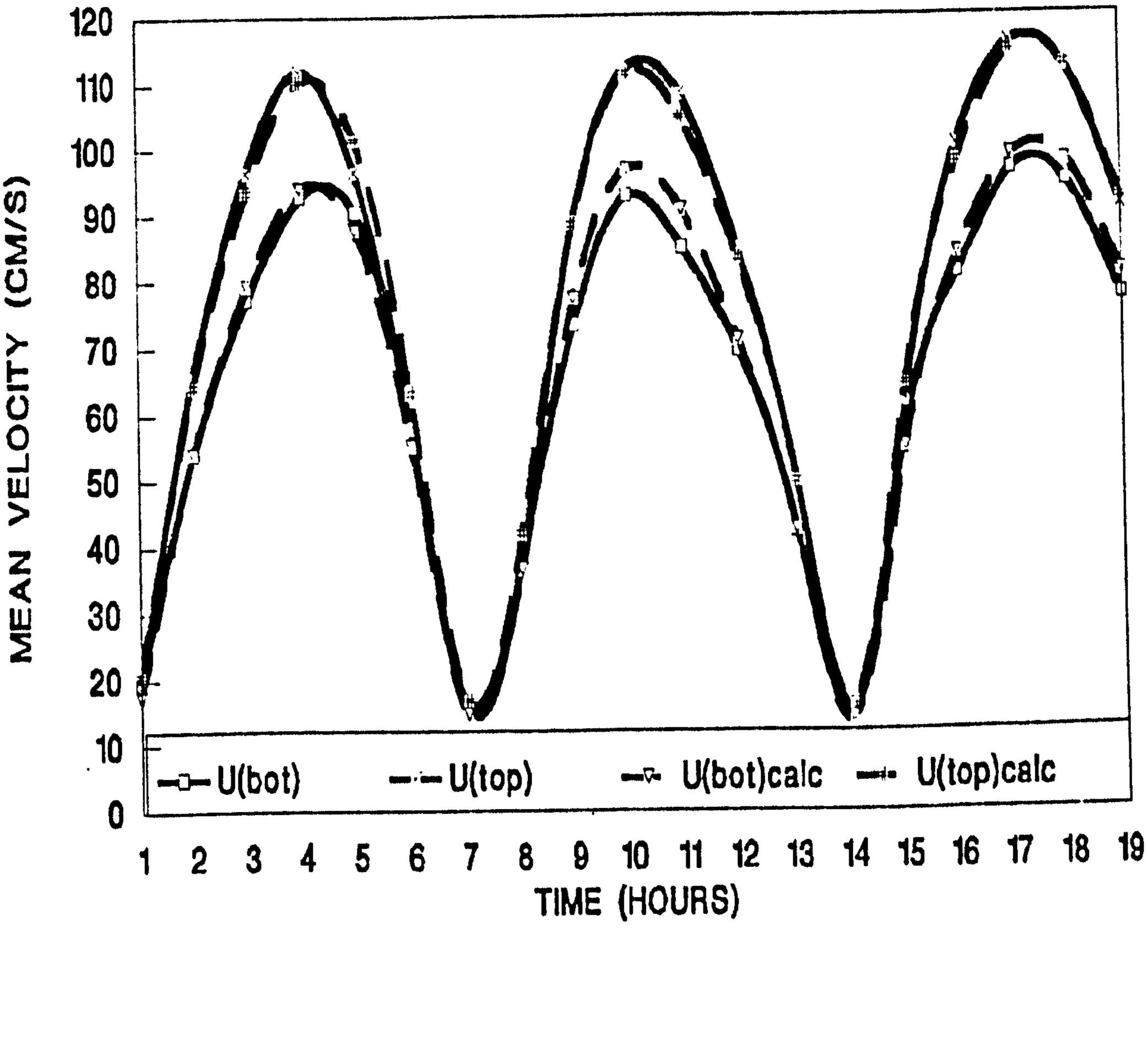

Figure 30. Calculated against measured mean velocities.

PARAMETER	
$U_{mean} = (U(h_1) + U(h_2))/2$	mean velocity found at 0.4 water depth - Chapter 3
$L = $ water depth	assumes boundary layer has reached the water surface
$u_L = \varepsilon^{1/3} L^{1/3}$	(2.52) with $\varepsilon = 0.3$ cm^2/s^3
$n_L = U_{mean}/11u_L$	(3.23) with N = 11
$\lambda = 0.05$ cm	(3.27) with $\nu = 0.014$ cm^2/s

Equation (3.33) was derived in Chapter 3 for eddies mixing momentum away from the bottom momentum at a constant rate:

$$U(h) = n_L u_L \log(h/\lambda) + 1.5 n_L u_L (h/L) + n_L u_L \qquad (3.33)$$

Comparing (3.33) with (7.2):

$$U(h) = n_L u_L \log(h/\lambda) + 1.5 n_L u_L (h/L) + 0.5 n_L u_L \qquad (7.2)$$

shows that the best fitting profile is as derived in Chapter 3 but with the criterion that:

$$U(\lambda) = 0.5 n_L u_L \qquad (7.3)$$

which is descriptive of a viscous sublayer of thickness λ at the wall. If the velocity distribution within this layer is linear we can write (Soulsby,1983):

$$\tau_0 = \rho\nu (\partial U/\partial y)_0 \approx \rho\nu n_L u_L/2\lambda \qquad (7.4)$$

which using (2.52) and (3.23) gives:

$$\tau_0/\rho \approx \upsilon U_0/2N \qquad (7.5)$$

where υ is the Kolmogorov dissipation scale velocity (Heathershaw 1979). If the boundary layer has grown to occupy the whole depth and ε is constant then (7.5) predicts that the bed stress should be directly proportional to the mean velocity. This is contrary to the constant stress layer hypothesis (Soulsby, 1983) which relates the square of the calculated friction velocity to the bed stress and predicts that the stress varies as U^2. Since from (3.50):

$$u^*/K = n_L u_L \qquad (3.50)$$

so that since n_L is proportional to U_0, u^{*2} is proportional to U_0^2 and (7.5) does not predict an equivalence between bed stress and Reynolds stress.

Tidal hysteresis

As has already been noted there was a reduced level of turbulent fluctuation measured by the current meters during the accelerating phase of the ebb tide. During this period the following effects were apparent:

a. The depth of water remained at the high water level while the mean velocity accelerated to almost its maximum ebb value. This is a phenomenum not noted after each slack low water where the water depth increased immediately the flood tide commenced.

b. The calculated value of λ increased during this period, indicating that the boundary layer had dropped away from the surface. There was insufficient accuracy in the method of calculating the mean profile from only two sensors to quantify by how much.

c. There was still an energy peak in the frequency spectra from this period at a frequency corresponding to a period of 350 s, i.e. to the lifetime of the largest eddies. The magnitude of the observed fluctuations was reduced.

d. The r.m.s. values of the streamwise and cross-stream

fluctuations were measured by both direct calculation and by measuring the total area under each derived spectrum. The results are plotted against mean current in Figure 31. The r.m.s. fluctuation level appears to follow a linear trend but with only half the value on the ebb as against the flood.

Development of the mean flow profile.

Below a velocity equal to $(U_1/2^{1/2})$, it is possible for the velocity profile between the bed and h = L/C to be created by a boundary layer of thickness L or L/C. From (3.63) at $U_0 = U_1/(2^{1/2})$:

$$n_L = 1/(2^{1/2}) \tag{7.6}$$

and from (2.52) with boundary layer thickness L:

$$n_L u_L = \varepsilon^{1/3} L^{1/3}/(2^{1/2}) \tag{7.7}$$

If the boundary layer is at L/C and is fully developed so that:

$$n_{L/C} = 1 \tag{7.8}$$

then from (2.52) and using $C = 8^{1/2}$:

$$n_{L/C} u_{L/C} = u_{L/C} = \varepsilon^{1/3}(L/C)^{1/3} = \varepsilon^{1/3} L^{1/3}/(2^{1/2}) \tag{7.9}$$

since (7.7) and (7.9) have the same value then the profile given by (7.2) will be the same. Above $U_0 = U_1/(2)^{1/2}$ it is not possible to mimic the mean profile with the smaller eddies otherwise their intermittency, $n_{L/C}$, would have to be greater than unity. A study of Figure 30 shows that the mean velocity at the top and bottom sensors became close at velocities less than about 75 cm/s. With $\varepsilon = 0.3$ cm^2/s^3 and N = 11, (3.65) gives $U_1 = 105$ cm/s, $U_1/(2^{1/2}) = 74$ cm/s. When the mean velocities at the top and bottom sensors are equal than the boundary layer has certainly dropped from the surface. It appears that the surface layers will not be affected by bottom generated turbulence at velocities less than about $U_1/(2)^{1/2}$, a velocity found 1-2 hours either side of slack water.

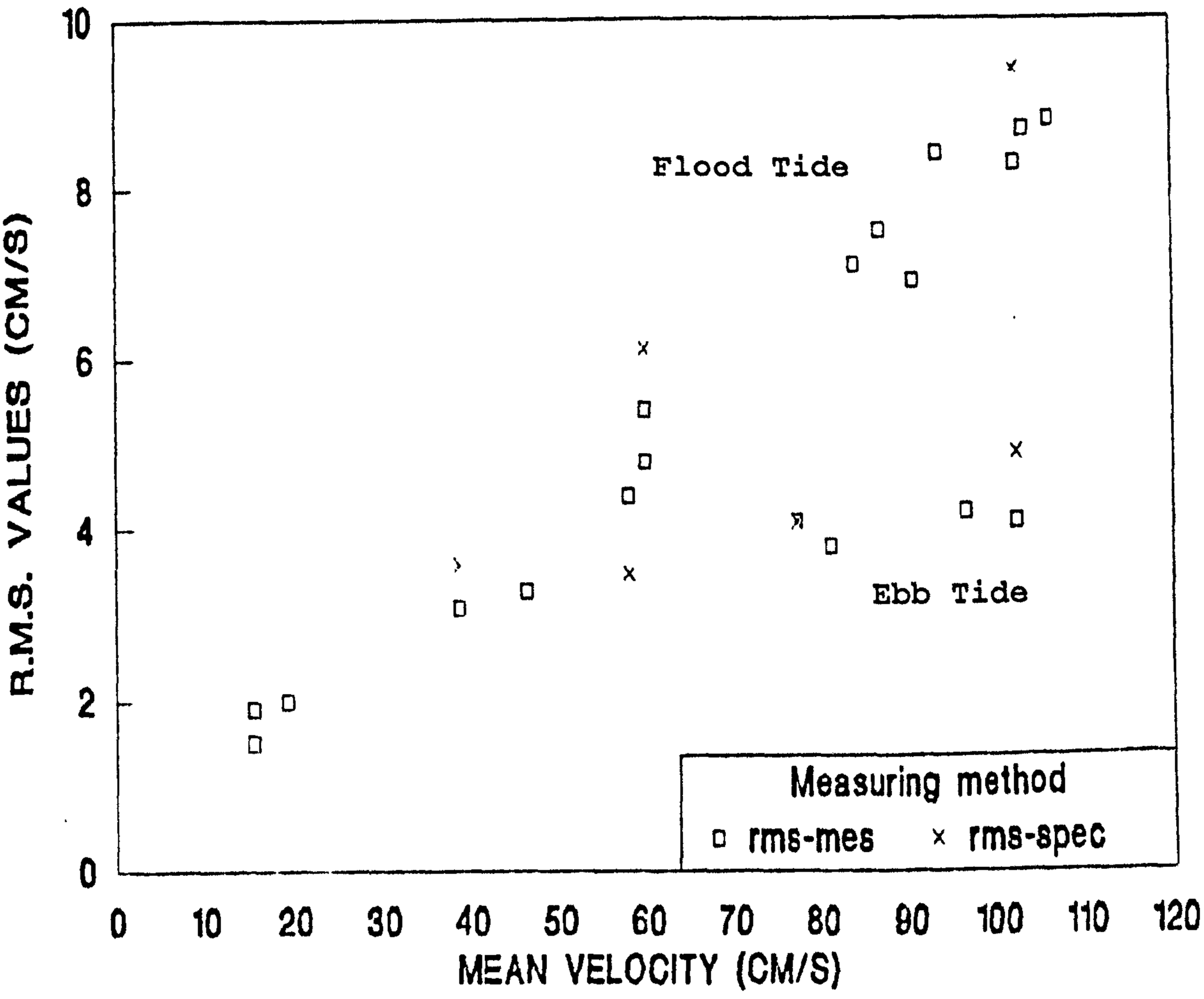

Figure 31. Measured r.m.s. fluctuation values plotted against mean velocity.

Modelling the tidal hysteresis.

The derivation of the mean velocity profile given in Chapter 3 can be changed to model the observed hysteresis above $U_0 = U_1/(2)^{1/2}$. The profile (7.3) is written in the following way for the boundary layer having thickness ℓ, where $\ell < L$:

$$U(h) = (L/\ell)^{1/3} n_L u_\ell (\log(h/\lambda) + 1.5h/L + 0.5) \qquad (7.10)$$

which reduces to (7.3) whatever the value of ℓ. The kinetic energy density in the production process, k_{prod}, is written as, following (2.66):

$$k_{prod} = (\ell/L)(3/2) n_L^2 u_\ell^2 \qquad (7.11)$$

$$(r.m.s.)_{prod} = (k_{prod})^{1/2} \qquad (7.12)$$

which is again correct when $\ell = L$. Equation (7.10) allows the mean profile to be modelled above $U_1/(2)^{1/2}$ without n_ℓ having to become greater than unity. Equation (7.11) predicts r.m.s. values which agree well with observation if the boundary layer remains at L/C over the ebb tide. Figure 32 plots the r.m.s. values from (7.12) against the measured values used in Figure 31, showing the agreement.

The calculated value of u^{*2} is found by modifying equation (3.49) to write:

$$u^{*2} = 0.3 (L/\ell)^{2/3} n_L^2 u_\ell^2 \qquad (7.13)$$

which preserves the relationship between u^{*2} and the turbulent kinetic energy given by (3.48) and gives values for the drag coefficient which fall within the band given by Bowden and Ferguson (1980) as typical of those found in the sea. The drag coefficient, Cd_{100} is defined from:

$$u^{*2} = Cd_{100} U_{100}^2 \qquad (7.14)$$

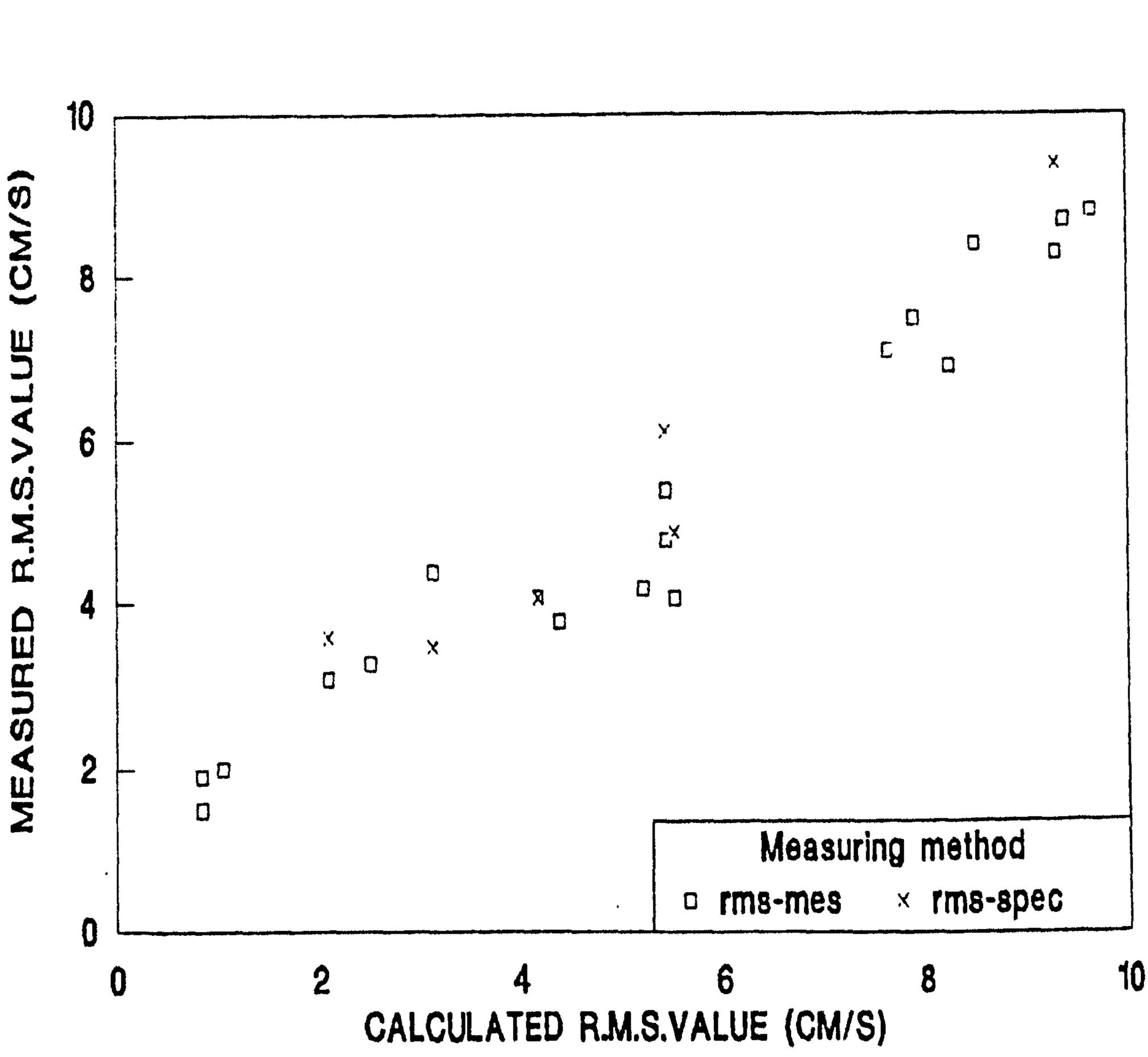

Figure 32. Calculated against measured r.m.s. fluctuation values.

and U_{100}, the velocity 1 m above the bed, is calculated from (7.2). Figure 33 plots the calculated values of the ratios given by (7.13) and (7.14), with the largest eddy size, ℓ, assumed to be L (equal to the water depth) on the flood, and L/C on the ebb.

Equations (7.10) and (7.13) are consistent with the Reynolds stress correlation being the driving function behind the mean velocity profile. To model the observed mean velocity the Reynolds stress has to remain proportional to u_L^2. Equation (7.11) for the kinetic energy implies that the production process reflects the total kinetic energy in the boundary layer, averaged over the full depth of water. Writing the total kinetic energy in the boundary layer, $KE_{\text{per unit area}}$, as:

$$KE_{\text{per unit area}} = \ell(3/2)u_\ell^2 \qquad (7.15)$$

then the kinetic energy density, k_{prod}, is given by:

$$k_{prod} = KE_{\text{per unit area}}/L = (\ell/L)u_\ell^2 \qquad (7.16)$$

which is of the same form as (7.11).

The description of the observed hysteresis by (7.10) and (7.11) is inconsistent with any theory that relates the Reynolds stress with the velocities within individual eddies. The stress is amplified by a factor, f, given by:

$$f = (L/\ell)^{2/3} \qquad (7.17)$$

for which no justification is immediately apparent. Furthermore when the boundary layer has largest eddy size L/C, the momentum is still transferred a distance L from the bed and the spectral peak remains at $1/t_L$. It is possible that the boundary layer has indeed grown to L but that the kinetic energy of the turbulence has remained at a lower level. If this is so then it may be that the boundary layer energy remains at preferred, discrete levels. Such discretisation of preferred energy levels is to be expected from the non-linearity of the governing equations. To investigate

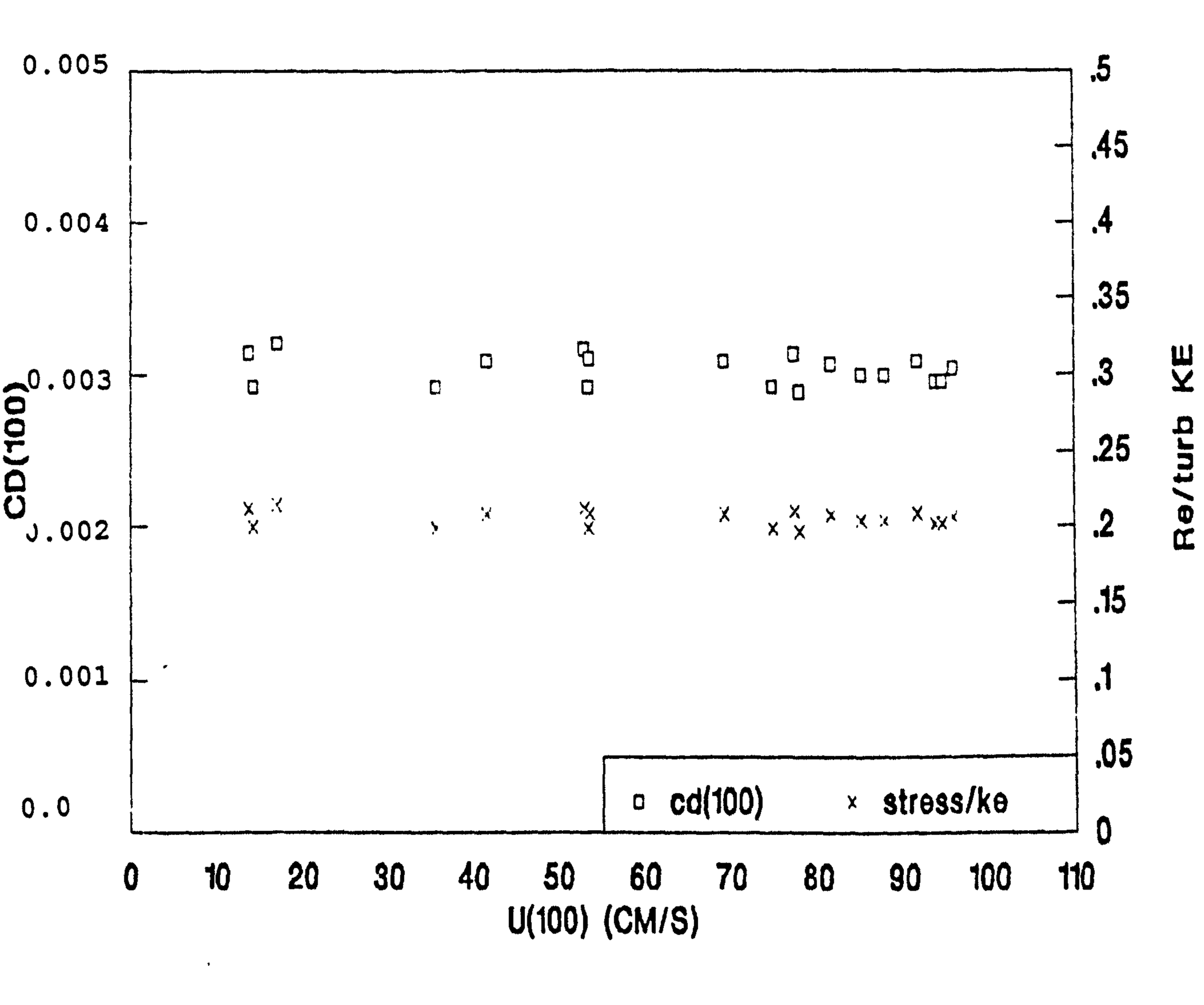

Figure.33. Calculated Cd_{100} and the ratio of $u*^2$/(turbulent KE) against U_{100}.

whether this phenomenum might occur it is necessary to study the time variation of the spectral components associated with the large eddies, those components lying around the spectral peak at $1/t_L$.

The component attractor.

It is difficult to calculate meaningful spectra from short records since to keep sufficient degrees of freedom to reproduce the underlying process a small number of Fourier calculation points has to be employed, resulting in a low level of resolution in the spectra. To try and elucidate the detailed variation in energy at the spectral peak frequency, $1/t_L$, it was decided to isolate those parts of the original signal associated with the peak. This was attempted by mathematically filtering the original signal to leave only Fourier components close to the spectral peak. Bendat and Piersol (1971) do not recommend any filtering method as being suitable for non-stationary data sets and Kinsman (1965) shows that the filtering method itself characteristically disturbs the output signal.

Two unrelated filtering techniques were therefore used and the results compared to establish whether the underlying process was being adequately represented. The first technique was to use the Hanning process (Chapter 5) and the second to use the direct cropping of Fast Fourier Transforms in the same manner as was used to produce the kinetic energy signal in Figure 28.

The Hanned results are discussed first. The raw speed and compass direction data were repeatedly smoothed using the Hanning process before u and v components were calculated. The effect of the smoothing was evaluated by plotting successive values of a resulting component against each other in three dimensions (a technique borrowed from chaos theory). At 100 smoothings the emergence of an underlying structure to the signal was unmistakable. Figure 34 shows a three dimensional plot of the resulting components u_{i-1}, u_i, u_{i+1} against each other for 200 smoothings. A few successive points have been connected to show the elliptical structure. The figure is flat, three-dimensional

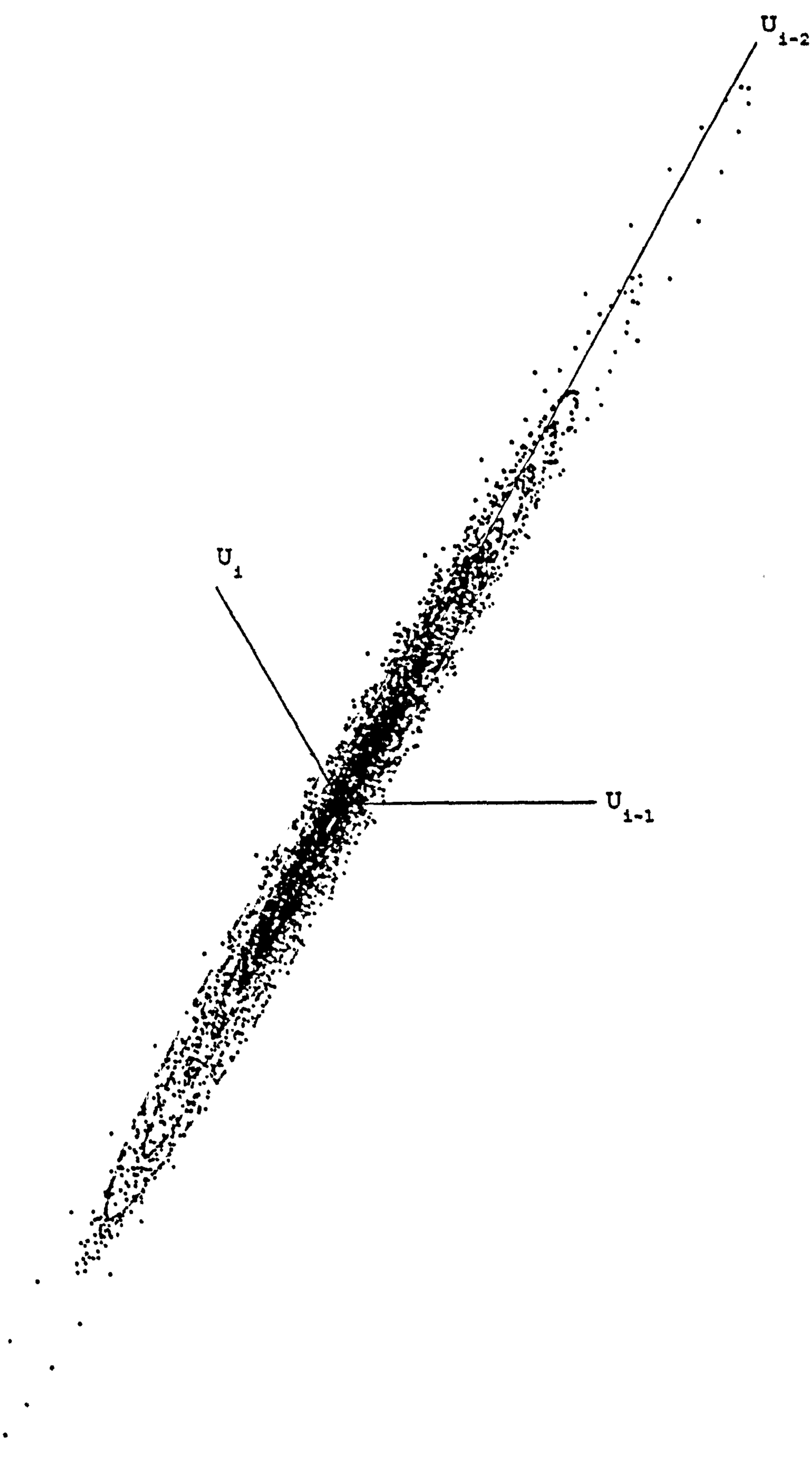

Figure 34. Three dimensional plot of successive u component values after smoothing of data.

and like an elongated set of Saturn's rings which never repeats itself. A similar plot is found for the v component. The plot appears to be a low dimensional manifestation of the strange attractor which may underlie the turbulent process. It will be termed a component attractor for convenience.

A more physically meaningful component attractor is shown in Figure 35. This is a plot of the derived u component against its change, Δu, in the preceding time step. It has a similar form to Figure 34. The v component attractor is similar but a little more symmetrically distributed. In this figure all the points have been connected by a smooth curve, but the basic period of each ellipse, however large, is 350 s, the period of the spectral peak.

To check that the attractor was not a function of the smoothing process the data were processed using Fast Fourier Transforms. The u and v components were produced from the raw data as described in Chapter 5 and the Fast Fourier Transform of the records produced using the FFT algorithm in the NAG FORTRAN library. The transform consists of a complex representation of the signal spectrum consisting of a number of pairs of discrete Dirac spikes equal to the total number of data points. These are evenly spread in frequency space between 0 and the Nyqist folding frequency.

The complex spectra were cropped by setting the values of the Dirac pairs to zero except for a chosen band around the spectral peak. The resulting complex series were transformed back to u and v signals which contained only the chosen band of Fourier components. As the allowed band was narrowed around the peak, the resulting plot of the component attractor again appeared. Its characteristics are identical to that produced by the Hanning process. If the cropping band is chosen carefully the attractors can be made almost identical.

Figure 36 is a plot of u against Δu achieved by the FFT technique. In this plot the spectra was severely cropped to demonstrate the gapped structure in the rings. It may be seen that

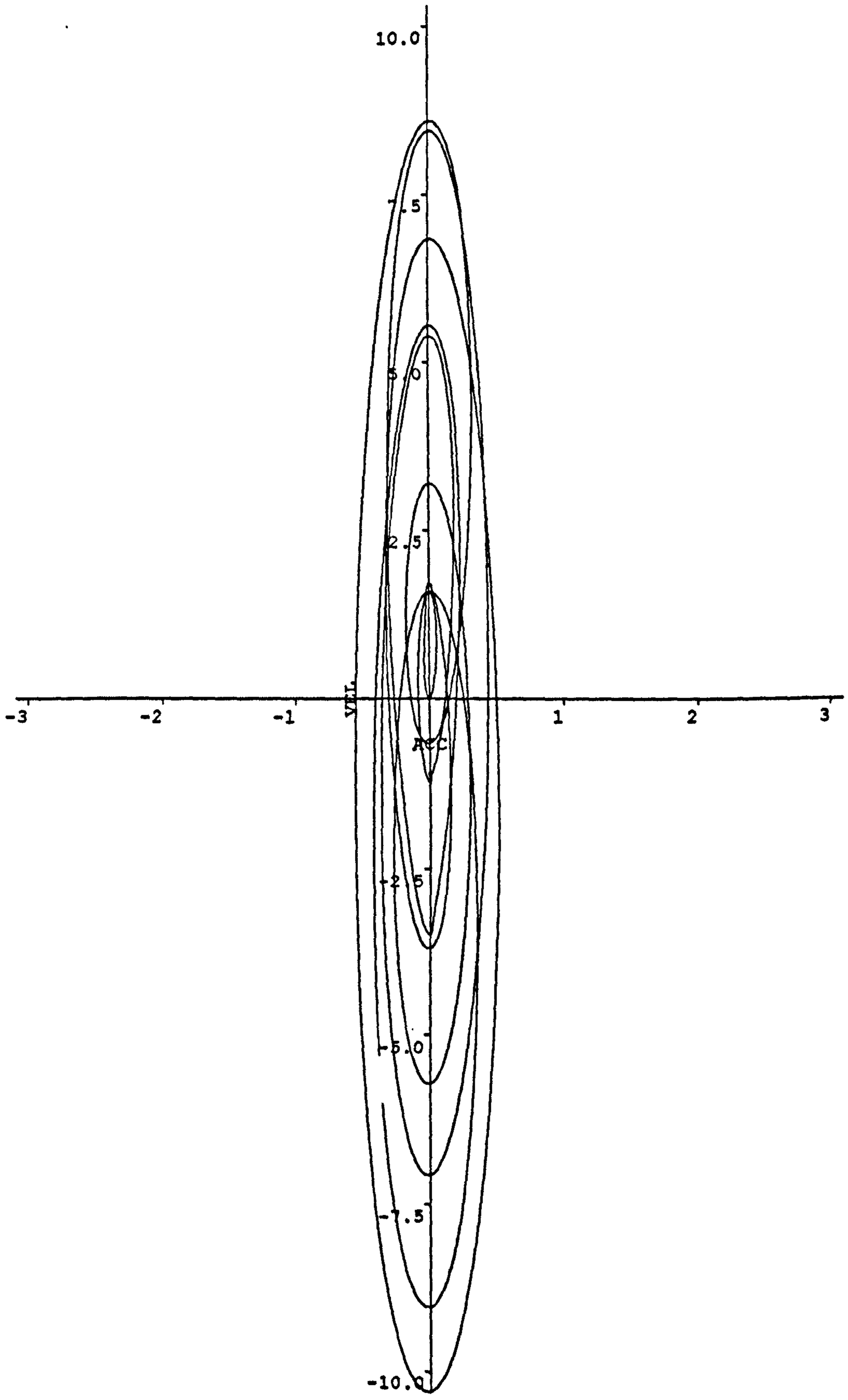

Figure 35. Plot of u against Δu.

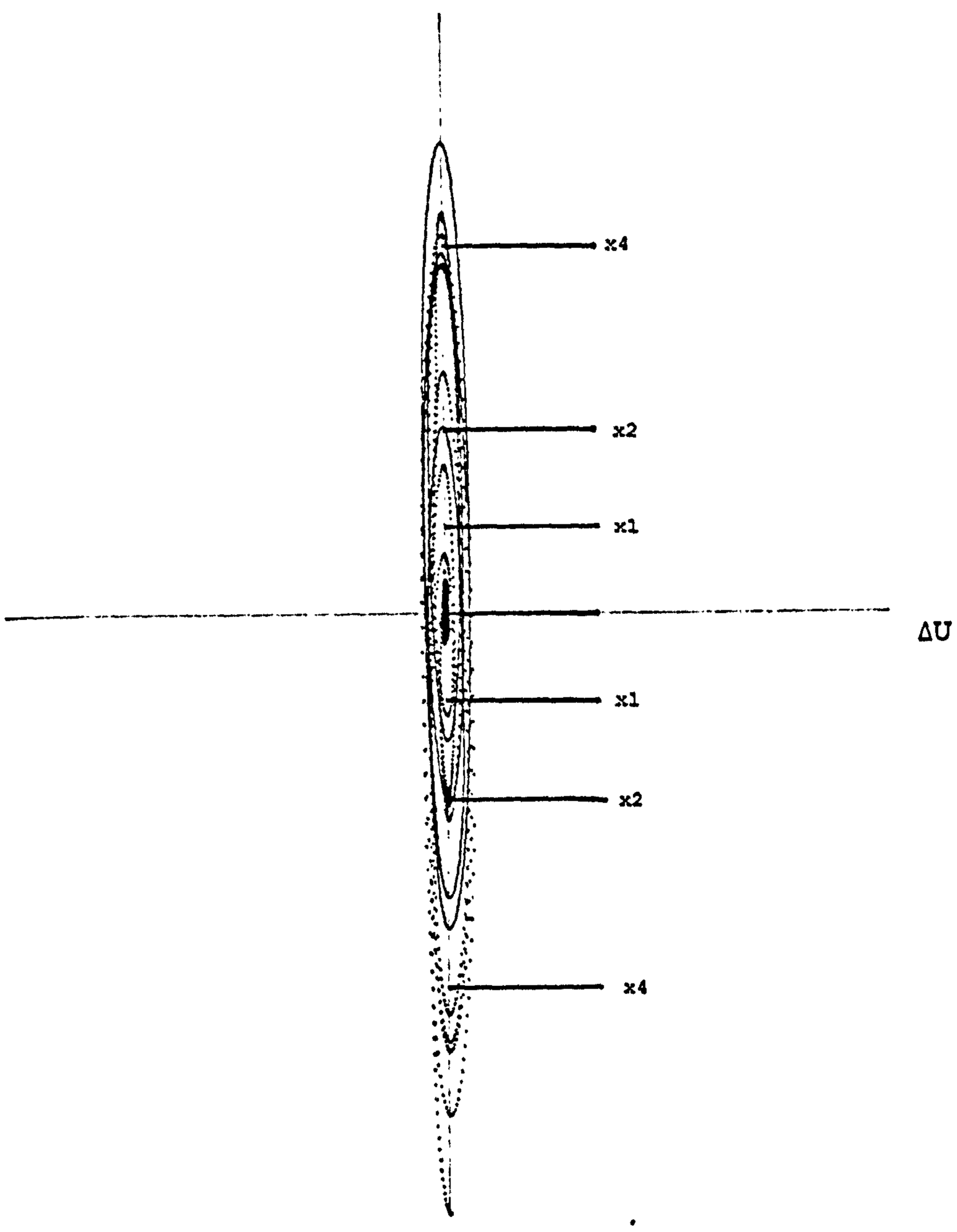

Figure 36. Plot of u against Δu achieved by cropping FFT spectrum.

the rings, although never repeating, are grouped in geometric series, each group having major axis magnitudes which are approximately half the next larger group. The implication is that over the record as a whole the kinetic energy at the frequency spectral peak tends to sit at discrete levels, each a factor of four different from the adjoining levels. As expected, the attractor was approximately half the size on the ebb as on the flood.

CHAPTER 7. A COMPUTER SIMULATION OF DISPERSION AT THE SEA SURFACE

A numerical model was written to test the dispersion theory derived in the preceding chapters. This code was developed on the PRIME mini-computer in the Department of Nuclear Science and Technology, Royal Naval College, Greenwich. The program was written in FORTRAN and used the NAG library facility for some statistical functions and GINO for the graphical output. The dispersion experiments against which the theory was to be tested were essentially two-dimensional measurements taken in the near surface region of the sea. These will be described in the next chapter. It was therefore decided that the code should only model two dimensions to save computing time. The code was subsequently extended to three-dimensions but is presented here in its two-dimensional form for simplicity, the extension being straight-forward.

Inputs to the program.

The following parameters were input to the program, several factors being included so a sensitivity analysis could be undertaken before the code was simplified to its final form:

PARAMETER	UNITS
Water Depth	m
Current Speed	m/s
Intermittency	$0.0 \leq$ intermittency ≤ 1.0
Spatial Anisotropy Factor	non-dimensional ≥ 0.0
Velocity Anisotropy Factor	non-dimensional ≥ 0.0
Correlation Factor	$0.0 \leq$ correlation factor ≤ 1.0
Switch Factor	$0.0 \leq$ switch factor ≤ 1.0
Spatial Randomness Factor	$0.0 \leq$ spatial randomness factor ≤ 1.0
Velocity Scalar	non-dimensional ≥ 0.0
Time Step	s
Energy Dissipation Rate	cm^2/s^3
Number of Eddy Sizes	non dimensional integer ≥ 1

The release was modelled as a continuous source from a fixed point. The current flowing past the point was assumed to be

rectilinear and steady during the release period. The release was one hour in duration and one marked particle was released at each time-step. The bottom turbulence was modelled as a sequence of fields of rectangular eddies which were superimposed over the marked particles as they moved with the mean current. The cross-stream dimension of the largest eddy size was equal to the water depth. The streamwise dimension was made equal to the cross-stream multiplied by the spatial anisotropy. The probability that a large eddy site was active was given by the intermittency factor which was calculated independently for each site using a random-number generator.

Whenever a grid of eddy sites was laid over the moving particles the physical position of the grid could be allowed to vary randomly using the spatial randomness factor. The marked moving particles were collected into the grid elements so that each set of particles within an eddy site were influenced by an eddy if the site was active. Since particles within an eddy do not leave it during its lifetime, the grids were placed and the particles collected only at the start of each eddy size lifetime. The group of particles influenced by each eddy were then given a velocity which continued to act on them throughout the lifetime of that grid, or eddy, size.

The code first calculated the counter for the main computational loop, and the lifetime count for the largest eddy size, (t_L divided by the time-step), from (2.42). Since eddies whose lifetime was less than the time-step could not be modelled, the code calculated the maximum number of eddy sizes that could be accommodated gave an error message if this was larger than the number demanded.

Counters were then calculated which were used in the main computational loop to determine at which step each eddy grid should be laid and velocities given to the grouped particles if the site was active. Lifetime counters were calculated for each size and used to decide at which step induced velocities should be lost. There was a small systematic error in the calculation due to

the use of integer counters. This was reported as an output and was generally found to be less than one percent.

Sorting the particles into discrete eddies.

The random number generator was initialised and the release started at a random stage of large eddy lifetime. The model commenced by updating the number of particles released and by initialising working array elements. The maximum dimensions of the existing pattern of particle positions was calculated so that eddy grids could be kept as small as possible.

A counter was used to check whether an eddy size should be initiated. If an eddy size smaller than the largest was due to commence then a sorting subroutine was called. A separate subroutine was called for the largest size. This was necessary since the smaller sizes occur only half as frequently as the largest size in the discrete eddy cascade. The streamwise or cross-stream eddy step length appropriate to that size was calculated and passed to the sorting subroutine. This defined the isotropic displacement vector component which eddies of that size were capable of achieving during their lifetime. The various methods which were used to parametise the motions induced by a particular eddy size are discussed further below.

The sorting subroutines divided the step-length by the lifetime count appropriate to the size to give an incremental length for each pass of the main loop. Particle position arrays which were used to keep track of the particles were shifted by a proportion of the eddy dimension dependent on the spatial randomness factor and saved as temporary working arrays. These were then used for particle sorting. Temporary arrays were then created to hold particle positions as integer multiples of eddy dimension appropriate to the grid in question. Further working arrays held the accurate position of each particle as a remainder in grid dimensions. Integer counters then selected each eddy in the grid in turn. A counter then sorted through the integer arrays to determine which particles were in that particular eddy site.

Having calculated the incremental step for the particles within that eddy grid site, velocity arrays associated with each particle were updated. The velocity arrays were multi-dimensional, each dimension holding the displacement required for a particular eddy size per main loop time-step. These velocity arrays were then returned to the main computational loop. The final part of each sorting subroutine updated the velocity arrays for the particles released since the size was last called. This was necessary to ensure a realistic discharge near the source while allowing sorting only at the beginning of each eddy life, rather than at every time-step.

The main loop continued by updating the particle position arrays by summing the elements of velocity arrays associated with each particle. A streamwise contribution from the mean flow was included in this position update. Since the smaller eddy sizes only exist for half their recurrence time a resetting subroutine then tested for the end of each small eddy size lifetime and returned the elements of the arrays velocity arrays to zero when required.

The model then established a sampling box whose size and position were defined as input parameters. The mean concentration and particle velocities in such a box were taken as representative of a fixed eulerian sensor. The particle velocities were calculated from the differences between particle positions at successive time-steps. A series of such boxes was generated in a cross-stream and stream-wise array, allowing eulerian spatial correlations and cross-correlations, frequency and wave number spectra and concentration intermittencies to be calculated. The correlations and cross-correlations and the frequency and wave-number spectra were calculated using the Blackman-Tukey method described in Chapter 5 (Bendat and Piersol, 1971). Lagrangian statistics could be calculated by following the motion of a series of particles and averaging.

Isotropic random eddy velocities.

The first implementation of the code gave all the particles

within an eddy grid site the same velocity. This formulation was chosen for its computational simplicity and because after many eddy lifetimes it produced realistic dispersion statistics.

Since two-dimensional surface mixing was being modelled, the particles were given randomly generated cross-stream and streamwise eddy velocities. These were calculated using (2.41) and by assuming that the vertical velocity component was completely suppressed at the surface. Brumley and Jirka (1987) have carried out near-surface turbulent velocity component measurement in a grid-stirred tank and shown that the vertical component is suppressed exponentially as the surface is approached, the energy being equally distributed to the horizontal components. Thus writing u for the streamwise fluctuation and v for the cross-stream:

$$k_\ell = \varepsilon^{2/3}\ell^{2/3} \qquad (2.41)$$

$$u^2 + v^2 = 2k_\ell \qquad (2.74)$$

The absolute value of the surface velocity generated by (2.74) and the input value of the energy dissipation rate could be varied using the velocity scalar. The induced surface velocities could be made anisotropic using the velocity anisotropy factor and neighbouring eddies could be made more or less likely to have velocity vectors in the same direction as each other using the correlation and switch factors.

Each time a grid was placed and a site selected a random number between zero and one was chosen and compared with the intermittency factor to determine if the site should be active. A second random number was compared with the switch factor to determine whether the incremental step should be positive or negative. A further similar comparison with the correlation factor determined the extent to which the signs of the cross-stream and streamwise steps should be correlated.

Results of the sensitivity analysis.

Typical output from the program is shown in Figure 37. The values for the input parameters are printed at the top of the figure and the eddy grid sizes on the right hand side. The width of the largest eddy size is equal to the water depth, 45 m in Figure 37. The following results were apparent after the sensitivity analysis:

a. The program ran very quickly when only calculating the large eddy grid, the particle tracking calculation for 1200 particles being completed in 2 or 3 s CPU time on the PRIME computer. The computing period became very much longer as the smaller eddy sizes were included, taking approximately 15 minutes CPU time for 3 eddy sizes. This is a function of the exponentially increasing number of FORTRAN DO loops containing IF statements.

b. The dispersion was unaffected by the smallest eddy sizes, being primarily driven by the large eddy size and the value of ε, which determines the frequency with which the large eddies appear and the velocity they produce. This is expected from (2.81) where the absolute dispersion coefficient was calculated from the sum of the coefficients from a cascade of eddy sizes:

$$\sigma^2 = (7/6) n_L u_L^2 t_L \, t \qquad (2.81)$$

c. The dispersion coefficient produced by the realisation followed equation (2.81) with a velocity scalar and velocity anisotropy both equal to 1, the coefficient being linearly dependent on n_L. If only the largest eddy size was modelled, then as Figure 38 shows, the dispersion coefficient was slightly reduced to $n_L u_L^2 t_L$ and the program gives a cruder realisation of the dispersion while running very much more quickly. The correlation factor and switch factor both distorted the dispersion pattern but had little affect on the amplitude of the meandering. The spatial randomness factor had no effect on the realisation except close to the source.

d. Although the meandering in Figure 37 is only crudely represented, the sensitivity analysis showed that the meandering

DEPTH = 45.0 M
SHIP SPEED = 1.0 M/S
INTERMITTENCY = 1.0
SPATIAL ANISOTROPY = 3.0
CORELLATION = 0.5
SPATIAL RANDOMNESS = 1.0
VELOCITY SCALAR = 1.0000
SWITCH FACTOR = 0.50

VELOCITY ANISOTROPY = 1.0
TIME STEP = 3.0 SECS
EPSILON = 0.90
NO OF EDDY SIZES = 3
SYSTEMATIC TIME ERROR = 0.43%

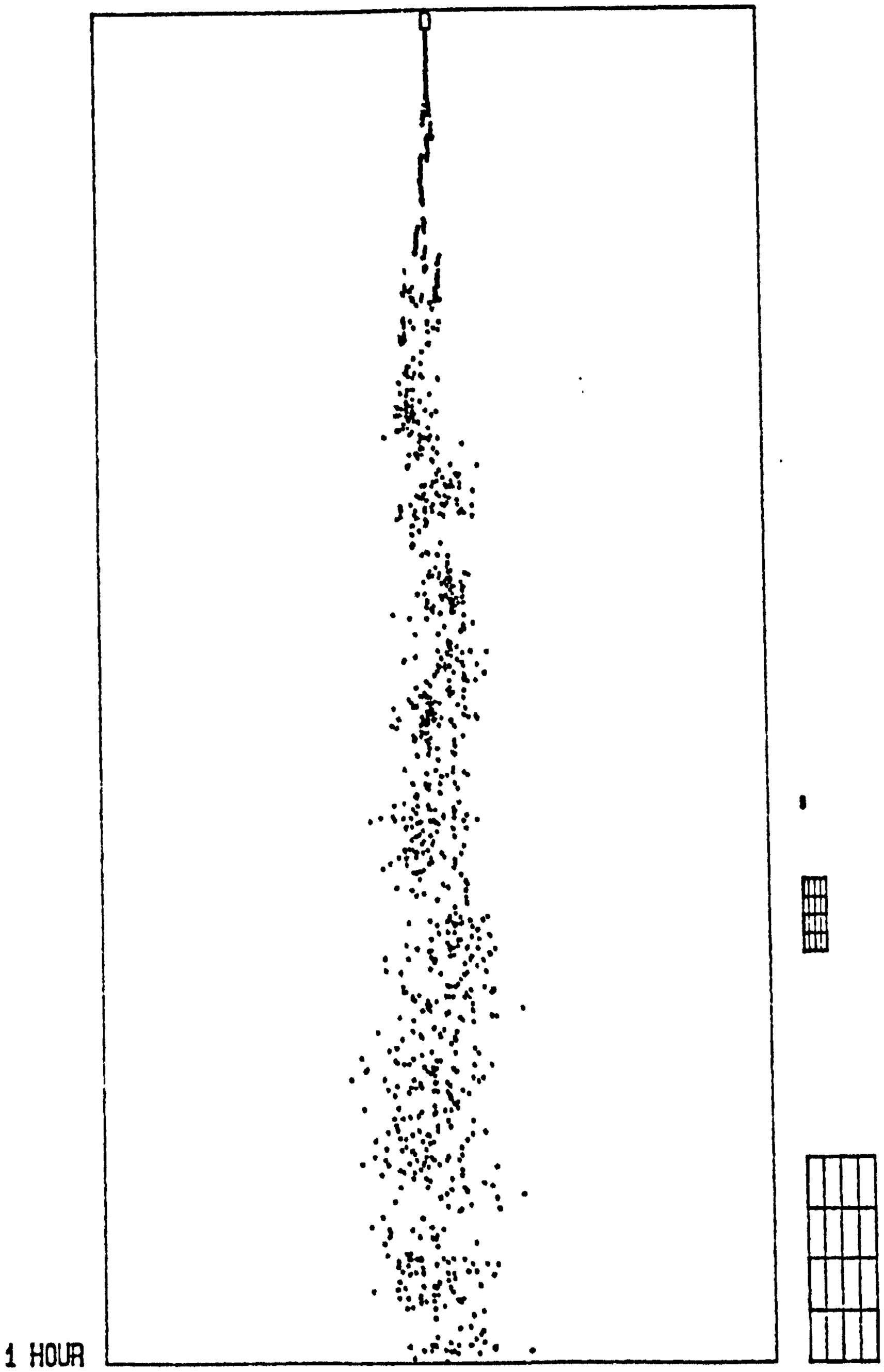

Figure 37. Dispersion from 3 eddy sizes.

DEPTH = 45.0 M
SHIP SPEED = 1.0 M/S
INTERMITTENCY = 1.0
SPATIAL ANISOTROPY = 3.0
CORELLATION = 0.5
SPATIAL RANDOMNESS = 1.0
VELOCITY SCALAR = 1.0000
SWITCH FACTOR = 0.50

VELOCITY ANISOTROPY = 1.0
TIME STEP = 3.0 SECS
EPSILON = 0.90
NO OF EDDY SIZES = 1
SYSTEMATIC TIME ERROR = 0.10%

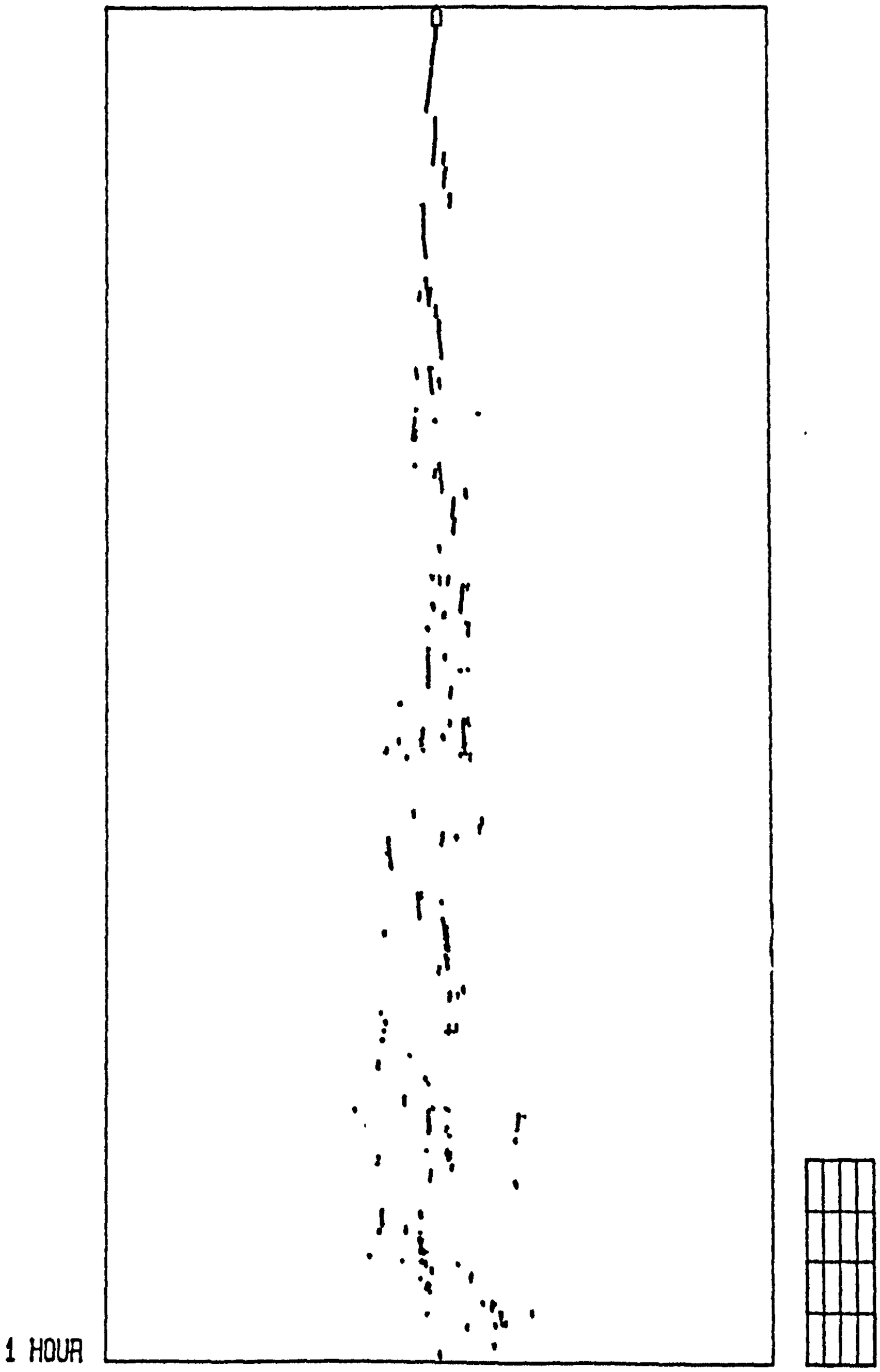

Figure 38. Dispersion from 1 eddy size.

wavelength and spatial anisotropy were linearly related, the wavelength being approximately equal to the large eddy streamwise dimension.

e. The sampling box size from which particle statistics were calculated was a variable of the program. After trying a range of sizes a sufficiently detailed measure of intermittency was produced by using a square box whose dimension was equal to the water depth. Figure 39 shows the average cross-stream intermittency from a sampling line made up of ten such boxes. Figure 39 allows a measure of absolute plume spreading to be calculated. An ensemble average of these intermittency plots was found to quickly approach a Gaussian distribution. The standard deviation of the Gaussian distribution increased with the square root of time as expected and the dispersion coefficient followed (2.81) dependent on the number of eddy sizes included in the model.

Figure 40 shows the Eulerian concentration fluctuation measured as a time series. This gives a measure of the peakiness of the signal as measured at a point. This plot was used for comparison with a dye release experiment described in the next chapter.

Implementation of the model.

In the light of the sensitivity analysis the velocity scalar, velocity anisotropy, spatial randomness, correlation and switch factors were removed as input parameters to the program. The values were fixed as follows:

PARAMETER	VALUE	EFFECT
Velocity scalar	1.0	eddy velocities as predicted by equation (2.74).
Velocity anisotropy	1.0	u and v fluctuation amplitudes equal.
Spatial randomness	0.0	no shift in grid position between implementations.

DEPTH = 45.0 M
SHIP SPEED = 1.0 M/S
INTERMITTENCY = 1.0
SPATIAL ANISOTROPY = 3.0
CORELLATION = 0.5
SPATIAL RANDOMNESS = 1.0
VELOCITY SCALAR = 1.0000
SWITCH FACTOR = 0.50
SAMPLING POSITION. STREAMWISE = 600.00M.
VELOCITY ANISOTROPY = 1.0
TIME STEP = 10.0 SECS
EPSILON = 0.90
NO OF EDDY SIZES = 1
SYSTEMATIC TIME ERROR = 0.81%
SAMPLING BOX SIZE = 30.00M

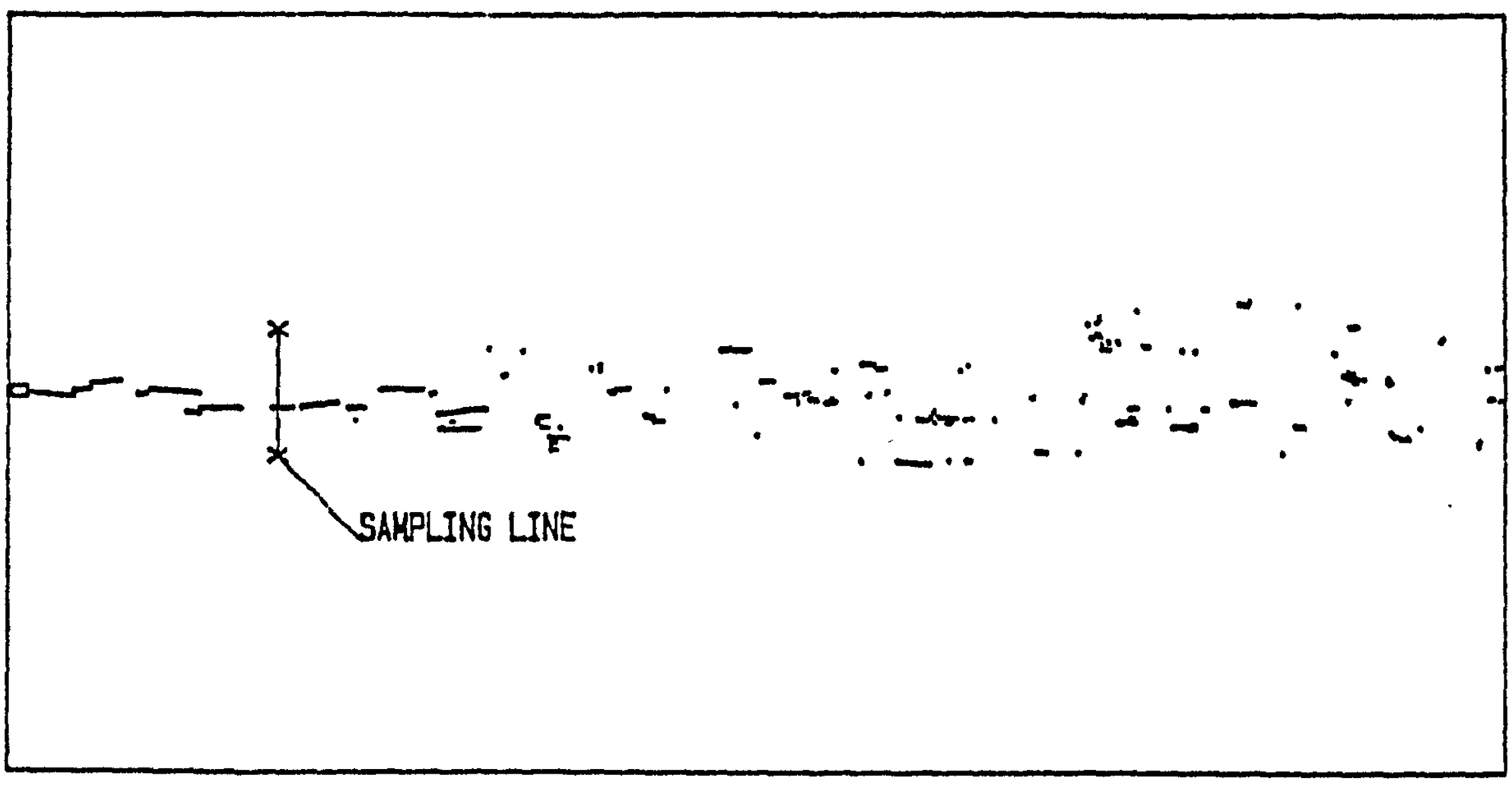

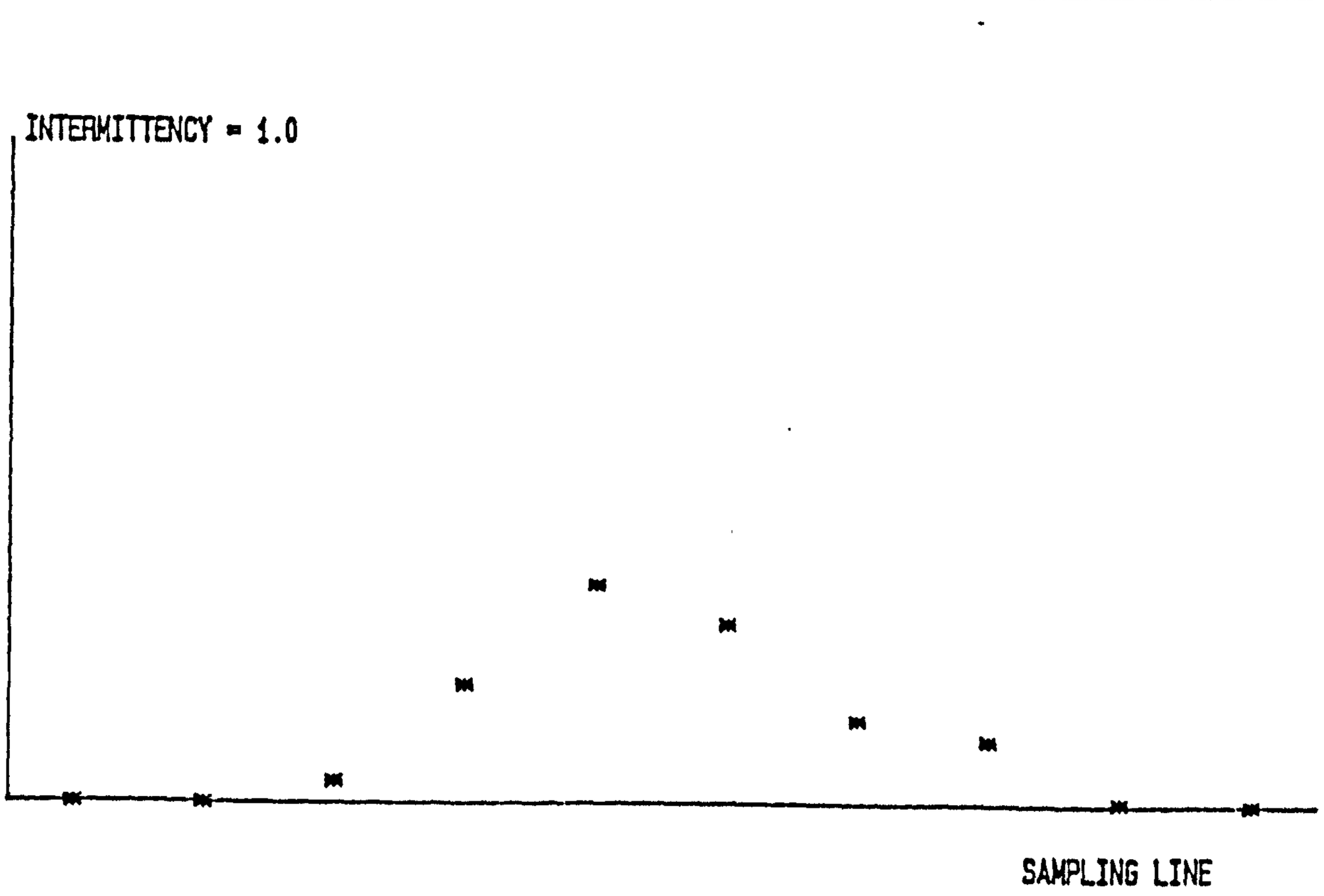

Figure 39. Cross-stream intermittency.

DEPTH = 45.0 M
SHIP SPEED = 1.0 M/S
INTERMITTENCY = 1.0
SPATIAL ANISOTROPY = 3.0
CORELLATION = 0.5
SPATIAL RANDOMNESS = 1.0
VELOCITY SCALAR = 1.0000
SWITCH FACTOR = 0.50
VELOCITY ANISOTROPY = 1.0
TIME STEP = 10.0 SECS
EPSILON = 0.90
NO OF EDDY SIZES = 1
SYSTEMATIC TIME ERROR = 0.81%
SAMPLING BOX SIZE = 30.00M
SAMPLING POSITION. STREAMWISE = 600.00M. OFFSET = 0.00

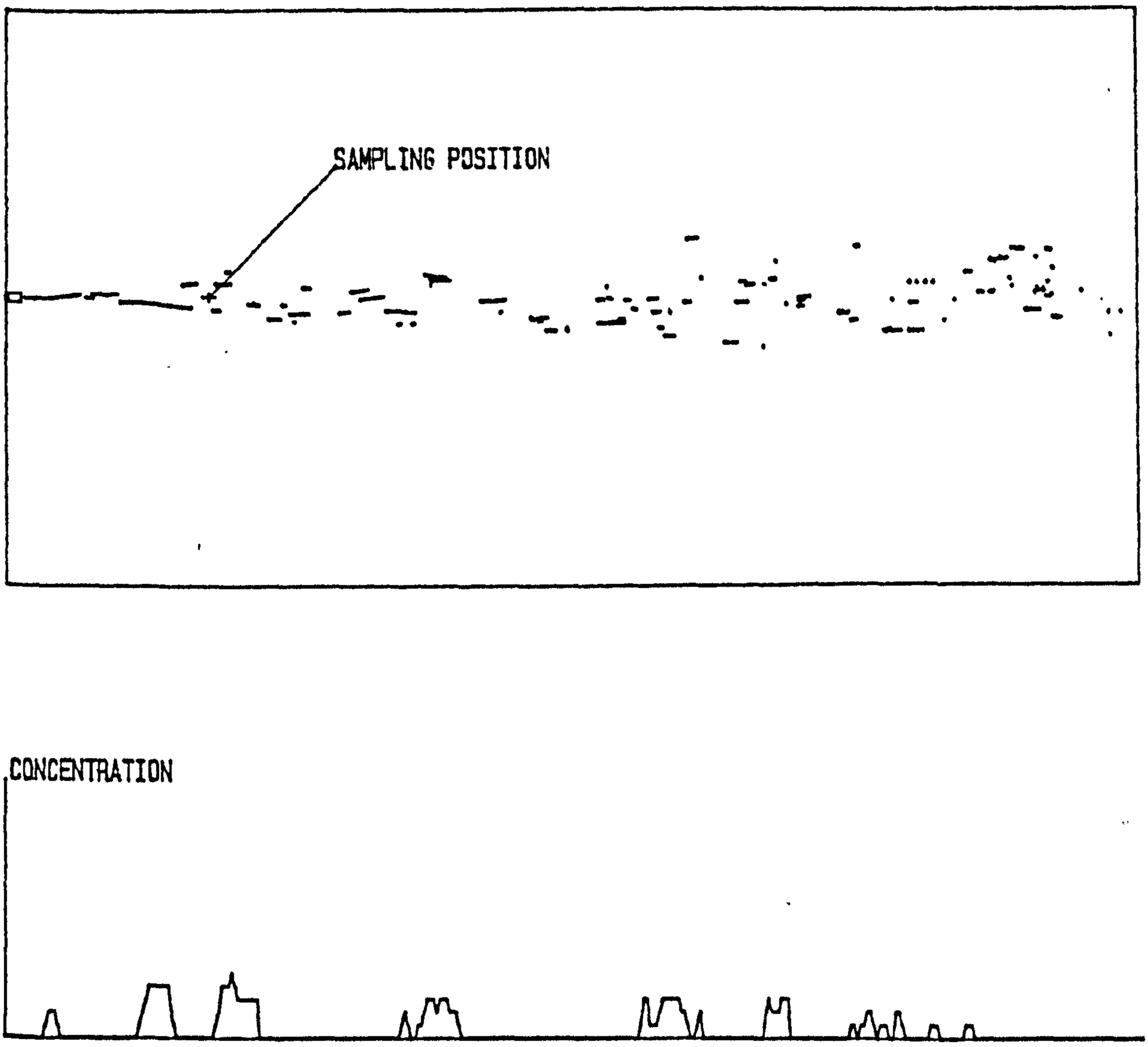

Figure 40. Eulerian concentration time series from the model.

Switch	0.5	no correlation between adjacent eddies.
Correlation	0.5	no correlation between u and v components.

The spatial anisotropy was set automatically by the program from (3.28). This was calculated by first determining the value of λ, the dissipation scale or model roughness length, from the value of ε using (3.34). The value of the energy dissipation rate, ε, remained an input to the code. The value of N was calculated from the water depth L as the integer part of log L/λ. Once ε, N and L are known, the value of U_1, the velocity at which the intermittency is unity, was calculated. The model was modified to allow mean flow variation throughout the release and the intermittency made equal to the ratio of current speed and U_1, as predicted by (3.63).

In order to increase the computational efficiency of the code it was decided that only the large eddies would be modelled individually. Thus the sorting routine and eddy velocities were retained for the large eddy size and the smaller sizes replaced by random dispersion, the dispersion coefficients of all the smaller sizes being summed in accordance with (2.86).

To model the cyclical nature of the production process fluctuation more effectively, the induced eddy velocities in the remaining large, spatially anisotropic, eddies was assumed to be sinusoidal. Thus the streamwise induced velocities were given a spatial sine distribution within each active eddy site, the amplitude of the fluctuation being adjusted to give the correct r.m.s. statistics and dispersion.

Correlations and spectra from the model.

Figure 41 shows a typical Eulerian velocity correlation and spectrum produced by the model. This was achieved by calculating the average velocity of the particles within the sampling box at each time step. The spectral peak is at $1/t_L$ and the logarithmic plot of the spectrum shows a σ^{-2} trend over part of the range. The

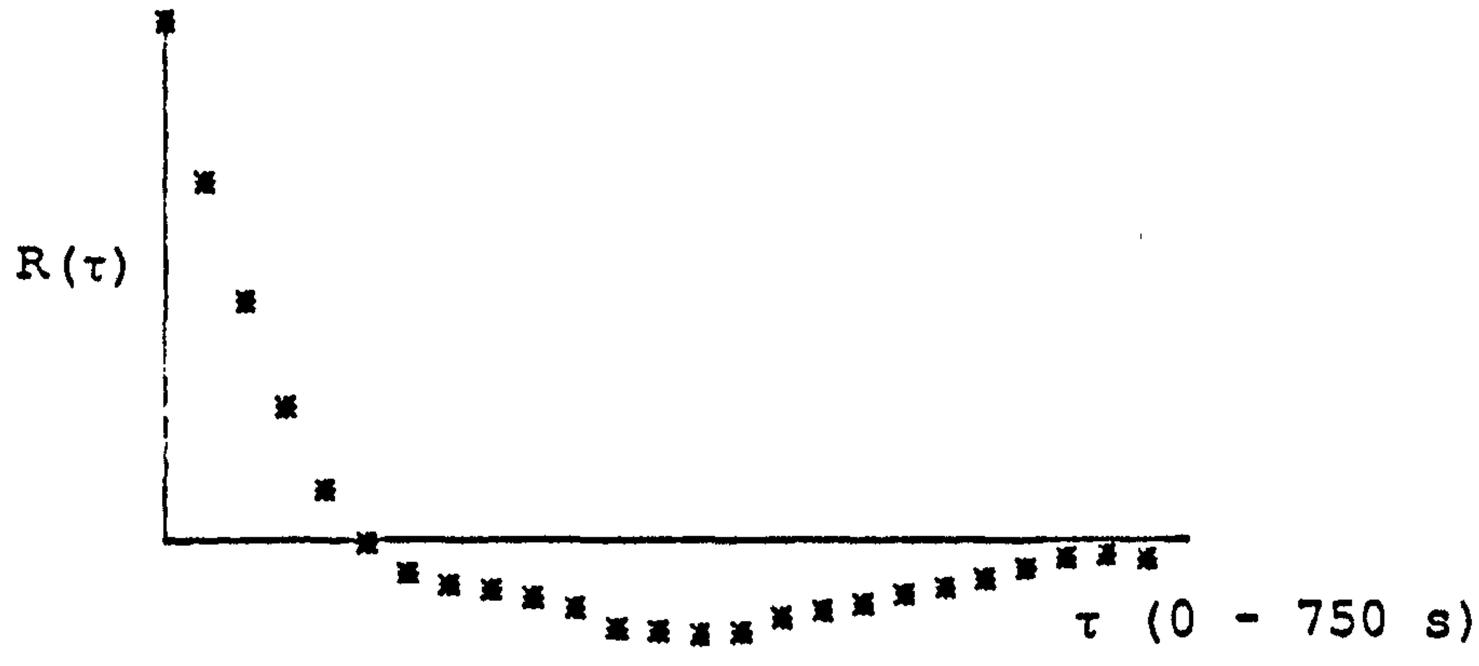

U FLUCTUATION CORRELATION

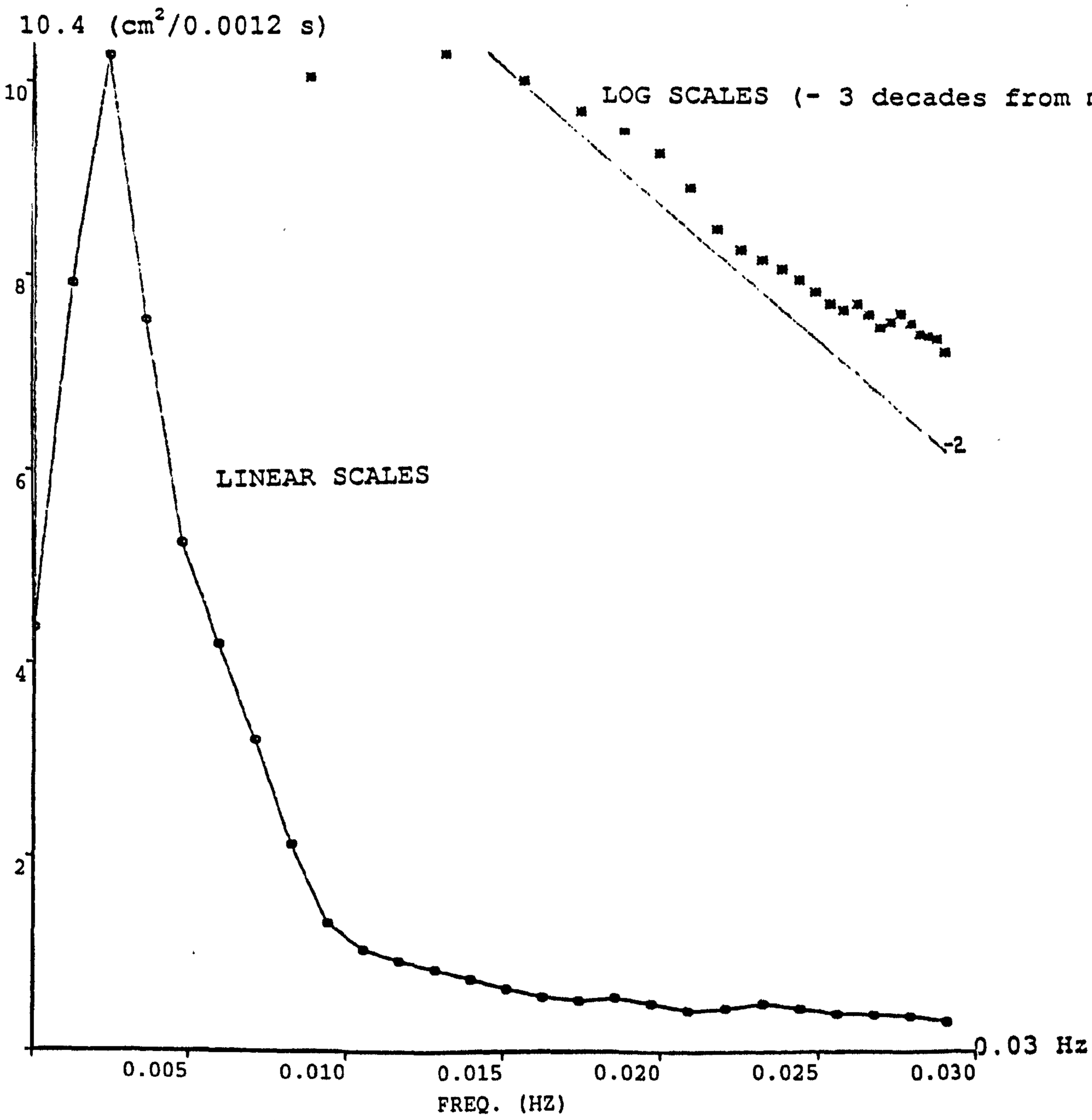

Figure 41. Typical frequency spectrum from the model.

concentration covariance and spectrum produced by the model will be discussed in the next chapter where they will be shown to have the same form as that found in the sea.

Figure 42 shows a wave-number spectrum calculated from the first version of the model which retained the smaller eddy sizes. The longditudinal correlation, R_{11}, is that between the simultaneous streamwise velocity fluctuations, u, at various streamwise separations. The transverse correlation, R_{22}, is that between the cross-stream fluctuations at the same points. F_{11} and F_{22} are the corresponding one-dimensional spectra taken by Fourier transforming the correlations. Both spectra show clear a $k^{-5/3}$ dependence over part of the wave number range. The isotropic relationship given by Tennekes and Lumley (1972) was used to calculate a measure of the three dimensional spectrum E(k):

$$E(k) = k^3 \, d/dk \, ((1/k) dF_{11}/dk) \qquad (8.1)$$

The spectrum E(k) calculated by this method closely followed the F_{22} spectrum. This is not as predicted by isotropic theory. Furthermore the ratio F_{11}/F_{22} is clearly not 4/3 as it should be for isotropy. The model velocities used to produce these spectra were isotropic and the intermittency was unity. It therefore must be the spatial anisotropy which distorts the correlations and spectra away from the values predicted by isotropic theory. The same result was obtained when the eddy velocities were modelled in a polar mode, the step length being appropriate to eddy size but the direction being random. Thus velocity isotropy itself is not sufficient to produce isotropic spectra. Spatial isotropy also has to be included.

Figure 43 shows typical output from the modified code. The meandering is much more clearly represented. The absolute and relative dispersion, meandering and intermittency predicted by the modified code is compared in the next chapter with dye and oil releases made at sea.

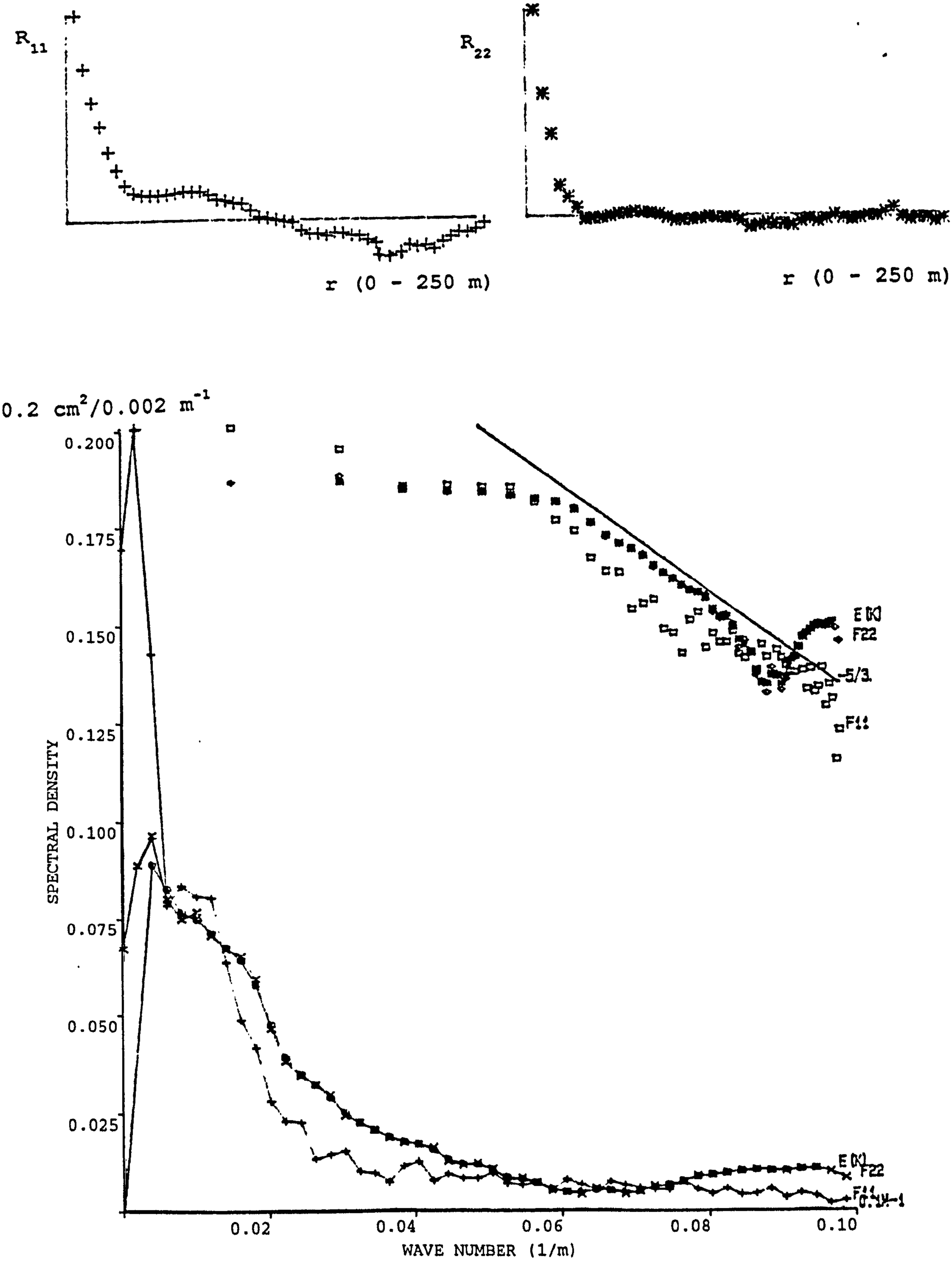

Figure 42. Typical wave number spectrum from the model.

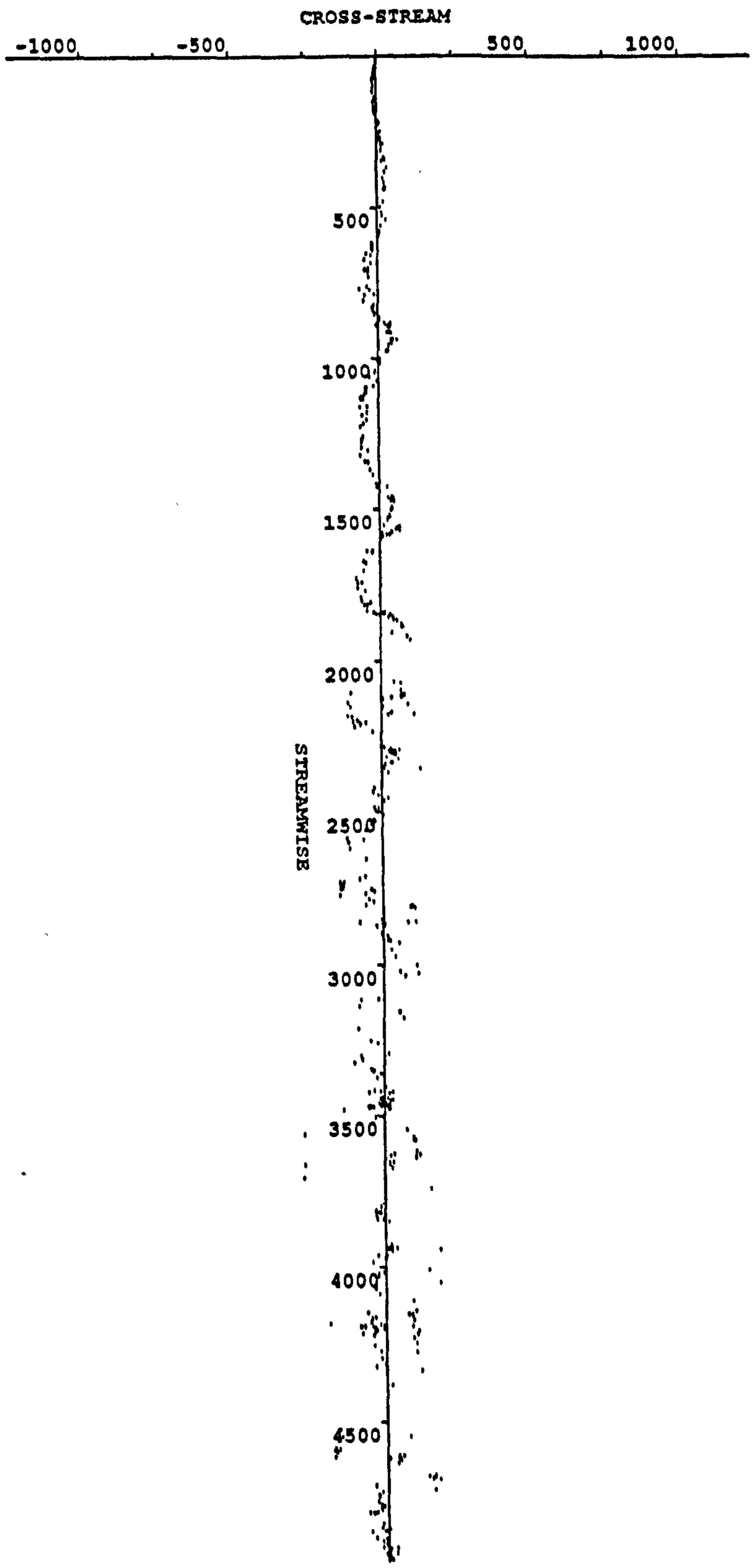

Figure 43. Typical output from final version of the model.

CHAPTER 8. COMPARISON OF SURFACE DISPERSION MODEL WITH OIL AND DYE RELEASE EXPERIMENTS.

The discrete eddy mixing model described in the previous chapter was used to simulate two large scale near-surface dispersion experiments, the first a series of Rhodamine B dye releases and the second an oil release. These were carried out by the Warren Spring Laboratory in the North Sea 35 miles off the coast at Ipswich. This area was chosen since there was known to be a considerable period of steady, rectilinear mean tidal flow (Elliott, 1986). The sea bed was sandy and flat with a depth of 45 m. The experiments were carried out in calm, windless conditions.

Dye release experiments.

The dye release experiments were carried out on 2 - 4 August 1988 and were specifically designed to establish the extent of the meandering. SEASPRING was anchored at 52°,9.6′ N, 2°, 30.7′ W and the dye releases carried out at the same stage of the tidal flow on the three successive days. The dye was released through a weighted pipe over the stern of SEASPRING. The pipe remained close to the sea surface and the dye was released at a rate of 55 litres/hour.

The dye concentrations were measured from SEATRUCK whose position was fixed by DECCA and checked by radar range and bearing from SEASPRING. SEATRUCK was fitted with two vertically supported sampling tubes which extended to 1 m and 5 m below the surface. Water was pumped continuously at a known rate through the tubes to recording fluorometers on SEATRUCK. By calibrating the fluorometers against known concentrations of dye, the recorded data could subsequently be processed to give concentration readings in ppb. The time delay between a sample entering each tube and reaching the fluorometer was accounted for in the data processing. The general arrangement for the dye releases and of SEATRUCK are shown in Figures 44 and 45.

SEATRUCK was limited to a low speed because of the underwater sampling tubes and was carried downstream by the mean current

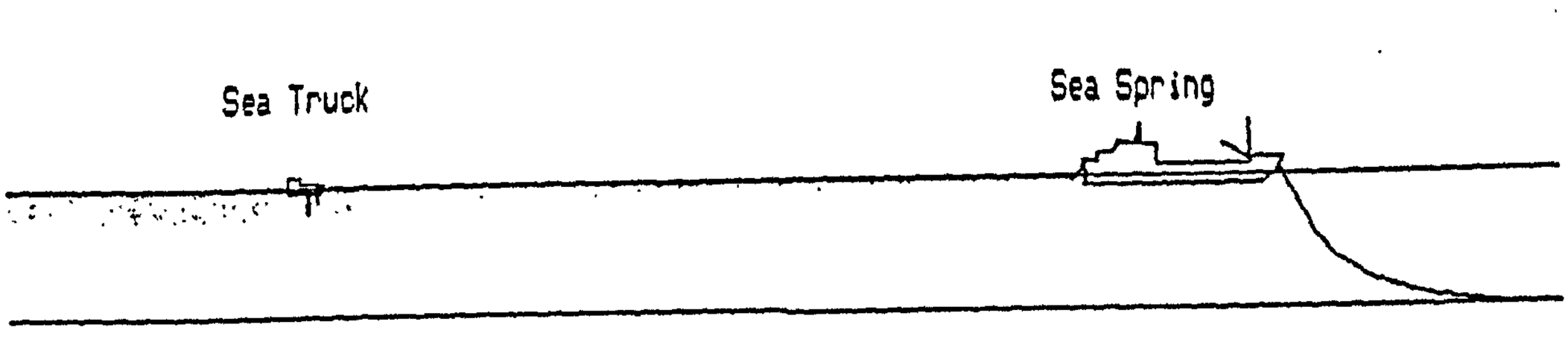

Figure 44. Deployment for dye release experiments.

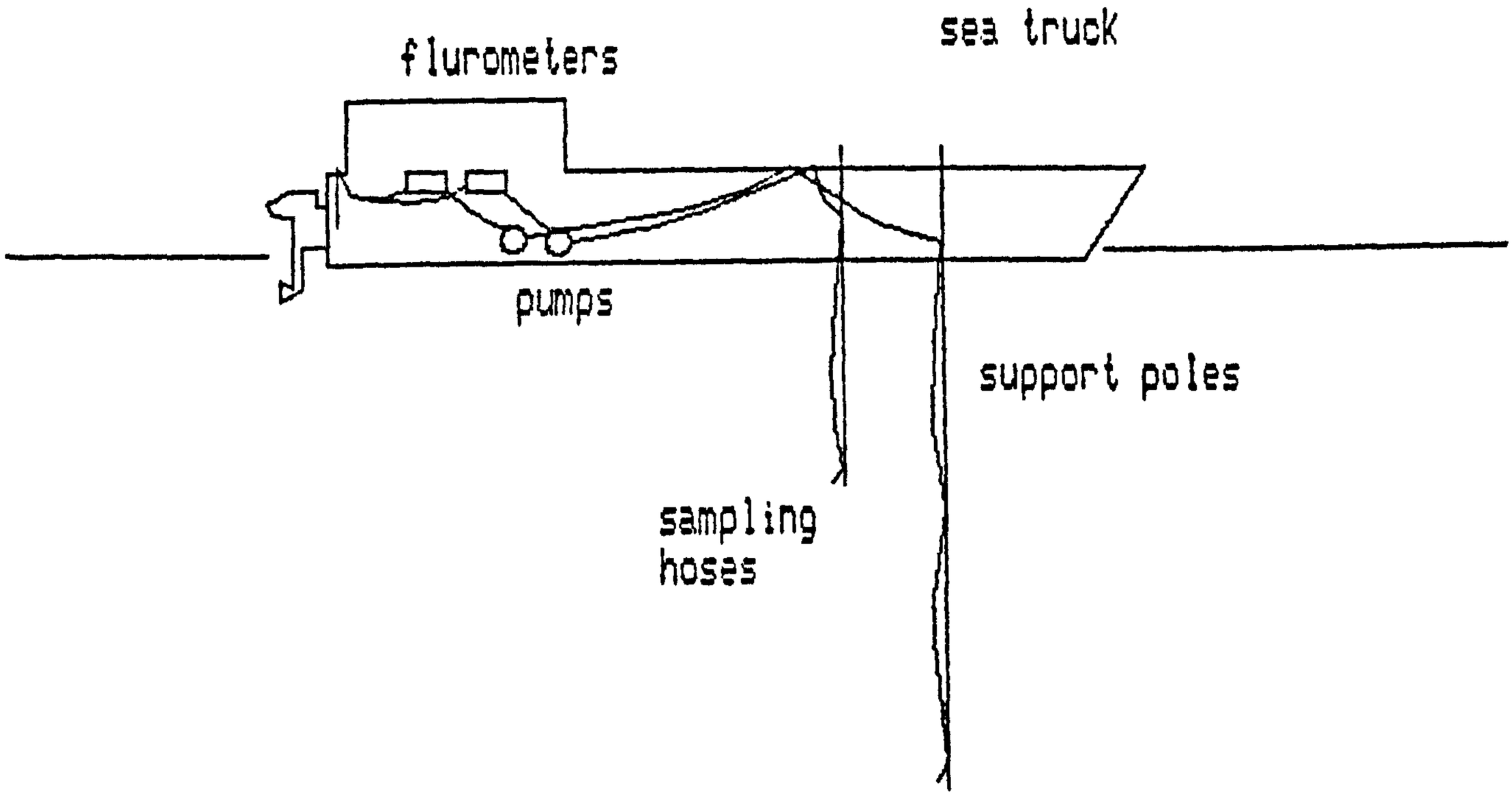

Figure 45. SEATRUCK sampling layout.

while carrying out each sampling crossing of the plume. The error from this effect was greatest when the widest sections of the plume were measured. On these occasions the position of SEATRUCK was fixed at the start and finish of each crossing so that the extent of the cross-stream spreading could be found accurately.

Sufficient crossings to characterise the plume had to be achieved before the mean flow conditions changed appreciably. Since SEATRUCK was restricted in speed and the plume dimensions were large, it was decided that the most important criterion on the mean flow was that it should remain uni-directional throughout the experiment. Thus on 2nd August, when crossings were made 11000 m downstream from SEASPRING, the dye had been released 3 hours previously. During this period the mean current direction varied by a maximum of 1.6% around its mean value of 204°. The two crossings achieved at this distance from the source were evenly distributed around a 204° bearing from SEASPRING showing that the current had also remained rectilinear over the plume dimension.

The variation in mean flow amplitude during the 3 hour period was 9% around its mean of 1 m/s. This is less significant since the plume width only varies slowly with distance from the source and a 9% error in converting distance from source to time since release is much less than the variability in the lateral measurements themselves. On the 3 August the plume measurements were taken out to 5000 m and the variation in mean flow was much less.

When "relative" diffusion experiments are carried out (Bowden and Lewis, 1973) the plume is traversed many times at the same location and an ensemble average of the spread of each profile around its centroid taken as a measure of plume width. In these experiments only one crossing of the plume was made at each downstream distance from the source and more scatter in the relative diffusion calculations was expected.

The true geographical position of each concentration profile

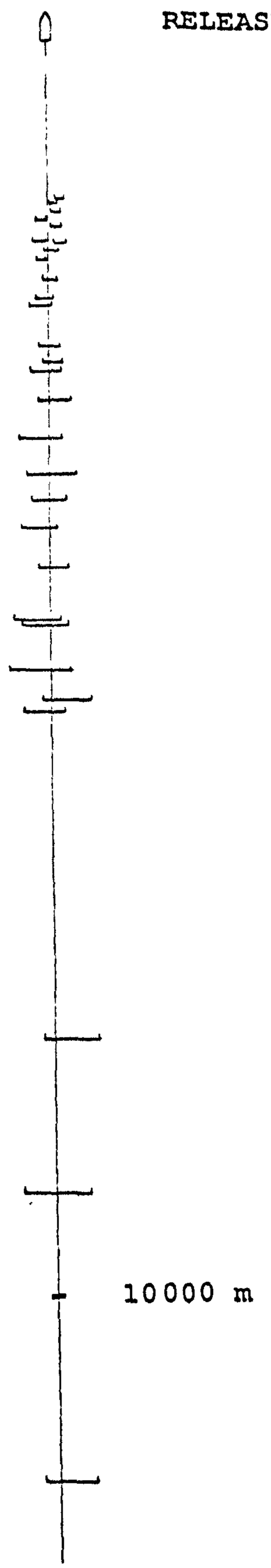

Figure 46. Plan of dye measurements.

was recorded so that each crossing could be plotted on a chart. Figure 46 shows the result for both plumes. The plot ignores the time at which each crossing was made. The full width of each concentration profile is shown. This was taken as the extent in each record where positive dye concentrations were found. In some of the near source records there was a difference in the plume width between the records taken at 1 m and 5 m depths. In these cases the larger dimension was recorded. Typical near source and far-field crossing realisations are shown in Figure 47. The standard deviation of each concentration profile was calculated using a computer code. These were similar at 1 m and 5 m and an average was taken as representative for each crossing.

The 5 m depth sensor did not record dye until 1500 m from the source on either day, indicating that the dye remains within the top 5 m for 25 minutes after release. The magnitude of the concentration peaks at 1 m and 5 m become approximately equal at 2000 m from the source. From 3000 m the profiles become very similar, indicating that the plume has mixed down to substantially more than 5 m deep. Near surface mixing mechanisms should therefore be effective for at least 30 minutes after a release in these conditions. Since measurements were not made at depths greater than 5 m, the realisations in Figure 46 are essentially two-dimensional.

For each crossing the maximum distance at which dye was found, measured from the centre line of the release (the mean flow bearing), was measured. Twice this distance was taken as an assessment of the full plume width, W, at that distance from the source. The result is plotted against time since release, calculated at 1 m/s mean flow, in Figure 48. Since the mean current in each case was 1 m/s, the time since release was equal to the distance from source in metres. The values all fall within an envelope given by:

$$W = 8.3\ t^{1/2} \qquad (8.1)$$

This envelope is shown in Figure 48. Equation (8.1) is the best

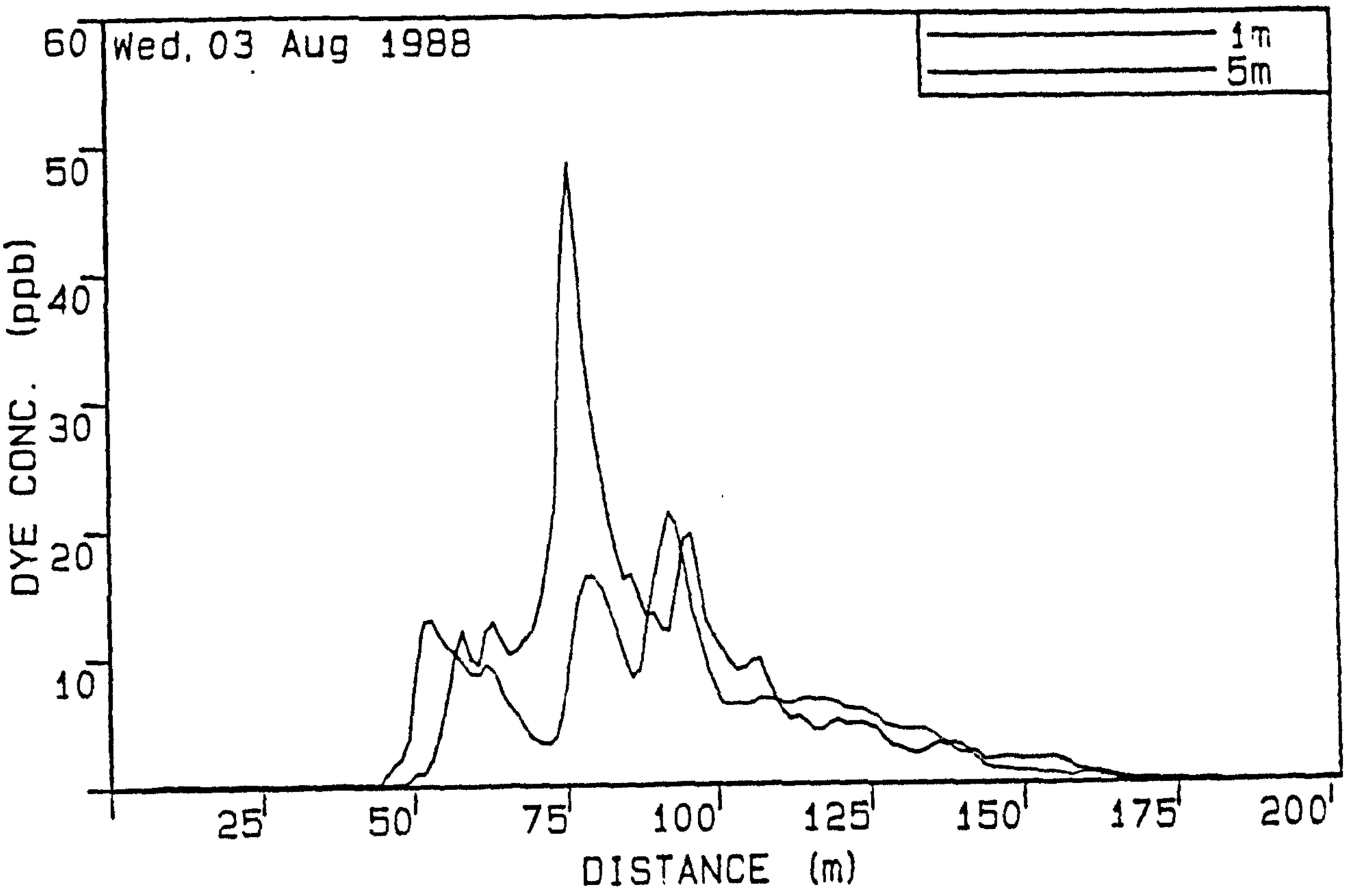

Figure 47. (top):Typical near source concentration profile. (bottom):Typical far-field concentration profile.

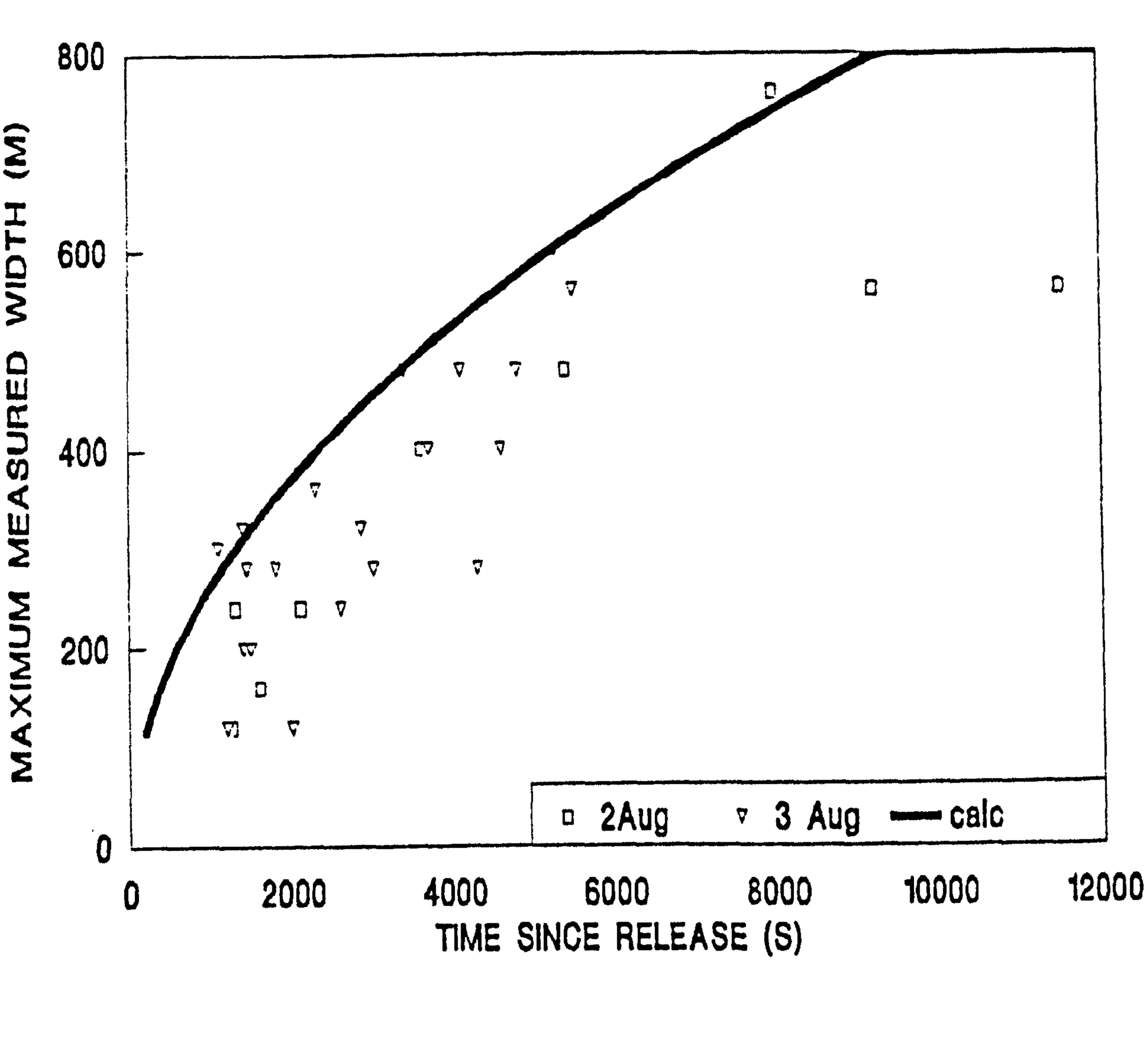

Figure 48. Full plume width against time since release.

assessment that can be made of the maximum extent of the absolute dispersion of the plumes.

The following definitions were made. All lengths are in metres.

SYMBOL	NAME	DERIVATION
W	full plume width	assessed from Figure 52 (equation 8.1)
w	individual crossing width	assessed from each profile (Figure 51)
σ	standard deviation of absolute diffusion	calculated as W/4 (equation (8.3))
s	standard deviation of relative diffusion	calculated from each profile (Figure 51)
m	standard deviation of the meandering	calculated (equation (2.91))
t	time since release	distance from source/ mean current

The calculated standard deviations, s, were plotted against the measured profile widths, w. With some scatter they were related by:

$$w = 4s \tag{8.2}$$

This relationship was expected from a Gaussian concentration distribution and has been established in relative diffusion experiments (Bowden and Lewis, 1973). Since the absolute diffusion is also Gaussian, the following relationship was assumed to calculate the standard deviation, σ:

$$\sigma = W/4 \tag{8.3}$$

The standard deviation of the meandering was then calculated from

(2.91):

$$m^2 = \sigma^2 - s^2 \qquad (2.91)$$

From (8.1) and (8.3), the standard deviation of the absolute diffusion was given by:

$$\sigma = 2.07\ t^{1/2} \qquad (8.4)$$

The standard deviation of the relative diffusion, s, was found to follow the following relationships:

$$s = 0.0002\ t^{3/2} \qquad t < 5000\ s \qquad (8.5)$$

$$s = 1.0\ t^{1/2} \qquad t > 5000\ s \qquad (8.6)$$

These relationships are shown in Figure 49. The $t^{3/2}$ behaviour is predicted for the growth of s during the explosive phase of growth in relative diffusion (see Introduction). Equations (8.4) - (8.6) will be used later in this chapter to derive the statistics of the meandering and the turbulence.

A further dye experiment was carried out on 4 August under similar tidal conditions as before. After one crossing which showed that the plume dimensions were similar to the previous days', SEATRUCK was anchored on the plume centre-line at a distance of 1600 m from SEASPRING. That the anchoring point was on the plume centre-line was established first by bearing from SEASPRING and then confirmed by observing that the plume fluctuated equally to either side of SEATRUCK during the experiment. The point concentration record is shown in Figure 50.

Point concentration record.

The intermittency factor of the dye concentration, γ, is defined as the proportion of the time at which dye is detected (see Introduction). Using this definition the point concentration record intermittency factor was 0.49. The intermittency decreased exponentially with threshold level so that if the chosen threshold

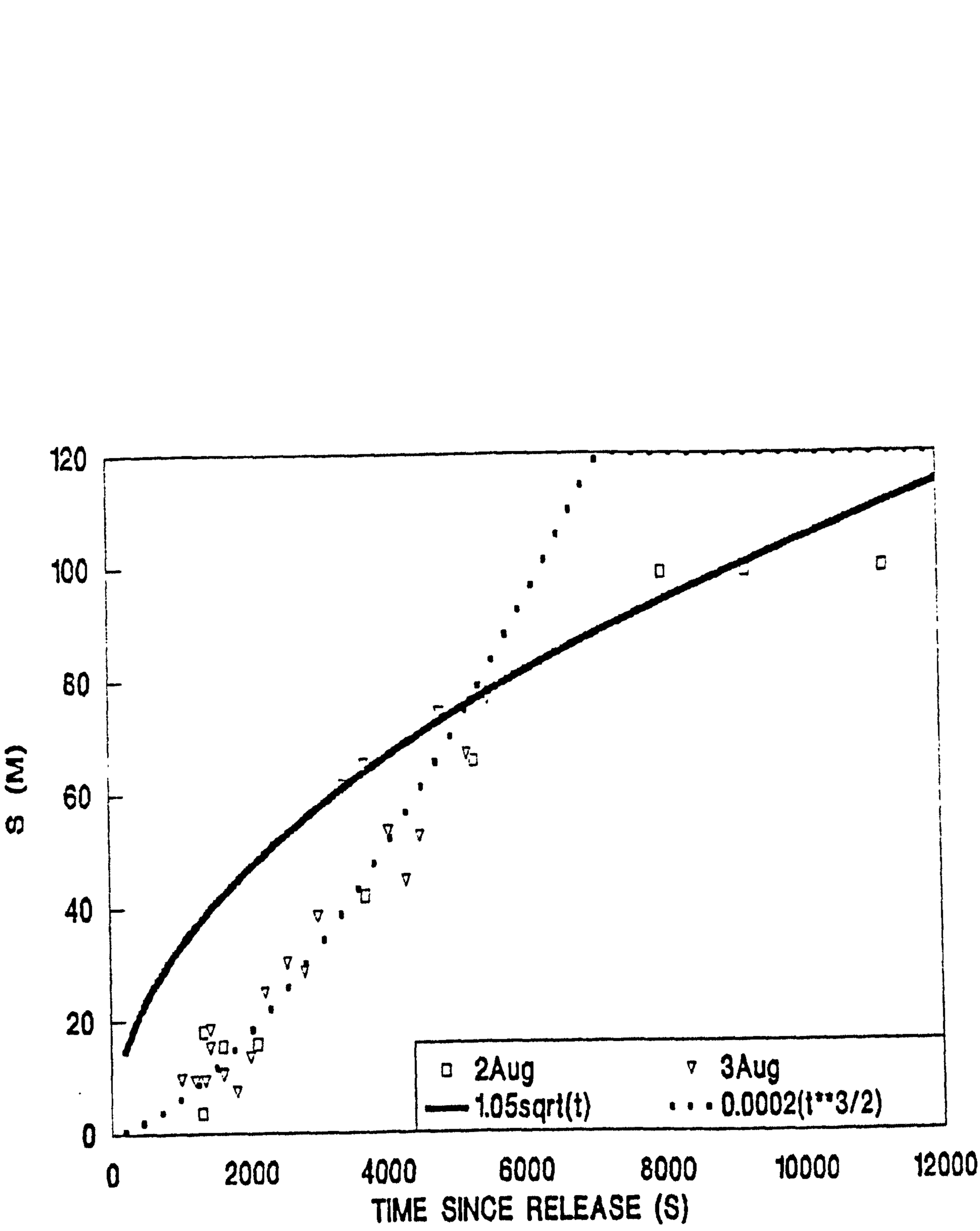

Figure 49. Standard deviation of relative diffusion against time since release showing two phases of growth.

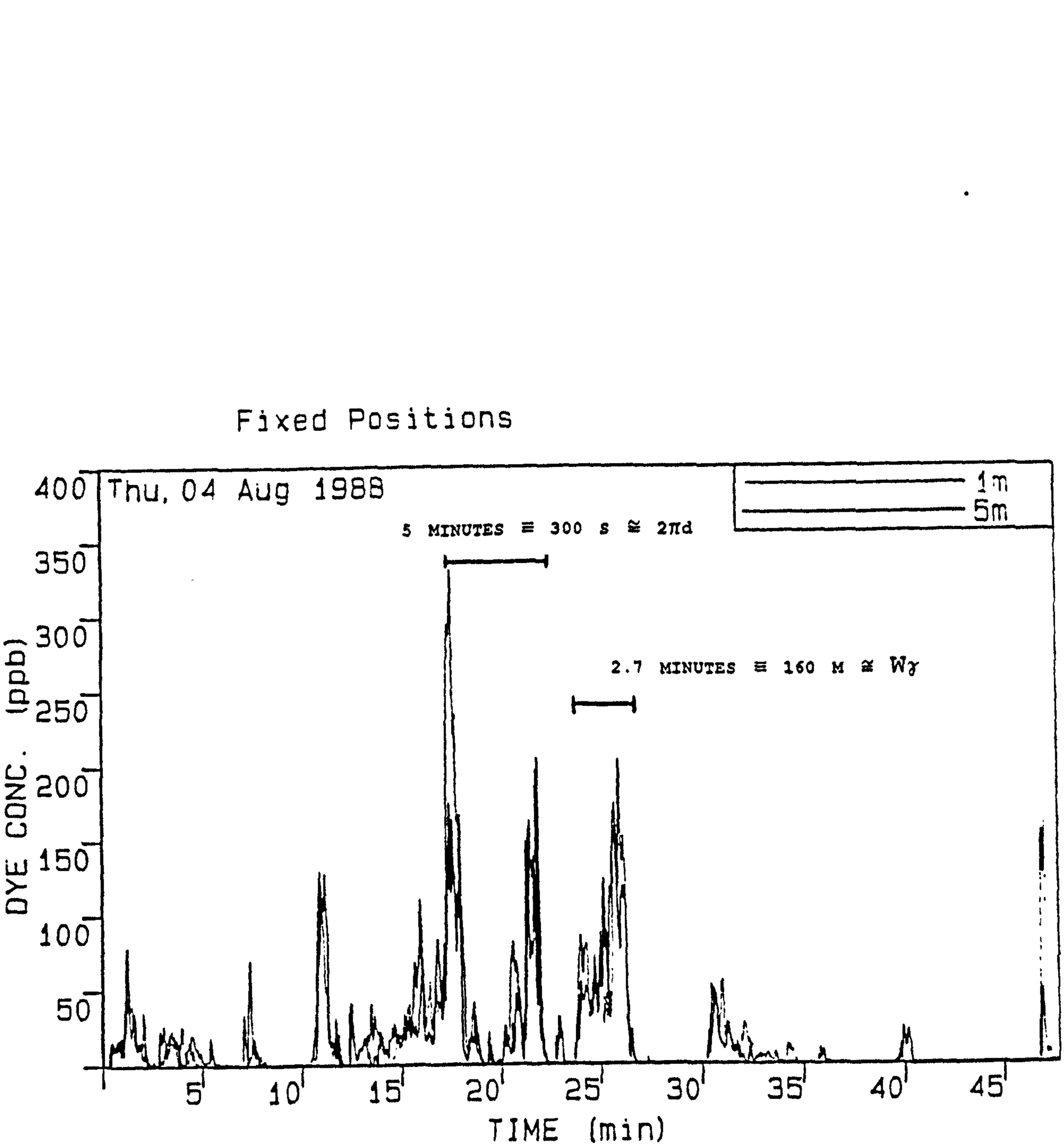

Figure 50. Point concentration record.

level was C_{thresh} and the intermittency, γ_{thresh}, was defined as the proportion of the time that the signal had a value greater than C_{thresh}:

$$\gamma_{thresh} = 0.49 \exp(-C_{thresh}/50) \qquad (8.7)$$

The significance of a relationship like (8.7) is that great care has to be taken in choosing the instrumentation threshold when intermittency measurements are made.

The mean value of the concentration is 30 ppb with a standard deviation of 51 ppb. This was greater than the mean and showed that the signal was highly kurtosed and intermittent. The peak to mean ratio was 10 for the largest observed peak. Equation (8.7) and the anomaly in the calculated standard deviation indicated that the fluctuation distribution might be log-normal. This distribution has been found in the atmosphere and was predicted by Csanady (1972) who considered a succession of random diluting impulses on a fluid packet moving through a field of turbulent eddies.

The probability distribution of the point concentration record is plotted against the logarithm of the concentration in Figure 51. The distribution is approximately Gaussian above the mean value, the distribution of low concentration values being difficult to measure. The probability distribution of peak values is plotted against the logarithm of the peak value in Figure 52. The distribution is approximately Rayleigh. Since the peak distribution of a narrow band Gaussian process is approximately Rayleigh (Pipes, 1958), these plots provide evidence that the fluctuation distribution is approximately log-normal.

The highest peak concentrations, C_{max}, from all the crossings carried out on 2 - 3 August were plotted against time since release. The maxima were contained by an envelope given by:

$$C_{max} = C_o/t^{7/3} \qquad (8.8)$$

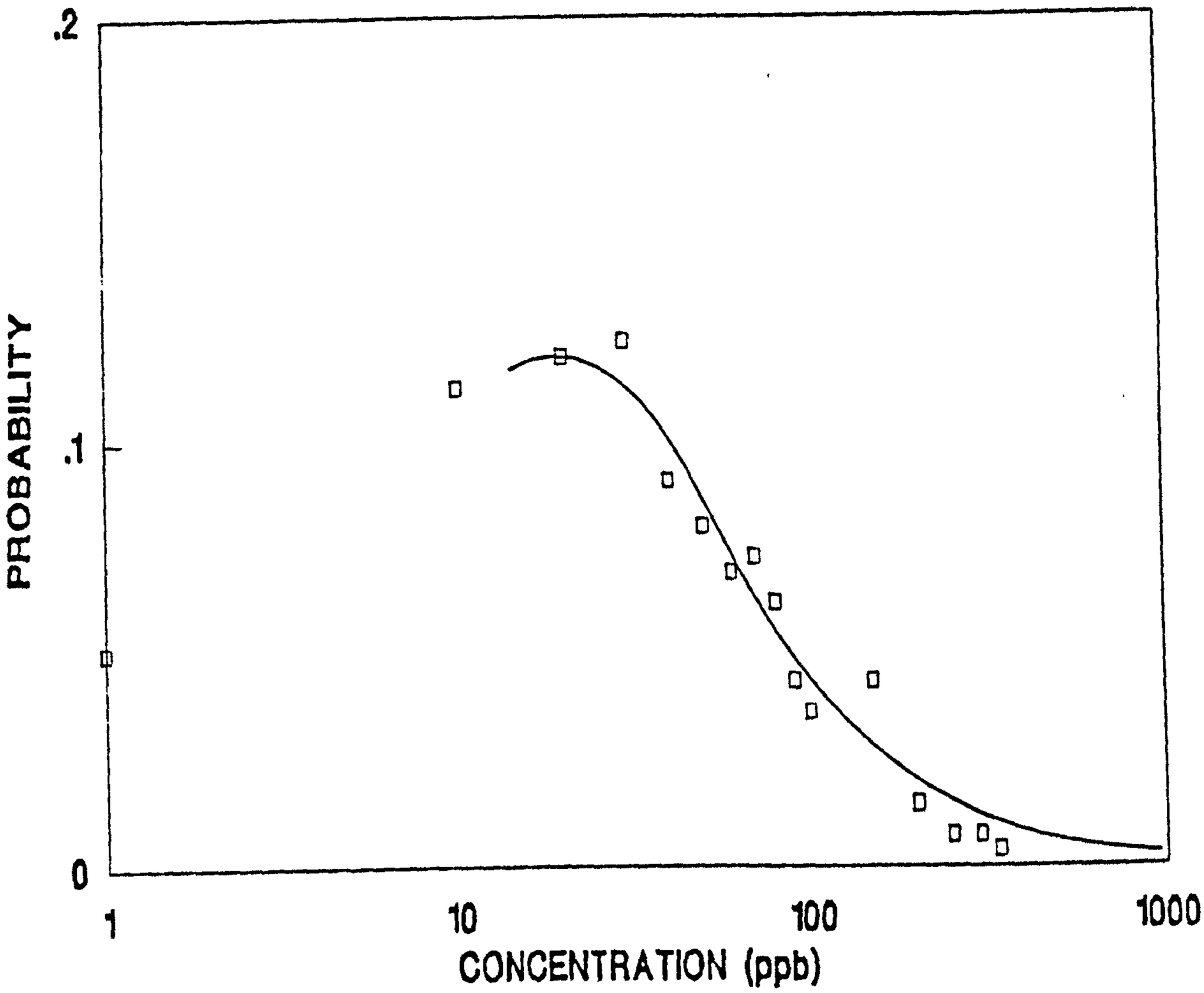

Figure 51. Point concentration probability distribution against logarithm of concentration.

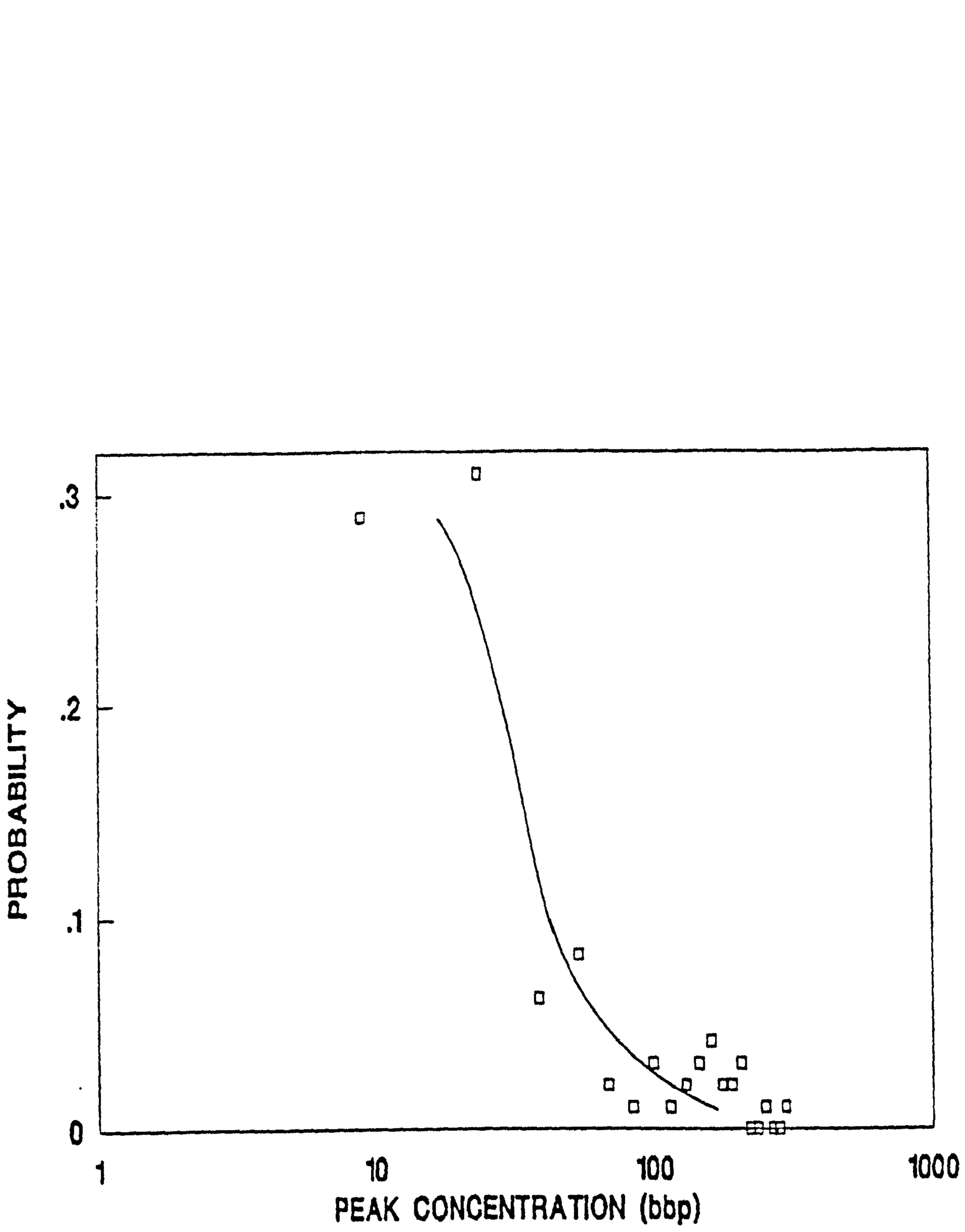

Figure 52. Probability distribution of peak values against logarithm of peak value.

where C_o was the initial concentration. A relationship such as (8.8) is required when the absolute concentration of a substance is hazardous.

The mean peak width (taken between points of zero concentration) was 95 s which corresponded to 95 m at a mean velocity of 1 m/s. The standard deviation of the peak widths was 70 m, showing the wide scatter in the results. A 2.7 minute timescale was apparent in the record and is marked on Figure 50. The record could be split into peaks that were close to multiples of this timescale, indicating that the passing plume elements might be characterised by a streamwise dimension of approximately 160 m. This value is close to W multiplied by the intermittency. From equation (8.1), W = 332 m. W x 0.49 = 162 m.

The mean period between peaks was difficult to establish because of the scatter at low concentrations. The mean period between the prominent peaks was 300 s with a standard deviation of 96 s. This period is shown on Figure 50 and corresponds to a length close to the sand dune wavelength predicted by Yalin (1977) of $2\pi d$ (where d is the water depth). In 45 m water, $2\pi d$ = 282 m.

Oil release experiment.

An oil release experiment was carried out on 22 August 1987. The experiment was part of a series of experiments in which the dispersive effect of various detergents on oil was being tested. The experiment was the only one of the series where conditions were the same as for the dye experiments reported above.

The release vessel, SEASPRING, maintained a constant position with respect to the sea bed during a one hour period when the surface velocity was steady at 1 m/s. There were no wind, waves or swell during the experiment. The position of SEASPRING was fixed by DECCA. The release position was within 1000 m of that from which the dye experiments were carried out.

About one hour after the discharge commenced the slick was photographed from the air from a height of 330 m using an

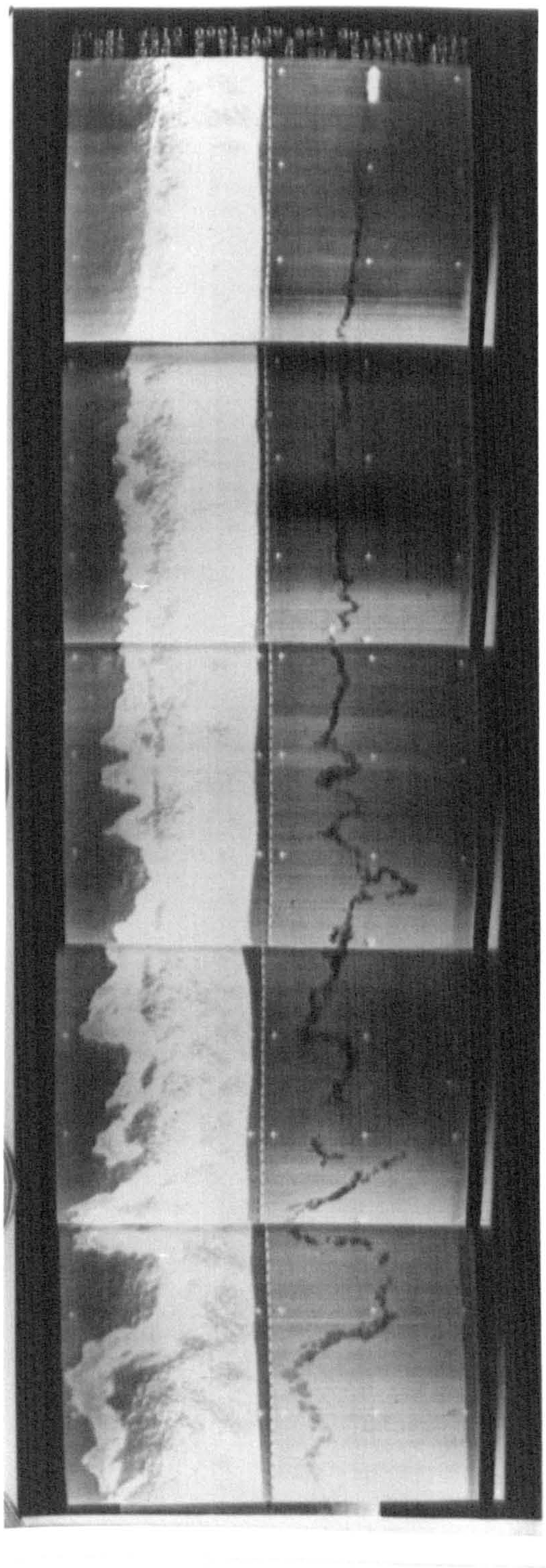

Figure 53. Electronic image of oil slick.

electronic camera. The aircraft flew up the reciprocal of the mean current bearing of 205°. The camera produced two simultaneous images of the slick. These are shown in Figure 53. The release vessel is at the top of each picture, and the white calibration marks at 200 m intervals. The slick was approximately 3000 m long and the meandering pronounced.

The left hand view in Figure 53 was taken through an ultra-violet filter and by showing the surface "sheen" gave a good indication of the full extent of the spread of oil at the sea surface. The right hand view was taken through an infra-red filter to show the bulk of the thicker surface oil.

The photographic strip was enlarged and the outline of the thicker oil slick traced and transferred to graph paper for subsequent analysis. The main axis of the slick, which was also the main current bearing from SEASPRING, was marked with points representing time since release at a mean flow of 1 m/s.

The meandering was assumed to be described by the centre line of the thicker oil. Since the outline of this part of the slick was ribbon-like and its cross-stream dimension remained small this was easily defined.

The meandering statistics were found by two methods. The first by directly measuring the cross-stream displacement, y, of the centre line at various times since release, t. In the second method an attempt was made to find the two-dimensional displacement of the slick centre line from the position which it would have occupied had the turbulence not been present.

The length of the centre line, measured from the source, was plotted against release time taken from the main axis. The centre line length, ℓ, was given by:

$$\ell = 0.12\ t^{4/3} \qquad (8.9)$$

with very little scatter. This indicated that the slick was

stretching along its centre line as the complexity of the meandering increased.

Equation (8.9) was then used to mark off the centre line of the slick in time since release. The following definitions were made and are illustrated in Figure 54.

SYMBOL	NAME	DERIVATION
W	total width of slick (absolute dispersion)	twice maximum displacement of sheen from axis
w	width of visible slick (relative dispersion)	measured from sheen
t	time since release along mean current bearing	calculated from current of 1 m/s
t′	time since release along slick centre line	calculated from equation (8.9)
y	cross-stream seperation between centre line and axis	measured at t
x	streamwise separaton between equivalent points on centre line and axis	measured at t
r	separation of equivalent points on centre line and axis	measured at t

It was found that the maximum values of W, y and r were described by:

$$W = 8.16\ t^{1/2} \qquad (8.10)$$

$$y_{max} = 3.2\ t^{1/2} \qquad (8.11)$$

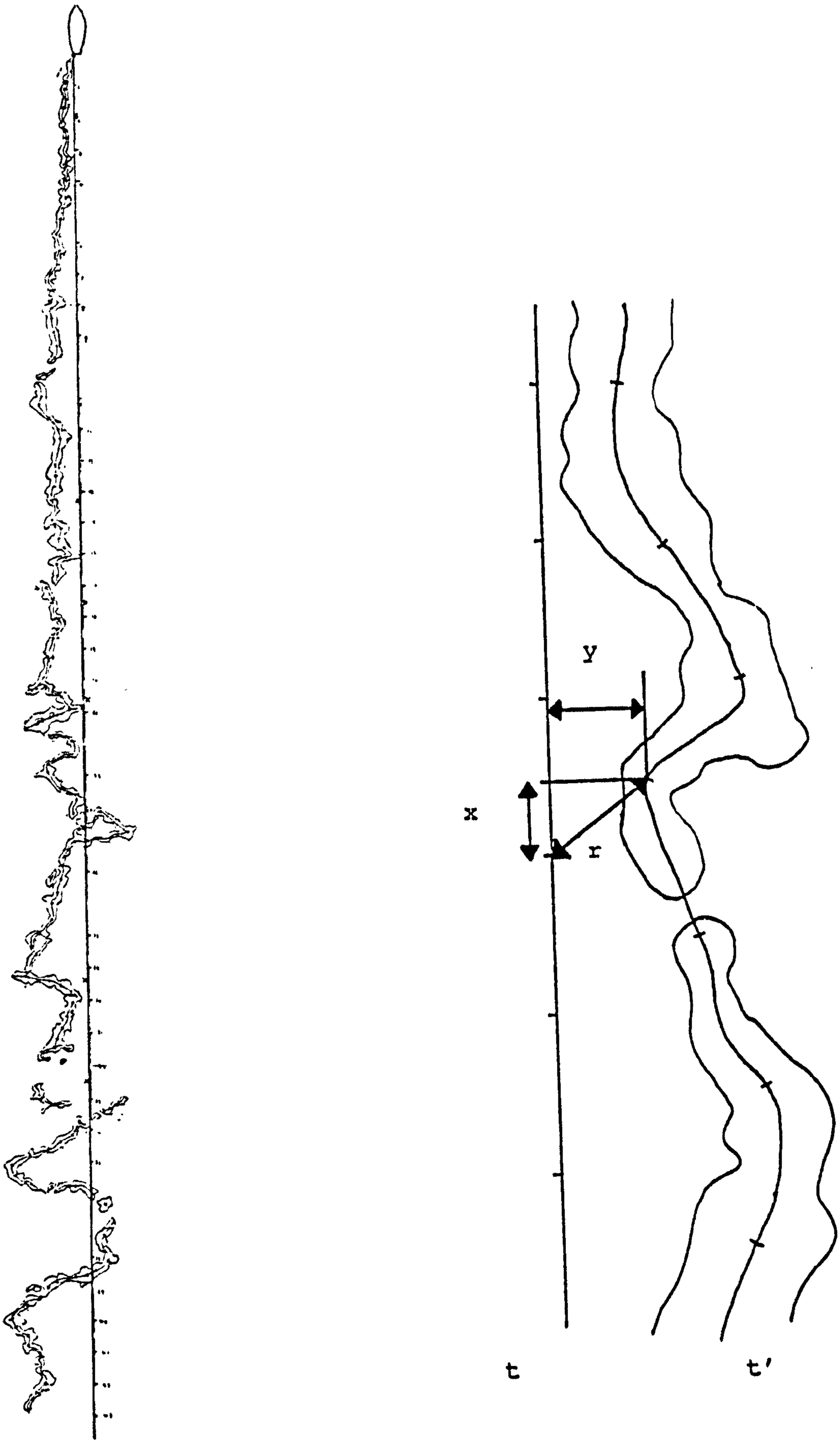

Figure 54. Definition of geometry for analysis of meandering.

$$r_{max} = 3.26\ t^{1/2} \qquad (8.12)$$

Beyond 1000 m from the source the cross-stream width of the sheen, w, is given by:

$$w = 0.00085\ t^{3/2} \qquad (8.13)$$

with little scatter. This equation, which is nearly the same as the one found for the dye releases, underestimates the width of the sheen close to the source. Quantitative comparison with relative diffusion theory is hampered by a lack of knowledge of oil drop size distribution (if it is in droplet form) and the response of a drop to turbulent impulses (Elliott, 1986). Surface tension will also affect surface spreading near the source. The near equivalence of (8.5) and (8.13) for relative diffusion and of (8.1) and (8.10) for absolute diffusion indicated that the oil was dispersed in the same manner as dye after about 20 minutes from release.

The statistics of r and y were analysed. Since both parameters increased with time two new variables were created:

$$r' = r/(t^{1/2}) \qquad (8.14)$$

$$y' = y/(t^{1/2}) \qquad (8.15)$$

From 1000m from the source the distribution of the values of r′ was found to be Rayleigh. The distribution is plotted in Figure 55. This distribution is expected from an isotropic two-dimensional random walk of fixed step length (see Introduction). The mean, $\eta(r')$, and standard deviation, $\sigma(r')$, of the distribution were given by:

$$\eta(r') = 1.88 \qquad (8.16)$$

$$\sigma(r') = 0.91 \qquad (8.17)$$

The standard deviation of y′ was found to be:

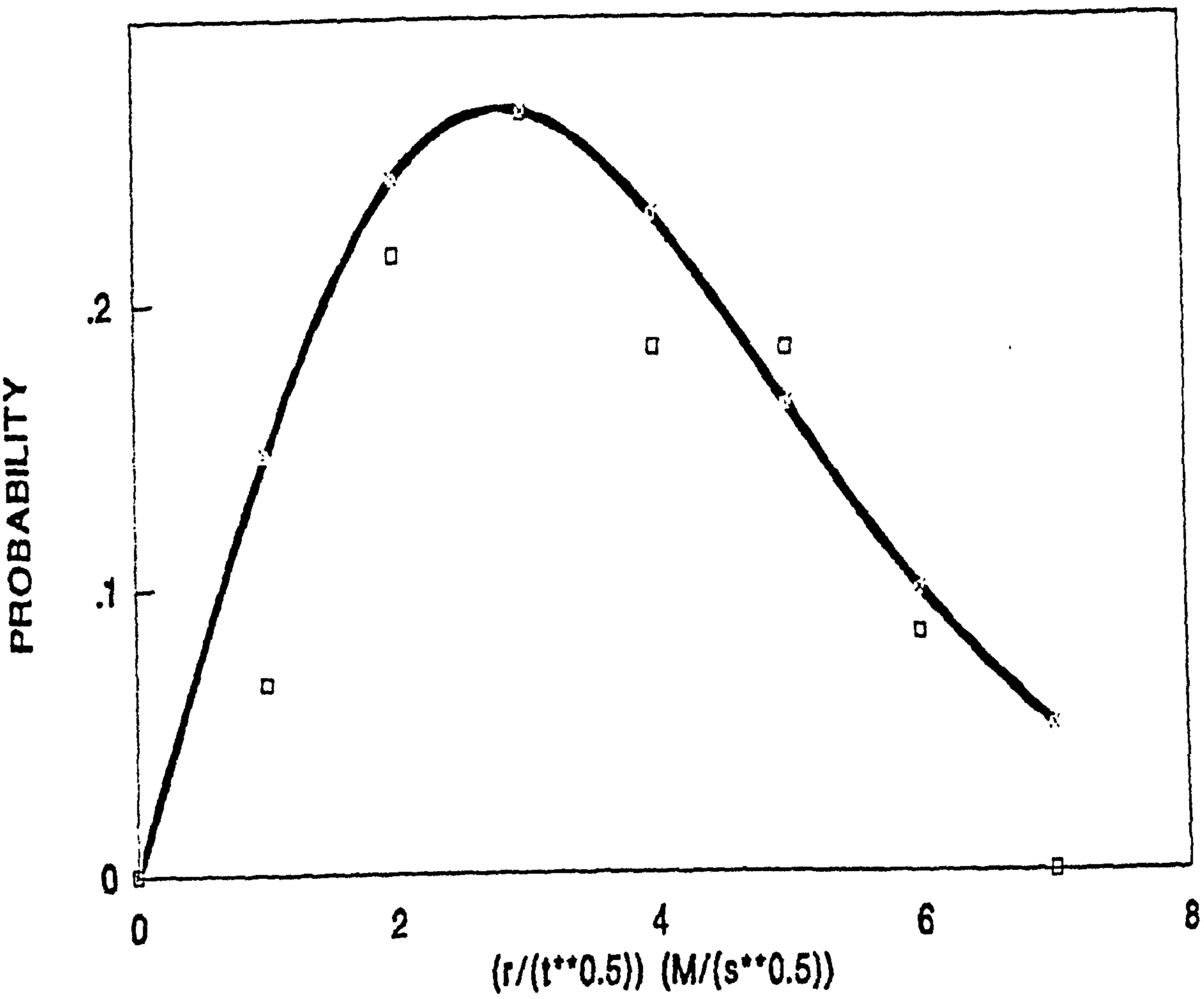

Figure 55. Rayleigh distribution of meandering displacement.

$$\sigma(y') = 1.79 \tag{8.18}$$

Equations (8.16), (8.17) and (8.18) may be rewritten in terms of r and y to give:

$$\eta(r) = 1.88\ t^{1/2} \tag{8.19}$$

$$\sigma(r) = 0.91\ t^{1/2} \tag{8.20}$$

$$\sigma(y) = 1.79\ t^{1/2} \tag{8.21}$$

Absolute dispersion and the mixing model.

The envelope describing the maximum cross-stream dimension of the dye releases was:

$$W = 8.3\ t^{1/2} \tag{8.1}$$

and for the oil release:

$$W = 8.16\ t^{1/2} \tag{8.10}$$

so that using equation (8.1) to describe W and (8.3) to give σ:

$$\sigma = W/4 \tag{8.3}$$

gives:

$$\sigma = 2.3\ t^{1/2} \tag{8.22}$$

If the surface spreading is caused by eddies which cause a simple random walk, step length $u_\ell t_\ell$ every t_ℓ then the absolute dispersion from all the eddies in the cascade is given by (2.101):

$$\sigma = 1.08\ n_L^{1/2}\ \varepsilon^{1/6} L^{2/3} t^{1/2} \tag{2.101}$$

so that substituting (8.22) into (2.101) and using L = 45 m gives:

$$n_L^3 \varepsilon = 0.13 \text{ cm}^2/\text{s}^3 \qquad (8.22)$$

Relative diffusion and the mixing model.

The relative dispersion of the dye was described by (8.5) and (8.6):

$$s = 0.0002\ t^{3/2} \qquad t < 5000 \text{ s} \qquad (8.5)$$

$$s = 1.0\ t^{1/2} \qquad t > 5000 \text{ s} \qquad (8.6)$$

In Chapter 2 the model predicted for a point source release:

$$s = 0.037\ n_L^{3/2} \varepsilon^{1/2}\ t^{3/2} \qquad (2.87)$$

$$s = 0.4\ n_L^{1/2} \varepsilon^{1/6} L^{2/3} t^{1/2} \qquad (2.99)$$

$$T_1 = 11.9\ t_L/n_L \qquad (2.91)$$

Equating (8.5) and (2.87) gives:

$$n_L^3 \varepsilon = 0.29 \text{ cm}^2/\text{s}^3 \qquad (8.23)$$

Equating (8.6) and (2.99) gives:

$$n_L^3 \varepsilon = 0.59 \text{ cm}^2/\text{s}^3 \qquad (8.24)$$

and putting T_1 equal to 5000 s in (2.91) gives:

$$n_L^3 \varepsilon = 0.26 \text{ cm}^2/\text{s}^3 \qquad (8.25)$$

Meandering and the mixing model.

The meandering statistics were calculated between 1000 m and 2500 m from the source. They were found to be:

$$\eta(r) = 1.88\ t^{1/2} \qquad (8.19)$$

$$\sigma(r) = 0.91\ t^{1/2} \qquad (8.20)$$

$$\sigma(y) = 1.79\ t^{1/2} \tag{8.21}$$

From the statistics of Rayleigh distributions given in (1.24), (1.25) and (1.26) we can write (Bartlett, 1978):

$$\eta(r)^2 = \pi m^2/4 \tag{8.26}$$

$$\sigma(r)^2 = (1 - (\pi/4))m^2 \tag{8.27}$$

$$\sigma^2(y) = m^2 \tag{8.28}$$

The measurements were taken within the explosive phase and the model predicts:

$$m^2 = 1.17 n_L \varepsilon^{1/3} L^{4/3} t - 0.0012\ n_L^3\ \varepsilon\ t^3 \tag{2.93}$$

so that using L = 45 m and $n_L^3\varepsilon \approx 0.3$ we can assess the relative size of each term in (2.93). At t = 1000 s, the first term is 200x the second. At 2000 s, 60x. Thus in this region (2.93) may be approximated by:

$$m^2 \approx 1.17 n_L \varepsilon^{1/3} L^{4/3} t \tag{8.29}$$

Using (8.19), (8.26) and (8.29) with L = 45 m gives:

$$n_L^3\varepsilon = 0.14\ cm^2/s^3 \tag{8.30}$$

Using (8.20), (8.27) and (8.29) with L = 45 m gives:

$$n_L^3\varepsilon = 0.08\ cm^2/s^3 \tag{8.31}$$

Using (8.21), (8.29) and (8.30) with L = 45 m gives:

$$n_L^3\varepsilon = 0.06\ cm^2/s^3 \tag{8.32}$$

<u>Establishing the value of the energy dissipation rate.</u>

The mean value of (8.22) - (8.25) and (8.30) - (8.32) is 0.22 cm^2/s^3 with a standard deviation of 0.17. The value of $n_L^3\varepsilon$ given in (8.24) is undoubtedly an over-estimate since the derivation of

(2.99) assumed that no dispersion from the largest eddy size was taking place. This must be occurring to some extent and would result in a lower value in (8.24). Furthermore (8.24) is very sensitive to the measured dispersion in (8.6) because of the 1/6 exponent in (2.99). Ignoring this result gives a mean of 0.16 cm^2/s^3 with a standard deviation of 0.07. Recalling (3.30):

$$n_L^3 \varepsilon = U_0^3/N^3 L \qquad (3.30)$$

shows that with L = 45 m, U_0 = 1 m/s and $n_L^3 \varepsilon$ = 0.16 cm^2/s^3, N = 11.

From (3.18) and (3.34):

$$N = \log L/\lambda \qquad (3.18)$$

$$\lambda = (\nu^3/\varepsilon)^{1/4} \qquad (3.34)$$

then values of ε between 0.26 cm^2/s^3 and 0.3 cm^2/s^3 give the required result with N = 11. These values are close to those found in 30 m of water and reported in Chapter 3.

Numerical simulation of the dye and oil experiments.

The surface dispersion code was found to best simulate the experiments with a value of ε equal to 0.3 cm^2/s^3. The absolute dispersion envelope, (8.1) was followed with precision. The meandering wavelength approximated to $2\pi d$ (the Yalin (1977) sand dune wavelength) over the same distances from source as for the oil release.

The accuracy of the relative dispersion was less easy to establish. The simulation was expected to be crude since the smaller eddies were modelled by (2.99) throughout the release. The program was modified to give real-time visual output and the envelope of the relative dispersion varied considerably as the release progressed. It proved impractical to track sufficient particles to establish (8.5) although (8.13) could be fitted to the relative dispersion between 1000 m and 2000 m from the source on some realisations.

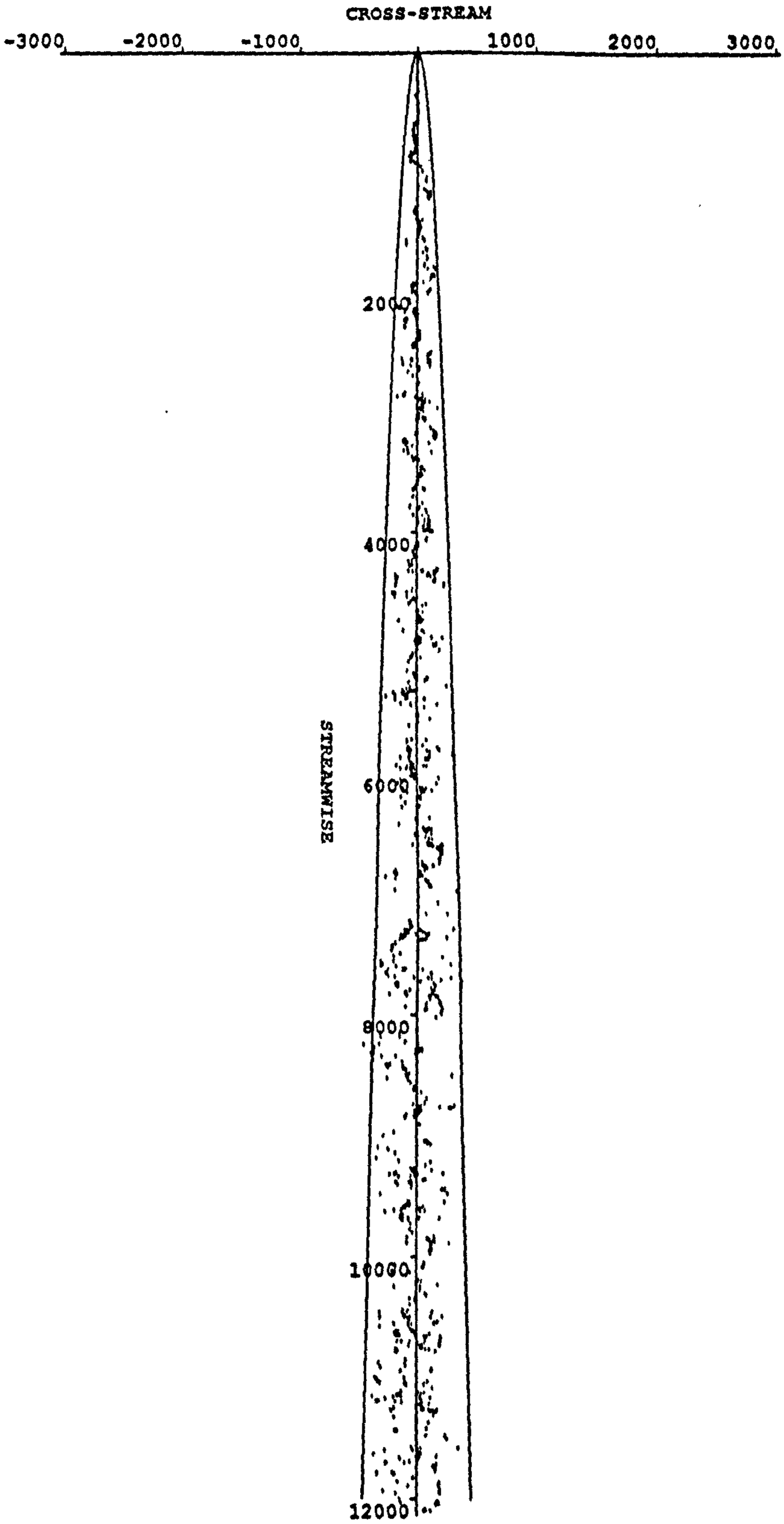

Figure 56. Simulation of dye release.

A typical realisation of the simulation of a dye release is shown in Figure 56. The concentration intermittency, γ, was calculated from point source records taken at varying cross-stream and streamwise distances from source. The cross-stream intermittency distribution was approximately Gaussian in the mean, peaking on the centre-line and going to zero at +/- W/2. The streamwise development of γ was more complex. From 0 m to approximately 1500 m from the source, the mean centre-line intermittency reduced linearly from 1 to 0.5. 1500 m was also the distance at which the 5 m fluorometer detected dye. From 1500 m to 3000 m, γ varied randomly between 0.5 and 0.7, a figure which was comparable with that found from Figure 50. From 3000 m to 5000 m, a distance equaivalent to T_1, the start of the second phase of growth in relative diffusion, γ returned to 1 approximately linearly with distance.

The concentration covariance and the concentration fluctuation spectrum were calculated from the point concentration record shown in Figure 50. This is compared with that calculated from the model in Figure 57. The model result is dependent on sampling box size and the comparison can only be qualitative. On that basis the simulation is close, indicating that the model is reproducing the point concentration fluctuation distribution realistically.

In Figure 58 the diffusion due to small eddies has been artificially reduced in order to highlight the meandering. This simulates the thicker oil in Figure 53. The meandering wavelength varies between approximately $2\pi d$ (the Yalin (1977) sand dune wavelength) which is shown in Figure 53 and $4\pi d$. This equates to the meandering of the oil release over the range shown in Figure 53.

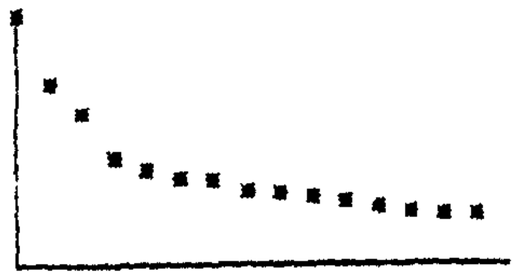

CONCENTRATION COVARIANCE

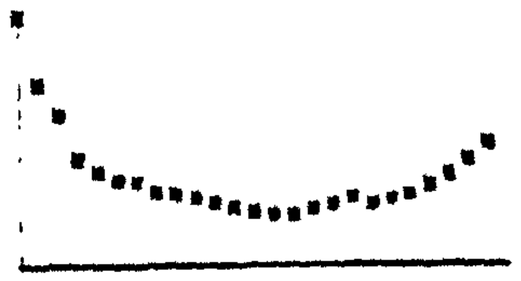

CONCENTRATION COVARIANCE

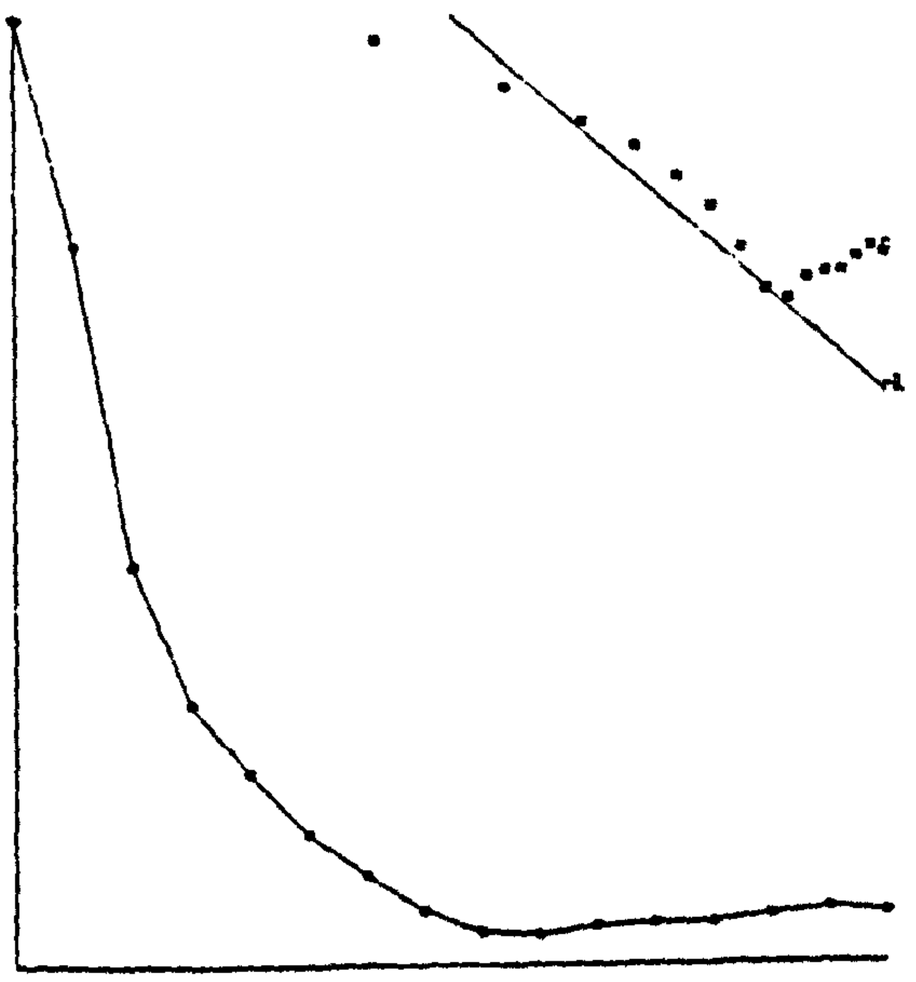

FREQUENCY SPECTRUM

MEASURED

FREQUENCY SPECTRUM

SIMULATED

Figure 57. Comparison of measured and simulated concentration covariance and spectrum from point source record.

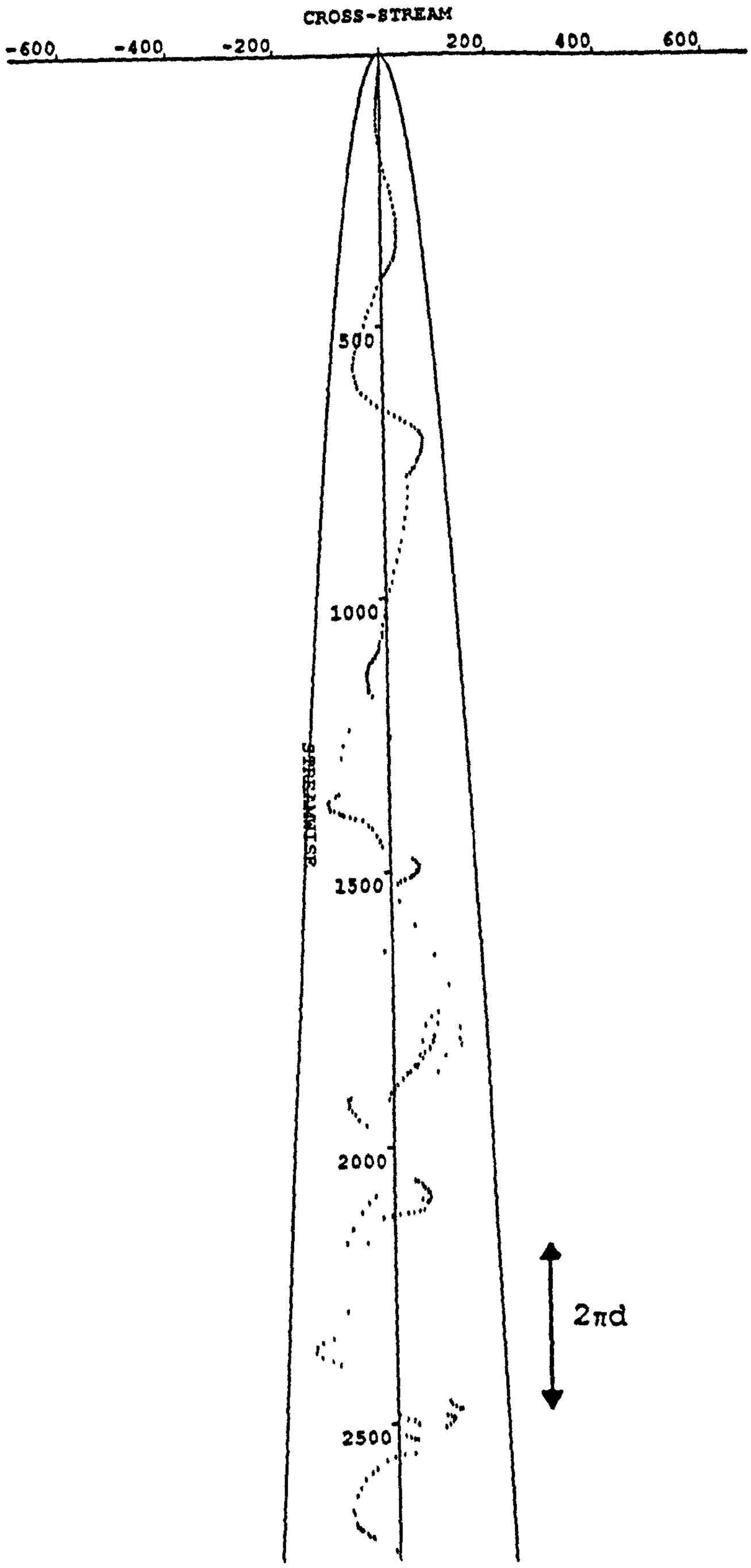

Figure 58. Simulation of thicker oil release to highlight meandering.

CHAPTER 9. SUMMARY OF RESULTS AND CONCLUSIONS.

The dissipation cascade.

A model of the turbulent dissipation cascade has been derived using a set of intermittent discrete eddy sizes. The kinetic energy density and lifetime of each eddy size are given by:

$$k_\ell = \varepsilon^{2/3}\ell^{2/3} \tag{2.41}$$

$$t_\ell = \varepsilon^{-1/3}\ell^{2/3} \tag{2.42}$$

where ℓ is a lengthscale describing the eddy size and ε the turbulent kinetic energy dissipation rate. If the breakdown process to smaller sizes is self-similar then to conserve kinetic energy and vorticity the eddy sizes are related by a fractional dimension C where:

$$C = 8^{1/2} \tag{2.63}$$

Equations (2.41) and (2.42) form part of many existing turbulence models and it is concluded that they should form the basis of any model which seeks to incorporate the spatial extent of individual eddies. When applied to simple geometries the cascade model can describe the development of grid generated turbulence and predict dispersion at the sea surface in a rectilinear mean current.

The turbulent production process.

A mean velocity profile was derived from the distance that eddies in the dissipation cascade can mix slow moving fluid away from the bed layer into the outer flow. Since the sizes are related by C, the profile is logarithmic. By equating the kinetic energy defect in the resulting profile with that of the largest eddies, so that the mean velocity profile is a result of the turbulent production process, there results:

$$U_0/N = n_L u_L \tag{3.28}$$

where U_0 is the mean surface velocity, L the boundary layer depth, $u_L^2 = k_L$ (equation (2.41)), and n_L the large eddy intermittency. The total number of discrete eddy sizes, N, is given by:

$$N = \log L/\lambda \tag{3.18}$$

It was concluded that λ could be associated with the Kolmogorov dissipation scale and, more significantly, that the turbulent production could equal dissipation for a value of N equal to 11. The result was that the mean velocity profile:

$$U(h) = n_L u_L \log h/\lambda + 1.5 n_L u_L + n_L u_L \tag{3.33}$$

was predicted for surface velocities less than a critical surface velocity U_1 given by:

$$U_1 = N u_L \tag{3.65}$$

so that below U_1 , ε remained constant and n_L was given by:

$$n_L = U_0/U_1 \tag{3.63}$$

A model of the Reynolds stress related the stress to the friction velocity used to characterise the mean velocity profile and predicted a constant stress layer near the bed. A model of the bursting sequence showed that the mean profile could be produced by a streamwise succession of eddies, size L, at related stages of production. For this reason, and from considerations of continuity, it was predicted that the development of the largest eddy size should exhibit group behaviour, there being $n_L N$ eddies in a streamwise group. The energy spectrum from such a group passing a fixed velocity sensor would show the production energy at a frequency equal to $1/t_L$ rather than at the frequency associated with the eddy passage time, invalidating Taylor's hypothesis for such spectra.

Turbulent spectra.

By considering how the energy from a particular eddy size would reflect into a one-dimensional spectrum the equations:

$$\Phi_1(k) = 1.7\, n_L \varepsilon^{2/3} k^{-5/3} \qquad (4.5)$$

$$\phi(\sigma) = 0.5 n_L \varepsilon\, \sigma^{-2} \qquad (4.18)$$

were derived from the dissipation cascade without reference to isotropy. These equations were used to propose an explanation for surface layer similarity scaling and the fact that the turbulence appears isotropic above $kh = 2\pi$ where h is the sensor height.

Current meter experiment.

A current meter experiment was carried out in 30 m of water over a complete tidal cycle. Correlations showed that the largest eddies in the flow were approximately cubic with a dimension equal to the water depth. These eddies were shown to move with the mean flow. Frequency spectra for the turbulent components peaked at $1/t_L$ showing that the current meters were responding to the fluctuations caused by the production process rather than to the passage of individual eddies. The horizontal velocity fluctuations were approximately isotropic.

The mean velocity measured at two heights closely followed (3.33) with $\varepsilon = 0.3$ cm^2/s^3 and $N = 11$. The large eddy intermittency was found by two methods and was proportional to current speed, validating (3.63). The value of ε was also found by fitting (4.18) to spectra derived for different intervals of the tidal cycle and by using (2.62) at the spectral peak frequency, $1/t_L$. The value again remained constant close to 0.3 cm^2/s^3.

During the ebb tide the turbulent kinetic energy was approximately a quater of the value found on the flood, despite the mean velocity profiles being similar. This could not be satisfactorily explained except by proposing that the boundary layer might adopt preferred energy states. If this were so then

the observations could be related to the discrete eddy cascade and a value of C given by (2.63).

To investigate the possibility that the boundary layer energy might vary in discrete steps the Fourier components of the spectral peak were isolated and transformed to give a signal descriptive of the large eddy production process. This signal was chaotic and is believed to be due to the strange attractor which underlies the turbulent process. By plotting the magnitude of this signal against its rate of change the discretised nature of the process was revealed.

Numerical simulation of surface dispersion experiments.

Two large scale dye releases and one oil release were analysed in terms of the dispersion predicted from the discrete dissipation cascade. The dispersion and meandering all followed the model equations with ε close to 0.3 cm^2/s^3. This was confirmed by a numerical simulation. These experiments were carried out in 45 m of water and the value of ε was the same as in the current meter experiment. Since this was carried out in 30 m of water it is concluded that the dependence of ε on water depth is slight.

A third dye release experiment resulted in a 45 minute concentration record taken at a fixed point 1600 m from the source. The intermittency and concentration spectrum from the record were reasonably well simulated by the dispersion model. The concentration fluctuation distribution was analysed and shown to be approximately log-normal with a peak to mean ratio reaching a maximum of 10. The model showed that the cross-stream concentration intermittency distribution was approximately Gaussian and that the centre-line concentration intermittency, γ, reduced linearly from unity to 0.5 over a distance approximately equivalent to that at which the dye was mixed throughout the water column. The value of γ then remained close to 0.5 for a distance equivalent to the end of the explosive phase of cloud growth, and subsequently returned to unity at the distance from source where the meandering became insignificant.

Concluding discussion.

The following paragraphs from the introduction gave the requirements of an improved turbulent dispersion model. These were that the model should:

a. Recognise the spatial distribution of eddies and the intermittency of the turbulence.

b. Give the mean velocity distributions found by observation.

c. Give the correct frequency and wave number spectral characteristics, possibly over a wider range than those derived for the inertial subrange.

d. Give values for parameters such as ε which are within the band of values measured by experiment.

e. Predict dispersion which agrees with the measurements of relative and absolute dispersion, meandering and intermittency.

f. Model the Reynolds stresses and justify the models currently in use for their prediction.

g. Give eddy characteristics which are derived from the fundamental equations of motion, so that the physics of the turbulent process is made more clear.

The model of dispersion by turbulent eddies developed in this thesis satisfies these requirements for dispersion by bottom generated turbulence in a rectilinear flow. In predicting the turbulent intensity, and consequent turbulent dispersion, there remains a significant unanswered question. It appears that the kinetic energy of a turbulent boundary layer might tend to adopt preferred, discrete, energy states. This behaviour is typical of systems whose governing equations are non-linear. If this phenomenum is real, then the prediction of turbulent dispersion becomes a much more complex problem.

It is possible to reproduce the component attractor presented in this thesis with non-linear equations. It has not yet proved possible to derive these from the Navier-Stokes equations. If this could be achieved then the discrete energy levels, and subsequent turbulent dispersion, might be predictable.

The model has been derived for, and tested in, rectilinear mean currents when the boundary layer has reached the surface. Under these restricted, but common, circumstances the value of the energy dissipation rate, ε, is found to remain constant at approximately 0.3 cm^2/s^3, and the turbulent intermittency to vary linearly with current speed. To find a value for ε the intermittency of the turbulence has to be accounted for and its variation in more complex geometries is as yet unknown. If ε is constant then in the simple geometry studied here the depth integrated turbulent kinetic energy equation simplifies to a non-linear equation for the intermittency, n_L. This may form another approach to the prediction of discrete energy levels and the development of turbulence in the sea.

The set of non-linear equations which reproduce the attractor can also be written in a form similar to the Langevin equation. In a simple random walk, the particle position is recalled at each time step and the particle given a randomly generated velocity. In the Langevin equation, the particle velocity is recalled and a random acceleration applied at each time step. In the form which mimics the attractor, the acceleration is recalled and a random rate of change of acceleration applied at each time step. A typical result, simulating the dispersion of one fluid particle in a constant current, is shown in Figure 59. The mean position of the particle meanders. It is therefore concluded that an in-depth study of the component attractor would form a fruitful basis for future research.

Figure 59. The dispersion of a single particle calculated from a modified form of the Langevin equation.

REFERENCES

Allen, C.M., (1982). Numerical Solution of Contaminant Dispersion in Estuary Flows. Proceedings of the Royal Society, London, A 381, 179-194.

Anwar, H.O., (1981). A Study of the Turbulent Structure of a Tidal Flow. Estuarine, Coastal Shelf Science., 13, 373-387.

Bartlett, M.S., (1978), An Introduction to Stochastic Processes with Especial Relation to Methods and Applications (3rd Edition). Cambridge University Press, London, 338pp.

Batchelor, G.K., (1950). The Application of the Similarity Theory of Turbulence to Atmospheric Dispersion. Quarterly Journal of the Royal Meteorological Society, 76, 133-142.

Batchelor, G.K., (1952). Diffusion in a Field of Homogeneous Turbulence, II- The Relative Motion of Particles. Proceedings of the Cambridge Philosophical Society, 48, 345-357.

Batchelor, G.K, (1967). An Introduction to Fluid Mechanics. Cambridge University Press, London, 615pp.

Bendat, J.S. and A.G. Piersol, (1971). Random Data; Analysis and Measurment Procedures. Wiley, London, 407pp.

Boussinesq, A., (1877). Theory de L'Ecoulement Turbulent. Mem. Pre. Par. Div. Sav., 23.

Bowden, K.F. and R.E. Lewis, (1973). Dispersion in Flow from a Continuous Source at Sea. Water Research, Pergammon Press, 7, 1705-1722.

Bowden, K.F. and S.R. Ferguson, (1980). Variations with Height of the Turbulence in a Tidally-Induced Bottom Boundary Layer. Reprinted from Marine Turbulence, edited by J.C.J. Nihoul, Elsever Publishing Co, 259-286.

Bradshaw, P., T. Cebeci and J.H. Whitelaw, (1981). Engineering Calculation Methods for Turbulent Flow. London Academic Press, London, 331pp.

Brumley, B.H. and G.H. Jirka, (1987). Near Surface Turbulence in a Grid-Stirred Tank. Journal of Fluid Mechanics, 183, 235-263.

Browne, L.W.R., R.A. Antonia and D.A. Shah, (1987) Turbulent Energy Dissipation in a Wake. Journal of Fluid Mechanics, 179, 307-326.

Cox, S.M., P.G. Darzin, S.C. Ryrie and K. Slater, (1990). Chaotic Advection of Irrotational Flows and of Waves in Fluids. Journal of Fluid Mechanics, 214, 517-534.

Csanady, G.T., (1972). Turbulent Diffusion in the Environment. Geophysics and Astrophysics Monographs, Vol 3. D Reidel Publishing Co, Boston, 248pp.

Durbin, P.A., (1983). Stochastic Differential Equations and Turbulent Dispersion. NASA Reference Publication 1103, 69pp.

Dwight, H.B., (1961). Tables of Integrals and Other Data. Macmillan, New York, 336pp.

Elliott, A.J., (1986). Shear Diffusion and the Spread of Oil in the Surface Layers of the North Sea. Dt. Hydrogr. Z., 39, 113-137.

Heathershaw, A.D., (1979). The Turbulent Structure of the Bottom Boundary Layer in a Tidal Current. Geophysical Journal of the Royal Astronmical Society, 58, 395-430.

Jones, W.P., (1971). Lamenarisation in Strongly Accellerated Boundary Layers. PhD Thesis, University of London, 412pp.

Jones, W.P. and B.E. Launder, (1972). The Prediction of Lemenarisation with a Two Equation Model of Turbulence. International Journal of Heat and Mass Transfer, 15, 301-345.

Kinsman, B., (1965). Wind Waves. Prentice Hall, Englewood Cliffs, New Jersey, 676pp.

Kim H.T., Kline, S.J. and W.C.Reynolds (1971). The Production of Turbulence near a Smooth Wall in a Turbulent Boundary Layer. Journal of Fluid Mechanics, 50, 133-160.

Kolmogorov, A.N., (1941). On degeneration of Isotropic Turbulence in an Incompressible Viscous Fluid. Dokl. Akad. Nauk. SSSR, 31, 538. (Translation in Friedlander, S.K. and L. Tapper, (1961). Turbulence: Classic Papers in Statistical Theory, Interscience, London, 496pp.)

Landahl, M.T. and E. Mollo-Christiansen, (1987). Turbulence and Random Processes in Fluid Mechanics. Cambridge University Press, London, 160pp.

Lamb, H., (1932). Hydrodynamics. (6th edition), Cambridge University Press, Cambridge, 738pp.

Launder, B.E., A. Morse, W. Rodi and D.B. Spalding, (1972). The Prediction of Free Shear Flows, a Comparison of the Performance of Six Turbulence Models. NASA Reference Publication, SP-311, 361-394.

Launder, B.E., G.J. Reece and W. Rodi, (1975). Progress in the Development of a Reynold's Stress Turbulence Closure. Journal of Fluid Mechanics, 68, 537-566.

Mandelbrot,B.B., (1983). The Fractal Geometry of Nature. W.H. Freeman and Co., New York, 468pp.

Mandelbrot,B.B., (1974). Intermittent Turbulence in Self-Similar Cascades: Divergence of High Moments and Dimension of the Carrier. Journal of Fluid Mechanics, 62, 331-358.

Nakamura, I., S. Sakai and M. Miyata, (1987). Diffusion of Matter by a Non-Buoyant Plume in Grid Generated Turbulence. Journal of Fluid Mechanics, 178, 379-403.

N.B.A. (Controls) Ltd, (1984). Manual for Self-Recording Current Meter. Model DNC 2, DNC 2B. N.B.A. (Controls) Ltd, Invincible Rd, Farnborough, Hants, 184pp.

Okubo, A. and H.H. Carter, (1966). An extremely Simplified Model of the Shear Effect on Horizontal Mixing in a Bounded Sea. Journal of Geophysical Research, 71, 5267-5271.

Okubo, A., (1967). The Effect of Shear in an Oscillatory Current on Horizontal Diffusion from an Instantaneous Source. Oceanology and Limnology, 1, 194-204.

Okubo, A. and R.V. Ozmidov, (1970). Empirical Dependence of the Coefficient of Horizontal Turbulent Diffusion in the Ocean on the Scale of the Phenomenum in Question. Izv. Atm. Oc. Phys. 6, 534-536.

Okubo, A., (1971). Oceanic Diffusion Diagrams. Deep-Sea Research, 18, 789-802.

Okubo, A., V. Andreasen and J. Mitchell, (1984).Chaos Induced Turbulent Diffusion. Physics Letters A, 105A 4-5, 169-172.

Ozmidov, R.V., (1965). Energy Distribution between Oceanic Motions of Different Scales. Bulletin of the Academy of Science, U.S.S.R, Atmospheric and Oceanic Physics, 1, 257-261.

Pipes, L.A., (1958). Applied Mathematics for Engineers and Physicists. (2nd Edition), McGraw-Hill, New York, 723pp.

Prandtle, L., (1925). Uber ein neues Formelsystem fur die ausgebildete Turbulenz. Z.A.M.M., 5, 136-142. (Nachr. Ges. Wiss. Gottingen, (1945). Math.-Phys, Kl., 6-19.)

Prandle, D., (1982). The Vertical Structure of Tidal Currents and other Oscillatory Flows. Continental Shelf Research, 1, 191-207.

Raudkivi, A.J. and R.A. Callander, (1975). Advanced Fluid Mechanics. Edward Arnold, London, 325pp.

Rogers,M. and P. Moin, (1987), The Structure of the Vorticity Field in Homogeneous Turbulent Flows. Journal of Fluid Mechanics, 176, 33-66.

Smith, T.J., (1982). On the Representation of Reynolds Stress in Estuaries and Shallow Coastal Seas. Journal of Physical Oceanography, 12, 914-921.

Soulsby, R.L., (1977). Similarity Spectra of Turbulence Spectra in Marine and Atmospheric Boundary Layers. Journal of Physical Oceanography, 7, 934-937.

Soulsby, R.L., (1983). The Bottom Boundary Layer of Shelf Seas. Phys Oceanog of Coastal and Shelf Seas, Ed B.Johns, Elsevier, Amsterdam, 189-266.

Taylor G.I., (1922). Diffusion by Continuous Movements. Proceedings of the London Mathematical Society, A 20, 196-199.

Tennekes,H. and J.L. Lumley, (1972). A First Course in Turbulence. MIT Press, London, 300pp.

Townsend, A.A., (1976). The Structure of Turbulent Shear Flow. Cambridge University Press, London, 315pp.

Tritton, D.J., (1977). Physical Fluid Dynamics. Van Nostrand Reinhold, London, 362pp.

Turner, J.S., (1973). Buoyancy Effects in Fluids. Cambridge University Press, London, 367pp.

Utami,T. and T. Ueno, (1987). Experimental Study on the Coherent Structure of Turbulent Open Channel Flow using Visualisation and Picture Processing. Journal of Fluid Mechanics, 174, 399-440.

Woods, J.D., (1977a). Paramterization of Unresolved Motions. Modelling and Prediction of the Upper Layers of the Ocean, Proceedings of a NATO Advanced Study Institute, Edited by E.B. Kraus, Pergamon Press, Oxford, 118-143.

Woods, J.D., (1977b). Information Theory Related to Experiments in the Upper Ocean. Modelling and Prediction of the Upper Layers of the Ocean,Proceedings of a NATO Advanced Study Institute, Edited by E.B. Kraus, Pergamon Press, Oxford, 263-284.

Yalin, M.S., (1977). Mechanics of Sediment Transport. Pergamon Press, Oxford, 298pp.

Yaglom, A.M., (1966). The Influence of the Fluctuation in Energy Dissipation Rate on the Shape of Turbulent Characteristics in the Inertial Interval. Sov. Phys. Dokl., 2, 26-29.